The University Of Sheffield.

The Role of microRNA-145 in the Tumour Microenvironment

By:
Genevieve E. Melling

A thesis submitted in partial fulfilment of the requirements for the degree of Doctor of Philosophy

The University of Sheffield
Faculty of Medicine, Dentistry and Health
School of Clinical Dentistry

June 2015

Dedicated in loving memory of ‘Grandpa Bagshot’,

William Arthur Mallinson, CBE (12 June 1922 - 17 November 2006).

Acknowledgements

Firstly, I would like to thank my supervisor Dan Lambert for his advice, guidance and encouragement over the last four years. Without your support, I wouldn't have dreamed of doing a Ph.D. and definitely would not be pursuing a career in research! I am hugely grateful for your optimism and for all the extra opportunities you have provided for me.

Thank you to the University of Sheffield for funding my Ph.D., and to Jim Catto, my second supervisor, for his valued input to the project.

A huge thank you to my Mum and Dad for the financial and loving support they have generously given me over my whole education. To my amazing Mum, thank you for all your uplifting words and everything you do to encourage me. I would also like to thank my Grandma who always has shown a keen interest and kind support.

I would like to thank Tasnuva Kabir, Emma Hinsley and Stuart Hunt for all your help with various lab techniques and for welcoming me into the department. I would also like to thank Brenka McCabe for all the technical support she has given. I would like to acknowledge Sarah Flannery, an excellent SURE undergraduate summer student, who helped me complete some of the molecular analysis of ADAMTS expression and versican cleavage work outlined in the thesis.

Thank you to all my friends and colleagues at the School of Clinical Dentistry for making it a wonderful place to work, especially to Chat, Kate, Charlotte and Raghu who were always there to cheer me up after a bad day!

To my good friend Ruth Mitchell, thank you for always being there for me, despite being the other side of the country, and spurring me on throughout my studies. Also, a big thanks goes to my housemate Maisha for looking after me for all these years!

Lastly, I would like to thank all my friends from my church especially Julia, and Sarah, my thesis writing buddy, for all your words of encouragement. Thanks foremost to God, whose grace is always sufficient.

Abstract

Background: Cancer associated fibroblasts (CAFs), are known to promote stromal-epithelial paracrine interactions, stromal remodelling and angiogenesis, within the tumour microenvironment. In oral squamous cell carcinomas, elevated expression of a myofibroblast CAF marker, alpha-smooth muscle actin (αSMA) and the matricellular proteoglycan versican are both predictive of invasive phenotypes and poor prognosis. The molecular mechanisms underlying myofibroblast transdifferentiation are poorly characterised. Here, the role of microRNA-145, a small non-coding RNA which negatively regulates multiple gene transcripts, was investigated in stromal fibroblasts.

Methods: Normal oral fibroblasts (NOFs) and fibroblasts isolated from OSCC (CAFs) were treated with cancer cell line conditioned medium and TGF-β1, and the expression of miR-145, versican and myofibroblasts markers αSMA, collagen-1a (COL1A1), and fibronectin-1 with extra domain A (FN1-EDA) were assessed by qRT-PCR, immunoblotting and immunocytochemistry. A synthetic precursor miR-145 was used to overexpress miR-145 in fibroblasts prior, or subsequent to, TGF-β1 treatment and the myofibroblast phenotype was investigated by assessing molecular markers, cell contractility and the ability to promote paracrine cancer cell migration. Versican expression was investigated and loss of function experiments were used to investigate its effect on myofibroblast phenotype. Putative genes involved in myofibroblast regulation were also assessed by qRT-PCR. Similar experiments were performed in primary dermal fibroblasts.

Results: CAFs had a significantly higher miR-145 expression than NOFs, but no difference in myofibroblast markers was observed. TGF-β1 induced the expression of miR-145 and myofibroblast markers, and promoted contractility and cancer cell paracrine migration. miR-145 gain of function experiments attenuated and rescued the TGF-β1-induced myofibroblast phenotype. miR-145 negatively regulated versican, and versican loss of function had a small effect on myofibroblast phenotype. miR-145 and versican had similar effects in dermal fibroblasts.

Conclusions: miR-145 inhibits and reverses oral and dermal myofibroblast transdifferentiation. Therefore, exogenously delivering miR-145 to the tumour microenvironment and fibrotic areas could potentially treat deleterious myofibroblasts.

Contents

List of Methods

List of Figures

List of Tables

List of Abbreviations

αSMA - Alpha Smooth Muscle Actin

ADAM - A Disintegrin and Metalloprotease

ADAMTS - A Disintegrin and Metalloprotease – with Thrombospondin motifs

BCA - Bicinchoninic Acid

BSA - Bovine Serum Albumin

BMDC - Bone Marrow Derived Cell

CAF - Cancer Associated Fibroblast

COL1A1 - Collagen 1a

CTGF - Connective Tissue Growth Factor

CXCL - C-X-C motif ligand 8

EBV - Epstein Barr Virus

ECM - Extracellular Matrix

EGF - Epidermis Growth Factor

EMT - Epithelial-to-Mesenchymal Transition

ET-1 - Endothelin-1

FAP - Fibroblast Activation Protein

FSP1 - Fibroblast Specific Protein 1

GAG - Glycosaminoglycan

HPV - Human papillomavirus

HRP - Horseradish Peroxidase

HNSCC - Head and Neck Squamous Cell Carcinoma

IL - Interleukin

IGF - Insulin- like Growth Factor

KLF-4/5 - Krüppel Like Factor- 4/5

LB - Lysogeny Broth

miRNA - miR – microRNA

MRTF-A/B - Myocardin Related Transcription Factor- A/B

MMP - Matrix Metalloproteinase

NF-κB - Nuclear Factor Kappa B

OSCC - Oral Squamous Cell Carcinoma

RNA - Ribonucleic Acid

RIPA - Radio-Immunoprecipitation Assay

RISC - RNA Induced Silencing Complex

PAI-1 - Plasminogen Activator Inhibitor -1

PBS - Phosphate Buffered Saline

primiR - primary microRNA

PremiR - Precursor microRNA

PDGF - Platelet Derived Growth Factor

qRT-PCR - quantitative Real Time – Polymerase Chain Reaction

SMC - Smooth Muscle Cell

SOC - Super Optimal broth with Catabolite repression

Sox - SRY- related high mobility group-Box

SRF - Serum Response Factor

TACE - TNF-α Converting Enzyme

TLR - Toll Like Receptor

TBS-T - Tris-Buffered Saline- Tween

TGF-β - Transforming Growth Factor Beta

TGF-βRII - Transforming Growth Factor Beta Receptor II

TNF-α - Tumour Necrosis Factor Alpha

UTR - Untranslated Region

VCAN - Versican

VEGF - Vascular Endothelial Growth Factor

VSMC - Vascular Smooth Muscle Cell

Chapter 1: Introduction

1.1 *Introduction to Cancer*

Cancer is the leading cause of mortality worldwide, it was estimated that 7.6 million people died in 2008 as a result of cancer (Globocan cancer project, International Agency for research on cancer (IARC)). Cancer is a collective term for diseases where normal cells undergo uncontrolled division and growth to form a tumour anywhere in the body. These tumours arise from normal cells that have mutations in key genetic pathways which control cellular proliferation, growth and apoptosis.

For many decades a major effort in medical research has been focused on pinpointing the genetic alterations present in cancer cells. This has shed light on the complex multi-stage process that is tumourigenesis and has highlighted the many somatic mutations, epigenetic changes, and chromosomal modifications that contribute to neoplasms and their progression. In the classic review by Robert Weinberg and Douglas Hanahan (2000), six key characteristics or 'hallmarks' that cells must possess to be cancerous were identified. They recognized that cells must become transformed to grow indefinitely without the need for the growth signals, to escape apoptosis, and to evade anti-growth signals, as well as having the ability to stimulate angiogenesis, invade tissue and metastasise (Hanahan & Weinberg, 2000). Since then research has elucidated that inflammation is critical in most tumours, and so has been labelled the 7th hallmark of cancer (Colotta *et al*., 2009). Furthermore, cancer has been likened to a 'wound that does not heal', hence inflammatory mediators have been recognised to play a part in cancer progression (Dvorak, 1986).

Like the initial oncogenesis within tumour cells, metastasis can also be seen as a multistage process and involves many molecular changes (Valastyan & Weinberg, 2011), sometimes described as the invasion-metastasis cascade. It involves: the local invasion of transformed cells through adjacent extracellular matrix and stroma, the intravasation of cells into nearby vasculature and/or lymphatics, the survival in the bloodstream, the dissemination to distant sites by extravasation, and the survival of the micro-metastases in their new environment enabling them to colonize and form a secondary tumours. The process of metastasis is responsible for 90% of deaths caused by cancer (Gupta & Massagué, 2006).

A significant event in the invasion-metastasis cascade is the epithelial-to-mesenchymal transition (EMT), whereby epithelial cells undergo changes in morphology, cell adhesion molecule expression and motility which collectively result in a phenotypic switch to a mesenchymal-like cell (reviewed in Thiery, 2002; Kalluri & Weinberg, 2009). The transition allows the deconstruction of the normal epithelial sheets to allow the migration and invasion of

the cells. This tissue re-organizational event is seen in wound healing and in early embryogenesis, but is also seen in carcinomas where transformed epithelial cells at the invasive front migrate through the basement membrane, a specialized dense extracellular matrix structure which provides a barrier at the basolateral side of cells (Kalluri & Zeisberg, 2006), and invade the surrounding stroma. EMT involves many molecular changes within the epithelial cells, but also requires the secretion of proteases and chemokines from surrounding stromal cells, namely fibroblasts and macrophages, to encourage their migration.

Through considerable research a view has emerged that malignant cells do not act autonomously, but grow, interact and adjust alongside a stromal environment. These stromal-epithelial interactions are a two-way paracrine cellular signalling mechanism which can stimulate changes in both the cancerous cells and the stroma to support the tumour's progression and its metastasis. In this way, the stroma 'evolves' alongside the tumour cells. An example of this was described by Hill *et al*., (2005) where they showed transformed epithelia that had undergone oncogenic stresses had non-cell autonomous effects on the surrounding 'non-malignant' stroma causing alterations and creating a more permissive environment in which a cancer could grow (Hill *et al*., 2005).

1.2 ***Head and neck cancers.***

Head and neck cancers mainly present, in around 90% of cases, as squamous cell carcinomas, referred to collectively as head and neck squamous cell carcinoma (HNSCC) (Sanderson & Ironside, 2002). HNSCC is defined as a tumour of squamous epithelial origin within the upper aerodigestive tract from the lips to the oesophagus. This region consists of paranasal sinuses, oral cavity, nasopharynx, oropharynx, larynx and the hypopharynx (Leemans, Braakhuis, & Brakenhoff, 2011). Tumours presenting in the oral cavity are the most common kind of HNSCC and are the sixth most prevalent cancer worldwide (American Cancer Society: Cancer Facts and Figures. 2009). Oral cancers mainly present as oral squamous cell carcinoma (OSCC), in 2008, the UK had an incidence of 8.49 per 100,000 people for oral and pharyngeal cancer with a 2.73 per 100,000 mortality rate (European cancer observatory database, IACR).

Most cases of HNSCC are diagnosed late, and some can develop from premalignant conditions, the most common ones being leukoplakia and erthyoplakia, which present as white and red patches respectively (Greer, 2006). Late stage HNSCC can be very aggressive with low survival rates and have only 40% 5 year survival due to high incidences of regional metastasis (Vikram *et*

al., 1984). Positive neck lymph node metastasis decreases the chance of survival by around 50% (Sotiriou *et al.*, 2004). Distant metastatic sites include the lung and liver (Lin *et al*., 2007). If caught at an early stage, however, prognosis is good. The standard treatment for HNSCC is platinum based chemotherapies combined with surgery.

Major risk factors of HNSCC include tobacco usage, alcohol consumption, genetic predisposition, and infection by certain high-risk human papillomaviruses (HPVs) especially in oropharyngeal squamous cell carcinomas, predominantly HPV-16 (Leemans *et al*., 2011) . A popular custom of chewing of khat or betel quid leaves, in certain countries, is associated with higher incidence of the disease. Also there have been occupational risks reported (Sanderson & Ironside, 2002). Epstein Barr Virus (EBV) has been identified to cause head and neck cancers, specifically those of the nasopharynx. Diet and oral health are also reported to have some influence in preventing cancer in the oral cavity, by promoting healthy oral epithelium.

The incidence of HPV positive tumours is increasing and is responsible for the rise in tongue, tonsil and oropharygeal neoplasms in the UK and US (Leemans, Braakhuis & Brakenhoff, 2011). The virus allows the integration of 2 oncogenes, E6 and E7, into the host cell's genome, these viral genes then inactivate endogenous tumour suppressor cell cycle regulators, p53 and retinoblastoma (RB), respectively to result in oncogenesis (Hausen, 2002). HPV positive status provides a good prognosis; however, smoking is correlated with high risk of death in oropharyngeal cancers (Ang *et al*., 2010).

Many of the molecular alterations contributing to the heterogeneous HNSCC cases remain poorly characterised. However, it is known that epidermal growth factor (EGF) signalling is aberrant in a larger number of HNSCC incidences, which is attributed to angiogenesis, increase tumour growth and invasion (Pai & Westra, 2009). The EGFR is overexpressed in around 90% of all HNSCC cases (Kalyankrishna & Grandis, 2006) and 30% are as a result of chromosomal amplifications (Sheu *et al.*, 2009). In addition, a constitutively active mutant form of EGFR has been identified in HNSCC, which caused hyperproliferation (Sok *et al*., 2006). Therefore, an effective clinically used treatment for certain HNSCCs is cetuximab, an EGF receptor monoclonal antibody. The response rate to cetuximab is around 20%, but when responsive it proves to be an effective treatment for patients with recurrent or metastatic HNSCC, on its own or in combination with chemo/radiotherapy (Burtness *et al.*, 2005; Sharafinski *et al.,* 2010).

A high proportion of OSCC have mutations in TP53 (the gene encoding p53), they are present even in HPV positive cells despite the inactivation of p53 mentioned previously (Leemans *et al.,* 2011). Most HNSCC have mutations in the TGF-β pathways which allow the loss of the inhibitory effect on proliferation. Interestingly, experimental loss of Smad4, necessary for TGF-β signal transduction into the nucleus, in mice caused spontaneous HNSCC (Bornstein, *et al.*, 2009). Other pathways reported to be altered in HNSCC are HGF signalling, NFκB, ET-1, renin angiotensin system and the PI3K-PTEN-AKT axis which are interconnected with TGF-β and EGF signalling (Leemans, Braakhuis & Brakenhoff, 2011).

In addition to altered intracellular signalling there appears to be a modified secretome in HNSCC. Stokes *et al.,* (2012) showed that HNSCC patients had elevated protease secretions (MMPs, ADAM and ADAMTS), whereas MMP9 levels were decreased in metastatic HNSCC. However, Lotfi *et al.*, (2015) found that serum from OSCC patients contained elevated MMP2 and MMP9, and this was found to be correlational with the presence of lymph node metastases.

As survival rates have not significantly increased over the last 40 years, and there are low survival rates for advanced stages of HNSCC, it is important that research is aimed at the development of further effective target-based therapies. Therefore, identifying druggable targets within the disease and identifying biomarkers would be hugely beneficial. Marsh *et al.,* (2011) found the best independent poor prognosis marker for OSCC to be of stromal origin, more accurately predictive than TNM staging or any tumour markers, highlighting the importance for investigating the oral tumour microenvironment for understanding tumour progression, and developing future therapeutics.

1.3 ***Tumour Microenvironment***

1.3.1 *Cells of the tumour microenvironment*

There are a variety of distinct non-malignant cell types surrounding transformed cells in solid tumours. Collectively, these cells and matrix are known as the tumour stroma, which plays an active role in cancer survival and progression. Similar to under normal physiological conditions, the transformed cells maintain an inter-communication with surrounding stromal cells. These stromal-epithelial interactions allow the neoplastic cells to provide factors that change the stromal cell phenotype to in-turn actively provide trophic paracrine signalling to encourage the metastasis of the tumour.

The non-malignant stromal cells can form up to 90% of the cells present in a tumour (Weinberg, 2006) and consists of a diverse population of specialised cells and a dense extracellular matrix. The cells that comprise the stromal environment include bone marrow-derived cells (BMDC), immune cells, vascular and lympathic endothelial cells, mesenchymal-derived smooth muscle cells, adipocytes, nerves, pericytes, fibroblasts and mesenchymal stem cells (reviewed in Joyce & Pollard, 2009). Many of these cells are usually protective and help to inhibit malignancy but within the cancer microenvironment they can be stimulated by the neoplasm to encourage its survival and metastatic dissemination into new sites.

Stromal cells can promote tumourigenesis in epithelial cells with genetic predisposition to be transformed. These compromised epithelial cells form tumours with less latency and greater efficiency when co-injected into mice with matrigel (basement membrane matrix derived from a sarcoma) or stromal fibroblasts (Elenbaas *et al.,* 2001; Noël *et al.,* 1993). Further information on the role of stromal fibroblasts in tumour progression will be discussed in section 1.4.

Irradiated mammary stromal cells were able to cause carcinomas when epithelial cells were added to mammary fat pads (Barcellos-Hoff & Ravani, 2000). However, the non-irradiated epithelial cell line used in the study (COMMA-D) despite being 'non-tumourigenic', caused a tumour in a sham-irradiated control (1 out of 6). This suggests that the irradiated stromal environment may reduce the latency of tumour formation, rather than inducing the transformation of the epithelial cells. Nonetheless, radiation has been reported to have numerous pro-tumourigenic changes to the stroma including, elevated EGF (Schmidt-Ullrich *et al.,* 1996) and TGF-β growth factor signalling, ECM modulation (Barcellos-Hoff *et al.,* 1993) and changes in the level of adhesion molecules (Akimoto *et al.,* 1998). So it is no surprise that radiation to the stroma has been associated with the initiation of tumours.

Stromal-epithelial interactions are paramount for tumour development. It is known that factors secreted by cancerous cells can activate the stromal compartment to support the tumour by releasing growth factors, chemokines, extracellular matrix proteins and proteases (reviewed in Allen & Louise Jones, 2011). An example of this was shown when human immortalised keratinocytes overexpressing PDGF-BB caused tumours to develop when injected in nude mice. This effect was not due to the keratinocytes, as they did not express a receptor to PDGF, but was a result of the activation and proliferation of adjacent fibroblasts which responded by signalling to the keratinocyte compartment to proliferate to form a tumour (Skobe & Fusenig, 1998).

Angiogenesis is a crucial event in the tumour microenvironment for the survival of newly formed tumours (Carmeliet & Jain, 2000). Stromal and tumour cells secrete endothelial growth factors which orchestrate neoangiogenesis; the main players belonging to the VEGF (vascular endothelial growth factor) family (Carmeliet *et al*., 1996). Neoangiogenesis in tumours allows the cells to receive the nutrients and oxygen that the tumour needs to grow as well as providing a route for dissemination to occur.

The regulation of the tumour microenvironment is key in promoting a permissive cancer environment for cancer progression. Therapeutically targeting the microenvironment is therefore a valid method of preventing the spread of cancers (reviewed in Hanna, Quick & Libutti, 2009). This could be achieved by attempting to regulate secretion of key growth factors found in the tumour environment, regulating the ECM remodelling by controlling the activity of MMPs (Kessenbrock, Plaks, & Werb, 2010), or controlling the secretion of ECM component from fibroblasts. Preventing the recruitment of immune cells, stopping angiogenesis, and preventing the activation of fibroblasts (discussed below) would also be beneficial to aid the prevention of tumour growth and metastasis. Possible future treatments will no doubt be combined therapies targeting both the underlying cause of malignancy in the oncogenic cells and targeting multiple aspects of the microenvironment.

An example of an approved drug that can target the microenvironment to halt tumour progression is bevacizumab (Avastin). Bevacizumab, a monoclonal antibody (mAb) to VEGF-A, works by blocking neovascularisation and is currently a used in combinational treatment for certain glioblastoma, metastatic colorectal cancers, advanced non squamous cell non-small cell lung cancers, advanced cervical cancer, platinum resistant ovarian cancer and metastatic kidney cancers (Avastin, 2012; accessed on 26.3.15).

1.3.2 *Extracellular matrix and its role in cancer.*

The extracellular matrix (ECM) is a meshwork of macromolecules including collagen, fibronectin, laminin, elastin and proteoglycans which provides a platform for cells to adhere to and to move on (Boy, 2002). The ECM is mainly synthesised and modified by stromal fibroblasts. Its assembly is regulated and it is remodelled under pathological and physiological conditions. The ECM is a crucial regulator of cellular shape, by manipulation of the cytoskeleton, cell behaviour, and cellular signalling (Kim, Turnbull, & Guimond, 2011). The extracellular matrix can be modulated by several growth factors including TGF-β1, PDGF, bFGF and EGF (Matrisian & Hogan, 1990).

Fibroblasts and macrophages secrete extracellular proteases in the form of matrix metalloproteinases (MMPs) and serine proteases which also modulate and re-organise the ECM (Kessenbrock *et al*., 2010). MMPs are a zinc-dependent secreted or, to a lesser extent, membrane bound protease family which act to degrade the ECM; thereby playing a key role in tumourigenesis and metastasis. Closely related to MMPs, are ADAMs, a class of predominantly transmembrane metalloproteinases. A subset of these, ADAM-TS (a disintegrin and metalloprotease- with thrombospondins) are secreted and can associate with the ECM. Members of the ADAM-TS function to modulate the stromal environment through the processing of collagen and the cleavage of the aggrecans (ADAMTS-1,-4, -5, -8, -9, -15). Also, ADAMTS-1 and -8 prevent VEGF- mediated angiogenesis through their TS motifs. (reviewed in Blobel, 2005).

Proteases achieve their pro-tumourigenic/metastatic influence by several methods: they aid the dissociation of cells, they can 'create a clear path' through the ECM for cells to migrate, they can release ectodomains of membrane bound growth factors (ADAMs), or release soluble growth factors sequestered in the extracellular matrix e.g. bFGF, TGF-β1, PDGF, and HB- EGF (reviewed in Joyce & Pollard, 2009; Blobel, 2005). Proteases also activate latent extracellular growth factors and other pro-MMPs which require proteolytic cleavage for their activation (Kessenbrock *et al*., 2010). For example, MMPs secreted from stromal fibroblasts process latent TGF-β1 in the pericellular space (Lyons, Keski-Oja, & Moses, 1988), and the active form can stimulate EMT in transformed epithelia and fibroblast activation (Bierie & Moses, 2006).

1.3.3 *Inflammation within the microenvironment*

Cancers often arise from sites of chronic inflammation (Colotta *et al*., 2009). This due, in part, to the immune cells present which secrete many chemokines, proteases and growth factors, for example TGF-β, TNF-α, ILs, MMPs, VEGFs, CXCL8 (C-X-C motif ligand 8) and COX-2 (cyclooxygenase 2) (reviewed in Murdoch *et al.*, 2008). These recruit more immune cells and promote changes in stromal cells to increase stromal-epithelial signalling that will support the formation of tumours. However, there is no simple correlation between other immune cells within a tumour and the prognostic outcome.

Bone marrow-derived macrophages are recruited to the tumour site by chemotaxis driven by tumour secreted chemokines CSF-1 (macrophage colony stimulating factor), MCP-1 (monocyte chemotactic protein-1), and VEGF (Bingle, Brown, & Lewis, 2002); here they are known as

tumour associated macrophages (TAMs). Macrophage infiltration within a tumour is indicative of a poor prognosis, in more than 80% of cancers (Joyce & Pollard, 2009). They infiltrate into the tumour to assist the destruction and clearance of transformed cells, but they are often activated to provide pro-tumourigenic signalling. One such signalling factor secreted by TAMs is TNF-α, which in turn activates the NF-κB pathway. This results in the survival and proliferation of the cancer cells through the downstream activation of anti-apoptotic proteins Bcl-XL and COX-2 (responsible for the production of prostaglandin E which causes many pro-oncogenic changes) (Weinberg, 2006). TNF-α has also been reported to increase cancer cell invasion by the enhanced secretion of matrix metalloproteases (MMPs), in particular MMP9 (Stuelten *et al.,* 2005).

Macrophages are differentially activated and can be classified as M-1 or M-2. M-1, or 'classically activated macrophages' are activated by IFN-γ, TNF-α (cytokines released by T cell helper 1) or pathogenic recognition patterns, whereas the M-2 subtype is activated by IL-4 and IL-13 (cytokines released by T cell helper 2) (reviewed in Laoui *et al.*, 2011). The M-1 population is involved in antigen presentation and hence promoting the immune system to target the tumour, alternatively the M-2 subtype is generally seen as pro-tumourigenic as it secretes cytokines and is capable of promoting angiogenesis (Joyce & Pollard, 2009).

High numbers of eosinophils, a class of leukocytes commonly seen in parasitic infections and allergic responses, have been identified as an indicator of poor prognosis in OSCC (Martinelli-Kläy et al., 2009). Their abundance within a tumour results in the increase in secretion of TGF-β, TNF-α, and interleukins (ILs) which aid the recruitment of inflammatory mediators to provide a more permissive environment for invasion of the cancer.

1.3.4 *Transforming growth factor-beta's role within the tumour microenvironment.*

There is a plethora of research that points to the effects of altered TGF-β signalling in tumourigenesis, both within the malignant cells and within the surrounding stroma. TGF-β's role in the tumour microenvironment is complex, due to its ability to halt cancer progression or actively encourage tumour formation and metastasis under certain circumstances. Many studies have shown that alterations in stromal-epithelial TGF-β signalling often result in neoplasms (reviewed in Bierie & Moses, 2006), its overexpression has been reported in many tumours. It often predicts angiogenesis and metastasis, and therefore prognosis (Bierie & Moses, 2006; Levy & Hill, 2006).

The canonical TGF-β signalling pathway, is part of a wider superfamily including activins, bone morphogenic proteins (BMPs), growth and differentiation factors (GDFs) and nodal which are important in important in development, differentiation and hormone and cell homeostasis (Weiss & Attisano, 2013). The TGF-β family itself are mainly involved with immunosuppression, ECM maintenance and apoptosis. There are 3 main TGF-β ligands TGF-β1, TGF-β2, TGF-β3, which work through transmembrane serine-threonine kinase receptors TGF-β RI, TGF-β RII, TGF-β RIII (Yue & Mulder, 2001). Mainly active TGF-β ligands bind to TGF-β RII which recruits and cross phosphorylates TGF-β RI, which in turn phosphorylates receptor smads, smad2 and smad3 which are joined with co-smad, smad4 and can translocate into the nucleus to regulate transcription.

TGF-β ligands can be secreted in their latent form and can be activated in several ways including cleavage by MMP2 and MMP9 (Yu & Stamenkovic, 2000), αvβ6 and other integrins *(Munger et al.,* 1999), thrombospondin-1 (Schultz-Cherry & Murphy-Ullrich, 1993) and by mechanical stress (Wipff et al., 2007). The latent forms of TGF-β have an N termini, which require cleaving, called the latency associated peptide (LAP), together they are referred to as the small latent complex (SLC) (Annes, Munger, & Rifkin, 2003). The SLC can be bound by the latent TGF-β binding protein 1 (LTBP1), both referred to as the large latent complex (LLC). The LLC can be sequestered within the ECM and in order for TGF-β to be activated it must be cleaved from the LAP and LTBP1.

An increase in TGF-β signalling in stromal fibroblasts promotes tumourigenesis (Kuperwasser *et al*., 2004). The group showed that when fibroblasts overexpressing TGF-β, HGF or both (*via* retroviral infection) were engrafted with human epithelia in a mouse mammary fat pad grafts, carcinomas developed, whereas those with normal stroma did not. It was argued that the some of the human epithelial cells added must have already undergone some genetic alterations to account for the speed at which the tumours arose.

However, separate studies showed the converse; that is, a loss of TGF-β signalling in stromal fibroblasts resulted in carcinogenic lesions (Bhowmick, Chytil, *et al*., 2004; Forrester *et al*., 2005). Genetic deletion of 2 introns of the TGF-β receptor II (TGF-βRII) in fibroblasts in mice (*via* a conditional Cre-lox recombination, under the control of a fibroblast specific promoter (FSP-1)) resulted in the increased proliferation of both the stromal fibroblast and epithelial compartments, allowing the formation of invasive neoplastic lesions in the prostate and forestomach (Bhowmick, Chytil, *et al*., 2004). The study implicates that TGF-β signalling is responsible for preventing the proliferation of both epithelial and stromal fibroblasts *in vivo*. They also showed evidence that the hyperproliferation seen when TGF-β signalling was lost was mediated through HGF, as HGF levels were elevated and c-Myc , the HGF receptor, was activated

in the mouse epithelial cells. A similar study in which a conditional TGF-β RII receptor knockout mouse was made, showed the same thing, that the loss of TGF-β signalling resulted in tumourigenesis (Forrester *et al*., 2005). TGF-β is important for tissue homeostasis, it control the inappropriate proliferation and differentiation of tumour cells, but also can be utilised in the tumour microenvironment to tumour growth, invasion and metastasis (Massagué, 2008).

There appears to be a switch in tumourigenesis when TGF-β signalling turns from being anti-tumourigenic to pro-tumourigenic. The presence of bone marrow derived cells in the tumour microenvironment has been suggested to be the cause of this change in response to TGF-β. Yang & Moses, (2008) put forward the hypothesis that transgenic attenuation of TGF-β signalling, for example by TGF-βRII or smad4 deletion, (Kitamura *et al*., 2007; Lu *et al.,* 2004; Yang *et al.*, 2008) acts to recruit Gr-1^{+}CD11b^{+} myeloid cells into the tumour microenvironment. Once adjacent to the tumour, these myeloid immune suppressive cells are stimulated to release more TGF-β and activate MMP secretion (MMP2, MMP13 and MMP14), promoting EMT, migration, angiogenesis and invasion of cancer cells.

TGF-β signalling is key in stromal organization, it is involved in the production and modulation of the ECM, as well as being able to inhibit proteases and increase production of proteases inhibitors (Ito *et al.,* 2004). Moreover, TGF-β1 is key in the activation of the epithelial to mesenchymal transition (EMT), hence has a role in metastasis (Bierie & Moses, 2006), it is also one of the main cytokines responsible for producing 'activated' stromal fibroblast.

1.4 ***Fibroblasts***

Fibroblasts are a dominant cell type found within the connective tissues embedded within the fibrillar matrix (a loosely organized ECM consisting of collagen I and fibronectin) (Tarin & Croft, 1969). They are the most abundant stromal cell type in the tumour environment and are responsible for the synthesis of the basement membrane and other extracellular matrix components (Allen & Louise Jones, 2011). Fibroblasts in tumours contribute towards a histologically desmoplastic stroma phenotype characterised by increased ECM resulting in a 'stiffening' of the tissue (Cardone *et al.,* 1997).

Fibroblasts are genetically heterogeneous and have poorly defined markers, which restrict their study (Kalluri & Zeisberg, 2006). Fibroblast specific protein 1 (FSP1), desmin, alpha smooth muscle actin (αSMA), vimentin and fibroblast activation protein (FAP) are examples of such fibroblasts markers, however none of the above are both completely exclusive to fibroblasts and

inclusive for all fibroblast subtypes (Kalluri & Zeisberg, 2006). Some markers are site or 'activational state' specific, for example desmin is found mainly within dermal fibroblasts; a list of CAF markers can be found in table 1.1. αSMA (gene name: ACTA2) is a commonly used marker of myofibroblasts, but this is not exclusive to myofibroblasts, it is also expressed in phenotypically normal fibroblasts, pericytes and smooth muscle.

Marker	Expression	Function/detail	Reference
αSMA	myofibroblast, SMC, low fibroblast,	Intermediate filament associated protein	(Tomasek *et al.,* 2002)
FAP (fibroblast activation protein)	Myofibroblast, fibroblasts	Transmembrane serine protease	(Rettig *et al.*, 1993)
Podoplanin	Myofibroblast, myoepithelial cell, lymph endothelial cell	Transmembrane glycoprotein, actin assembly and migration	(Wicki & Christofori, 2006)
Paladin 41g	Myofibroblast, smooth muscle cell	Cell adhesion, motility and actin assembly	(Najm & El-Sibai, 2014)
Cadherin-11	Myofibroblast, smooth muscle cell	Involved in actin cytoskeletal scaffolding	(Vered *et al.*, 2010)

Table 1.1: Fibroblast markers. Reviewed in (De Wever *et al.,* 2008; Kalluri & Zeisberg, 2006)

In addition to the cell surface and cytoskeletal markers listed in table 1.1. Myofibroblasts have secreted extracellular markers including various collagens, mainly type I, III, IV and V (Hinz, 2007), SPARC (secreted protein acidic rich in cysteine), tenascin- c, fibronectin 1 with extra domain A isoform (FN1-EDA), MMPs (MMP) and TIMPs (De Wever *et al.,* 2008; Kalluri & Zeisberg, 2006). Most of which play a role in matrix remodelling and invasion. As no markers exclusively identify myofibroblasts it is necessary to use a combination of markers to study myofibroblasts experimentally.

1.5 ***Cancer Associated Fibroblasts***

A large subsection of fibroblast within tumours display an 'activated' phenotype, termed cancer associated fibroblast (CAFs; or carcinoma/ tumour associated fibroblasts). These CAFs are heterogeneous and show slightly different phenotypes and form distinct populations with different markers and characteristics. Higher recruitment or activation of CAFs in tumours may reflect the prognostic outcome (Cardone *et al.,* 1997). The number of CAFs within tongue squamous cell carcinomas have been found to be directly correlated with disease outcome (Bello *et al.*, 2011).

The mechanisms by which these CAFs arise are under dispute (Augsten, 2014; Kalluri & Zeisberg, 2006). There are numerous hypotheses, one of which is that normal fibroblasts are activated by signals in their environment to undergo the genetic changes to transform their phenotype to become myofibroblasts. Such stimuli include exogenous toxins e.g. alcohol and cigarette smoke, DNA damaging agents, radiation and endogenous stimuli from an adjacent arising tumour. It is also argued that myofibroblasts are transdifferentiated smooth muscle cells, pericytes, fibrocytes or mesenchymal stem cells. Another theory is that the myofibroblasts are epithelial cells which have undergone EMT (Kalluri & Neilson, 2003).

The secretome of CAFs creates an environment, which encourages invasion and angiogenesis. CAFs are known to secrete an array of growth factors, cytokines and proteases which act to remodel the stroma and promote tumour progression, including: EGF, IL-6, bFGF, SDF-1, VEGF, HGF, EGF, TGF-β, CXCL14, IL-1, IL-6, IL-8 MMPs, and TIMPs *(Otranto et al., 2012; Studebaker et al.,* 2008).

1.5.1 *The role of fibroblasts in the tumour microenvironment.*

There have been multiple studies looking at the effect of CAFs in tumour progression compared to phenotypically normal fibroblasts in co-culture. CAFs have been shown to create a permissive environment for tumours to proliferate. For example, in an *in vivo* 3D co-culture model of breast tissue study, both normal fibroblasts and CAFs were able to reduce the proliferation of a normal mammary epithelial cell line. However, when a genetically altered mammary cell line was introduced in the co-culture, only normal mammary fibroblasts and not mammary CAFs were able to prevent the proliferation (Sadlonova *et al.,* 2005). It is possible that the fibroblast's capacity to negatively regulate proliferation is due to enhanced TGF-β signalling, described earlier. When TGF β RII is deleted in fibroblasts (Bhowmick *et al.,* 2004) both the tumour and

the stroma overproliferate. Taken together these studies may suggest that CAFs are only able to stimulate already transformed epithelial cells (Sadlonova *et al.,* 2005).

A similar 3D culture study showed that CAFs could promote proliferation in the same normal mammary fibroblast cell line (Shekhar *et al.,* 2001). Sadlonova *et al., (2005)* observed that the previous study used a higher fibroblast to epithelial cell ratio than they had, and when using the same ratio of CAF to epithelia cell they indeed saw that CAFs permitted the proliferation of normal epithelial cells. This suggests that it is not only the activational state of the adjacent fibroblast but the number that can influence a tumour.

Some studies have suggested that CAFs have transforming abilities (Hayashi & Cunha, 1991) However, a study from Olumi *et al.*, (1999) gave evidence to suggest that epithelial cells must already be transformed to benefit from stromal fibroblasts. They compared the abilities of CAFs and normal stromal fibroblasts to both initiate and support tumour progression in a prostate cancer model. In the study, CAFs were grown with initiated or normal prostatic epithelial cells and studied *in vitro*, as well as being used in collagen grafts in mice. CAFs were only able to initiate carcinoma formation when grafted with initiated cancer epithelial cell line BPH-1. Similarly *in vitro* examination showed that CAFs cause tumourigenic hallmarks such as increased epithelial proliferation and decreased cell death only when co-cultured with genetically abnormal epithelial cells. Overall the study suggested that CAFs encourage tumour progression when a carcinoma is already initiated, rather than being involved in the initial genetic transformation of the cells (Olumi *et al.,* 1999).

1.5.2 *Myofibroblasts*

Myofibroblast-like CAFs share a phenotype similar to myofibroblasts present in wounds and fibrosis (Hinz *et al.,* 2007). Myofibroblasts are characterised by an altered shape, an elevated expression in alpha smooth muscle actin (αSMA) (Hinz *et al.,* 2001), increased proliferation, elevated secretion of metalloproteases (specifically MMP- 2, 3 and 9), extracellular matrix components (Rodemann & Müller, 1991), growth factors and cytokines (Bhowmick *et al.,* 2004) (figure 1.1). Myofibroblasts are also characterized ultra-structurally by having contractile cytoskeletal microfilaments, increased focal adhesions comprising gap junctions and adherens, and having cell to cell and cell to matrix attachments (reviewed in Hinz., 2007).

In normal wound healing myofibroblasts play an important role in the granulation layer, contracting to close the open wound. Physiologically normal wound healing can be divided into

3 phases, the inflammatory phase, proliferation phase and the regeneration phase (reviewed in Darby *et al.*, 2014; Otranto *et al.,* 2012). In the inflammatory phase, is immune cells infiltrate into the wound and release cytokines. The proliferation phase allows the generation of the granulation layer, in which neoangiogenesis, proliferation and activation of fibroblasts into myofibroblasts occurs. It is in this phase where myofibroblasts contract and close the open wound. The final phase is the regeneration phase where there is extensive remodelling of the granulation tissue; this is achieved mainly by ECM modifications by MMPs. There is also the deposition of collagen type I and elastin in this phase. The myofibroblasts then undergo apoptosis (Desmoulière *et al.,* 1995). Organ fibrosis and fibromatosis occur when myofibroblasts are inappropriately and chronically activated. One reason for this continuous activation of myofibroblasts is a delay in apoptosis (Teofoli *et al.,* 1999).

Myofibroblasts are often found in desmoplastic reactive stromas of invasive tumours (Kawashiri *et al.,* 2009). Myofibroblasts promote tumour growth and angiogenesis *via* the secretion of chemokines, ECM molecules and growth factors. Orimo *et al.,* (2005) showed that human breast CAFs, which experimentally behaved like myofibroblasts and were mostly positive to αSMA, strongly promoted tumour growth and angiogenesis within a human xenograft and that this was facilitated by stromal cell derived factor-1 (SDF-1)/ CXCL12. The elevated levels of SDF-1 contributed to tumour growth, *via* the paracrine activation of CXCR4 receptors leading to proliferation, and neoangiogenesis *via* the recruitment of endothelial progenitor cells (EPCs) which are principal in forming new blood vessels. Interestingly the researchers showed a statistically significant positive correlation between the CAFs' contractility and their likelihood to form tumours, suggesting that the myofibroblast sub-population of the CAFs are the most tumourigenic. Immunohistochemical analysis of patient samples showed αSMA positive CAFs also co-localised with the staining for SDF-1 suggesting that the pro-tumourigenic characteristics of myofibroblasts could be mediated by the secretion of SDF-1 (Orimo *et al.,* 2005). SDF-1 is one example of how a secreted molecule in the tumour microenvironment can have pleiotropic effects to result in tumour progression.

Many studies investigating myofibroblasts in the tumour microenvironment suggest that they cause aggressive invasive tumours, however very few studies to date have shown their prognostic value. They have been shown to predict unfavourable outcomes in OSCC, colorectal, and breast tumour types studied (Kellermann *et al.,* 2007; Tsujino *et al.,* 2007; Surowiak *et al.,* 2007). For OSCC, αSMA stromal staining, indicating the presence of myofibroblasts was the strongest independent marker of poor prognosis (Marsh *et al.,* 2011). In this study, all aspects

of the tumour were classified; stage, grade, type of invasion, lymph node, tumour depth and surgical margins as well as sex and age, and immunohistochemistry was performed for αSMA, αvβ6, EGFR, EP4 (prostaglandin receptor), p53, and p16. αSMA was found to be the most predictive of mortality, with ~50% of patients with high αSMA staining dying within 3 years. This study also investigated oral myofibroblasts *in vitro* using organotypic models and transwell migration assays and found that they promoted the invasion of OSCC cell lines, attributing to their aggressive phenotype.

The presence of myofibroblasts has been identified to correlate with the classification of bladder tumours. An immunohistochemistry study using sections from both non-invasive and invasive UCCs identified that, in this cohort, myofibroblasts were only present in the invasive bladder tumours (Alexa *et al.,* 2009). Whereas in a similar study, myofibroblasts were found in both non-invasive and invasive bladder carcinomas, however an alternative pattern of distribution between non-invasive and invasive tumours was seen (Shimasaki *et al.,* 2006).

1.5.3 *Senescent fibroblasts*

Another fibroblast phenotype which is found in abundance in CAF populations is the senescent fibroblast (Campisi & Fagagna, 2007). These are defined as having undergone indefinite growth arrest (in G0) but still metabolically active. Like myofibroblasts, they have an altered secretome, which includes some common released MMPs and cytokines e.g. IL-6. The secretome of senescent cells is termed the senescence associated secretory phenotype (SASP) (Coppe *et al.,* 2009). They are distinctive from myofibroblasts as they have an increase in p16 and p21. Senescence can be induced in a number of ways, for example exposure to irradiation, natural ageing, DNA damaging and chemotherapeutic agents. *In vitro*, treatment with cisplatin, H_2O_2 and allowing fibroblasts to undergo many rounds of cell division (replicative senescence) are ways of inducing this phenotype (reviewed in Rodier & Campisi, 2011).

Distinct CAF phenotypes have been identified surrounding genetically stable or genetically unstable OSCCs (GS-OSCC or GU-OSCC). Lim *et al.,* (2011) classified OSCCs depending on the presence of inactivating mutations/ chromosomal deletions of TP53 and $p16^{INK4A}$ and found that fibroblasts surrounding genetically unstable OSCCs (GU-OSCC; loss of TP53/$p16^{INK4A}$) were senescent and have a transcriptionally different profile to fibroblasts from GS-OSCCs (wild type TP53/$p16^{INK4A}$). This senescence, associated with CAFS from GU-OSCCs, was induced by ROS, TGF-β1 and TGF-β2 secreted by GU- keratinocytes (Hassona *et al.,* 2012). The GU-OSCC senescent CAFs had oxidative DNA damage indicated by 8-oxo-dG, SA-β gal staining and

increased expression of a profile of oxidative stress genes. GU-OSCC CAFS also were able to induce the invasion of a H357 cancer cell line. A more recent study showed that this invasion, which was only induced by GU-OSCC not GS-OSCC or normal keratinocytes, was attributed to the presence of active MMP2 in GS-OSCC CAF SASP (Hassona *et al.,* 2014).

Fibroblast activation may not be classified accurately in the literature, research groups use slightly different markers/criteria to classify different fibroblasts. It may be that myofibroblasts and senescent fibroblasts may not be exclusive phenotypes. A possible hypothesis is that myofibroblasts are a middle phenotype between normal fibroblasts and senescent fibroblasts. Jun & Lau, (2010) hypothesise that myofibroblasts can become senescent in chronic fibrosis through CCN1 mediated oxidative stress. Understanding the molecular mechanism behind the acquisition of both will help to understand if they are completely distinct phenotypes.

1.5.4 *Regulation of the myofibroblast transition.*

The molecular mechanisms underlying the transdifferentiation from phenotypically normal fibroblasts to myofibroblasts remain to be fully delineated. Two autocrine loops have been considered to be responsible for the transdifferentiation of myofibroblasts, TGF-β and SDF-1. (Kojima *et al.,* 2010) and *in vitro* it can be modelled by exogenous application of TGF-β1 (Rønnov-Jessen & Petersen, 1993). In various fibroblasts including cardiac, pulmonary, dermal and oral/gingival fibroblasts (Desmoulière *et al.,* 1993; Hinz *et al*., 2001; Lewis *et al*., 2004; Reed *et al*., 1994). Connective tissue growth factor (CTGF/ CCN2), endothelin-1 (ET-1) and angiotensin II (Ang II) have also been implicated promoting fibrosis and inducing myofibroblasts, suggesting that they may also play a role in this transdifferentiation process (Bai *et al*., 2013; Garrett *et al*., 2004; Swigris & Brown, 2010).

Myofibroblasts can be induced from primary oral fibroblasts by co-culture with the modified OSCC-derived cell line VB6 cell line (H357 oral cancer cell line stably transfected with αvβ6) (Marsh *et al*., 2011). An inhibitor to αvβ6 integrin, showed that it was required for the activation of latent TGF-β1, which had been previously shown in other cells, and that αvβ6 was required for myofibroblast transdifferentiation. Immunohistochemical analysis showed that αSMA staining was correlational αvβ6 staining suggesting that the integrin is responsible for myofibroblast activation in tumourigenesis perhaps through TGF-β1 activation. In addition to TGF-β signalling, αvβ6 also acts as a receptor to fibronectin, and tenascin-c (Annes, Chen, Munger, & Rifkin, 2004), and is overexpressed in many tumours including colon (Bates *et al*.,

2005), lung (Elayadi *et al*., 2007), cervical (Hazelbag *et al*., 2007) breast (Moore *et al*., 2014) and OSCCs and is associated with poor prognosis (Thomas, Nyström, & Marshall, 2006). As it is not expressed highly on healthy epithelia, but on epithelial cells undergoing remodelling, for example in wound healing, embryogenesis or in cancers (Breuss *et al*., 1995), targeting αvβ6 has great shown potential for anti-cancer therapies, especially in breast in combination with trastuzumab, a HER2 monoclonal antibody (Moore *et al*., 2014). However, it is important to note that, like TGF-β signalling discussed above, αvβ6 appears to have dual roles as both a tumour suppressor and a promoter. Blocking αvβ6 or the downstream TGF-β pathway in pancreatic ductal adenocarcinoma (PDAC) causes an increase in the proliferation and invasion of PDAC cells, therefore works as a tumour suppressor through the activation of smad4 in this circumstance (Hezel *et al*., 2012).

A study of the role of MRTF-A/B (Myocardin related transcription factors A and B) in rat embryonic fibroblasts highlighted their role in myofibroblast transdifferentiation. MRTF A and B are important transcription factors similar to myocardin which along with serum response factor co-activate smooth muscle contractile genes (including αSMA) which are under the control of a CArG box. Using a MRTF-A/B targeting siRNA resulted in the reduction of TGF-β1 mediated smooth muscle contractile genes associated with the myofibroblast phenotype (Crider, *et al.,* 2011), this study also suggested that MRTF-A was sufficient to induce the myofibroblast phenotype. Another study showed that MRTF-A expression was required for myofibroblasts associated contractility and showed that a small drug known to induce myofibroblasts, isoxazole, worked through MRTF-A (Velasquez *et al*., 2013).

Smad3 has been identified to work together with MRTF-B to fine tune the controlled expression of CArG induced smooth muscle genes in epithelial cells (Masszi *et al*., 2010). Smad3, a main downstream effector of TGF-β signalling, has been found to bind MRTF-B and inhibit it's action on the αSMA promoter in a porcine renal tubular epithelial cell line induced to become myofibroblasts by a combined low calcium and TGF-β1 treatment.

The extracellular environment appears to have a large influence on myofibroblast transdifferentiation. Fibroblasts can undergo myofibroblast transdifferentiation in response to a stiff environment, it is an important mechanism in fibrosis and has been shown in many fibroblasts using collagen gels including gingival (Arora, Narani, & McCulloch, 1999), aortic (Chen, *et al.,* 2011), cardiac (Galie, Westfall, & Stegemann, 2011) and pulmonary (Goffin *et al*., 2006). One study MKL1 (also known as MRTF-A) loss of function study showed that MRTF-A was required for matrix stiffness induction of myofibroblast phenotype (Huang *et al*., 2012)

Contraction of 3D collagen gels has also been shown to be able to activate latent TGF-β1 (Wipff *et al.,* 2007). Further evidence for MRTF-A being involved in TGF-β1 induced myofibroblast transdifferentiation, PGE2 is able to inhibit αSMA expression through the regulation of MRTF-A and SRF (Penke *et al*., 2014).

ECM molecules have also been reported to induce myofibroblasts. Versican, an extracellular proteoglycan (discussed in detail in section 1.7) has been reported to be necessary for dermal myofibroblast transdifferentiation (Hattori *et al*., 2011). In one study, which used genetically modified TIMP knockout mice referred to as TIMPless, the dysregulation of the ECM by the action of ADAM10 was able to induce myofibroblast like CAF phenotype (Shimoda *et al*., 2014).

In addition an isoform of fibronectin has been implicated to be important as marker and inducer of the myofibroblasts phenotype. Fibronectin is an extracellular glycoprotein, made up of two identical ~220 kDa sized monomers. It is found in two forms, plasma or cellular fibronectin in the ECM. The cellular form allows the incorporation of 2 extra type III domains A and B (EDA and EDB, respectively) by alternative splicing (Pankov & Yamada, 2002). Fibronectin with extra domain A (FN1-EDA) expression can be induced on TGF-β treatment (Balza, Borsi, Allemanni, & Zardi, 1988; Borsi, Castellani, Risso, Leprini, & Zardi, 1990) and is commonly found in the ECM of activated fibroblasts (Kalluri & Zeisberg, 2006) and therefore used as a marker of myofibroblast transdifferentiation in this study.

The accumulation of FN1-EDA has found to be necessary for TGF-β1 dermal myofibroblast transdifferentiation (Serini *et al*., 1998). It also has been labelled pro-fibrotic, essential for pulmonary fibrosis and TGF-β responsiveness (Muro *et al*., 2008) and is found at higher levels in idiopathic pulmonary fibrosis (Kuhn & McDonald, 1991). Proposed mechanisms for FN-EDA pro-fibrotic action are through TLR signalling as it has been shown to act as a TLR4 ligand (Bhattacharyya *et al*., 2014) it has also been reported to interact with α4β1 (Shinde *et al*., 2015) and α4β7 integrins activating MAPK/ERK1/2 signalling (Kohan, *et al.,* 2010) which results in induction of αSMA expression. FN1-EDA has other reported roles within the tumour microenvironment, it is documented to promote EMT through α9β1 (Ou *et al*., 2014; Sun *et al*., 2014), and neoangiogenesis through increasing in expression of VEGF-C (Xiang *et al*., 2012).

Exosomes, secreted extracellular vesicles that are passed between communicating neighbouring cells, are released by cancerous cells. Exosomal TGF-β cargo is responsible for the induction of the myofibroblast transition in stromal fibroblasts (Webber *et al.,* 2010). microRNA 21 expression promotes TGF-β1 induced myofibroblast transition within ovarian fibroblasts, and

appears to regulate the transition through its target PCD4 (programmed cell death 4) (Yao *et al*., 2011). Another microRNA, miR-146a has been reported to negatively regulate TGF-β1 induced myofibroblast activation. miR-146a was able to regulate TGF-β effector Smad4 protein level (Liu *et al.,* 2012), however the authors only judged the inhibition of myofibroblast activation based on αSMA expression and no functional assays were performed. Also, microRNA-31 has also been reported to act cell autonomously within fibroblast to prevent CAF activation. Its expression is lost in endometrial CAFs compared to matched controls and its overexpression prevents *in vitro* cancer cell invasion and migration; this is thought to be due to the loss of its target homeobox gene SATB2, whose expression stimulated those traits (Aprelikova *et al*., 2010). Interestingly, all the aforementioned microRNAs have roles in the regulation of metastasis. miR-21 promotes metastasis, whereas both miR-146a and miR-31 expression prevent metastasis (Hurst, Edmonds, & Welch, 2009)

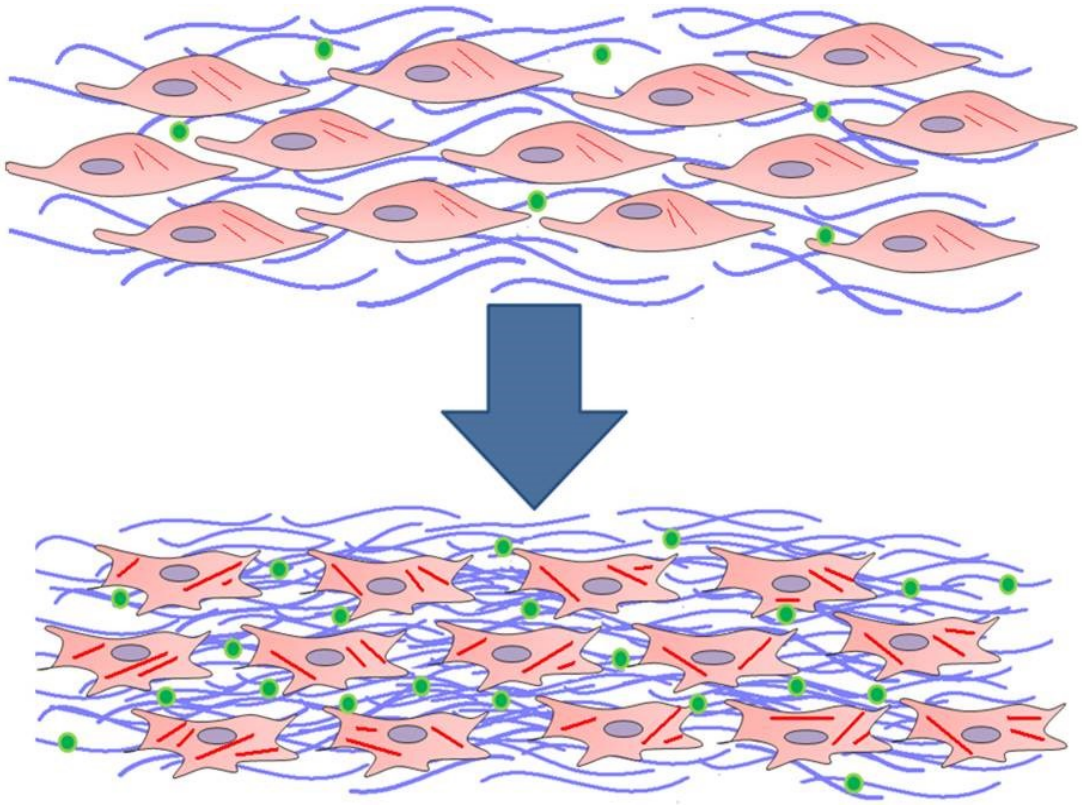

Figure 1.1 Myofibroblast transition schematic. Normal stromal fibroblasts can become activated in the tumour microenvironment to become myofibroblast-like cancer associated fibroblasts (CAFs). These myofibroblasts, are characterised by an altered shape, an increase in alpha smooth muscle actin (αSMA) stress fibres (shown in red), and a contractile phenotype. They are also responsible for the enhanced secretion of extracellular matrix components (shown in blue), cytokines and proteases (shown in green) which meditate further stromal-epithelial interactions to support tumour growth and metastasis.

1.5.5 *Genetic alterations in CAFs*

CAFs are generally considered to be genetically stable, however there is some evidence in the literature that supports the view that tumours may have genetic alterations in the stroma, specifically in CAFs. This view is controversial in the field, and many think that recently reported genetic alterations within the stroma is artifactual and is a result of tumour cell contamination. Nonetheless, attempts have been made to identify the consequential associated altered stromal-epithelial signalling.

Genetic mutations within the stromal compartment have been identified in the HNSCC tumour microenvironment and found to be capable of altering the signalling in both the stoma and epithelia (Bebek, Orloff, & Eng, 2011). Commonly the genetic mutations and chromosomal alterations that occur within the stroma are frequently found in malignant cells also, for example mutations in the P53 gene TP53. Loss of heterogeneity/ allelic imbalance studies have also identified that there were TP53 mutations within invasive breast carcinoma CAFs, but not the epithelium, and this was found to be correlated with positive lymph node status (Patocs *et al*., 2007). It seems apparent that p53 in fibroblasts plays a non-autonomous role to halt proliferation, neoangiogenesis and metastasis within a tumour (reviewed in Bar, Moskovits & Oren, 2010). P53-null fibroblasts, when co-inoculated with tumour cells in mice, had less latency in forming tumours than wild type fibroblast controls (Kiaris *et al*., 2005). Loss of p53 in these cells also drives angiogenesis *via* the loss of regulation of anti-angiogenic thrombospondin-1 (Tsp1; Dameron *et al.*, 1994). It is thought that under normal physiological conditions p53 downregulates chemokine SDF-1/CXCL12 in fibroblasts, when p53 is lost within the fibroblasts there is an increase in the secretion of SDF-1 hence providing pro-migratory and invasion signals to encourage metastasis (Moskovits *et al.,* 2006).

Hill *et al.*, (2005), when studying the co-evolution of the stromal and epithelial compartment in a prostate cancer murine model in which Rb is inactive, found that p53 is needed in the stromal compartment to prevent fibroblast proliferation. The authors hypothesized that transformed epithelium puts an oncogenic evolutionary selective pressure for p53 inactivation on the stroma, by paracrine growth factor signalling. Functional p53 will prevent the proliferation of the fibroblasts whereas cells lacking p53, or with a mutant p53, can proliferate creating a more reactive stromal environment which can secrete additional factors to support the tumour evolution. Another group has found that cancer cells can produce factors which prevent the activation of stromal p53 (Bar *et al*., 2009). Of course the loss of p53 does not have to result

from a null or inactivating mutation or chromosomal alteration, it could be a result of epigenetic or signalling changes within the stromal cells.

The expression of tumour suppressor PTEN has also been reported to be lost in stroma (Kurose *et al*., 2002). The genetic deletion of PTEN in a conditional fibroblasts specific knockout was responsible for increased tumourigenesis when used in a mammary tumour model, associated with ECM remodelling, angiogenesis and macrophage infiltration (Trimboli *et al*., 2009).
A subpopulation of fibroblasts, which were positive for FSP1, in oro-pharyngeal squamous cell carcinomas had inactivated (hyperphosphorylation) tumour suppressive retinoblastoma (Rb) (Pickard *et al*., 2012). *In vitro* studies showed that fibroblasts depleted of Rb increased the invasion of transformed epithelium in 3D organotypic cultures. This was found to be due to increased stromal levels of KGF (keratinocyte growth factor; also known as fibroblast growth factor 7; FGF7) which drives invasion through increased secretion of MMP1 *via* the activation of the AKT pathway. This suggests that altered paracrine signalling mediated from transformed epithelium may promote the oncogenic activation of the adjacent fibroblasts.

1.5.6 *FSP1 positive fibroblasts*

Furthermore an FSP1 positive CAF subpopulation has been reported to be distinct from the population of αSMA positive myofibroblasts (Sugimoto *et al.,* 2006). Most studies show that FSP1 positive fibroblasts are scattered throughout the tumour stroma whereas αSMA positive fibroblasts were mainly found located next to blood vessels (Zhang *et al.,* 2011); however pericytes have αSMA expression, possibly confounding interpretation of these findings.

Although a discrete CAF population, FSP1 positive CAFs also appear to have a pro-tumourigenic role. Studies using FSP1 knockout mice have revealed that the presence of FSP1 is needed for metastasis and increases the incidence of tumour formation (Grum-Schwensen *et al*., 2005). In a two-stage *in vivo* mouse carcinogenesis model FSP1 positive fibroblasts proliferated at an early stage of carcinogenesis, when they were depleted from the model there were decreased levels of inflammatory mediators IL-6 (interleukin-6), TNF-α (tumour necrosis factor-alpha), and MCP-1 (monocyte chemotactic protein -1), the latter was found to recruit macrophages to further add to tumour progression (Zhang *et al.*, 2011). FSP1 has however been shown to mark invasive carcinoma cells, which may explain why the depletion of FSP1 so dramatically reduces metastasis (Strutz *et al*., 1995).

FAP (fibroblast activation protein), another marker of CAF phenotype, is also involved in stromal fibroblasts' influence on tumourigenesis. FAP, also found on pericytes, is a type II transmembrane peptidase belonging to the dipeptidylaminopeptidase family. Experimental deletion and pharmacological inhibition of FAP resulted in the attenuation of tumour growth and myofibroblast activation both in models of lung and colon cancer (Santos, Jung, Aziz, Kissil, & Puré, 2009), suggesting that targeting the stromal compartment can have a marked effect on both the tumour and stroma.

1.5.7 *Fibroblasts as drug targets*

CAFs are identified as a suitable drug target for treating the tumour microenvironment, this is partly due to them being generally non proliferative and genetically stable. CAFs have also been implicated in aiding drug resistance in cancer cells (Johansson *et al*., 2012; Kinugasa, Matsui, & Takakura, 20144), therefore targeting CAFs alongside current therapies may be beneficial. The presence of CD-44 positive CAFs were found to protect lung cancer cells from the toxic effects of 5-FU (Kinugasa *et al.,* 2014). Of relevance to HNSCC, several studies have implicated HGF, which is secreted by CAFs, to interfere with EGF signalling (Wang *et al*., 2009; Yamada *et al*., 2010) and recently a study found that CAFs secretions prevent the action of cetuximab via the action of MMPs (Johansson *et al*., 2012). However, this study failed to use normal fibroblasts to investigate whether normal fibroblasts may infer a similar resistance to cetuximab.

1.5.8 *CAFs in HNSCC*

The body of evidence points towards the pro-tumourigenic role of CAFs in tumour progression. Over the past 10 years much research has been done to investigate CAFs effects in HNSCC. Barth *et al*., (2004) were the first to show myofibroblasts in OSSC stroma (Barth *et al.,* 2004). Subsequent studies revealed that they are indicative of poor prognosis (Kellermann *et al*., 2007) and suggest significantly lower 5 year survival rates and are more likely to have local reoccurrence (Vered, *et al.,* 2010). Marsh *et al.,* (2011; discussed in section 1.3.3) showed that the presence of myofibroblasts predicted aggressive OSCC with poor patient outcomes.

Many groups have attempted to identify the ways in which myofibroblasts modulate tumour cells. Myofibroblasts were shown to increase tumour volume when injected, with SCC9 cell lines, into nude mice (Sobral *et al*., 2011). These myofibroblasts were identified to be secreting activin

A, a member of the TGF-β superfamily, which was responsible for the influence on tumour proliferation and tumour volume.

Conditioned media from OSCCs were able to transdifferentiate gingival myofibroblasts, this was found to be due to the secretion of TGF-β1, in turn the myofibroblast were shown to secrete HGF/SF (scatter factor) to promote the paracrine invasion of the OSSC cells (Lewis *et al*., 2004b). In addition, SF has been previously shown to induce the expression of MMP2 and MMP9 in H357 cells and normal oral keratinocytes (Bennett *et al.,* 2000), highlighting the elegant ways that malignant cells and stroma synergistically interact. MMP2 and MMP9 have also been shown to be released by SSC9 cells in response to myofibroblasts conditioned media, to promote tumour invasion (Sobral *et al*., 2011). Kellermann *et al*., (2008) also confirmed this two way cross-talk showing that tongue SCC cells can transdifferentiate fibroblasts to myofibroblasts, which in turn release factors which influence the SCC cells by increasing their proliferation. Several groups have also showed that myofibroblasts release factors which stimulate OSCC migration and invasion.

1.6 ***MicroRNAs***

1.6.1 *Introduction to microRNA*

MicroRNAs are evolutionary conserved short non-coding RNA, of 18-22 nucleotides in length, which have a post-transcriptional role in the control of gene expression (Ambros *et al*., 2003). Each microRNA has a seed sequence of 2-7 nucleotides which gives the microRNA specificity for its targets (reviewed in Huntzinger & Izaurralde, 2011). The microRNA seed sequence binds to near perfect complementary sequences mainly in the 3' untranslated region (UTR) of their mRNA targets and less frequently to complementary sequences in the coding region of their target. The nature of the binding reflects the fate of the transcript; if the mature microRNA binds perfectly to the 'seed' sequence, the mRNA is degraded by the RISC (RNA induced silencing complex) components. If it does not bind perfectly, the transcript is downregulated either because translational machinery cannot carry out translation, or the mRNA is deadenylated (Giraldez *et al*., 2006). Each microRNA has multiple targets and has pleiotropic effects; hence as a class they converge on almost all genetic pathways. As they have many targets they can play integral roles in transcriptional networks and cellular phenotypes. According to bioinformatics data, as a class they are the most common method by which the cell controls expressional heterogeneity and they make up 30% of all genetic regulatory molecules (Lim *et al*., 2005).

1.6.2 *microRNA biogenesis*

MicroRNAs undergo post-transcriptional processing into their mature form by a series of RNase III enzymes (figure 1.2.) (reviewed in Chong *et al.*, 2010; Siomi & Siomi, 2010). The precursor microRNAs are transcribed in the nucleus as a long hairpin stem loop primary microRNAs, and then are processed by a complex including Drosha, a RNase III enzyme, and DGCR8 (also known as Pasha), a RNA binding protein. The result of the Drosha/DGCR8 cleavage is around 70 nucleotide stem loop precursor pre-miRNA. This is able to be transported through nuclear pores by Exportin-5 mediated export using Ran small GTPase. Once in the cytosol, the pre-microRNA is subsequently processed by another RNase III enzyme, Dicer, to become a single stranded RNA between 22-23 nucleotides in length. As a mature miRNA of around 22 nucleotides it is then incorporated into the RNA Silencing Complex (RISC complex) which mediates the silencing of the target mRNA transcript.

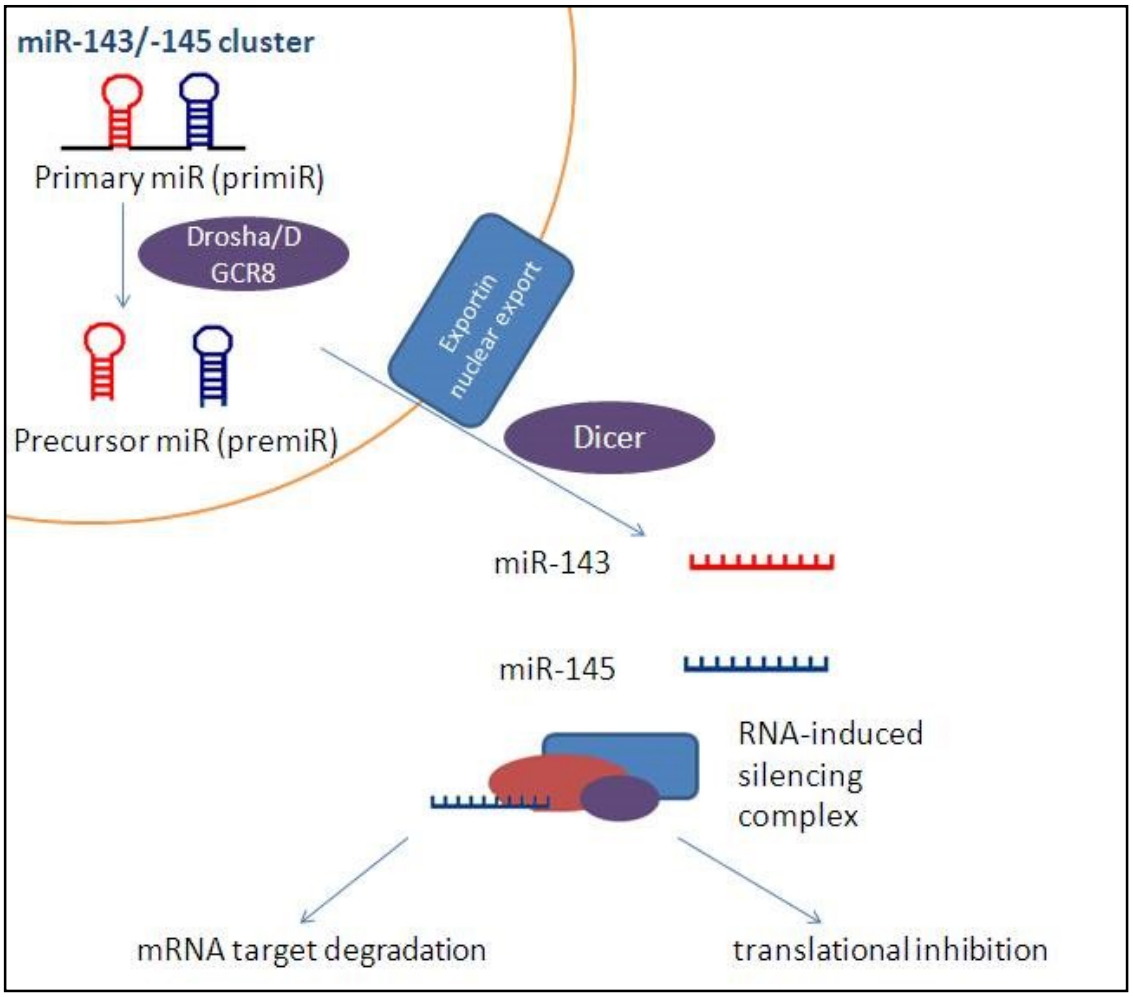

Figure 1.2. The biogenesis of microRNA-143/-145 cluster: a simplified schematic. microRNA-143/145 cluster is co-transcribed as a bicistronic pair as a stem-loop primary transcript, this is then cleaved by the Drosha/ DGCR8 in the nucleus to a smaller stem-loop precursor miR around 70 nucleotides in length. The premiR is exported from the nucleus by exportin-5, in the cytosol it that is further cleaved by dicer to a mature miR which can then be incorporated into the RISC complex to result in the downstream inhibition of target transcripts (figure modified from Rangrez *et al*., 2011).

1.6.3 *microRNAs in malignancies*

microRNAs can act as tumour suppressors or as oncogenes, termed oncomiRs. miRNAs were first identified to be misregulated in cancers when miR-15 and miR-16-1 where located at the 13q14 locus which is commonly deleted within B-cell chronic lymphocytic leukaemia (CLL) (Calin *et al*., 2002). These microRNAs have since found to negatively regulate the expression of the anti-apoptotic BCL2, therefore providing a mechanism for the formation of leukaemia (Cimmino *et al*., 2005). The primary precursor to miR-15-1, and miR-16a has even been identified to be mutated in some cases of CLL (Calin *et al*., 2005).

More than half of the known microRNAs are found at fragile sites in chromosomes, where deletions, amplifications and translocations may occur, explaining why they are commonly misregulated in malignancies (Calin *et al*., 2004). Translocations have also been reported to result in the swapping, shortening or loss of 3'UTRs leading to inappropriate targeting or loss of regulation over specific mRNAs targets, perhaps leading to tumourigenesis (Mayr, Hemann, & Bartel, 2007).

microRNA-21, an 'oncomiR' overexpressed in many cancers, contributes to oncogenesis by targeting PTEN and tropomyosin-1 (TPM-1), amongst other tumour suppressor genes (Zhu *et al*., 2008). In addition, the overexpression of this miR in glioblastoma cells has been associated with modulation of the ECM leading to increased invasion as it targets two MMP inhibitors (reviewed in Gabriely *et al.*, 2008; Wentz-Hunter & Potashkin, 2011).

Differential microRNA expression profiles have been reported between invasive and non-invasive bladder urothelial carcinomas (Wszolek *et al.*, 2009), highlighting their potential use as biomarkers. Invasive UCC displayed high levels of miR-21 and miR-99a whereas they had low levels of certain miRs, some of which had previously been reported to be involved in EMT: miR-30, miR-31, mir-141, miR-200a, miR-200b, miR200c. The reintroduction of the miRs (except miR-30b) resulted in an *in vitro* reduction of invasion, suggesting that the loss of these miRs directly orchestrates the invasion process. Tumours with low expressional levels of miR-200c, miR-141,

and miR-30b, had dramatically lower survival rates. It is thought that expression of the miR-200 family is required to be reduced to allow EMT to occur (reviewed in Korpal & Kang, 2008) and has been reported to be downregulated in several invasive tumours. It is found to be downregulated in OSCC and saliva from these patients (Wiklund *et al*., 2011) and is found to be significantly reduced in the urine of bladder tumour patients (Wang *et al.,* 2012).

microRNAs have been hypothesised to have alternative roles in the mechanisms leading to metastasis. microRNA-21 and micro-RNA 29a have been reported to behave as ligands for the TLR (Toll-like receptor) family of receptors (Fabbri *et al.,* 2012). The microRNAs were transported to the macrophage by cancer exosomes. This activation of TLR 8 leads to the downstream activation of NF-κB subsequently leading to the secretion of TNF-α and IL-6 to evoke a pro-metastatic response.

Some miRs have been identified to play important roles in stroma remodelling. miR-21 has been shown to have several effects in modulating the stroma, and stromal-epithelial interactions in several tumour types (Bullock *et al.*, 2013; Kadera *et al.,* 2013; Uozaki *et al.,* 2014). miR-21 overexpressing fibroblasts promote colorectal cancer cells invasion through the regulation of MMP2, give protection against oxaliplatin, and were shown to promote myofibroblast transdifferentiation (Bullock *et al.,* 2013). However, MRC5, a foetal fibroblast lung cell line were used in this study, there is some concern using foetal fibroblasts as a model for adult fibroblasts (Rolfe & Grobbelaar, 2012; Walraven *et al.,* 2014). However, another study showed if miR-21 was inhibited this prevented the myofibroblast transdifferentiation (Yao *et al.,* 2011) in MRC-5 cells, a foetal lung fibroblasts cell line. Interestingly, miR-21 has been identified to be expressed the oral tumour stroma and predict poor prognosis (Hedbäck *et al.,* 2014).

1.6.4 *The 143/145 microRNA cluster.*

The microRNA 143/145 cluster is found on chromosome 5 (q33.1) as around 2kb (Liu *et al.,* 2012) co-transcribed as a bicistronic primary microRNA pair.

The cluster is involved in the transcriptional networks regulating vascular smooth muscle cell (VSMC) fate (Cordes *et al.,* 2009; Davis-Dusenbery *et al.,* 2011; Xin *et al.,* 2009). miR-143/5 are central in regulating myocardin and myocardin related transcription factors. These genes, along with serum response factor (SRF) activate the transcription of contractile smooth muscle genes including αSMA, through the binding of CArG box (a DNA sequence motif found in SMC gene promoters). There is also a CArG box in the upstream enhancer of miR-143/5 (Xin et al., 2009),

allowing them to be in a central feedback cascade controlling VSMC differentiation and maintenance.

TGF-β1 and BMP4 are both involved in promoting smooth muscle repair, and are able to induce the expression of the cluster in VSMCs (Davis-Dusenbery *et al.,* 2011; Long & Miano, 2011). The cluster fine tunes the smooth muscle phenotype by regulating myocardin and MRTFs, miR-145 has been shown to directly target MRTF-B and also some negative regulators of myocardin for example KLF4/5 (Krüppel like factor 4/5) (Xin *et al.,* 2009). miR-143/5 was shown to regulate KLF4 expression, with miR-145 having a more dominant effect (Davis-Dusenbery *et al.,* 2011). In addition to negatively regulating myocardin, KLF4 can bind SRFs to prevent its binding to myocardin or MRTFs and alter the CArG box chromatin to prevent the activation of SMC genes (Liu *et al.,* 2004), therefore KLF4 also controls the expression of the miR-143/5 cluster through the CArG box.

PDGF causes dedifferentiation of the VSMC, to a more proliferative phenotype, through the downstream loss of myocardin expression due to its negative regulation of miR-145 *(Cheng et al.,* 2009). miR-143 complements the action of miR-145 by targeting Elk-1, a transcription factor able to inhibit smooth muscle differentiation through regulating myocardin (Cordes *et al.,* 2009). Once induced to become smooth muscle cells the cluster is downregulated to allow proliferation, therefore PDGF contributes towards a proliferative smooth muscle phenotype whereas TGF-β1 and BMP4 contribute towards a contractile phenotype.

These studies have suggested that miR-145 is key in SMC differentiation, however, a miR-143/145 knockout mouse study showed a show that the cluster is dispensable for the differentiation (Xin *et al.,* 2009). However, these mice did possess vasculature with reduced vascular tone, and were unable to respond to vascular injury due to their inability to switch between the proliferative and contractile phenotypes. This study showed that both miR-143 and miR-145 have predicted targets that are involved in actin cytoskeleton organisation (Rho Kinase and Rock 1), actin polymerisation (actin-related protein 2/3 complex, and gamma actin) and actin binding (various targets including cofilin; Xin *et al.,* 2009). MiR-143/145 have also been discovered to target Fascin Homolog 1 (FSCN1), which is also involved in actin maintenance as a actin bundling protein (Liu *et al.,* 2012). miR-143/5 cluster has been reported to have been transferred from vascular smooth muscle cells to endothelial cells via specialised cell-cell connections called tunnelling nanotubes (Climent-Salarich *et al.*, 2015).

Databases such as DIANA have identified multiple predicted targets of miR-145 within the TGF-β signalling family. Recently, some of these predicted targets have been verified, TGF-βRII (Zhao *et al.,* 2015) and smad3 (Huang *et al.,* 2014). TGF-β1 has also been shown to induce the expression of the miR-143/5 cluster (Long & Miano, 2011), suggesting that miR-145 could be an integral part of TGF-β signalling.

miR-145 is overexpressed in pulmonary arterial hypertension (PAH), and chronic hypoxia mouse models of PAH (Caruso *et al.,* 2012), however it's molecular contribution to pathogenesis is yet to be outlined. Pulmonary arterial hypertension, is a disease caused by vascular smooth muscle cells proliferating in arteries of the lung, resulting in a narrowing of the pulmonary blood vessels increasing the pulmonary blood pressure and eventually leads to right heart failure. Preclinical studies have shown potential for using anti-miR-145 oligonucleotides to inhibit miR-145-mediated effects in PAH (McLendon *et al.,* 2014).

The loss of microRNA-145 is reported to be involved in chondrocyte differentiation, as it directly targets the 3'UTR of a critical transcription factor in chondrogenesis, Sox-9 (Yang *et al.,* 2011). As well as being key in specialised differentiation, miR-145 plays an important role in general differentiation. In embryonic stem cells miRNA-145 is upregulated when cells are differentiating this allows the downregulation of its pluripotency gene targets KLF4, OCT4, and SOX2 (Xu *et al.,* 2009). Additionally, miR-145 also has reported involvement in the gut epithelial and smooth muscle cell maturation (Zeng, Carter, & Childs, 2009).

1.6.5 *miR-143/145 tumour suppressor activity*

The co-transcribed microRNA-143/145 cluster has been documented to be downregulated in many malignancies. microRNA-145 was first identified in humans in colorectal adenocarcinomas, where it was found to be downregulated compared to normal colonic tissue (Michael *et al.,* 2003). Its expression has since been reported to be to be lost in a number of human malignancies including: B cell, bladder, breast, liver, lung, ovary, prostate, pituitary, colorectal, (reviewed in Suh *et al.*, 2011) and head and neck malignancies (Oesophageal SCC (Wu *et al.*, 2011), and nasopharyngeal (Chen *et al.,* 2009)

The miR-143/-145 cluster is thought to have a role in oncogenesis as loss of expression has been found in early stage colorectal adenomas (Akao *et al.,* 2010). In colorectal cancers the mature forms of both miR-143 and miR-145 are downregulated, however the precursor levels aren't, suggesting that the processing of the miRs is altered contributing to oncogenesis (Michael *et al.,*

2003). Other studies have identified differential post-transcriptional processing of miRNAs via the regulation of the processing machinery (reviewed in Siomi & Siomi, 2010; Chong *et al.*, 2010). miR-143/5 processing has been identified to be specifically regulated by drosha *via* p53 (Suzuki *et al.,* 2009). DNA damage causes p53 to indirectly interact with non-coding RNA processing machinery Drosha to increase the cleaving of the co-transcribed pre-miR-143 and pre-miR-145 to their mature forms.

One way miR-143 could contribute towards carcinogenesis is *via* the downregulation of KRAS, this has been explored in oral cancer. Chen *et al.,* (2009) used a luciferase reporter assay to show that miR-143 directly targets KRAS through binding to its 3'UTR. The loss of KRAS results in attenuation of ERK 1/2 phosphorylation in the MAPK signalling pathway, and is responsible for the loss of proliferation and increased apoptosis seen when miR-143 is upregulated in cells.

MiR-143/5 is involved in a KRAS feedback loop, and acts as a break to prevent oncogenic RAS signalling. An active KRAS mutant repressed the expression of the miR-143/145 cluster *via* a RREB1 (Ras-responsive element-binding protein-1) in the cluster's promoter (Kent *et al.,* 2010). Also, miR-145 was found to target RREB1, in addition to miR-143 targeting KRAS, allowing for feedback loops to be established within Ras oncogenic signalling. Moreover, when miR-143 and miR-145 were re-expressed in a mutant KRAS positive pancreatic ductal adenocarcinoma cell line, the cells were unable to form tumours in immunocompromised mice, perhaps suggesting that miR-143/145 cluster mediates the tumour suppressive activity associated with KRAS, on top of the other oncogenic signalling on which the miRs converge (Kent *et al.,* 2010).

As the downregulation of the miR-143/-145 cluster is important in cancers and tumour initiation, the therapeutic implications of this have been highlighted. Kitade & Akao, (2010) have attempted to overcome the limitation of nuclease digestion presented by RNAi based therapeutic strategies, by the chemical addition of an aromatic residue to the passenger stand of the miRNA duplex, this gave the miR-143 5 to 8- fold increased stability. Introduction of this modified miR-143 intravenously into colon tumour mice models, resulted in the dose – responsive reduction in tumour size.

Another reported function of miR-143 is regulating cancer metabolism (R. Fang et al., 2012). The activity of the metabolic pathway mTOR results in the upregulation of hexokinase 2 isoform (HK2), an enzyme associated with aerobic glycolysis which is commonly upregulated in tumours. This upregulation greatly benefits tumour growth as it provides ATP by binding and facilitating an ATP transporter ion channel, VDAC, in the outer mitochondrial membrane. The regulation is

achieved through the negative regulation of miR-143, which targets HK2 *via* binding to its 3'UTR in cancer cell lines (Peschiaroli *et al.,* 2012).

The miR-143/5 cluster has also been implicated in the EMT process. Both miR-143 and miR-145 were found to be at lower levels in the bone metastasis compared to the primary prostastic tumour site (Peng *et al.,* 2011). This study found that overexpression led to an inhibition of the EMT process in both *in vitro* assays and *in vivo* studies. In addition, miR-145 has been shown to suppresses cellular invasion (Sachdeva & Mo, 2010), *via* directly targeting mucin-1, a cell surface proteoglycan pro-metastatic gene. Studies from bladder tumours have revealed that miR-143/5 cluster targets plasminogen activator inhibitor -1 (PAI-1), an inhibitor of serine protease plasminogen (which cleaves plasminogen to plasmin, another protease involved in coordinating fibrinolysis) involved in various processes including fibrosis, angiogenesis and ECM component degradation and is commonly upregulated in cancers (Villadsen *et al.,* 2012).

MicroRNA-145 has been implicated to be involved with growth factor signalling pathways. The Insulin like growth factor (IGF) has been noted to be one of the pathways affected. miR-145 targets both a receptor type 1 insulin-like growth factor receptor I (IGF RI) and IRS-1, a docking protein which transduces the insulin signal from the receptor to downstream cystolic signalling proteins. miR-145 was found to directly target IRS-1 3'UTR through 2 separate binding sites (shown by luciferase reporter assay), the ectopic expression of miR-145 resulted in decreased IRS-1 protein levels but there was an increase in IRS-1 mRNA transcript levels suggesting that miR-145 acts to prevent the translation of IRS-1 and that there may be a positive feedback loop involve (La Rocca *et al.,* 2009). In this study they failed to the downstream effectors of the IGF pathway e.g. Ras or MAPK/ERK pathway. In their study, mir-145 transfection correlated with growth inhibition, which can be assumed to be due to the loss of IRS-1. Truncation experiments confirmed that miR-145 was able to negatively regulate translation of IGF-R1 by binding to its 3'UTR.

Research has shown that miR-145 could be used as a putative biomarker. Low levels of miR-145 correlate with an aggressive cancer and poor prognosis in prostate. The downregulation of the miR-143/145 cluster is strongly associated with OSCC (oesophageal SCC), and also the incidence of lymph node metastasis (Liu *et al.,* 2012). Interestingly the downregulation of miR-143 and miR-145 was statistically associated with heavy drinking and smoking habits. The microRNA 143/-145 cluster are one of several microRNAs which are significantly downregulated in HPV positive cases of PSCC (pharyngeal squamous cell carcinoma) compared to HPV negative (Lajer *et al.,* 2012).

Sachdeva *et al.,* (2009) showed that tumour suppressor p53 negatively regulates proto-oncogene c-myc through the induction of miR-145. They discerned that PI3K/ Akt pathway is able to mediate the induction of miR-145 expression *via* p53. As the PI3K/AKT and p53 pathways are central and converge on many downstream signalling networks, miR-145 regulation is important in normal cellular growth and the cell cycle. In particular they revealed that p53 is able to bind to a p53 response element in miR-145's promoter sequence and activate its transcription, miR-145 in turn directly targets transcription factor and proto-oncogene c-myc. Their data suggests that miR-145's tumour suppressor characteristics are at least in part due to the silencing of c-myc (Sachdeva *et al.,* 2009). Suh *et al.*, (2011) studied 47 cancer cell lines and found a strong correlation between p53 mutations and the hypermethylation, hence downregulation, of miR-145. The authors showed that a mutant form of p53 was unable to induce miR-145 expression, perhaps highlighting why the loss of basal levels of miR-145 is so common in cancers. As mentioned previously p53 is also able to regulate miR-145 at the processing level as well as the transcriptional level (Suzuki *et al.,* 2009).

Despite the above data, the miR-143/5 cluster has been recently suggested to be expressed exclusively in the mesenchymal compartment of the gut in mice and humans (Chivukula *et al.,* 2014), despite previous studies implicating a role for the miR-143/5 cluster as a tumour suppressor in colorectal epithelium (Akao *et al.,* 2010; Chen *et al.,* 2009). The authors of this controversial paper suggest that previous results could have been due to mesenchymal contamination. They investigated whether the expression of miR-143/5 in epithelium could be a result of the aberrant Wnt pathway inducing its expression in early oncogenesis and subsequently it being downregulated in tumour progression. Using mice models of adenomas with constituently active Wnt, they found no evidence of miR-143/5 expression changing, suggesting that the downregulation of miR-143/5 in previous studies must be a result of mesenchymal contamination. Conditional knockout studies showed that miR-143/5 in the mesenchymal compartment was found to be required for normal epithelial regeneration through regulating IGF signalling in intestinal subepithelial myofibroblasts.

1.6.6 *miR-143/-145 cluster and the tumour microenvironment.*

MiR-145 has recently been identified as a potential helpful biomarker in several cancers. miR-145 is downregulated in the serum of ovarian cancer (Liang *et al.,* 2015) and in the saliva of patients with OSCC compared with healthy controls (Zahran *et al.,* 2015)

MicroRNA microarrays comparing CAFs isolated from invasive bladder tumours and normal fibroblasts isolated from foreskin showed a significant downregulation in the miRNA-143/145 cluster in the CAFs; however the same down regulation was not seen when they attempted to validate using qRT-PCR analysis of a small cohort (n=3) (Enkelmann *et al.,* 2011). Conversely in the same study, both microRNA microarray and qRT-PCR data revealed an upregulation of miR-16 and miR-320 in bladder CAFs compared to normal bladder fibroblasts. Studies from cardiac and pulmonary fibrosis have reported miR-145 to promote the myofibroblasts phenotype, suggesting miR-145 may play a role in regulating fibroblast transdifferentiation towards myofibroblasts (Gras *et al.,* 2015; Wang *et al.,* 2014; Yang *et al.*, 2013).

Data from our lab has shown that miR-145 is involved with stromal-epithelial interactions (Pal *et al.,* 2013). Normal oral fibroblasts downregulate miR-145 is response to cigarette smoke, which in turn promotes the paracrine migration of OSCC cancer cell lines.

Angiogenesis may be regulated in part by miR-145 expression. miR-145 targets p70S6K1 which is immediately downstream of mammalian target of rapamycin/ (mTOR), a molecule central in the cellular functions such as apoptosis, cell cycle regulation, proliferation and growth (Xu *et al.,* 2012). Xu *et al*., showed that miR-145, *via* loss of p70S6K1, is capable of halting angiogenesis and cellular growth by the inhibition of angiogenic regulators HIF-1α and VEGF. They hypothesised that loss of tumour miR-145 expression results in the downstream activation of angiogenic factors *via* the mTOR pathway.

Data from Lu *et al*., (2013) confirmed unpublished data from our lab that suggests miR-145 targets the transmembrane protease ADAM-17. They showed that miR-145 directly targets ADAM-17 *via* binding to its 3'UTR, and downregulates EGFR expression. ADAM-17 is also referred to as TNF-α converting enzyme (TACE), due to its ability to process TNF-α, therefore overexpression of ADAM-17 due to loss of inhibition by miR-145, could increase the release of TNF-α in the inflammatory response. ADAM-17 also cleaves heparin-binding EGF-like growth factor (HB-EGF) (Merlos-Suárez *et al.,* 2001), therefore miR-145 may indirectly increase EGF growth signalling to promote EMT and tumour growth (Hinsley *et al.,* 2012). ADAM-17 has also been reported to play a role in angiogenesis, so loss of miR-145 may promote neovascularisation through ADAM-17. miR-145 has been published to target other proteases including MMPs, for example MMP-11 (Wu *et al.,* 2014)

ADAMTS levels are also important in cancer, like ADAMs, they can influence growth factor signalling and ADAMTS-1 and -4, are involved in proteolytic cleavage of an extracellular

proteoglycan versican. This cleavage produces a form which can function independently. Both cleaved and uncleaved versican are strongly implicated in the tumour microenvironment. miR-143 has been reported to post-transcriptionally regulate versican, in smooth muscle cells by binding to its 3' UTR (Wang, Hu, & Zhou, 2010). Preliminary data from our lab also suggest that miR-145 is able to regulate versican levels. This study aims to assess this regulation and its significance within CAFs.

1.6.7 *miRNA therapies*

miRNA mimics and antimirs are being developed for the therapeutic treatment of diseases or and cancer. The development of this new class of drugs comes with several challenges to overcome in addition to ensuring that the miRNA has minimal off-target effects (reviewed in van Rooij, Purcell, & Levin, 2012). Nucleic acids are unstable and are subject to degradation by nucleases, therefore an appropriate delivery system needs to be used for protection and also to ensure delivery to the appropriate cells. RNAs have a negative charge and therefore the miRNA needs to be of a neutral charge, to be uptaken into a cell. Various technologies have been developed to overcome these limitations. To overcome nuclease degradation nucleic acids can be stably modified. Locked nucleic acids (LNA) have been generated (Koshkin et al., 1998), these have an extra bridge between 2'O and 4' on the ribose moiety, making the nucleic acid more stable. Peptide nucleic acids (PNA) have also been synthesised, where the nucleic acids phosphodiester backbone is replaced with N-(2-aminoethyl)-glycine, these are also neutrally charged so it does not require further packaging (Zhang, Wang, & Gemeinhart, 2013). Delivery vectors *in vitro* can be viral vectors or lipid liposomal based however these are not suitable for in vivo use as they inflict an immune response and are toxic (Zhang *et al.,* 2006). Most commonly studied delivery technique in vivo is the polyethylenimide (PEI) polymer, are long pronated polymers which can bind nucleic acid (Boussif *et al.,* 1995) which can package the nucleic acids for delivery.

Targeting the miR cargo to the correct cells is the next challenge to overcome. PNAs can be directly targeted to the tumour microenvironment. AntimiR-155 was conjugated to a pHLIP peptide with an ability to be induced into an alpha helix transmembrane structure at low pH, in the tumour microenvironment, which can be incorporated into adjacent cells' plasma membrane (Cheng *et al.,* 2015). In an acidic environment (around pH 6), like that found in tumours, sites of inflammation or ischaemia, the pHLP peptide can incorporate into the plasma membrane of surrounding cells, the disulphide bond between pHLP and the antmiR is reduced

in the cytosol and the antimiR is released to decrease miR-155 levels by RNAi. This treatment strategy was tested on mouse miR-155 overexpressing lymphoma model, where it was able to reduce miR-155 levels, reduce tumour size and increase survival.

Some miRNAs show incredible potential as they target many oncogenes at once for example miR-34, which a mimic is currently in phase 1 clinical trials for the treatment of primary advanced liver cancer. The drug MRX38, a miR-38 mimic encapsulated in liposomal based delivery system, is in a phase 1 clinical trials. Another miR therapy in clinical trials is antimiR-122 (drug name: Miravirsen) which seems to be so far successful in Phase 2a trials for treating hepatitis C infection (Gebert *et al.,* 2014). A miR-145 inhibitor is currently in preclinical studies for use in treating pulmonary arterial hypertension (Caruso *et al.,* 2012) which is being developed by miRagen Therapeutics, Inc. (miRagen Therapeutics | microRNA Based Therapeutics)

1.7 ***Versican***

Versican (VCAN, also known as PG-M, and CSPG-2) is a large extracellular chondroitin sulphate proteoglycan which is a member of the aggrecan family. Other members of this gene family include aggrecan, neurocan and brevican; these structurally similar molecules all have roles in extracellular matrix (ECM) assembly. Versican is widely expressed in adult connective tissues in smooth muscle, skin, blood vessels, glandular epithelium, and nervous system (Bode-Lesniewska *et al.,* 1996; Yao *et al.,* 1994).

Versican is a large structurally complex proteoglycan approximately 74 - 450 kDa in size (Ricciardelli *et al.,* 2009). Proteoglycans are proteins that contain glycosaminoglycan (GAG) chains. Versican is classed as a chondroitin proteoglycan as it has 15 - 20 chondroitin sulphate side chains attached to its GAG domains. The versican gene spans 15 exons on chromosome 5 (Nasos, Zimmermanng, & Iozzon, 1994), and two GAG exons are alternatively spliced, to produce 4 isoforms V0, V1, V2, and V3 (Zimmermann & Ruoslahti, 1989). Each isoform consists of two globular domains G1 and G3, but differs by the presence of two GAG chains, α and β. G3 has two EGF repeats and lectin binding domains (Lebaron, 1996). V0 is the full length versican which contains both α and β GAG domains, V1 contains only β GAG, V2 contains only α GAG domain and V3 contains no GAG domains, in addition to the two globular domains (figure 1.3.; reviewed in Ricciardelli *et al.*, 2009) Each isoform, therefore, has slightly different functions in physiological and pathological situations.

Versican's name reflects its biological versatility both in development, maintenance and disease. It has roles in many cellular processes e.g. adhesion, proliferation, migration and apoptosis (Ricciardelli *et al.,* 2009). It is an integral part of the extracellular matrix and interacts with several key extracellular matrix components, such as fibronectin, collagen I and laminin (Wu *et al.,* 2005). Like other members of the aggrecan gene family, versican is able to interact with hyaluronan (a ubiquitous polysaccharide present in the ECM; HA) and form aggregates, associating with it through versican's N terminus (G1 domain) (LeBaron, Zimmermann, & Ruoslahti, 1992) and also through its GAG chains (Wu *et al.,* 2005). Versican is also known to interact with hyaluronan's receptor CD44, it is thought to behave as a ligand, independent of hyaluronan binding as there is an association in the presence of hyaluronidase (Kawashima *et al.,* 2002*)*. CD44, versican and HA have been reported to form a complex (Hattori *et al*., 2011). Hyaluronan also can influence cellular signalling, it can activate EGF signalling by interacting with EGFR (Simpson *et al.,* 2010), in addition to converging on the NFκB pathway, through physically interacting with TGF-β receptor I at the cell membrane. Through this interaction, HA is able to activate the TGF-β RI leading to the activation of the TGF-β pathway and increase migration in a breast metastatic cell line (Bourguignon *et al.*, 2002). On the other hand, HA can dampen the TGF-β response through CD44 and TGF-β RI interaction in proximal tubular epithelial cells (Ito *et al.,* 2004). The differences seen could reflect the different CD44 isoforms in the diverse cell types.

CD44 has also been found to act as a docking platform for MMP9 (Yu & Stamenkovic, 1999). Docked MMP9 was shown to, in turn cleave latent TGF-β2 and TGF-β3 (Yu & Stamenkovic, 2000) promoting tumour invasion and angiogenesis.

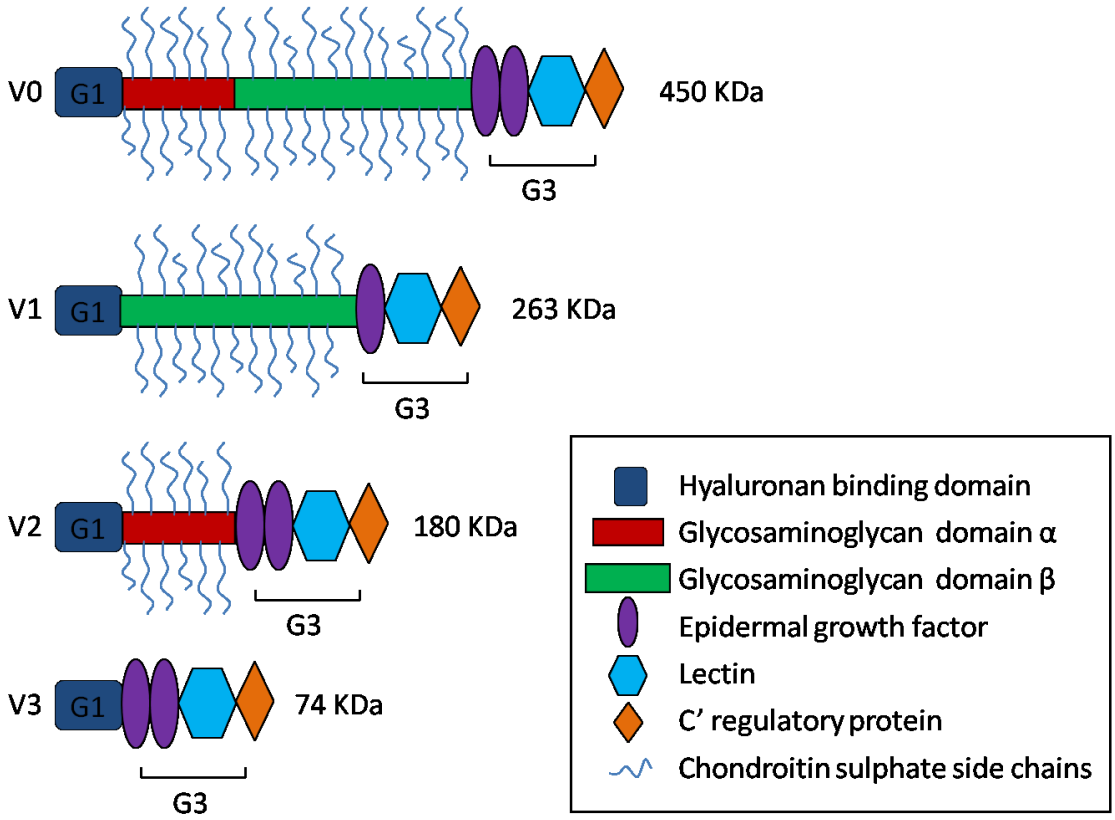

Figure 1.3. A schematic showing the structure of the versican isoforms.
Modified from (Ricciardelli et al., 2009)

There are several CD44 isoforms that have implicated roles in HNSCC, such as chemosensitivity to cisplatin, cellular proliferation and migration (Wang *et al.*, 2009). CD44, and therefore HA have been reported to activate EGF signalling, a pathway aberrantly activated in a large proportion of HNSCC cases. Bourguignon *et al.*, (2002) showed that CD44 and EGFR form a complex. Several studies have showed that interaction can lead to the downstream activation of tumour associated signalling pathways Ras, Rho A, MAPK and PI3-K (reviewed in Wang & Bourguignon, 2011). Furthermore, CD44 is used as a cell surface marker to identify the presence of cancer stem cells in breast and prostate, implicating further its significance in cancers.

HA and versican complex formation is crucial in regulating the ECM structure and cellular phenotype. Mice embryonic fibroblasts expressing a versican construct with decreased ability to interact with HA (due to a subdomain deletion in the G1 domain), Cspg2Δ3/Δ3, undergo premature senescence due to a less stable ECM (Suwan *et al.*, 2009). These Cspg2Δ3/Δ3 cells have markedly reduced amount of versican and HA in the extracellular environment, in the mutant cells HA was only found associated with CD44 at cell membranes suggesting that efficient HA and versican interaction is required for HA to amalgamate into the ECM and for

complete matrix assembly. The authors proposed that a decrease in versican and HA complexes resulted in a greater amount of free HA activating CD44, leading to the downstream activation of MAPK allowing early senescence. It could be hypothesized that the opposite could be true, a pathological accumulation of versican in the tumour environment leading to a larger ECM with increase HA accumulation and subsequent lower CD44 activation and less ERK1/2 phosphorylation resulting in increased survival and proliferation.

1.7.1 *Versican in cancer.*

In the tumour environment, versican is secreted mainly by the fibroblasts in the adjacent stroma. This secretion is elevated by paracrine signalling from the cancer, as shown in studies where conditioned media from cancer cell lines induced an increase in release of versican in mammary fibroblasts (Ricciardelli *et al.,* 2009; Sakko *et al.,* 2001). Specifically TGF-β1 induces versican secretion in human smooth muscle cells, gingival fibroblasts amongst other normal cell types (Haase *et al.*, 1998; Kähäri, Larjava & Uitto, 1991). The presence of a TGF-β1 antibody was able to block induced versican expression in response to both exogenous TGF-β1 and conditioned media in prostate fibroblasts (Sakko *et al.,* 2001), suggesting that TGF-β1 signalling is one of the primary ways that cancer cells are able to regulate versican levels. In addition to expression by stromal cells, versican mRNA has been detected in the cytosol of epithelial tumour and melanoma cell lines (Gulyás & Hjerpe, 2003; Touab *et al.,* 2002).

High stromal versican levels are correlated with poor prognostic outcome and a more aggressive phenotype in many cancers, including breast (Ricciardelli *et al.,* 2002), pharyngeal (Pukkila *et al.,* 2004) oral squamous cell carcinoma (Pukkila *et al.*, 2007), and bladder (Said *et al.,* 2012). In addition, versican expression has been detected to be greater in metastatic sites (Pukkila *et al.,* 2004). The same study's data suggested that versican expression is greater in the earlier stages of pharyngeal tumours, however similar immunohistological studies have not seen any correlation with versican expression and the staging (Pukkila *et al.,* 2007; Suwiwat *et al.,* 2004). The presence of versican also increases the chance of relapse in prostate and breast malignancies. One study showed that high peritumoural versican levels were 6 fold more likely to relapse (Ricciardelli *et al.,* 2002). On the other hand, versican levels found in epithelial cells have been indicative of a longer disease free survival in colon cancer (de Wit *et al.,* 2012).

Versican can cause proliferation and inhibit apoptosis in NIH3T3 fibroblasts (Sheng *et al.*, 2005). Versican is an anti-adhesive molecule due to its negatively charged chondroitin sulphate side

chains (Ricciardelli *et al*., 2009), therefore another method by which it could promote cancer progression and relapse is by allowing cancer cell invasion through a non-cohesive extracellular matrix, allowing dissemination of cancer cells. It also destabilises focal adhesions between cells which is believed to permit cellular proliferation and hence tumour growth.

Versican has been implicated in muscle invasive bladder carcinomas, where it is expressed highly (Said *et al.,* 2012). Rho-GTP dissociation inhibitor 2 (Rho-GDI2), a molecule preventing invasion which is lost in these tumours, works through the action of versican. When Rho-GDI2 was introduced into a bladder urothelial cell line, versican expression was decreased by more than 8-fold. Specifically, GDI was able to downregulate V1 and V3 isoforms. When Rho-GDI2 was introduced into a cancer urothelium and macrophage co-culture system there was a decrease in versican expression and a reduction in the release of pro- inflammatory mediators MCP-1 (also known as CCL2) and IL-6, suggesting that versican induces an inflammatory response resulting in the recruitment of macrophages. The presence of macrophages was shown to be crucial for the GDI2-mediated upregulation of versican to promote invasion and metastasis, as the depletion of macrophages in mice inhibits versican's ability to stimulate lung-metastasis. This study eloquently revealed versican's pro-metastisic role through the regulation of inflammation with the tumour microenvironment.

Versican has been found to act as an agonist for TLR-2 (Toll-like receptor-2) present on macrophages resulting in activation and subsequent secretion of chemokines TNF-α (tumour necrosis factor-alpha) and IL-6 (interleukin-6) (Kim *et al.,* 2009). These metastatic mediators can then recruit more inflammatory mediators, increase permeability of blood vessels and activate the NF-KB pathway which is anti-apoptotic and pro-proliferative; all of which will aid metastasis. This *in vivo* study went on to show that both recombinant knock out of TLR-2 and the silencing of versican, in the cancer cells used to inoculate the mice, significantly attenuated metastatic spread and improved survival. It was clear from this study that versican is able to strongly affect the tumour microenvironment by behaving as a ligand, however it is not clear whether this effect was through its association with hyaluronan.

Extracellular versican levels are responsible for change in cellular phenotype. Hattori *et al*., (2011) reported that pericellular, the extracellular compartment surrounding the cell, accumulation of versican, *via* the loss of ADAMTS-5 mediated cleavage, was responsible for the acquisition of myofibroblast phenotype within dermal fibroblasts. ADAMTS-5 -/- knockout mice dermal fibroblasts had an attenuation of versican cleavage shown by a reduction in detection, *via* immunoblotting, of an epitope specific to the ADAMTS-5-cleaved versican product (DPEAAE

epitope) compared to the wild type. Moreover there was an increase in the unprocessed versican levels shown by an increase in detection of anti-GAGβ which is present in both V0 and V1. These ADAMTS-5-/- fibroblast had an extensive pericellular matrix and characteristics that resemble myofibroblasts: altered cell shape, increased αSMA expression, and greater contractility (Hattori *et al.,* 2011). This phenotype could be rescued by the addition of ADAMTS-5 and by crossing ADAMTS-5 -/- mice with haploinsufficient VCAN, suggesting that the phenotype was due to accumulation of versican. Again, heterologous expression of full-length versican induced a myofibroblast phenotype within ADAMTS-5 -/-, VCAN hdf/+ fibroblasts; suggesting that it was in fact accumulation of pericellular versican inducing dermal myofibroblast differentiation.

Hattori *et al.*, (2011) also showed evidence to suggest that the myofibroblast phenotype was related to increased TGF-β signalling and HA. ADAMTS-5 -/- fibroblasts had an increase in psmad 2/3 levels, and when an inhibitor to TGF-β R was added there was a reduction in αSMA expression and contractility. Likewise, inhibiting the synthesis of HA, which had previously been shown to be involved with the myofibroblast transition (Meran *et al.,* 2007), had the same ameliorating effect on the myofibroblast phenotype. This study further exposes the links between HA, versican, and TGF-β signalling, and indeed the action of ADAMTS family members, which appear to contribute towards myofibrotic phenotype (Hattori *et al.,* 2011).

ADAMTS-1 and -4 are able to proteolytically cleave versican at the Glu441-Ala442 bond resulting in a truncated form of versican (Ricciardelli *et al.*, 2009). This cleaved version of versican co-stained with both ADAMTS-1 and ADAMTS-4 in malignant prostate cancer sections. A separate study has suggested that higher levels of this cleaved form in cancers contributes to invasion, as an antibody to the neoepiptope formed by ADAMTS cleavage inhibited cancer cell migration (Arslan *et al.,* 2007). How these cleaved products of versican contribute to cancer and metastasis needs to be explored further.

1.7.2 *Regulation of versican*

Versican expression is regulated by a number of molecules including a range of cytokines and growth factors. Platelet derived growth factor (PDGF), was able to stimulate an increase in versican levels in human gingival fibroblasts and arterial smooth muscle cells, where PDGF was also able to cause a greater number of HA/versican aggregates (Evanko *et al.,* 2001). Other growth factors, EGF and IGF-1 (Syrokou *et al.,* 1999), as well as steroid hormones, (Russell *et al.,*

2003) androgens (Read *et al.,* 2007), and IL-α (Qwarnström *et al.,* 1993), to name a few, have also been reported to increase versican levels.

microRNA-143 has been identified to post-transcriptionally regulate versican. Wang *et al,* (2010) showed that myocardin is responsible for the downregulation of versican *via* transcriptional activation of miR-143, in smooth muscle cell differentiation. miR-143 is able to directly bind to a complementary sequence within the versican 3'UTR to result in the downregulation of versican in smooth muscle cells. However, co-transcribed microRNA-145 did not bind to versican's 3'UTR (Wang *et al.,* 2010). Scanning bioinformatical databases did not reveal any putative binding sites within the versican gene. However, preliminary data from our lab suggests that miR-145 may regulate versican.

1.8 ***Aims and Objectives***

The main aim of this study was to assess the role of miR-145 within fibroblasts in the tumour microenvironment, termed cancer associated fibroblasts (CAFs). As myofibroblast CAFs are the most well characterised CAF and are recognised to promote invasive tumours with poor prognositic value, the roles of miR-145 within the myofibroblast phenotype of CAFs were assessed. The main hypothesis was that miR-145 regulates the myofibroblast phenotype in CAFs.

The study intended to assess the expression of miR-145 in fibroblasts isolated from OSCCs and normal oral fibroblasts treated with TGF-β1 (induced myofibroblasts) and to use miR-145 mimics and antimiRs to test the gain of function and loss of function effects of miR-145 on the myofibroblast phenotype. The study planned to investigate the myofibroblast phenotype by assessing the expression of molecular myofibroblast markers, contractility and ability to promote the paracrine migration and invasion of an oral cancer cell line.

The work outlined in this thesis aimed to identify and validate novel targets for miR-145. The study intended to validate preliminary data that suggested miR-145 regulates extracellular proteoglycan versican, and understand the nature of this regulation. In addition to investigating the role of versican in regulating the myofibroblast phenotype.

The main objectives of the study were to:

- Optimise the dose and time duration of TGF-β1 treatment for inducing the myofibroblast phenotype in normal oral fibroblasts (NOFs).
- Characterise normal oral fibroblasts and fibroblasts isolated from OSCC, CAFs, responses to TGF-β1 and conditioned media from oral cancer cell lines, by assessing common markers of myofibroblast phenotype by assessing the presence of α- smooth muscle actin (αSMA) stress fibres, the increased expression of extracellular matrix markers collagen 1a (COL1A) and fibronectin-1 with extra domain A (FN1-EDA), increased ability to contract, and increase ability to promote the paracrine migration and invasion of cancer cells.
- Investigate the ability of the conditioned media from oral cancer cell lines cal27, H357 and VB6 to promote the myofibroblast phenotype in NOFs and CAFs.
- Determine the expression of molecular markers of myofibroblasts in fibroblasts isolated from genetically stable and unstable OSCCs compared to normal oral fibroblasts.
- Assess the expression of microRNA-143 and miR-145 in TGF-β1 induced myofibroblasts and CAFs compared to NOFs.
- Perform miR-145 gain of function and loss of function experiments within TGF-β1 induced myofibroblasts and CAFs and assess the expression of myofibroblast markers.
- Investigate the effect of miR-145 in fibroblast‘s promoting paracrine migration and invasion of H357 cells.
- Examine the expression of versican isoforms in TGF-β1 induced oral myofibroblasts and CAFs.
- Investigate the expression of versican in NOFs and CAFs overexpressing miR-145.
- Investigate how miR-145 regulates versican by cloning versican’s regulatory regions.
- Examine the effect of a versican siRNA on the myofibroblast phenotype in TGF-β1 induced myofibroblasts.
- Determine the regulation of versican in the tumour microenvironment by investigating metalloproteases which cleave versican in induced myofibroblasts and CAFs.
- Confirm targets for miR-145 which had been previously published and identifying new target to understand the role of miR-145 in the myofibroblast phenotype better.
- Investigate the role of miR-145 and versican in the myofibroblast phenotype of dermal fibroblasts, and establish whether they have the same effect as it does in oral fibroblasts.

Chapter 2: Materials and Methods

2.1 ***Materials***

2.1.1 *Reagents*

All chemicals used were purchased from Sigma Aldrich (UK), unless otherwise stated.

2.1.2 *Recombinant proteins and peptides*

Recombinant human transforming growth factor-beta 1 (TGF-β1) was purchased from R & D systems (UK) and reconstituted in 4 mM hydrochloric acid with 1 mg/ml bovine serum albumin (BSA) at a concentration of 20 µg/ml. Endothelin-1 synthetic peptide, which has sequence matched with porcine and human was purchased from Sigma Aldrich, and was made up in sterile water to a concentration of 10 µM. Recombinant platelet derived growth factor-BB (PDGF-BB) was purchased from R & D systems (UK), and reconstituted in 4 mM HCl to a final concentration of 100 µg/ml. All peptides and recombinant proteins were stored at −20^{o}C and used within a month following reconstitution.

2.1.3 *Cell lines*

The cell lines used in this study are shown in table 2.1

Table 2.1 Head and neck cell lines used.

Cell Line Name	Tissue Origin site	Source
BICR16	OSCC tongue	Provided by K.Hunter
Cal27	OSCC tongue	Purchased from ATTCC
H357	OSCC tongue	Gift from S.Prime (University of Bristol)
VB6 ($\alpha_v\beta_6$ integrin stable transfection)	OSCC tongue	Generated by G.Thomas (at Eastman Dental Institute UCL (Thomas *et al*., 2001))

2.1.4 *Primary cells*

Human normal primary cells were isolated with South Yorkshire ethical committee approval at the Charles Clifford Dental hospital). Fibroblasts isolated from OSCCs were kindly given by Prof. Ricardo Coletta at University of Campinas, Piracicaba, Sao Paulo, Brazil. Fibroblasts isolated from genetically characterised OSCCs were given by Prof Ken Parkinson, and isolated at Beatson Institute for Cancer Research (Lim *et al.,* 2011). All Primary cells used are listed in the table 1.2.

Table 2.2 Human primary cells used

Cell Type	Cell name	Source
Normal gingival Fibroblasts	OF26, DENF008, DENF316, DENF319	Charles Clifford Dental Hospital, Sheffield
	MNF4, MNF5, MNF6	Prof Ricardo Coletta (University of Campinas, Sao Paulo)
	HNOF1, HNOF2, HNOF5	Prof Ken Parkinson (Lim *et al.*, 2011)
Fibroblasts isolated from Genetically stable OSCC	BICR37, BICR59, BICR69, BICR70, BICR73	Prof Ken Parkinson (Lim *et al.*, 2011)
Fibroblast isolated from genetically unstable OSCC	BICR3, BICR18, BICR31, BICR63, BICR78	Prof Ken Parkinson (Lim *et al.*, 2011)
Fibroblasts isolated from OSCCs	MCA, MC5, MC6, MC15	University of Campinas, Sao Paulo - Prof Ricardo Coletta
Fibroblasts from dysplasias	E2	Prof Ken Parkinson (Lim *et al.*, 2011)
Dermal Fibroblast	HDF	Promocell
	HDF 283, HDF286	Prof Sheila MacNeil

2.1.5 *Bacterial Strains*

The chemically component E.coli strain DH5α was purchased from New England BioLabs (UK), and was used for propagating plasmid DNA.

2.1.6 *Antibodies*

Mouse anti-human alpha smooth muscle actin (anti-αSMA) monoclonal antibody (clone 1A4; 1:1,000 for western blotting), mouse anti-human β-actin monoclonal antibody (clone AC-74; 1:4,000 for western blotting), and rabbit anti-human glyceraldehyde 3-phosphate

dehydrogenase (GAPDH) monoclonal antibody (1:7,500 for western blotting) were purchased from Sigma Aldrich (UK). Goat anti-human full length versican polyclonal antibody was bought from R & D systems (UK) (1:1,000, for western blotting). Rabbit anti-human neoepiptope versican (ab19345) polyclonal antibody (1:1,000, for western blotting) was purchased from Abcam (UK). The secondary horseradish peroxidase (HRP) conjugated antibodies used were anti-rabbit IgG (Cell Signalling Technologies; 1:5,000) , anti-mouse IgG (Cell Signalling Technologies; 1:3,000) and ZyMAX^{TM} rabbit anti-goat IgG (Invitrogen, UK; 1:3,000).

2.1.7 *Plasmids*

The pGL3 basic plasmid vector was purchased from Promega (UK).

2.1.8 *Tissue Culture*

All reagents used in tissue culture were purchased from Sigma Aldrich (UK): Dulbecco's modified eagle medium (DMEM), foetal bovine serum (FBS), L-glutamine, phosphate buffered saline (PBS), trypsin /EDTA (ethylenediaminetetraacetic acid), Ham's F12 media, epidermal growth factor (EGF), cholera toxin, insulin, hydrocortisone, insulin, adenine, amphotericin B, penicillin and streptomycin, 3,3,5-tri-iodothyronine, and apo transferrin. Difco trypsin, for use in the isolation of primary cells, was purchased from BD Worldwide (UK).

Reduced serum OptiMem and Oligofectamine transfection reagents were purchased from Life Technologies (UK). Fugene HD 6 from Promega (UK) was used in Dual Luciferase reporter assay to introduce vectors into reciprocal B16 cells.

All culture plates were purchased from Griener Bio one (UK). Porous membrane (8μm) transwell inserts for use in cell migration assay were purchased from Scientific Laboratory Supplies (SLS; UK). Glass coverslips with a diameter of 13mm were purchased from VWR International (UK).

2.1.9 *Oligonucleotides*

Synthetic oligonucleotides for gain of function/ loss of function experiments were bought from Life Technologies (UK) and shown in table 2.3.

Table 2.3: List of oligonucleotides.

Oligonucleotide	Part number
Versican siRNA	AM16708 14606
MRTF-B siRNA	AM16708 115972
Silencer select negative siRNA #1	4390843
Silencer select negative siRNA #2	4390847
Negative premiR control #1	AM17110
Negative premiR control #2	AM17111
premiR miRNA precursor 143	AM17100 PM19855
premiR miRNA precursor 145	AM17100 PM11480
antimiR miRNA inhibitor antimiR-145	AM17000 AM11480

2.1.10 *Primers*

Primers were synthesised by Sigma Aldrich, and the sequences are shown in Table 2.4.

Table 2.4. SYBR green primer sequences

Primer	**Sequence**	**Reference**
U6 Forward	5’ CTCGCTTCGGCAGCACA 3’	(Baroukh *et al*., 2007)
U6 Reverse	5’ AACGTTCACGAATTTGCGT 3’	(Baroukh *et al*., 2007)
αSMA Forward	5’ GAAGAAGAGGACAGCACTG 3’	(Yue *et al*., 2008)
αSMA Reverse	5’ TCCCATTCCCACCATCAC 3’	(Yue *et al*., 2008)
Versican Forward	5’CTGATAGCAGATTTGATGCCTACT GC 3’	(Wang *et al*., 2010)
Versican Reverse	5’ GTGGTTCTTTGGATAAACTGGGTGA TG 3’	(Wang *et al*., 2010)
Fibronectin-1 with EDA (FN1-EDA) domain Forward	5’ TGGAACCCAGTCCACAGCTATT 3’	
Fibronectin-1 with EDA (FN1-EDA) domain Reverse	5’ GTCTTCTCCTTGGGGGTCACC 3’	
Collagen 1a (COL1a) Forward	5’GTGGCCATCCAGCTGACC 3’	
Collagen 1a (COL1a) Reverse	5’ AGTGGTAGGTGATGTTCTGGGAG 3’	
Connective Tissue Growth Factor (CTGF) Forward	5’ GGGAAATGCTGCGAGGAGT 3’	
Connective Tissue Growth Factor (CTGF) Reverse	5’AGGTCTTGGAACAGGCGCTC 3’	

Matrix metalloprotease 2 (MMP2) Forward	5’ AATAATTCCGCTTCCAGGGCACATCC ‘3	
Matrix metalloprotease 2 (MMP2) Reverse	5’ TTATTGCGGTCGTAGTCCTCAGTGGT ‘3	
Myocardin Forward	5’ CGAGTCTGATCCGGAGAAAGG 3’	
Myocardin Reverse	5’ CTGTGAAAGAGGCCATAAAAGGTAA 3’	
Myocardin Relative Transcription Factor –A (MRTF-A) Forward	5’ TGTGTCTCAACTTCCGATGG 3’	
Myocardin Related Transcription Factor –A (MRTF-A) Reverse	5’ TTCACCTTTGGCTTCAGCTC 3’	
Myocardin Relative Transcription Factor –B (MRTF-B) Forward	5’ GCAACTGCTGCACAAATAACC 3’	
Myocardin Related Transcription Factor –B (MRTF-B) Reverse	5’ TTGATAAAGGGCTGCTGGAC 3’	
TGF-β Receptor II Forward	5’ AGTCGGATGTGGAAATGGAGG 3’	
TGF-β Receptor II Reverse	5’ GGAAACTTGACTGCACCGTTGT 3’	

Sox9 Forward	5'GACCAGTACCCGCACTT 3'	(van Baal *et al*., 2012)
Sox9 Reverse	5' TTCACCGACTTCCTCCG 3'	
Krüppel like factor 4 (KLF4) Forward	5' CCCAATTACCCATCCTTCCT 3'	(Davis-Dusenbery *et al*., 2011)
Krüppel like Factor 4 (KLF4) Reverse	5' CGTCCCAGTCACAGTGGTAA 3'	
Krüppel like Factor 5 (KLF5) Forward	5' CTTCCACAACAGGCCACTTACTT 3'	(C. Chen, Bhalala, Qiao, & Dong, 2002)
Krüppel like Factor 5 (KLF5) Reverse	5' AGAAGCAATTGTAGCAGCATAGGA 3'	

2.2 ***Methods:***

2.2.1 *Cell culture*

Isolation of primary cells from oral biopsies

Human primary normal oral fibroblasts were isolated from biopsies taken from patients at the Charles Clifford Dental Hospital undergoing routine dental treatments with informed consent (see section2.2.5).

Isolation of normal oral keratinocytes.

Biopsy tissue was incubated in 0.1% (w/v) Difco trypsin at 4 ^{o}C overnight to remove the epithelium. Keratinocytes were obtained from the biopsies by gentle scraping of the connective tissue into the Difco trypsin, using a scalpel. The remaining tissue was used to isolate normal oral fibroblasts (section 0). The tryspin mixture containing the keratinocytes was subsequently centrifuged at 1200 rpm for 5 min, resuspended in Green's media and grown on an irradiated mouse fibroblast feeder layer (i3T3). Green's media, is made up of 66% (v/v) DMEM, 21.6% (v/v) Ham's F12 media, 5 ng/ml epidermal growth factor (EGF) 8.47 ng/ml cholera toxin, 5 µg/ml

Insulin, 4 µg/ml Hydrocortisone, 5 µg/ml Insulin, 0.025 µg/ml Adenine, 0.625 µg/ml Amphotericin B, 100 i.u./ml Penicillin, 100 µg/ml Streptomycin, 1.36 ng/ml 3,3,5-Tri-iodothyronine, and 5 µg/ml Apo Transferrin. This study did not use the keratinocytes subsequently.

Isolation of normal oral fibroblasts.

After the isolation of normal oral keratinocytes, the remainder of the biopsy was finely cut up using the scalpel and left in 0.5% collagenase A at 37 ^{o}C in a CO_2 humidified incubator overnight. After 14-18 h incubation the collagenase and cells were centrifuged at 2000 rpm for 10 min. The cells were resuspended, and grown in Dulbecco's modified eagle medium (DMEM) supplemented with 10% (v/v) foetal bovine serum (FBS) and 2 mM L-glutamine, supplemented with 0.625 µg/ml ampotericin B and 100 i.u./ml penicillin and 100 µg/ml streptomycin, in a T75 tissue culture flask.

Routine Cell Culture

Primary fibroblasts were used within 3–9 passages. Primary normal oral fibroblasts were maintained in antibiotic free DMEM containing 10% (v/v) FBS, and 2 mM L-glutamine. The primary fibroblasts were routinely grown in T175 treated culture flasks. Fibroblasts isolated from OSCCs were cultured in the above media supplemented with penicillin and streptomycin (100 i.u.ml and 100 µg/ml, respectively). Human dermal normal fibroblasts were cultured in fibroblast growth media with additional fibroblast supplement (Promocell, UK) and supplemented with penicillin and streptomycin (100 i.u./ml and 100 µg/ml) and 0.625 µg/ml ampothericin B. Fibroblast culture media was changed once a week.

Cell lines, unless otherwise stated, were cultured in DMEM media containing 10% (v/v) FBS with 2 mM L-glutamine. Cal27 cell line was grown in DMEM with high glucose content (4500mg/ml glucose and L-pyridoxine.HCl). SCC4 cell line was cultured in medium consisting of DMEM: F12 Ham's Nutrient Media supplemented with 400 ng/ml hydrocortisone, 2mM L-glutamine and 10% (v/v) FBS. All cell lines were routinely cultured in T75 flasks, passaged once a week and the culture media was changed twice a week.

When confluent, all primary cells and cell lines were passaged using trypsin/EDTA (trypsin/ ethylenediaminetetraacetic acid. The cells were washed twice with phosphate buffered saline (PBS), and an appropriate amount of trypsin/EDTA was added according to the flask size (2 ml for T175, 1.5 ml for T75, 600 µl for T25, and 300 µl for 6 well plate), and the flask was placed in the incubator for 2-5 min. After separation of cells from the culture flask or plate, serum

containing media was used to neutralise the enzymatic action of the trypsin/EDTA. The cell suspension was then centrifuged at 1000 xg for 5 min, resuspended in fresh culture media and the appropriate amount was placed in a new flask to grow.

All cells were incubated at 37 ˚C with 5% (v/v) CO_2. Around every 3 months, all cells were checked for the presence of mycoplasma using the EZ- PCR mycoplasma kit (GeneFlow) on conditioned media from the cells.

Freezing down cells for cryoprotecting

Cell pellets were resuspended in a freezing down media containing 10% (v/v) DMSO (dimethyl sulfoxide), 50% (v/v) FBS and 40% (v/v) cell specific culturing media so that the media contained around <5 x 10^5 cells per ml. Cryovials containing 1 ml of the cell suspension were placed in a Nalgene 'Mr Frosty' freezing container (ThermoScientific), filled with isopropanol to allow slow freezing of the cells, of -1^oC per minute. The freezing container was placed at 80 ^oC for 24 h before the cryovials were placed in liquid nitrogen for long term storage. To recover the cells were thawed quickly and mixed with pre-warmed culture media, centrifuged at 1,000 xg for 5 min, to remove the DMSO, then resuspended in culture media and grown in T25/T75 flasks depending on the number of cells.

Seeding cells onto coverslips.

Prior to seeding the cells the coverslips were sterilised in the culture plates by the addition of 70% industrial methylated spirits (IMS) and incubated for 20 min, the plates were then left to dry and subsequently washed twice with PBS to remove any IMS. Cells were seeded normally (250,000) into six well plates containing coverslips.

Cell line conditioned media preparation

Cal27, H357 or $\alpha_v\beta_6$ stably transfected H357 cells were seeded at 1x10^6 cells/flask in T25 (high cell density) or T75 (low cell density) and left overnight. The media was then replaced with 1 ml (high cell density) or 3 ml (low cell density) of the respective serum free media, after 24 h this conditioned media was collected for immediate use or stored at −20 ^oC for future use within 3 weeks.

TGF-β1 Treatment

Oral fibroblasts were seeded at 250,000 cells/well in a 6-well plate. They were grown in serum free DMEM plus L-glutamine 24 h before being subsequently treated with 0.5-50 ng/ml recombinant human TGF-β1 (reconstituted in 4 mM HCl plus 1 mg/ml BSA) for 48 h. After treatments the media was collected, and stored at −20 ^oC for future use in a cell migration assay.

siRNA and pre-miRNA Transfection

Primary human oral fibroblasts were transfected in a 6 well plate at a density of 250,000 cells/well (around 60% confluency). Versican siRNA, myocardin related transcription factor- B (MRTF-B) siRNA, premiR-143, premiR-145 and antisense miR-145 oligonucleotides (Life technologies) were transiently transfected into oral fibroblasts using an oligofectamine (Invitrogen) lipid-based protocol, scramble siRNA and silencer siRNA #1, silencer siRNA #2, Cy3 fluorescently labelled conjugated silencer siRNA #1 (negative siRNA non-targeting controls) or negative premiR control #1 (Life Technologies) were used as controls. 50nM synthetic precursor microRNA or siRNA were mixed with Oligofectamine and OptiMEM I (Life-Tech) and added to the cells. After 4 h, 500 µl 20% (v/v) FCS DMEM plus L-glutamine or OptiMEM, depending on whether serum starvation was required, were added. Cells were incubated in the transfection media for 24 h, and subsequently used in functional assays and/or treated with 5 ng/ml TGF-β1.

Fibroblast conditioned media preparation

Conditioned media was collected for downstream use in paracrine cancer cell transwell migration assays. Media was collected from fibroblasts that had been transfected (section 1.2.1.10) then treated with TGF-β1 for 48 h (this was the same media that was used to treat the fibroblasts and was exposed to the cells for 48h). The fibroblasts which were treated with TGF-β1 for 48 h then subsequently transfected were grown in the transfection mixture for 24 h, then the media was replaced with 1 ml serum free media to generate conditioned media and to allow downstream transfection effects to occur. Conditioned media was frozen for a maximum of 3 weeks, then before use it was thawed to 37 ^{o}C and centrifuged at 2500 xg.

Harvesting Cells

Cells were then harvested using trypsin/EDTA (Sigma), collected in 0.1% (w/v) bovine serum albumin (BSA) plus DMEM and L-glutamine, washed in phosphate buffered saline (PBS) and pelleted for downstream RNA/protein analysis. To examine extracellular versican levels fibroblasts were harvested via scraping into 30 µl RIPA (Radio-Immunoprecipitation Assay) buffer (Sigma) on ice.

Cell Migration Assay

Conditioned media collected from the transfected and TGF-β1 (5 ng/ml) treated fibroblasts was thawed, passed through a 0.2 µM filter and 500 µl placed into the bottom of the well in a 24-well plate. H357 cells, previously serum-starved using DMEM supplemented with L-glutamine, were resuspended into 0.1% (w/v) BSA DMEM plus L-glutamine (2 mM) and seeded at a density of 100,000 cells/well into the top of the migration transwell chamber (Scientific Laboratory

Supplies). The chamber was placed on top of filtered conditioned media (through a 0.2 μm pore) from untreated, treated and/ or transfected oral fibroblasts. Cells were allowed to migrate for ~18 h at 37^{O}C and 5% (v/v) CO_2. The transwell chambers were swabbed to remove non-migrated cells in the top of the chamber, washed in PBS and placed in 100% (v/v) methanol for 10 minutes to fix the migrated cells to the underside of the membrane. These cells were then stained using 0.1% (w/v) crystal violet, placed in PBS and imaged at 4 randomly selected fields of view per transwell at 40x magnification using a light microscope. Migrated cells were then counted using the ImageJ Software.

Collagen I gel contraction assay

Collagen gels were prepared, on ice, by the mixing rat tail collagen I in a 1:1 ratio with 10X concentrated DMEM. Transiently transfected or un-modified normal human primary oral fibroblasts were resuspended in 10% (v/v) FCS DMEM (and L-glutamine) and added to the collagen at a density of 250,000 cells, or 100,000 per well, and 0.5 M NaOH was used to neutralise the solution. The gel mixture was placed into a 24-well plate and incubated at 37 ^{O}C with 5% (v/v) CO_2 for 45 min. DMEM with 10% (v/v) FBS was then added to the gels and left to incubate for 4 h, after serum starvation overnight. The gels were carefully detached from the sides of the wells and treated with 5 ng/ml TGF-β1. Photographs were taken at 24 h and 48 h, the contractility of the gels was then measured by the measuring the diameter of the gel, using ImageJ.

2.2.2 *Molecular cloning*

Preparation of versican promoter- pGL3-basic construct

Total DNA was isolated from fibroblasts using Wizard® Genomic DNA Purification kit (Promega). The putative versican promoter region was amplified from human genomic DNA. Primer design was based on -653 +118 around the transcriptional start site (Rahmani *et al*., 2005; Nasos, Zimmermanng, & Iozzon, 1994; Read *et al*., 2007) including sequences for Mlul I and Kpn I restriction endonucleases. The following primers were used:

Long Forward 5’ AATAGGTACCGAATTCTTACACTTTCCCTCTAGGTCC

Short Forward 5’ AATAGGTACCGAATTCTTACATTTCCC

Long Reverse 5’ AATAACGCGTTGTCCACAACACCTAATGTTCT

Short Reverse 5' AATAACGCGTTGTCCACAACACCTAA

Standard PCR was performed with Phusion DNA polymerase (NEB), using Phusion buffer 5X HF. Amplification was carried out using a thermal cycle of 98 ^{o}C for 30 s, then 40 cycles of: 98 ^{o}C for 10 s, 60 ^{o}C for 30 s, 72 ^{o}C for 30 s and a final extension 72 ^{o}C for 10 min.

The resulting amplicon was subsequently ligated into a luciferase reporter vector (pGL3-basic vector; Promega), which contains a gene for ampicillin resistance. The ~750 bp PCR product was purified using a PCR clean up column (Qiagen) before double digestion with restriction endonucleases Mlu I and Kpn I (NEB) buffered by NEB buffer 2 and incubated at 37 ^{O}C for ~6 h. The pGL3b vector was also subjected to double digestion using the same enzymes. The two digested DNA fragments were then electrophoresed on a 1% (w/v) agarose gel and the correct band size was excised and the DNA was extracted using a gel extraction kit (Bioline). The linearised vector and DNA product were then ligated at different ratios of 1:3 and 1:5 (vector: product) using T4 ligase (NEB). Ligation mixtures were then transformed in chemically competent E.Coli.

Transformation of the Construct into Chemically Competent E.Coli.

The ligation mixture (2 µl) was added, on ice, to DH5-alpha chemically competent E. coli (NEB) for 30 min. The cells were then heat shocked at 42 ^{O}C for 30 s, and placed back on ice for 5 min. The cells were then grown in SOC (super optimal broth with catabolite repression) medium (NEB) shaking vigorously (250 rpm) at 37 ^{O}C for 1 h before being spread on amplicilin (100 µg/ml) LB (Lysogeny Broth) plates, to select for amplicin resistance, and incubated at 37 ^{O}C overnight. Colonies were randomly selected and grown overnight in amplicilin LB broth at 37^{o}C with shaking.

Colony Screening

Plasmid miniprep from selected colonies was performed using QIAprep Spin Miniprep Kit (Qiagen). These preps were then subjected to a number of screens to assess whether the cloned sequence was integrated into the plasmid. Firstly, a PCR using the original primers used to amplify the promoter region was performed using GoTaq® Flexi Polymerase (Promega) supplemented with 1.2 mM $MgCl_2$. Secondly an overnight digest was performed on the preps using Mlu I. The PCR products/ digested DNA were electrophoresed on 1.2% (w/v) agarose gel to visualise the size of the DNA. Minipreps which appeared positive for the cloned sequence

were verified by DNA sequencing, performed at Core Genomic Facilities, University of Sheffield Medical School, using pGL3-basic primers forward RVprimer3 5´-CTAGCAAAATAGGCTGTCCC-3´ and reverse GLprimer2 5´-CTTTATGTTTTTGGCGTCTTCCA-3´ (Sigma) (sequences were obtained from Promega pGL3-basic guidelines). Sequences were viewed using Finch TV software and analysed using Blast (NBCI).

Luciferase Reporter Assay

pGL3-basic luciferase reporter vector containing the versican promoter region, VCANp-Luc (0.1, 0.5, 1, or 10 µg) was co-transfected with Renilla plasmid control (0.1 µg) using Fugene 1 µl/0.3 µg (Promega) into B16 cell line, supplemented with 0.5% FCS, for 48 h. VCANp-Luc and Renilla control vector transfected cells were also co-transfected with premiR-145, premiR-143 or pre-miR negative control #1 (50 nM), to examine the transcriptional effect miR-145 has on the versican promoter. Cells were lysed using passive lysis buffer (Promega) and Renilla and Firefly Luciferase activity was measured using a dual-luciferase reporter assay kit (Promega) using a Glowmax microplate luminometer (Promega). Firefly luciferase levels were normalised to Renilla luciferase to assess promoter activation.

2.2.3 *Molecular analysis*

Primer design for quantitative Real Time PCR (qRT-PCR)

The primers used for SYBR green qRT-PCR are mentioned in table 1.2. Some sequences for the primers were taken from previous publications, primer sequences without references were designed in house. The transcript sequences were found using mRNA RefSeq (PubMed, NBCI) database and isoform domains were located using Ensemble. Primers for SYBR Green qPCR were designed so the product would be around 100 nucleotides, and where appropriate they were intron spanning. Primers were designed to be sequences between 18-23 nucleotides in length. Primers were *in silico* validated via the primer BLAST tool (NCBI) and were checked to be appropriate for PCR use with a GC content of 35–65%, a melting temperature of 60–68^{o}C and minimal or no primer dimer/ secondary structures formation.

Primer validation and measuring primer efficiency

Primers were *in silico* validated using the primer BLAST tool (NCBI). A dissociation melt curve step was used when performing qRT-PCR to ensure the primers were only amplifying one product. The amplication efficacy was calculated for each set of primers by creating a standard curve via serially diluting cDNA generated using 2 µg RNA starting template. The CT values generated from a qRT-PCR reaction were plotted against the log of the amount of starting

genetic material. The slope of this graph was calculated using graphpad prism 6. This number was then used in the ThermoFisher qPCR amplification efficiency calculator to work out the % efficiency and the amplification factor which can be incorporated into delta delta CT method, specific to each primer set when calculated the relative quantification of a certain gene.

Real Time quantitative PCR (qRT-PCR) Analysis

Total RNA was extracted from pelleted fibroblasts using the RNeasy (Qiagen) kit according to the manufacturer's instructions. RNA was quantified using a Nanodrop 1000 spectrophotomer (Thermo). RNA isolated from normal and diseased bladder urothelium and stromal tissue was provided by Dr Jim Catto. RNA (100 ng) was then reversed transcribed using a high capacity cDNA Reverse Transcription kit (Applied Biosystems), according to the manufacturer's protocol using a DNA engine Peltier Thermal cycler (MJ Research). Specific mature microRNAs were reverse transcribed using 10 ng of RNA using specific Taqman Reverse Transcription microRNA probe/primers for miR-143, miR-145 and RNU 48 as a control (Applied Biosystems). cDNA was then used in SYBR green or Taqman real time quantitative PCR reaction using a 7900HT fast Real Time-PCR system. Sequences of primers used for SYBR analysis (Sigma) are supplied in table 1.1. Taqman probes for microRNA-143, miR-145, RNU 48 and versican isoforms V0, V1, V2 and V3 were purchased from Applied Biosystems. Quantification was calculated using delta delta CT values and were normalised to endogenous controls U6 (SYBR green), β2macroglobin (B2M) or RNU 48 (Taqman).

qRT-PCR analysis

The quantification of gene expression was calculated via the delta delta C_T method ($2\Delta\Delta C_T$) (Livak & Schmittgen, 2001). The C_T value is the number of thermal cycles at which the amount of fluorescence reaches a detectable threshold. It corresponds to the amount of template at the start of the reaction.

$$2^{-\Delta\Delta CT} = \Delta C_T(test) - \Delta C_T(control)$$

$$\Delta C_T = C_T(target) - C_T(reference\ gene: U6)$$

Amplification efficiencies for each set of primers were assessed by using a standard curve of cDNA. 2 µg RNA was reverse transcribed and serially diluted to create 6 standard dilutions, which were used in a qRT-PCR reaction for a particular SYBR green primer. CT values were plotted on a semi-log scale the line of best fit was calculated (Bio-Rad). The efficiency (E) is calculated:

$$E = 10^{-1/slope}$$

Which can be made into a percentage:

$$\%\, E = (E - 1) \times 100\%$$

Only primer sets with <80% efficiency were used in this study (see appendix).

Western Blotting

Cell lysates were prepared by adding 30 µl RIPA buffer supplemented with complete mini protease inhibitor cocktail (Roche) and benzonuclease (Sigma) to cell pellets washed in PBS. Alternatively the RIPA buffer was added directly to the wells to lyse the cells, in order to not lose any extracellular matrix components. The protein concentration was then assessed using a bicinchoninic acid (BCA) assay kit (Thermo) using BSA to generate a standard curve. Absorbance of standards and test samples was measured at 595 nm using a POLARstar Galaxy spectrophotometer (BMG LABTECH).

If appropriate, total protein lysates were treated with chondroitinase ABC (Sigma; 0.003–0.01 units/ml) at 37^{o} C for 3 h, or on ice as a control. Total protein (20-30 µg) was resolved by 3–8% (w/v) SDS-polyacrylamide gel (Life-Technologies) electrophoresis (SDS-PAGE) in Tris-acetate buffer (Life-Technologies). The protein was transferred onto a nitrocellulose membrane (Millipore) by wet transfer or iBlot dry transfer (Invitrogen), blocked with 5% (w/v) milk and 3 % (w/v) bovine serum albumin (BSA) in Tris buffered saline with 0.05% (v/v) Tween 20 (TBS-T) to prevent non-specific binding. The primary antibody was diluted in aforementioned blocking solution and incubated at 4 ^{O}C overnight. The membrane was washed 3 times (for 5 min each) with TBS-T, and subsequently incubated with a horseradish peroxidase- conjugated (HRP) secondary antibody diluted 1 in 3000 in the above blocking solution, for 1 h at room temperature. The membrane was then washed 3 times in TBS-T, and developed using enhanced chemoluminescent (ECL) Western Blotting Substrate (Pierce) and HRP activity of the secondary antibody was exposed on an x-ray film (Thermo Scientific) and developed using a Compact X4 Developer (Xograph Imaging Systems).

Nitrocellulose membranes were stripped of antibodies by incubation in 50 ml stripping buffer (62.5 nM Tris, 2% (v/v) SDS, 100 mM β-mercaptoethanol) at 50 ^{o}C for 30 min. The membranes were then washed 4 times with TBS-T, and blocked and reprobed as above.

Densitometry

The size of detected bands by immunoblotting were quantified used ImageJ analysis software. The scanned blot was converted to an 8- bit image and boxes were drawn, of the same size, around each band assigning them a lane using the 'plot lanes' command. The area of each analysed lane was measured, which corresponds to the size of the band. These were adjusted against the size of the loading control bands to calculate the relative protein quantification and the process repeated for each repeat.

Immunocytochemistry

For visualising the α smooth muscle actin stress fibres the fibroblasts were stained with a FITC conjugated anti-alpha smooth muscle actin mouse antibody (clone 1A.4; 1:100). Fibroblasts were seeded on coverslips (see section0) and transfected and/or treated. The coverslips were then removed, and the cells remaining in the culture plate could be harvested and used for molecular analysis. The fibroblasts on the coverslips were washed with PBS twice and subsequently fixed using 100% methanol for 10 min. Fibroblasts were then permeabilised by using 4 mM sodium deoxycholate (diluted in PBS), by washing with it once and then keeping the coverslips in 4 mM sodium deoxycholate for 10 min. Coverslips were then blocked in 2.5% (w/v) BSA in PBS for 30 min before incubating in 25 µl FITC-conjugated αSMA diluted in blocking buffer antibody overnight in the dark at 4 ^{o}C. After antibody incubation, the coverslips were washed twice with PBS, keeping the coverslips in the dark to prevent the FITC bleaching. The coverslips were mounted on normal microscope slides using mounting media containing DAPI (vectorshield). The slides were viewed using a Ziess Axioplan 2 fluorescence light microscope at 40x, and imaged using Proplus 7.0.1 image software. The fluorescence intensity was measured using ImageJ software. The background fluorescence was subtracted, pixel intensity measured and normalised to the cell number to give the quantified fluorescent intensity per cell.

2.2.4 *Statistical Analysis*

Where appropriate data was subjected to a two- tailed student's t-test to test for statistical significance. The student's t-test was either paired or unpaired, paired was used when the same patient cells were used in the same experiment, but treated or transfected differently, and unpaired was used when the cells/ RNA being compared were taken from different patients. T-tests were carried out in Microsoft excel.

All graphs were drawn and other statistical analyses were performed, using GraphPad Prism 6. The Pearson correlation coefficient was used to assess the correlation between mRNA expression of αSMA and V0/V1 versican in CAFs. Mann Whitney U statistical tests were used to

assess the difference in expression patterns between CAFs and NOFs for specific genes. Multiple ANOVAs were used for assessing any statistical difference between subsets of CAFs and NOFs. Error bars on graphs represent the standard error mean (SEM), unless otherwise stated.

2.2.5 *Ethical Approval*

The isolation of human primary normal fibroblasts from dermal, gingival or buccal tissue and from OSCCs has been ethically reviewed by Sheffield Research Ethics Committee (09/H1308/66 and 13/NS/0120, respectively).

Chapter 3: The characterisation of stromal oral fibroblasts.

3.1 *Aims and objectives*

The aim of the work presented in this chapter was to characterise the response of normal oral fibroblasts (NOFs), and fibroblasts isolated from OSCCs to TGF-β1 or conditioned medium from cancer cells, in inducing the myofibroblast phenotype. The chapter objectives were to optimise the conditions of the TGF-β1 and conditioned media (from oral cancer cell lines) treatments in CAFs and NOFs, by assessing the effect on the expression of markers of myofibroblast. In addition, work outlined in this chapter planned to compare the expression of myofibroblast markers and the miR-143/5 cluster between CAFs and NOFs, and its expression in induced myofibroblast.

3.2 *The characterisation of normal oral fibroblasts*

Fibroblasts are the most abundant cell type within the tumour microenvironment and have been reported to be responsible for promoting stromal remodelling and disease progression (Kalluri and Zeisberg, 2006; Bhomwick *et al*., 2004). There are many different subtypes of cancer associated fibroblasts, or CAFs, within the tumour microenvironment with different roles. Some are noted to be tumour suppressive and others types are known to actively promote a desmoplastic stroma and a more invasive tumour, for example the myofibroblast-like CAF.

In order to study the role of fibroblasts within the tumour microenvironment and to investigate any role microRNA-145 may possess in controlling tumour stromal interactions of fibroblasts, normal gingival fibroblasts were cultured and exposed to factors that are prevalent in the tumour microenvironment and that are known to promote changes in normal fibroblasts *in vitro* to them behave more like *bona fide* oral CAFs surrounding tumours.

TGF-β1, a growth factor with pleiotropic roles within the tumour microenvironment (Bierie and Moses, 2006), has been used to induce the oral myofibroblast phenotype in several previous studies (Smith *et al*., 2006, Sobral *et al*., 2011). Many studies in fibroblasts from different origins use TGF-β1 treatments ranging from 0.25 ng/ml to 10 ng/ml to induce a myofibroblast phenotype (Kojima *et al.,* 2010; Lewis *et al.,* 2004; Serini *et al.,* 1998; Thannickal *et al.,* 2003). Numerous have shown a TGF-β1 dose of 5 ng/ml sufficient to induce a myofibroblast phenotype (Desmoulière *et al.,* 1993; Grotendorst, Rahmanie, & Duncan, 2004; Yao *et al.,* 2011). Our lab also found that a concentration of 5 ng/ml TGF-β1 was sufficient for inducing a significant induction of the myofibroblast phenotype in the NOFs tested as judged by the expression of myofibroblast marker alpha smooth muscle actin (figure 3.1), so this dose was used subsequently in this study.

A time-course experiment of TGF-β1 treatment was performed to assess the changes over myofibroblasts markers over a 72 h treatment period. NOFs treated with 5 ng/ml TGF-β1 or serum free media for 24 h, 48 h, or 72 h. Fibroblasts were harvested and total protein lysate and RNA extracted for qRT-PCR for myofibroblast markers. After 24 h and 48 h TGF-β1 treatment caused αSMA to be significantly upregulated by ~13 fold, after 72 h αSMA levels were ~2.5 fold higher than their respective untreated control (figure 3.1A). Immunoblotting using a monoclonal antibody for αSMA showed that there was a small increase in αSMA protein with TGF-β1 treatment at each time point (figure 3.1B).

Additional myofibroblast markers, COL1A1 and FN1-EDA were also assessed at each time point of TGF-β1 treatment by qRT-PCR. In these NOFs, there was no significant difference in COL1A1 transcript levels at each time point between untreated and TGF-β1 treated fibroblasts. At 24 h TGF-β1 treated DENF319s had a ~1.1 fold, not significant, increase in COL1A1 transcript levels (figure 3.2A), compared with 48 h and 72 h were the COL1A1 transcript levels had decreased by ~0.8 and ~0.65 fold (not significant) relative to untreated at each of the time points, respectively. On the other hand TGF-β1 caused a significant increase by ~6, ~7.5, and ~4.5 fold in FN1-EDA transcript levels, relative to each untreated time point (figure 3.2B).

Immunoblotting total protein lysates from NOFs treated with 5 ng/ml TGF-β1, revealed that the treatment caused a trend of an increase in αSMA protein, quantified to be ~6 fold greater than untreated NOFs (figure 3.3 A and B).

αSMA is a contractile cytoskeletal component which contributes to the contractile nature of myofibroblasts, and helps to remodel the surrounding stromal environment (Hinz *et al*., 2001). Myofibroblasts use their contractility most obviously in wound healing to bring the granulation layer of wounds together, before re-epithelisation (Skalli and Gabbiani, 1988). The ability of fibroblasts to contract, therefore, is a marker of the myofibroblast phenotype, and contractility assays are commonly used to verify the phenotype of myofibroblast in *in vitro* studies. The contractility of fibroblasts was assessed here using a rat tail collagen I contractility assay. Fibroblasts were mixed with rat tail collagen 1 and DMEM, at a density 250,000 per well and left to form a gel. These gels were detached from the well and TGF-β1 containing media or serum free media was added for 48 h. The amount of contraction was assessed by the reduction of the gel diameter. TGF-β1 (5 ng/ml) was able to induce NOF contraction (figure 3.3C).

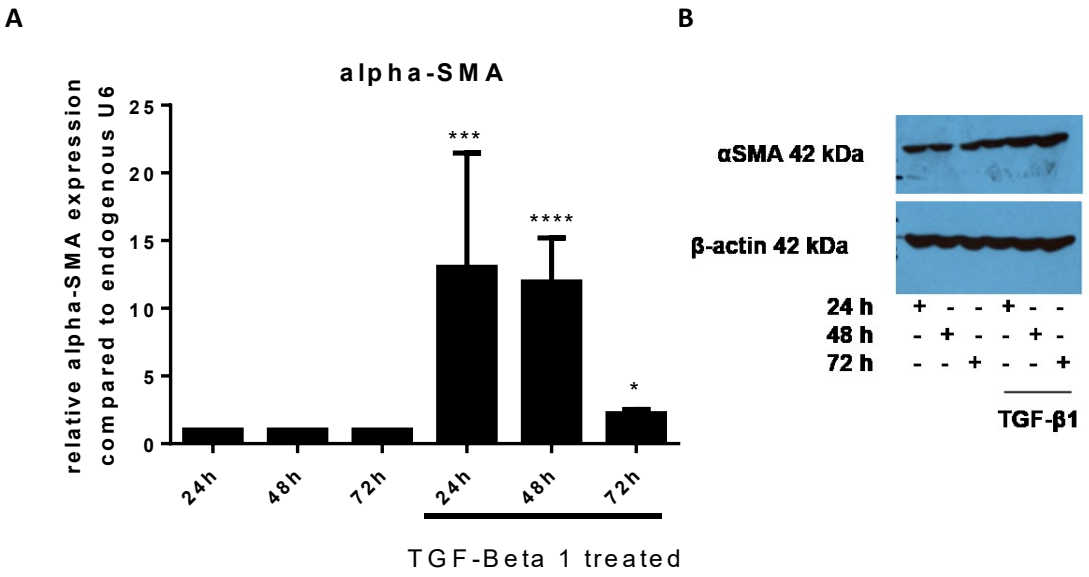

Figure 3.1: TGF-β1 treatment caused an increase in αSMA expression. DENF319 NOFs were seeded at a cell density of 250,000/ 6 well overnight, then serum starved for 20 h and subsequently treated with 5 ng/ml TGF-β1, or serum free media as a control for 24 h, 48 h and 72 h. After treatment fibroblasts were harvested, and used for molecular analysis. RNA was isolated, quantified and 100 ng was used in a total cDNA preparation. qRT-PCR was performed with the cDNA with primers to amplify αSMA and U6 as a reference gene (A). Cell pellets were lysed with protein RIPA lysis buffer and 20 µg total protein was resolved on a 3–8% (w/v) tris acetate gel and transferred to a nitrocellulose membrane for immunoblotting. A monoclonal αSMA antibody was used to detect αSMA protein and β-actin was used as a loading control (B) Each bar on the figure represents the mean relative quantification of αSMA transcript levels compared to endogenous U6, for each treatment relative to the relevant untreated timepoint. Statistical analysis was performed by a paired two tailed student's t-test, and statistical significance is shown on the figure by *p<0.05, ***p<0.001, ****p<0.0001 compared to the control at each timepoint. Error bars represent the SEM. N=3, independent experiments.

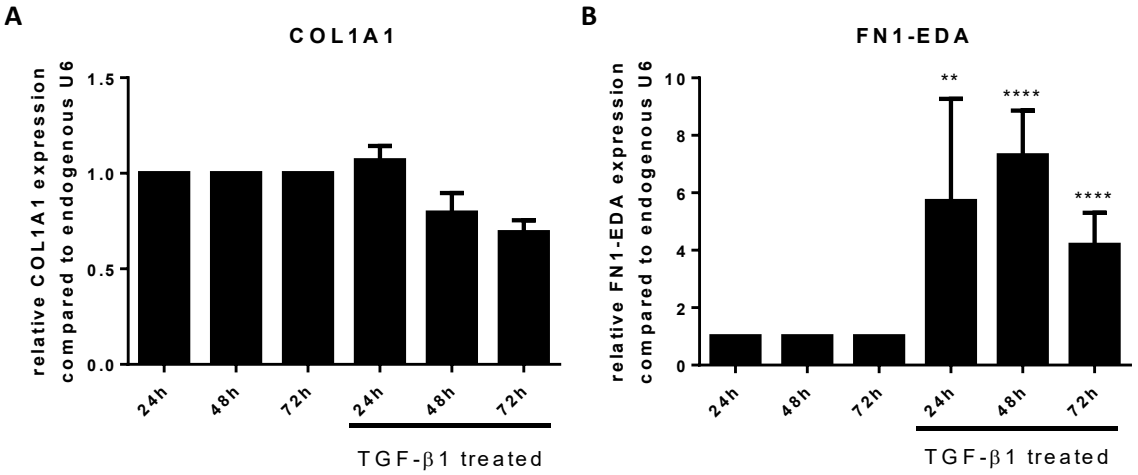

Figure 3.2: TGF-β1 treatment resulted in an increase in the expression of myofibroblast marker FN1-EDA, but not COL1A1 in DENF319s. DENF319 NOFs were seeded at a cell density of 250,000/ 6 well overnight, then serum starved for 20 h and subsequently treated with 5 ng/ml TGF-β1, or serum free media as a control for 24 h, 48 h and 72 h. After treatment fibroblasts were harvested, and used for molecular analysis. RNA was isolated, quantified and 100 ng was used in a total cDNA preparation. qRT-PCR was performed with the cDNA with primers to amplify COL1A1, FN1-EDA and U6 as a reference gene. Each bar on the figure represents the mean relative quantification of COL1A1 (**A**) and FN1-EDA (**B**) transcript levels compared to endogenous U6, for each treatment relative to the relevant untreated timepoint. Statistical analysis was performed by a paired two tailed student's t-test, and statistical significance is shown on the figure by **p<0.01, ****p<0.0001, compared to the control at each timepoint. The significance is compared to the untreated equivalent transfection. Error bars represent the SEM. N=3, independent experiments.

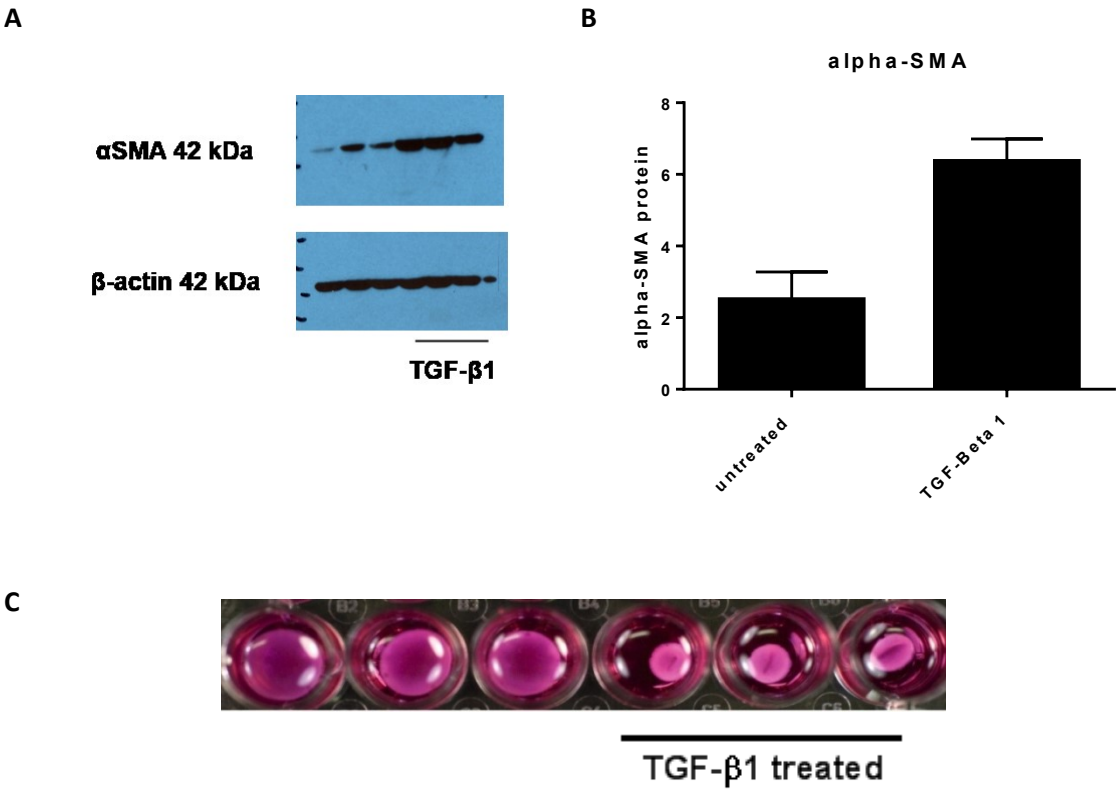

Figure 3.3: TGF-β1 treatment caused non-significant increase in αSMA protein in NOFs and induced fibroblasts contraction. (**A** and **B**) DENF319 NOFs were seeded at a density of 250,000 per six wells were treated with TGF-β1 for 48 h or serum free as a control. Cell pellets were lysed with protein RIPA lysis buffer and 20 µg was resolved on a 3–8% (w/v) tris acetate gel and transferred to a nitrocellulose membrane for immunoblotting. A monoclonal αSMA antibody was used to detect αSMA protein and β-actin was used as a loading control. In **A**, serum free treated cell lysates were run in lane 1 – 3, and TGF-β1 treated lysates were run in lane 4-6. The amount of αSMA detected was quantified by densitometry using ImageJ and shown in **B**. Error bars represent SEM. N=3, technical repeats. **C** NOFs were counted and resuspended in a 1:1 mixture of rat tail collagen 1 (in 0.1 M acetic acid): DMEM and neutralised with NaOH, at a density 250,000 NOFs per 300 µl collagen gel. The mixture was aliquoted into wells (300µl/well) and left to set in an incubator at 37 ^{o}C with 5% (v/v) $CO_{2.}$ After the gels had set, media was added to the wells at 4 h later the media was replaced with serum free media for overnight serum starvation. The gels were detached from the sided of the wells and treated with 5 ng/ml TGF-β1, or serum containing as a control. The figure shows a representative photograph of gels after 48 h TGF-β1 treatment (**C**). N=4, independent experiments.

Immunocytochemistry was performed on NOFs treated with 5 ng/ml TGF-β1 for 48 h using a FITC-conjugated αSMA antibody, to assess whether TGF-β1 treatment was able to induce αSMA stress fibres which are typical of the myofibroblast phenotype. NOFs (DENF319) were seeded onto coverslips, then TGF-β1 treated for 48 h. The coverslips were methanol fixed, permeabilised, incubated with FITC-αSMA antibody in PBS containing 2.5% (w/v) BSA and mounted onto slides using a DAPI containing medium to visualise the nucleus. A negative control was used to assess whether the fibroblasts possess any background fluorescence, this was performed by just blocking the fibroblasts on coverslips with the PBS containing 2.5% (w/v) BSA rather than incubating with the primary FITC-αSMA antibody. TGF-β1 treatment induced myofibroblast-like αSMA stress fibres compared to controls (figure 3.4). The negative control showed that the NOFs had little or no detectable auto-fluorescence.

Within the tumour microenvironment, it is thought that fibroblasts can be transdifferentiated into heterogeneous CAF phenotypes by a number of stimuli e.g. HGF, PDGF-BB, IL-8, EGF, ET-1, SDF-1, FN1-EDA, have all been published to play a role (mentioned in Chapter 1). *In vivo* it is likely a combination of cancer and stromal derived growth factors play an important role in the transdifferentiation of myofibroblasts. Therefore, the effect of oral cancer cell-derived secreted factors on the fibroblast phenotype was assessed by treating NOFs with OSCC cell lines Cal27, H357 and VB6 (H357 cell line stably overexpressing αvβ6) conditioned media. It has been previously published that a H357 cell line stably overexpressing αvβ6 integrin causes myofibroblast transdifferentiation in oral fibroblasts, which are capable of promoting the paracrine invasion of OSCC cells (Marsh *et al*., 2011). The effect of Cal27, an invasive OSCC cell line, H357 and VB6 conditioned media's effect on fibroblast phenotype was assessed by qRT-PCR and immunoblotting in NOFs and CAFs.

TGF-β1 was used as a positive control, which resulted in a ~13 fold increase in αSMA transcript levels in DENF316 cells (figure 3.5A). TGF-β1 treatment of NOFs also caused a ~2.25 fold and ~3.25 fold increase (not significant) in αSMA protein levels (figure 3.6 and 3.7). Conditioned media from Cal27 cell line caused a significant ~3.5 fold increase in αSMA transcript levels when used to treat NOFs (figure 3.5A), there was no increase in αSMA protein compared to untreated controls (figure 3.6A and B), immunocytochemistry visualised that was stronger αSMA staining in Cal27 treated cells, but there was no visual induction of αSMA stress fibres (figure 3.6C).

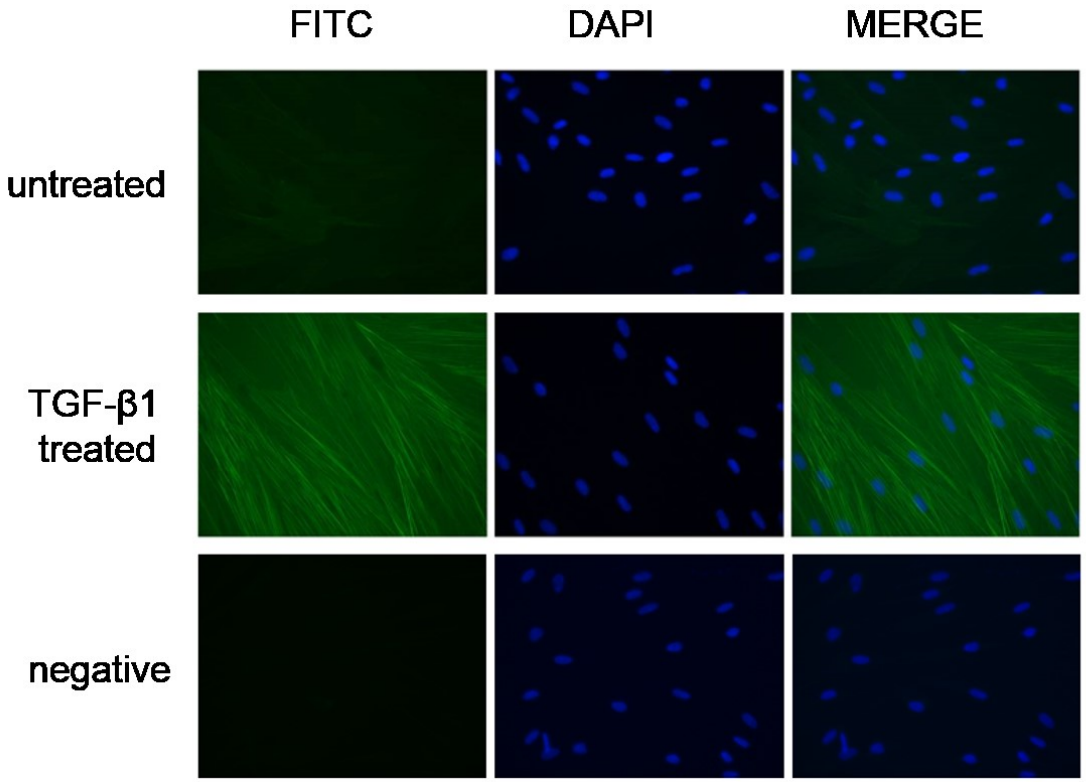

Figure 3.4: TGF-β1 induced αSMA stress fibre formation in NOFs. DENF319 NOFs were seeded at a density of 250,000 per 6 well plates with 8mm coverslips in the bottom, cells were serum starved for 20 h then treated with 5 ng/ml TGF-β1 for 48 h. The coverslips were washed in PBS, before being fixed in 100% methanol for 10 min, they were then permeablised using 4 mM sodium deoxycholate for 10 min, and blocked using 2.5% (w/v) BSA in PBS for 30 min before incubation with a primary FITC-conjugated αSMA antibody at 4 ^{o}C overnight. The coverslips were then washed in PBS before mounting on microscope slides using DAPI containing mounting medium. Fluorescent images were taken using a microscope, using Pro-plus 7 imaging software at 40x magnification. Negative control were coverslips incubated with 2.5% BSA in PBS rather than incubated with the FITC-αSMA antibody. Representative pictures are shown. N<3, independent experiments.

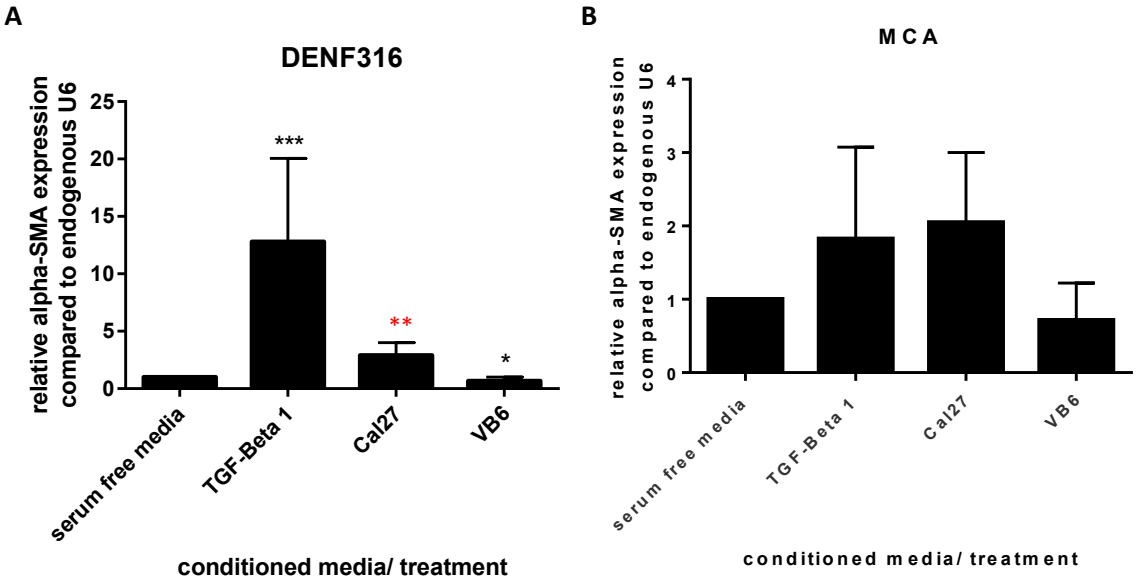

Figure 3.5: NOFs treated with conditioned media from Cal27 cancer cell line had an increased expression of αSMA. NOFs (DENF316; A) and CAFs (MCA; B) were seeded at a density of 250,000 per six well, serum starved for 20 h and treated with serum free media, 5 ng/ml TGF-β1, or conditioned media collected from a Cal27 or VB6, a H357 cell line stably transfected with the integrin αvβ6, for 48 h. The conditioned medias were collected by seeding $1x10^6$ of the cancer cell line in a T75 flask, overnight before conditioning serum free media for 24 h using serum free medium. After treatment, fibroblasts were harvested and the RNA was isolated and used to generate cDNA for qRT-PCR analysis using primers designed to amplify αSMA and U 6, as an endogenous control. Each bar on the figure represents the mean relative quantification of αSMA transcript levels compared to endogenous U6, for each treatment relative to untreated. Statistical analysis was performed by a paired two tailed student's t-test, and statistical significance is shown on the figure by *p<0.05, **p<0.01, ***p<0.001. The significance is compared to the αSMA levels in the fibroblasts treated with serum free media. Important significant data highlighted in red. Error bars represent the SEM. N=3, independent experiments.

VB6 and H357 cells were plated at two different densities and used to collect conditioned media for NOF treatment, allowing two different concentrations of conditioned media to be tested. The high density conditioned media was prepared by seeding $1x10^6$ cells in a T25 flask leaving overnight and placing 1 ml serum free media for 24 h to be conditioned. The low density conditioned media was prepared by seeding $1x10^6$ cells in a T75 flask, leaving overnight and placing 3ml serum free media for 24 h to be conditioned. VB6 conditioned media caused a significant decrease in αSMA transcript levels (by ~0.35 fold) (figure 3.5A), but an increase in αSMA protein levels (by ~1.25 fold not significant; figure 3.6 A and B) in NOFs. The high density VB6 and H357 conditioned media caused a ~1.2 fold increase (not significant) in αSMA protein, compared to untreated NOFs (figure 3.7). The low density VB6 conditioned media treatment (less concentrated), seemed to have caused a larger increase (not significant) in αSMA protein compared to the high density VB6 conditioned media. The low density conditioned media treatment caused a ~2 fold increase in αSMA protein in the NOFs, compared to untreated NOFs and the low density H357 conditioned media caused a trend of a ~1.4 fold increase in αSMA protein. Immunocytochemistry revealed that VB6 was unable to induce significant stress fibre formation (figure 3.6C), although there were slightly more individual fibroblasts with strong αSMA stress fibre staining.

The effect of conditioned media on the transdifferentiation of fibroblasts was also tested on MCA CAFs, fibroblasts isolated from an OSCC. NOFs treated with TGF-β1 and cal27 conditioned media caused an increase in αSMA transcript levels by ~1.8 fold and ~3 fold respectively (figure 3.5B; not significant) and the treatment of MCA CAFs with VB6 conditioned media resulted in a ~0.3 fold decrease (not significant) in αSMA in these fibroblasts. Interestingly, TGF-β1 treatment did not induce a significant increase in αSMA expression.

3.3 ***A comparison of normal oral fibroblasts to oral cancer associated fibroblasts***

The NOFs used in this study were isolated from human gingiva of patients from the Charles Clifford Dental Hospital commonly undergoing a tooth extraction, these cells are labelled with the prefix DENF or OF. Some NOFs, referred to as HNOFs, were used as comparisons for the CAFs were provided by Prof. Ken Parkinson. The CAFs were isolated from OSCC were from either the University of Campinas, Sao Paulo, (MCA, MC15 and MC6) or the Beatson Institute for Cancer Research (BICR-3, -59, -63, -70). BICR CAFs were isolated from either genetically stable or unstable OSCCs and previously well characterised (Hassona, *et al.,* 2014; Hassona *et al.*, 2013; Lim *et al.,* 2011).

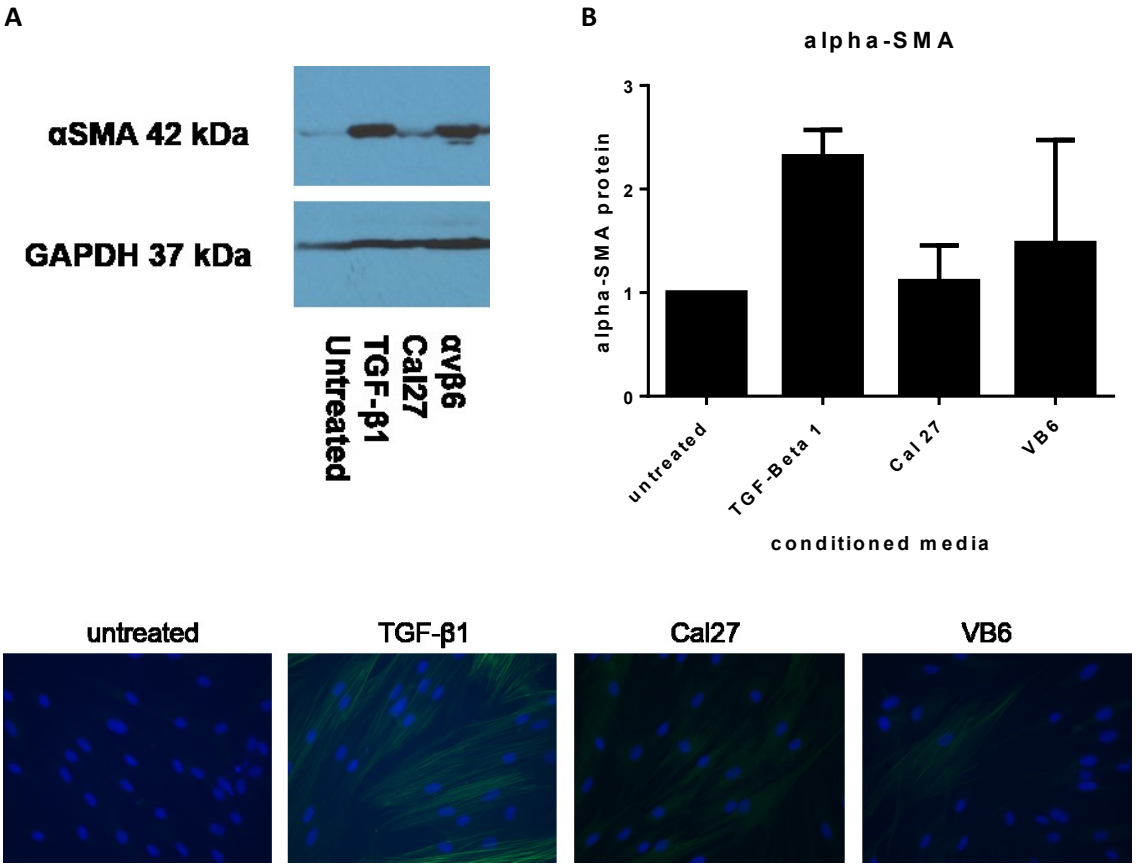

Figure 3.6: Conditioned media from VB6 cancer cell line caused no increase in αSMA protein, and no αSMA stress fibre formation. NOFs were seeded at a density of 250,000 cells per 6 well and left overnight before being were serum starved for 20 h and treated with serum free media, 5 ng/ml TGF-β1, or conditioned media from Cal27 or VB6, a H357 cell line stably transfected with the integrin αvβ6, for 48 h. (**A** and **B**) After treatment, fibroblasts were harvested and total protein lysates were extracted with RIPA buffer. Total protein was quantified using a BCA assay and 20 µg was resolved on a 3–8% (w/v) tris acetate gel, transferred to a nitrocellulose membrane for immunoblotting with a monoclonal anti- αSMA antibody and GAPDH as a loading control. Each bar on the figure represents the mean relative quantification of αSMA protein levels compared to endogenous GAPDH (**B**). Error bars represent the SEM. (**C**) Glass coverslips were placed in 6 well plates and 250,000 DENF319 NOFs were seeded as normal, serum starved and treated with serum free media, 5 ng/ml TGF-β1, or conditioned media from Cal27 or VB6. After treatment, the coverslips were washed in PBS, before being fixed in 100% methanol for 10 min, they were then permeablised using 4 mM sodium deoxycholate for 10 min, and blocked using 2.5 % (w/v) BSA in PBS for 30 min before incubation with a primary FITC-conjugated αSMA antibody at 4 ^{o}C overnight. The coverslips were then washed in PBS before mounting on microscope slides using DAPI containing mounting medium. Fluorescent images were taken using a microscope, using Pro-plus 7 imaging software at 40x magnification. Representative pictures are shown. N=2, independent experiments.

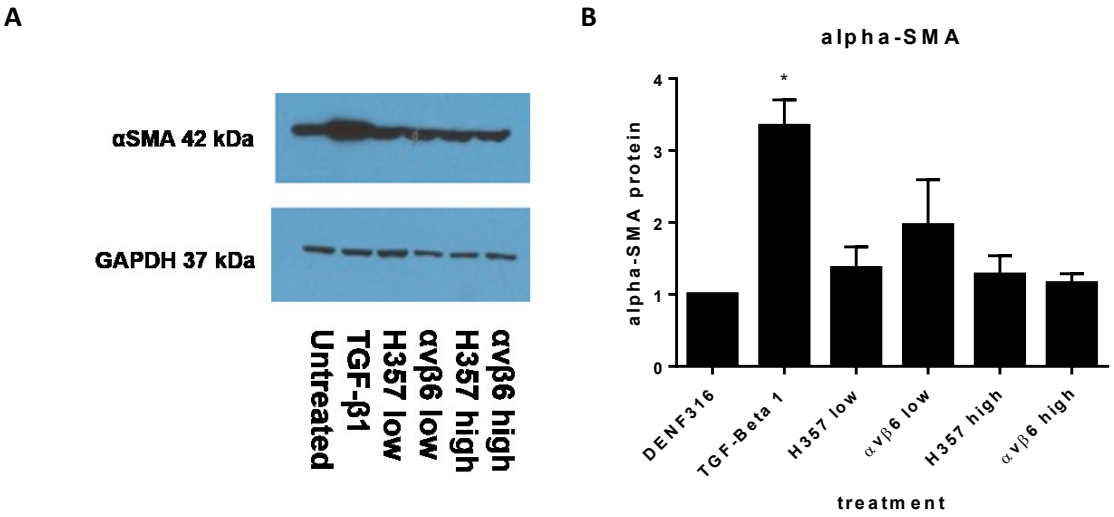

Figure 3.7: Conditioned media from cancer cell lines had no effect on αSMA protein. NOFs treated with were serum starved and treated with serum free media, 5 ng/ml TGF-β1, or conditioned media from H357 cancer cell lines and VB6, a H357 cell line stably transfected with the integrin αvβ6, at high and low density, for 48 h. The high density conditioned media was prepared by seeding $1x10^6$ cells in a T25 flask leaving overnight and placing 1 ml serum free media for 20 h to be conditioned. The low density conditioned media was prepared by seeding $1x10^6$ cells in a T75 flask, leaving overnight and placing 3ml serum free media for 20 h to be conditioned. After conditioned media treatment, fibroblasts were harvested and total protein lysates using RIPA buffer. Total protein was quantified using a BCA assay and 20 µg was resolved on a 3–8% (w/v) tris acetate gel, transferred to a nitrocellulose membrane for immunoblotting with a monoclonal anti- αSMA antibody and GAPDH as a loading control. Each bar on the figure represents the mean relative quantification of αSMA protein levels compared to endogenous GAPDH. Statistical analysis was performed by a paired two tailed student's t-test, and statistical significance is shown on the figure by *$p<0.05$. The significance is compared to the αSMA levels in the fibroblasts treated with serum free media. Error bars represent the SEM. N=3, independent experiments.

As there was a certain amount of biological variability amongst NOFs and CAFs, and to assess if CAFs are able to maintain their phenotype *in vitro,* a fibroblast screen of 10 NOFs and 10 CAFs was used to assess if there was any difference between the two groups, and within the subtypes of the groups i.e. between genetically stable and unstable CAFs, or between NOFs from Sheffield NOFs and BICR NOFs. The NOF and CAF population were assessed by examining the molecular myofibroblast markers by immunoblotting and qRT-PCR.

Immunoblotting for αSMA protein, revealed that there was no clear difference between αSMA expression between NOFs and CAFs. BICR31, BICR37 and BICR63 had a higher amount of αSMA immunoreactivity in these samples (figure 3.8). However, this immunoblot was only performed once, due to some of the CAFs being slow growing and time constraints. Also, not all CAFs and NOFs were compared in this small cohort.

On the other hand, all NOFs and CAFs available in this study were used in the qRT-PCR analysis. There was a small, not significant, increase (average ~1.1 fold) in αSMA expression in the CAF population compared to the NOFs (figure 3.9A). By comparing the αSMA expression of the different types of CAFs and NOFs from different institutions, there was no difference between NOFs and BICR NOFs and CAFs from genetically stable and unstable OSCC had a similar αSMA expression (figure 3.9B).

There was no difference in the average expression of FN1-EDA between NOFs and CAFs, but there was more variability between the difference types of CAFs and NOFs from different institutes (figure 3.10). BICR NOFs expression of FN1-EDA was ~3 fold higher than NOFs from Sheffield and CAFs from genetically stable OSCCs had on average ~3 fold higher FN1-EDA expression than CAFs from genetically stable OSCCs, however these trends did not reach statistical significance using a Mann Whitney U test.

For collagen 1a (COL1A1), CAFs on average had a ~1.2 higher expression (not significant) than NOFs (figure 3.11). BICR NOFs expression of COL1A1 was on average ~1.4 fold higher than NOFs, and CAFs from genetically stable OSCCs had ~1.3 fold higher expression of COL1A1 than CAFs from genetically unstable OSCCs (figure 3.11B), however this data was not found to be significant.

To investigate whether CAFs were able to release factors which stimulated paracrine migration of OSCC cancer cell lines, a transwell migration assay was used. Conditioned media from NOFs, DENF316 and DENF319, and CAFs from Brazil, MCA, and MC15 were collected and placed in the bottom of a transwell to be used as a chemo-attractant for stimulating cancer cell migration.

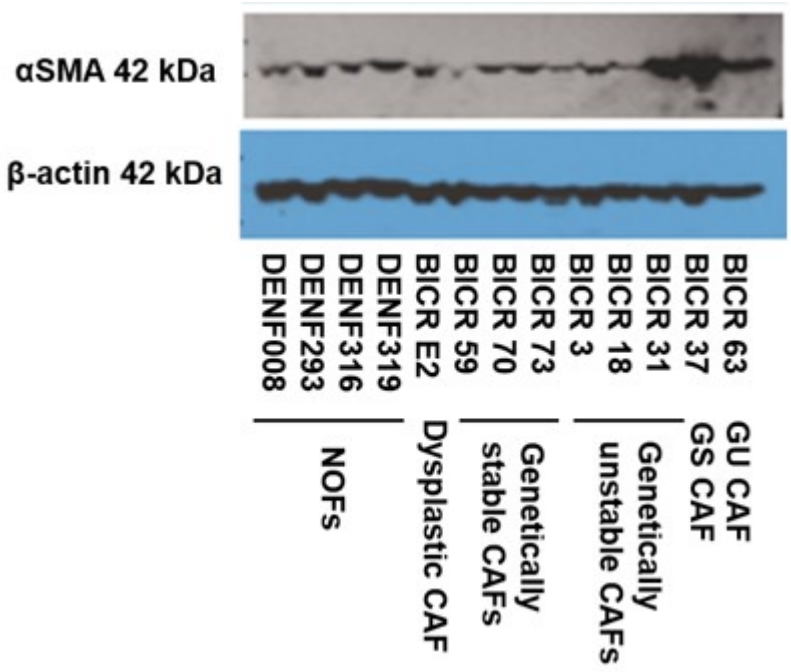

Figure 3.8: There was no difference in αSMA protein expression between CAFs isolated from genetically stable and unstable tumours, and NOFs. CAFs isolated from genetically stable OSCCs (N=4), unstable OSCCs (N=4), oral dysplasia (N=1), all originally from Prof Erik Parkinson and NOFs (from Sheffield; N=4) were cultured. Cell pellets from these cultures were then resuspended in RIPA protein lysis buffer and total protein was quantified using a BCA assay. Total protein lysates (20µg) were resolved on 3–8% (w/v) tris acetate gels and transferred onto nitrocellulose membranes for immunoblotting. A monoclonal anti-human αSMA antibody was used to detect αSMA levels in this CAF/NOF screen. β-actin was used as a loading control. N=1.

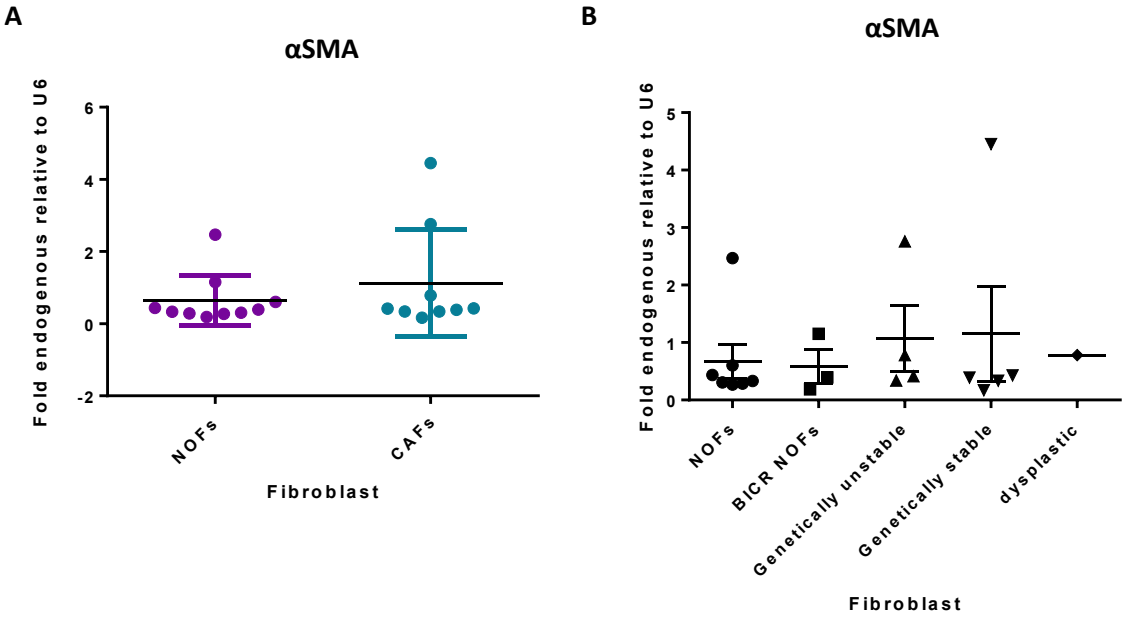

Figure 3.9: There was no difference in αSMA transcript expression between the NOFs and CAFs tested. Fibroblasts isolated from OSCC, CAFs (9), and NOFs (10) were grown, RNA was isolated and 100 ng was used to generate total cDNA for qRT-PCR analysis using primers designed to amplify αSMA, and U 6, as an endogenous control. The fold endogenous change of target αSMA compared to reference gene U 6 is plotted on each graph, each dot representing a different NOF/CAF. The line represents the mean fold endogenous for each set of fibroblasts. **A** compares the expression of αSMA between NOFs and CAFs, whereas **B** shows the expression of αSMA in different subsets of CAFs. Error bars display the SD.

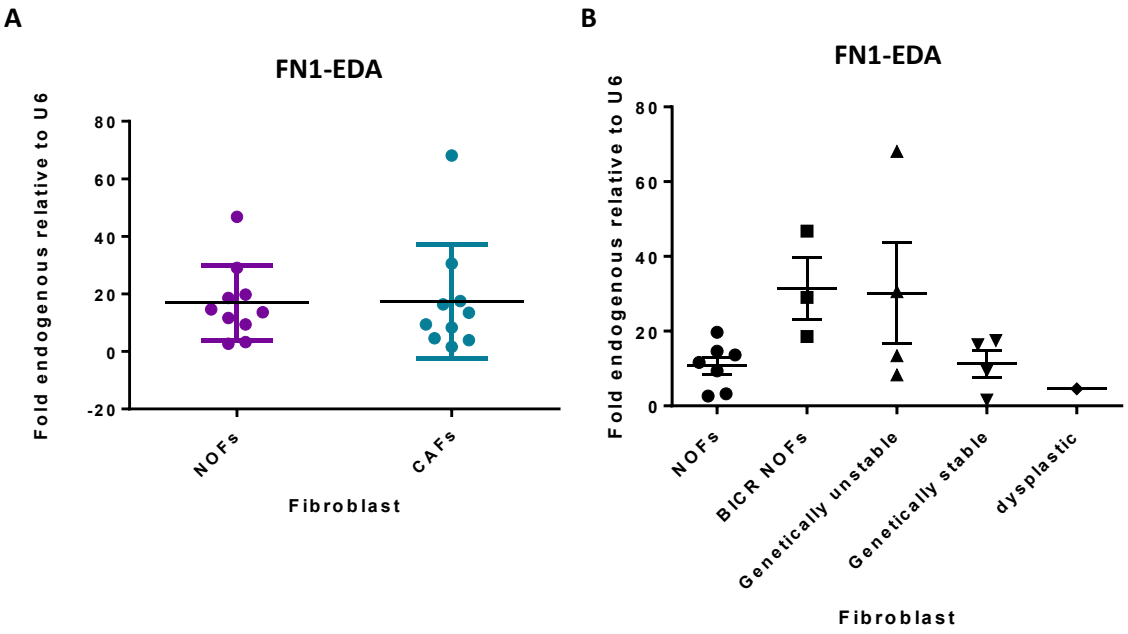

Figure 3.10: There was no difference in FN1-EDA expression between the NOFs and CAFs tested. Fibroblasts isolated from OSCC, CAFs (9), and NOFs (10) were grown, RNA was isolated and 100 ng was used to generate total cDNA for qRT-PCR analysis using primers designed to amplify FN1-EDA, and U 6, as an endogenous control. The fold endogenous change of target FN1-EDA compared to reference gene U 6 is plotted on each graph, each dot representing a different NOF/CAF. The line represents the mean fold endogenous for each set of fibroblasts. **A** compares the expression of FN1-EDA between NOFs and CAFs, whereas **B** shows the expression of FN1-EDA in different subsets of CAFs. Error bars display the SD.

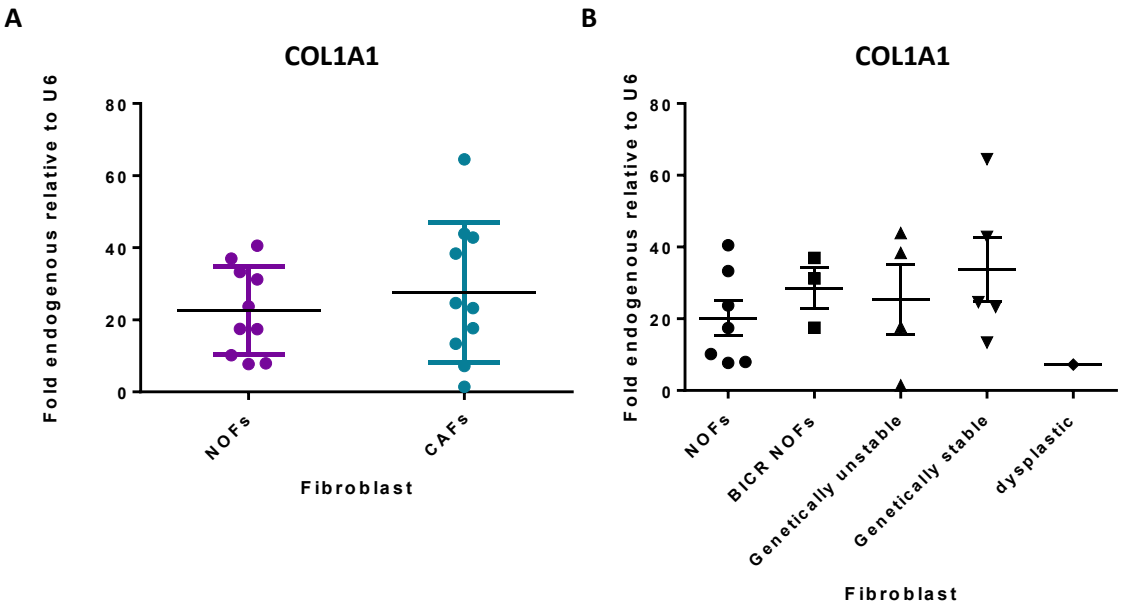

Figure 3.11: There was no difference in COL1A1 expression between the NOFs and CAFs tested. Fibroblasts isolated from OSCC, CAFs (10), and NOFs (10) were grown, RNA was isolated and 100 ng was used to generate total cDNA for qRT-PCR analysis using primers designed to amplify COL1A1, and U6, as an endogenous control. The fold endogenous change of target COL1A1 compared to reference gene U6 is plotted on each graph, each dot representing a different NOF/CAF. The line represents the mean fold endogenous for each set of fibroblasts. **A** compares the expression of COL1A1 between NOFs and CAFs, whereas **B** shows COL1A1s expression in different subsets of CAFs. Error bars display the SD.

H357 cells were seeded in the top of a transwell migration chamber with an 8 μM porous membrane to allow migration through to the media for 38 h. Cells were then fixed to the membranes and stained with 0.1% (w/v) crystal violet. Photographs were taken at 40x with a light microscope of 4 representative views, and counted to calculate relative migration. Conditioned media from DENF316, DENF319, MCA and MC15 all stimulated a similar level of H357 migration (figure 3.12).

3.4 *miR-143/miR-145 cluster in stromal oral fibroblasts*

miR-143 and miR-145 have been identified as tumour suppressors miRNAs in OSCCs. A previous study from our lab identified miR-145 as been downregulated in gingival fibroblasts in response to cigarette smoke extract, and that it plays a key role in stromal epithelial interactions in OSCC (Pal *et al*., 2011). miR-145 is also reported to be downregulated in invasive bladder CAFs and in scleroderma, an autoimmune fibrotic disorder. Therefore, it can be hypothesised that miR-145 plays a role in the myofibroblast-like CAF phenotype and is important in regulating stromal-epithelial interactions. To investigate this in this study, first the endogenous expression of miR-143 and miR-145 was assessed in NOFs and CAFs by qRT-PCR.

The expression of mature of both miR-143 and miR-145 was significantly higher in CAFs compared to NOFs in our study (figure 3.13). The expression of miR-143 in CAFs was ~20 fold higher than in NOF, and the expression of miR-145 was ~4 fold higher. The expression of miR-143 was ~2 fold higher in CAFs isolated from genetically stable OSCC compared to genetically unstable OSCCs. But the statistically significant result was the difference in miR-143 between CAFs isolated from genetically stable OSCC and the NOFs from Sheffield (~63 fold higher in CAFs; figure 3.14A). The expression of miR-145 in CAFs from genetically stable OSCC was ~13 fold higher than NOFs from Sheffield, again the only significant difference between the different subtypes in the cohort (figure 3.14B). There was ~1.6 fold higher expression of miR-145 in CAFs isolated from genetically stable OSCC compared to unstable OSCCs.

The effect of TGF-β1 on mature miR-145 expression was assessed by qRT-PCR. 4 NOFs, DENF316, DENF319, DENF008 and OF26 were each treated with TGF-β1, RNA isolated and used for specific miR-145 and RNU 48 cDNA preparation for qRT-PCR analysis. This revealed that TGF-β1 treated NOFs have a greater expression of mature miR-145 (figure 3.15). This difference was found to be statistically significant in 2 of the 4 NOFs tested, DENF319 (~1.5 fold increase) and OF26 (~1.4 fold increase). Although not found to be statistically significant, TGF-β1 treatment resulted in a

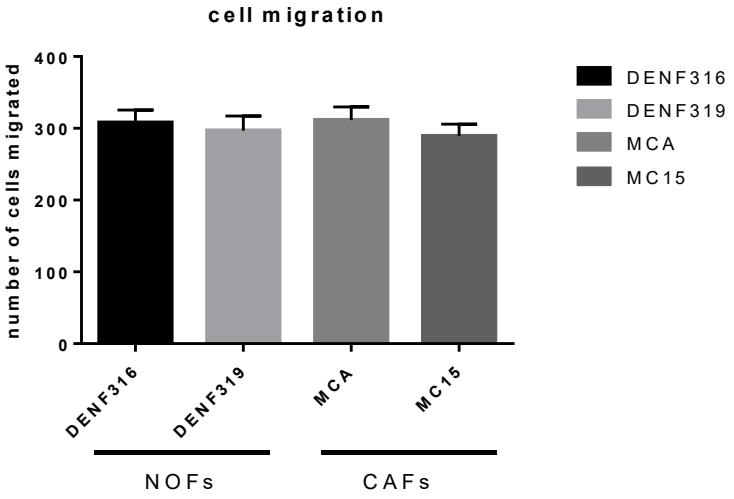

Figure 3.12: NOFs and CAFs stimulated a similar level of paracrine H357 migration. Conditioned media was collected from DENF316, DENF319 (NOFs), MCA and MC15 (CAFs). Conditioned media was prepared by seeding fibroblasts at a density of 250,00 per six well plate, leaving overnight and then leaving serum free media for 24 h to condition. The conditioned media was spun at >2500xg to remove cellular debris then placed in the bottom of a transwell migration assay plate. H357 cells were seeded at 100,000 cells per well into an 8µm porous transwell with 1 mg/ml mitomycin c and allowed to migrate for 38 h. The ability of the conditioned media to promote migration was assessed by methanol fixing cells attached to the membrane after 38 h, staining the cells with 0.1% (w/v) crystal violet, taking photographs at 40x, and calculating the average number of cells in the representative photographs. Error bars represent the SEM. N=3, independent experiments.

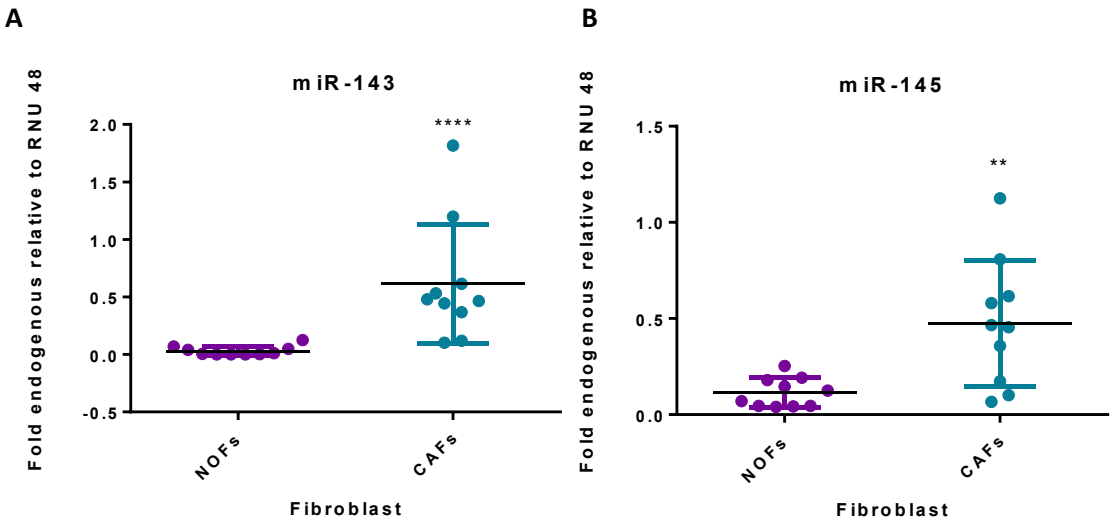

Figure 3.13: CAFs had a greater expression of miR-143 and miR-145 than NOFs tested. Fibroblasts isolated from OSCC, CAFs (10), and NOFs (10) were grown, RNA was isolated and 10 ng was used to generate cDNA for qRT-PCR analysis using primers designed to amplify miR-143, miR-145 and RNU 48, as an endogenous control. The fold endogenous change of target miR-143 (**A**) or miR-145 (**B**), compared to reference gene RNU 48 is plotted on each graph, each dot representing a different NOF/CAF. The line represents the mean fold endogenous for each set of fibroblasts. Statistical analysis was performed by Mann-Whitney test, and statistical significance is shown on the figure by **p<0.01, ****p<0.0001. Error bars display the SD.

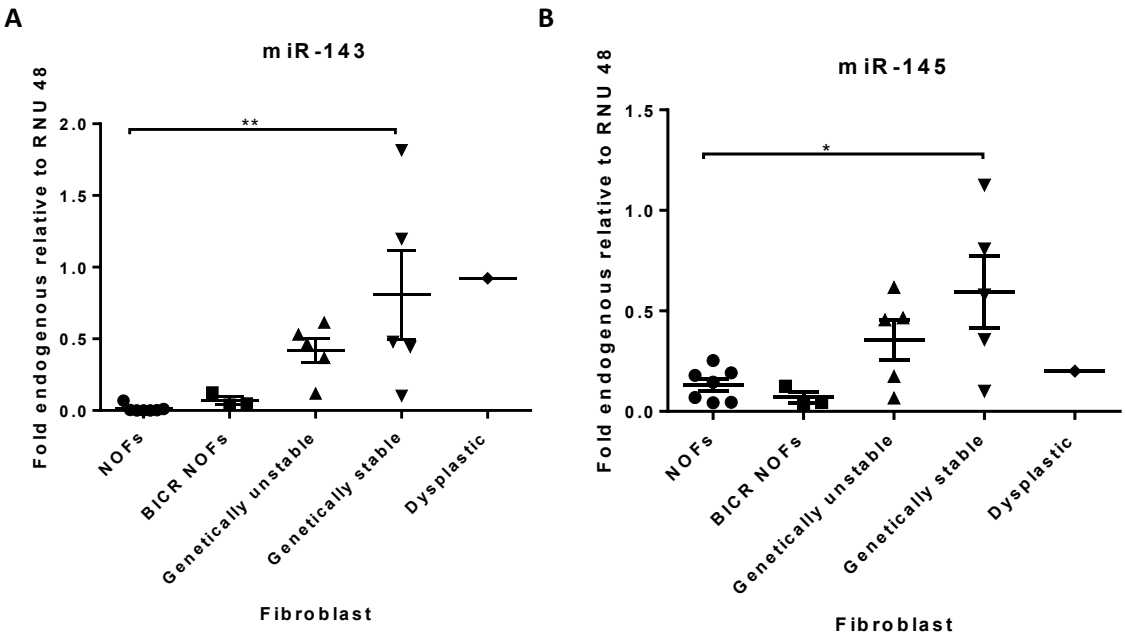

Figure 3.14: miR-143 and miR-145 expression was higher in CAFs isolated from genetically stable compared to NOFs. CAFs isolated from genetically stable OSCCs (N=5), unstable OSCCs (N=5), oral dysplasia (N=1), normal gingiva (BICR NOFs; N=3) all originally from Prof Ken Parkinson and NOFs (from Sheffield; N=7) were cultured. RNA was isolated and 10 ng was used to generate cDNA for qRT-PCR analysis using gene specific primers (Taqman) designed to amplify miR-143, miR-145 and RNU 48, as an endogenous control. The fold endogenous change of target miR-143 (**A**), and miR-145 (**B**) compared to reference gene RNU 48 is plotted on each graph, each dot representing a different NOF/CAF. The line represents the mean fold endogenous for each set of fibroblasts. Statistical analysis was performed by multiple ANOVA, and statistical significance is shown on the figure by *p<0.05, **p<0.01. Error bars display the SD.

~2 fold and ~1.2 fold increase in miR-145 expression in DENF316 and DENF008 respectively. Again, there was some variability in the miR-145 expression in response to TGF-β1.

The effect of TGF-β1 on miR-143 and miR-145 expression was also examined by performing qRT-PCR on NOFs treated with varying doses of TGF-β1. The TGF-β1 dose response samples were used to assess miR-143 and miR-145 expression (figure 3.16). DENF316s were treated with 0.5, 5 or 50 ng/ml TGF-β1 for 48 h, and molecularly assessed by qRT-PCR for mature miR-143 and miR-145 levels. miR-143 expression, decreased (by ~0.25 fold) with 0.5 ng/ml TGF-β1, and then increased to ~1.25 and 1.5 after 5 and 50 ng/ml treatment respectively. There was a steady trend in an increase in miR-145 expression with the increment of TGF-β1 treatment at 5 ng/ml (~1.5 fold) and 50 ng/ml (~2 fold). The trend suggests that TGF-β1 caused the increased expression of miR-143 and miR-145, however the increases did not reach statistical significance.

The effect of TGF-β1 on miR-145 expression was also examined in CAFs. 4 CAFs; BICR-3, BICR-59, BICR-63 and BICR-70 were each treated with TGF-β1, RNA isolated and used for specific miR-145 and RNU 48 cDNA preparation for qRT-PCR analysis. This experiment was performed in duplicate for each CAF, so repetition is needed to validate the findings. But the data suggest that TGF-β1 is able to increase the expression of miR-145 in CAFs also (figure 3.17). The miR-145 levels increase by ~4.5 (significant), ~3 and ~12.5 fold in BICR-59, BICR-63 and BICR-3 respectively. In BICR-70 CAFs, however, there was no increase in miR-145 after TGF-β1 treatment (~0.5 fold decrease).

Next, the effect oral cancer cell lines conditioned media have on NOF and CAF miR-145 expression was assessed. DENF316 (NOF) and MCA (CAF) were treated with conditioned media from Cal27 and VB6, a stably expressing integrin αvβ6 H357 cell line, and used for qRT-PCR to assess miR-145 levels compared to serum free treated and TGF-β1 controls. In both DENF316 and MCA fibroblasts, αvβ6 conditioned media treatment caused the significant downregulation of miR-145 (~0.5 fold decrease, compared to untreated fibroblasts; figure 3.18). In DENF316 and MCA both TGF-β1 and Cal27 conditioned media caused no significant change in miR-145 levels. Contrary to data described above TGF-β1 did not cause any increase in miR-145 levels, and cal27 conditioned media treatment resulted in a small decrease in expression, but ~0.25 fold compared to untreated controls. In MCA CAFs, TGF-β1 caused a small increase in miR-145 levels (~1.25 fold, not significant) and Cal27 conditioned media had no effect.

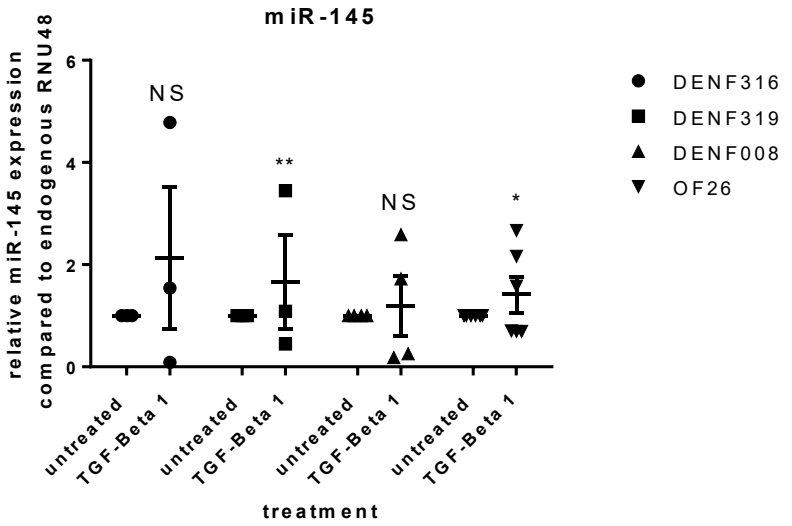

Figure 3.15: TGF-β1 caused an increase of miR-145 expression only in certain NOFs. DENF316, DENF319, DENF008 and OF26 were seeded at a density of 250,000 cells per six well overnight, serum starved for 20 h and treated with 5 ng/ml TGF-β1, or serum free media as a control for 48 h. After treatment fibroblasts were harvested, RNA isolated and 100ng was used in a total cDNA preparation. qRT-PCR was performed with the cDNA with gene specific primers (Taqman) to amplify miR-145 and RNU 48 as a reference gene. Each dot on the figure represents the relative quantification of miR-145 transcript levels compared to endogenous RNU 48, for each treatment relative to untreated, the line represents the mean relative difference. Statistical analysis was performed by a paired two tailed student's t-test, and statistical significance is shown on the figure by *p<0.05, **p<0.01. The significance is compared to the untreated equivalent transfection. Error bars represent the SEM. N=3-7, independent experiments.

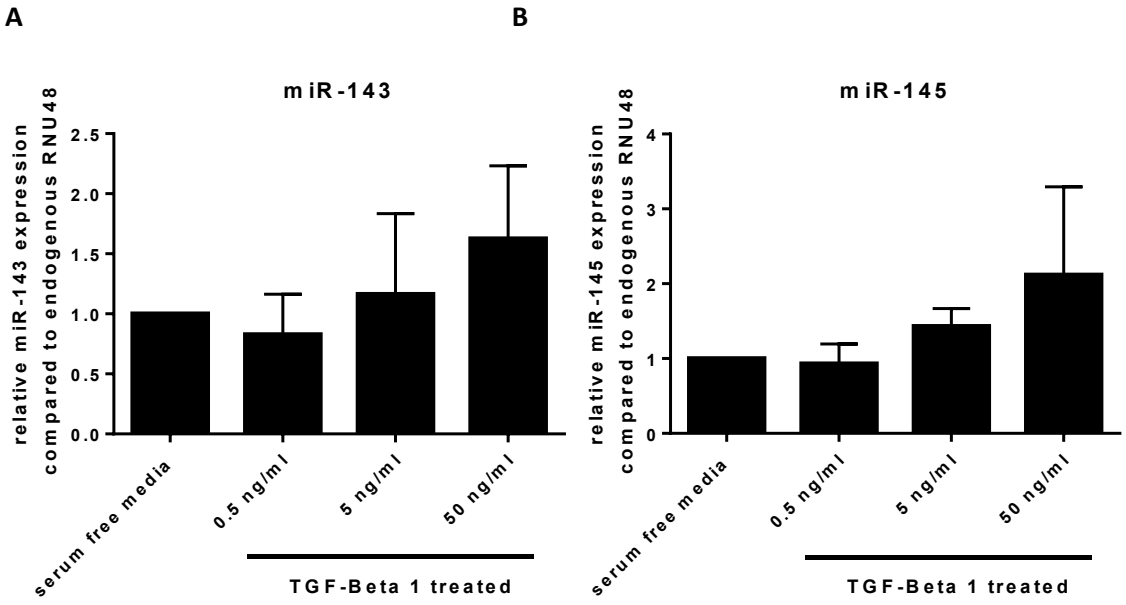

Figure 3.16: Dose response of TGF-β1 treatment caused a trend of increasing miR-143 and miR-145 expression. DENF316 normal oral fibroblasts were seeded at a density of 250,000 cells per 6 wells overnight, serum starved for 20 h and subsequently treated with 0.5, 5 or 50 ng/ml TGF-β1, or serum free media as a control for 48 h. After treatment fibroblasts were harvested, total RNA isolated and 10 ng used in miRNA specific cDNA preparation using specific primers to mature miR-143, miR-145 and RNU 48. qRT-PCR was performed with the cDNA with primers to amplify miR-143, miR-145 and RNU 48 as a reference gene. Each bar on the figure represents the mean relative quantification of miR-143 (**A**) or miR-145 (**B**) transcript levels compared to endogenous RNU 48, for each treatment relative to the relevant untreated. Error bars represent the SEM. N=3, independent experiments.

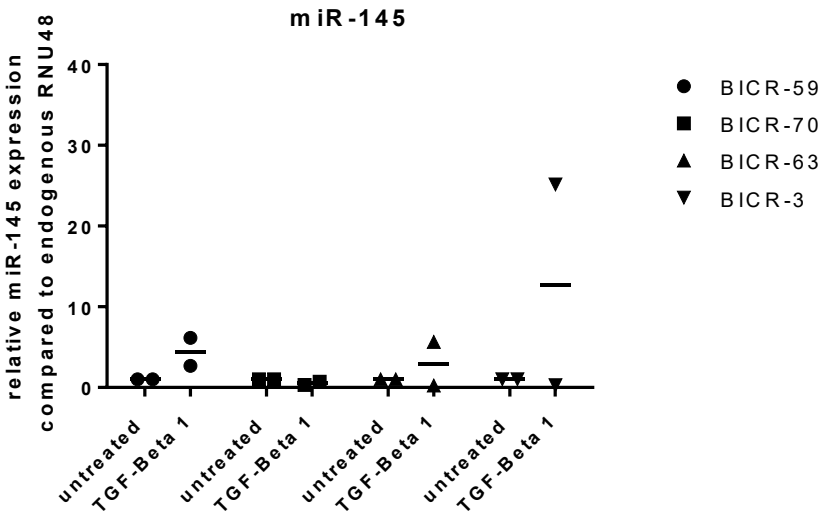

Figure 3.17: TGF-β1 caused an trend of an increase in miR-145 expression in CAFs, but not in BICR-70. BICR-3, BICR-59, BICR-63, and BICR-70 were seeded overnight at a density of 250,000 cells per 6 wells, serum starved for 20 h before subsequent treatment with 5 ng/ml TGF-β1, or serum free media as a control for 48 h. After treatment fibroblasts were harvested, RNA isolated and 10 ng was used in cDNA using gene specific primers to amplify miR-145 and RNU 48 (Taqman). qRT-PCR was performed with the cDNA with primers to amplify miR-145 and RNU 48 as a reference gene. Each dot on the figure represents the relative quantification of miR-145 transcript levels compared to endogenous RNU 48, for each treatment relative to untreated, the line represents the mean relative difference. N=2, independent experiments for each CAF.

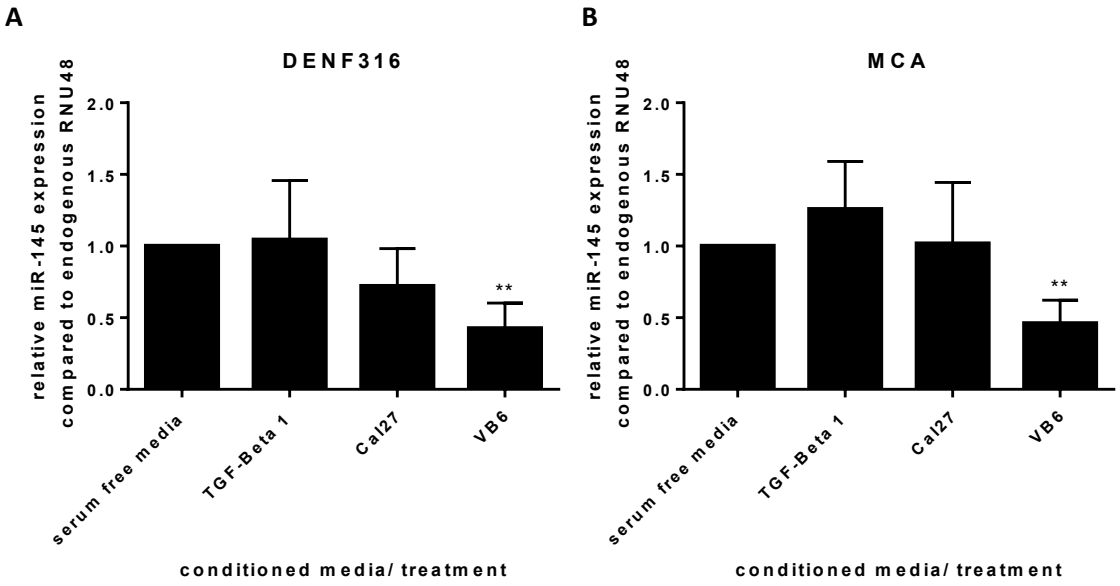

Figure 3.18: NOFs and CAFs treated with VB6 conditioned media had decreased expression of miR-145. NOFs (DENF316; **A**) and CAFs (MCA; **B**) were seeded at a density of 250,000 cells per 6 well, serum starved for 20 h and treated with serum free media, 5 ng/ml TGF-β1, or conditioned media collected from a Cal27 or VB6, a H357 cell line stably transfected with the integrin αvβ6, for 48 h. Conditioned media was collected by seeding the cell line at a density of $1x10^6$ in a T75 overnight and replacing with 3 ml serum free media to condition for 24 h. After treatment, fibroblasts were harvested and the RNA was isolated and 10 ng was used to generate specific cDNA for mature miR-143, miR-145 and RNU48 using gene specific primers (Taqman). qRT-PCR analysis was performed using primers designed to amplify miR-145 and RNU 48, as an endogenous control. Each bar on the figure represents the mean relative quantification of miR-145 transcript levels compared to endogenous RNU 48, for each treatment relative to untreated. Statistical analysis was performed by a paired two tailed student's t-test, and statistical significance is shown on the figure by **$p<0.01$. The significance is compared to the miR-145 levels in the fibroblasts treated with serum free media. Error bars represent the SEM. N=3, independent experiments.

3.5 ***Summary***

In this chapter, the effect of TGF-β1 and conditioned media from cancer cell lines on NOFs on markers of myofibroblasts transdifferentiation and the miR-145 expression were assessed. Conditioned media from Cal27, H357, and VB6 did not significantly induce myofibroblast transdifferentiation of NOFs, however Cal27 and VB6 showed some increase in αSMA transcript and protein levels respectively. Conditioned media from VB6 was able to significantly downregulate miR-145 expression. TGF-β1 treatment induced significant upregulation of myofibroblasts molecular markers αSMA and FN1-EDA, and also induced αSMA stress fibre formation and contraction of the fibroblasts. The optimal duration of TGF-β1 treatment for inducing myofibroblast transdifferentiation was optimised to be for 48 h (5 ng/ml). TGF-β1 treatment increased the expression of miR-145 in NOFs and CAFs. There was no identified difference in the expression of myofibroblasts markers between NOFs and CAFs, however the expression of miR-143 and miR-145 in CAFs was significantly higher than that in NOFs.

Chapter 4: The role of miR-145 in the control of pro-tumourigenic phenotypic changes in stromal oral fibroblasts.

4.1 *Aims and objectives*

The overall aim of this chapter was to investigate the role of miR-145 in oral myofibroblast transdifferentiation. To do this, the objectives were to use gain of function and loss of function experiments to assess the effect of miR-145 on the NOF and CAF induced myofibroblasts phenotypes by looking at molecular myofibroblast markers and fibroblasts contractility. In addition, this chapter planned to determine whether manipulating miR-145 expression in NOFs and CAFs had any paracrine effects on cancer cell migration and invasion, by using transwell assays using conditioned media from the fibroblasts as a chemotaxis stimulus.

4.2 *miR-145 inhibited markers of oral myofibroblast transdifferentiation.*

Myofibroblasts are typically characterised by having contractile cytoskeletal αSMA stress fibres (Hinz, 2007). TGF-β1 is able to induce transdifferentiation of normal fibroblasts to myofibroblasts in many different fibroblasts including human gingival fibroblasts (Lewis *et al*., 2004). In order to investigate the effect of miR-145 on the myofibroblast phenotype, two primary NOF cultures were transiently transfected with a synthetic premiR-145 oligonucleotide to overexpress mature miR-145, and were subsequently treated with 5 ng/ml TGF-β1 for 48 h. A negative non-targeting premiR was used as a control, and the effect of overexpressing co-transcribed miR-143 was also investigated using premiR-143. The effect on myofibroblast phenotype was molecularly assessed by qRT-PCR and immunoblotting. Fibroblasts were harvested after TGF-β1 treatment and used for total protein or RNA extraction. The expression of the well-characterised myofibroblast molecular markers αSMA, collagen 1a (COL1A1) and specific fibronectin 1 isoform with extra domain A (FN1-EDA), were all assessed by qRT-PCR. The best-described marker of myofibroblast transdifferentiation, αSMA, was also assessed via immunoblotting and immunocytochemistry.

Synthetic oligonucleotides of premiR-143 and premiR-145 were used to overexpress mature miRNA levels in the NOFs tested. The precursor miRNA is in the form of a chemically synthesised double stranded RNA which is processed by the cell's machinery to result in the correct miRNA strand being introduced into the RNA induced silencing complex (RISC), leading to downstream effects on gene expression by binding to complementary sequences in the 3'UTRs of mRNA targets. To assess whether these precursor miRNAs were effective in overexpressing the mature miRNAs, specific cDNA was generated using miR-143, miR-145 or RNU 48 Taqman probes. The cDNA preparations were then used in qRT-PCR reactions to assess the levels of each miRNA

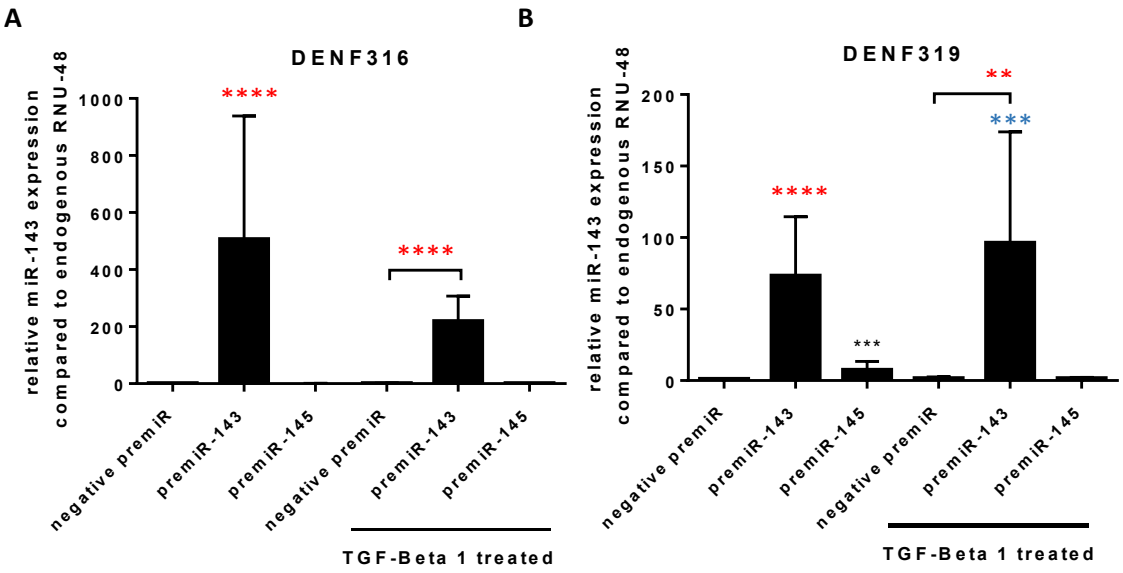

Figure 4.1: premiR-143 transfection resulted in the overexpression of mature miR-143. Two primary NOFs, DENF316 and DENF319 (**A** and **B** respectively), were seeded at a density of 250,000 cells per six well and transiently transfected with premiR-143, premiR-145 or a negative non-targeting premiR (50 nM) 24 h prior to treatment with 5 ng/ml TGF-β1 for 48 h. After treatment, fibroblasts were harvested and the RNA was isolated and 10ng was used to generate specific miR-143 and RNU 48 cDNA using specific Taqman probes. qRT-PCR analysis was performed using primers for miR-143 and RNU 48 (Taqman). Each bar on the figure represents the mean relative quantification of miR-143 transcript levels compared to endogenous RNU 48, for each transfection plus/minus treatment relative to untreated negative premiR. Statistical analysis was performed by a paired two tailed student's t-test, and statistical significance is shown on the figure by ***p<0.001 and ****p<0.0001. If not indicated by a bar, the black significance asterix are compared to the untreated, negative premiR transfected, negative control. Blue significance asterix indicate significance compared to the untreated counterpart, e.g. premiR-143 transfected, TGF-β1 treated compared with premiR-143 transfected, untreated. Important significant data is shown in red. Bars also indicate statistical comparisons. Error bars represent the SEM. N=3, independent experiments.

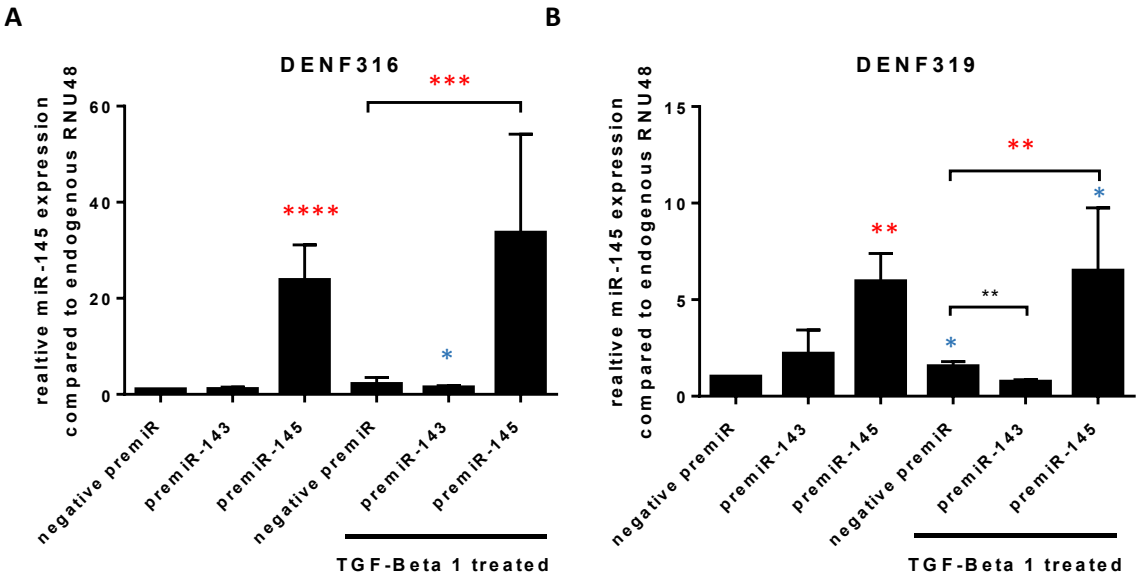

Figure 4.2: premiR-145 transfection resulted in the overexpression of mature miR-145. Two primary NOFs, DENF316 and DENF319 (**A** and **B** respectively), were seeded at a density of 250,000 cells per six well and transiently transfected with premiR-143, premiR-145 or a negative non-targeting premiR (50 nM) 24 h prior to treatment with 5 ng/ml TGF-β1 for 48 h. After treatment, fibroblasts were harvested and the RNA was isolated and 10ng was used to generate specific miR-145 and RNU 48 cDNA using specific Taqman probes. qRT-PCR analysis was performed using primers for miR-145 and RNU 48 (Taqman). Each bar on the figure represents the mean relative quantification of miR-145 transcript levels compared to endogenous RNU 48, for each transfection plus/minus treatment relative to untreated negative premiR. Statistical analysis was performed by a paired two tailed student's t-test, and statistical significance is shown on the figure by *p<0.05, **p<0.01, ***p<0.001, ****p<0.0001. If not indicated by a bar, the black significance asterix are compared to the untreated, negative premiR transfected, negative control. Blue significance asterix indicate significance compared to the untreated counterpart, e.g. premiR-143 transfected, TGF-β1 treated compared with premiR-143 transfected, untreated. Important significant data is shown in red. Bars also indicate statistical comparisons. Error bars represent the SEM. N=3, independent experiments.

relative to RNU 48, a small nuclear RNA used as endogenous reference gene. RNU 48 was selected from a screen of endogenous controls including RNU 44, B2M and U6, as it showed the least fluctuation in CT values between samples. Transfection of premiR-143 in NOFs for 24 h resulted in an overexpression of mature miR-143 (Figure 4.1). Transfection of premiR-145 resulted in the overexpression of mature miR-145 (Figure 4.2). TGF-β1 treatment caused an increase in endogenous miR-145 expression in DENF319 (B), but not in DENF316 (A). Of interest, the overexpression of miR-143 and miR-145 was several fold higher in DENF316 then DENF319, and TGF-β1 caused a significant increase in miR-145 levels in DENF319 and not in DENF316 NOFs. Surprisingly, premiR-145 transfection also caused a premiR-145 transfection also caused a small but significant increase in miR-143 in DENF319 in the absence of TGF-beta, but not in its presence (Figure 4.1B). However, this was only observed in one of the primary cultures tested so requires further investigation.

As seen previously in chapter 3, TGF-β1 caused an increase in αSMA expression in NOFs. In both primary NOFs used, TGF-β1 caused a significant increase in αSMA transcript levels in fibroblasts transfected with negative premiR, and with premiR-143 (Figure 4.3). The two primary fibroblasts show some differences in αSMA expression in response to TGF-β1 treatment and the overexpression of miR-143 and miR-145. TGF-β1 treatment caused a greater response in DENF316 than DENF319, TGF-β1 caused a ~110 fold increase in αSMA expression in DENF316 NOFs compared to ~11 fold in DENF319 NOFs. Overexpression of miR-143 caused a reduction in the TGF-β1 mediated αSMA expression compared to negative premiR transfected NOFs, the TGF-β1 increases were ~34 fold (compared to ~110 fold; significant) and a ~10 fold (compared to ~11 fold; not significant) in DENF316 and DENF319 respectively (Figure 4.3A and B). In DENF316, the reduction in TGF-β1 mediated αSMA between negative premiR transfected and premiR-1 a significant reduction in the activation of αSMA expression.

In contrast, fibroblasts transfected with premiR-145 do not show an increase in αSMA at transcript and at protein levels. miR-145 overexpression inhibited the increase in αSMA expression, associated with TGF-β1 treatment, in both the NOFs tested. NOFs overexpressing miR-145 had a 95% and 82% (DENF316 and DENF319 respectively) reduction in TGF-β1 associated increase in αSMA compared to treated negative premiR control. miR-145 overexpression also prevented the TGF-β1 induced increase in αSMA protein, whereas miR-143 did not (figure 4.3C). Untreated DENF319 overexpressing miR-145 also had a significant decrease in αSMA.

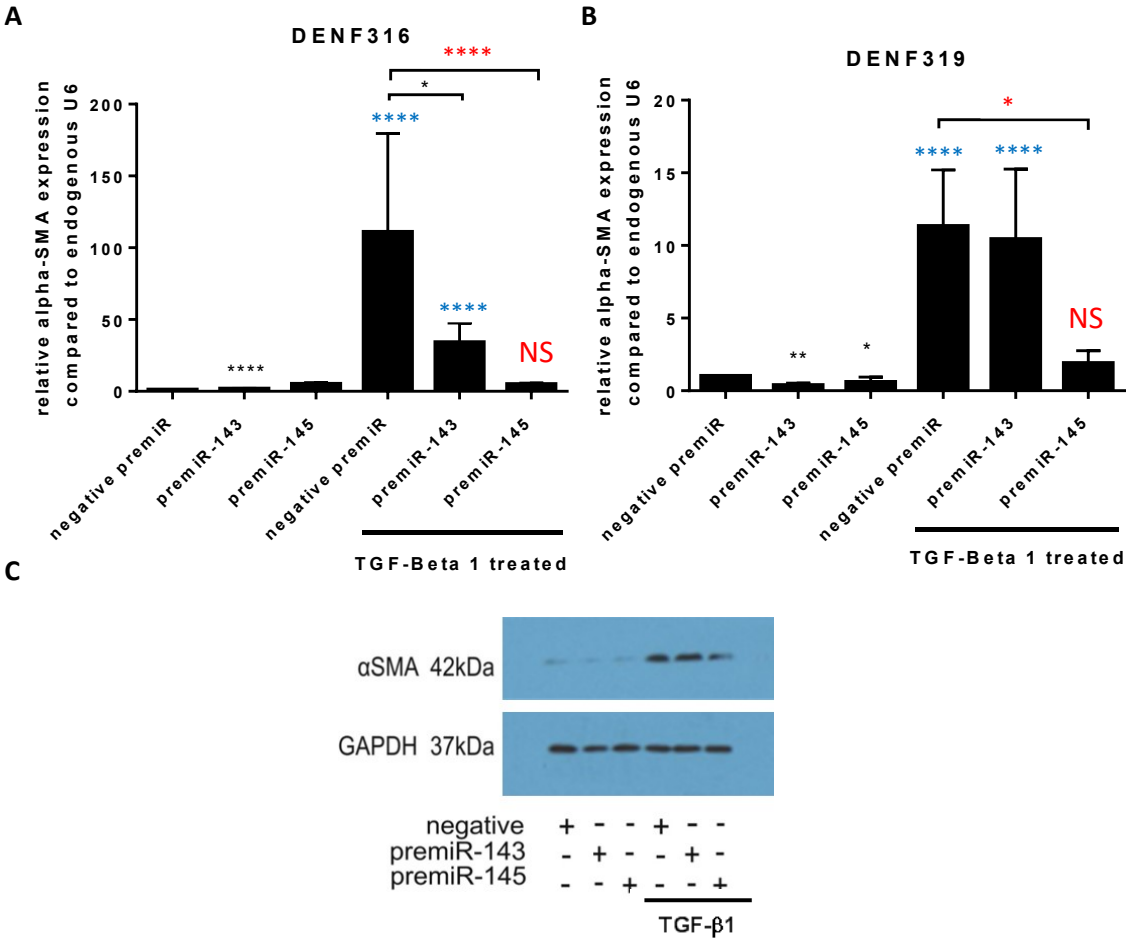

Figure 4.3: miR-145 overexpression attenuated TGF-β1 induced α smooth muscle actin expression. Two primary NOFs, DENF316 and DENF319 (**A** and **B** respectively), were seeded at a density of 250,000 per six well, and were transiently transfected with premiR-143, premiR-145 or a negative non-targeting premiR (50 nM) 24 h prior to treatment with TGF-β1 for 48 h. After treatment, fibroblasts were harvested and the RNA was isolated, quantified and 100 ng was used to generate cDNA for qRT-PCR analysis using primers designed to amplify αSMA and U6, as an endogenous control. Each bar on the figure represents the mean relative quantification of αSMA transcript levels compared to endogenous U6, for each transfection plus/minus treatment relative to untreated negative premiR. Statistical analysis was performed by a paired two tailed student's t-test, and statistical significance is shown on the figure by *p<0.05, **p<0.01, ***p<0.001, ****p<0.0001. If not indicated by a bar, the black significance asterix are compared to the untreated, negative premiR transfected, negative control. Blue significance asterix indicate significance compared to the untreated counterpart, e.g. premiR-143 transfected, TGF-β1 treated compared with premiR-143 transfected untreated. Bars also indicate statistical comparisons. Important significant data is shown in red. Error bars represent the SEM. **C** Total protein lysates were prepared from the NOFs transfected with each premiR, then TGF-β1 treated. Protein lysate was prepared using RIPA protein lysis buffer, quantified and 30 µg was run on a 3–8% (w/v) tris acetate gradient gel and transfected to a nitrocellulose membrane and immunoblotted for αSMA and GAPDH as the loading control. The figure shows a representative blot. N=3, independent experiments for each NOF.

Myofibroblasts are often identified in vitro by visualising their striking cytoskeletal αSMA stress fibres. To investigate the effect of miR-145 overexpression on the integrity of these stress fibres, NOFs were seeded onto coverslips in order to perform immunocytochemistry using a FITC-conjugated αSMA antibody. Once seeded, NOFs were transiently transfected with premiR-143, premiR-145 or negative premiR, then treated with TGF-β1. The TGF-β1 treatment caused a significant increase in mean fluorescence intensity (by 4.5 fold), and caused the formation of αSMA stress fibres, which are typical of myofibroblasts (figure 4.4). In fibroblasts overexpressing miR-143 there was no difference in the amount of αSMA stress fibres visualised, but a slight reduction in the mean fluorescence per cell (not significant). However, in fibroblasts overexpressing miR-145 there was a marked reduction in the amount of fluorescence and stress fibres present, however this did not reach significance.

To investigate miR-145's functional effect on the myofibroblast phenotype, a collagen 1 contractility assay was used to assess the effect of miR-145 on the TGF-β1-induced oral myofibroblast-associated contractility. NOFs transiently transfected with premiR-143, premiR-145 or negative premiR were resuspended in a mixture of rat tail collagen I: DMEM, allowed to set and used to assess TGF-β1 stimulated contraction. In this study, TGF-β1 was shown to significantly cause contraction of the gels, consistent with the myofibroblast phenotype (seen in figure 3.4C). miR-145 was able to significantly reduce TGF-β1's ability to induce gel contraction, shown by the lack of reduction in gel diameter (Figure 4.5). miR-143 overexpression also caused a smaller, but significant reduction in induced myofibroblast contractility.

Next, other known markers of myofibroblast transdifferentiation were analysed to investigate whether miR-145 was able to affect the whole myofibroblast phenotype or just αSMA expression. A specific fibronectin-1 isoform, fibronectin with extra domain A (FN1-EDA), is reported to be a bona-fide marker of myofibroblasts as well as being necessary for myofibroblast transition (Serini *et al*., 1998). In both NOFs analysed, FN1-EDA gene expression was increased in TGF-β1 induced myofibroblasts (figure 4.6) by ~3 fold in DENF316 (this did not reach statistical significance) and ~1.6 fold in DENF319. The overexpression of miR-143 had different effects on the TGF-β1 induced myofibroblast phenotype in the two NOFs. In DENF316, overexpression caused a further increase in FN1-EDA on TGF-β1 treatment (~12 fold, compared to negative premiR, untreated NOFs) compared to TGF-β1 treated NOF transfected with control premiR (Figure 4.6A). However, in DENF319, overexpression of miR-143 did not cause a significant change (~1.3 fold compared to negative premiR transfected, untreated NOFs) in FN1-EDA levels on TGF-β1 treatment compared to TGF-β1 treated NOF transfected with control

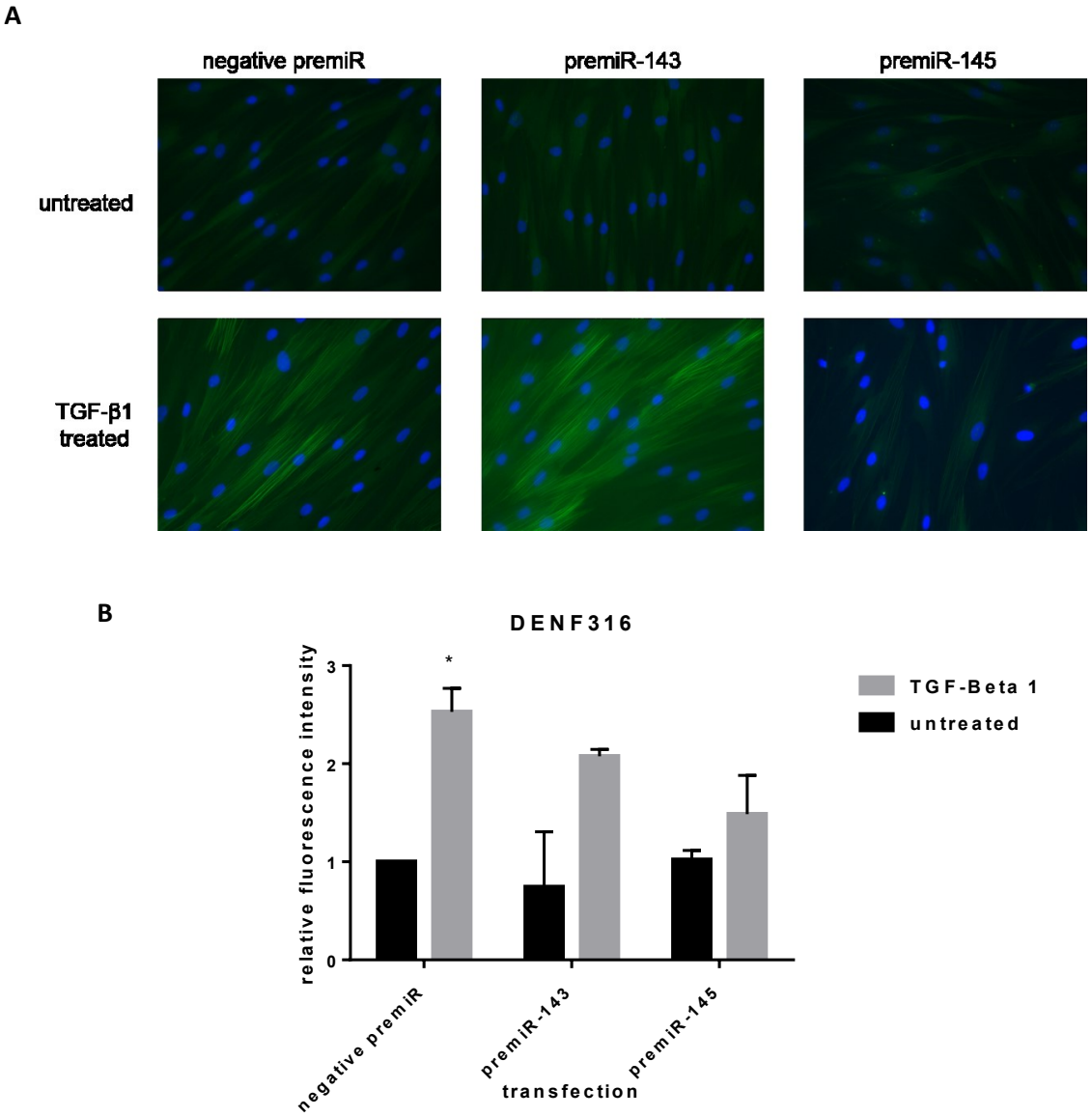

Figure 4.4: miR-145 overexpression prevented αSMA stress fibre formation. NOFs were seeded at a density of 250,000 cells per six well onto coverslips overnight, then were transiently transfected with negative premiR, premiR-143 or premiR-145 (50 nM) for 24 h prior to being treated with TGF-β1 for 48 h. The coverslips were washed in PBS, before being fixed in 100% methanol for 10 min, then permeablised using 4mM sodium deoxycholate for 10 min, and blocked using 2.5% (w/v) BSA in PBS for 30 min before incubation with a primary FITC-conjugated αSMA antibody at 4 ^{o}C overnight. The coverslips were then washed in PBS before mounting on microscope slides using DAPI containing mounting medium. Fluorescent images were taken using a microscope, using Pro-plus 7 imaging software at 40x magnification. Representative pictures are shown in **A.** The amount of fluorescence intensity per cell was quantified using Image J, and displayed in **B** as the mean relative fluorescent intensity for DENF316. Statistical analysis was performed by a paired two tailed student's t-test, and statistical significance is shown on the figure by *$p<0.05$, negative premiR treated compared to treated. Error bars show the SEM. N=3, independent experiments.

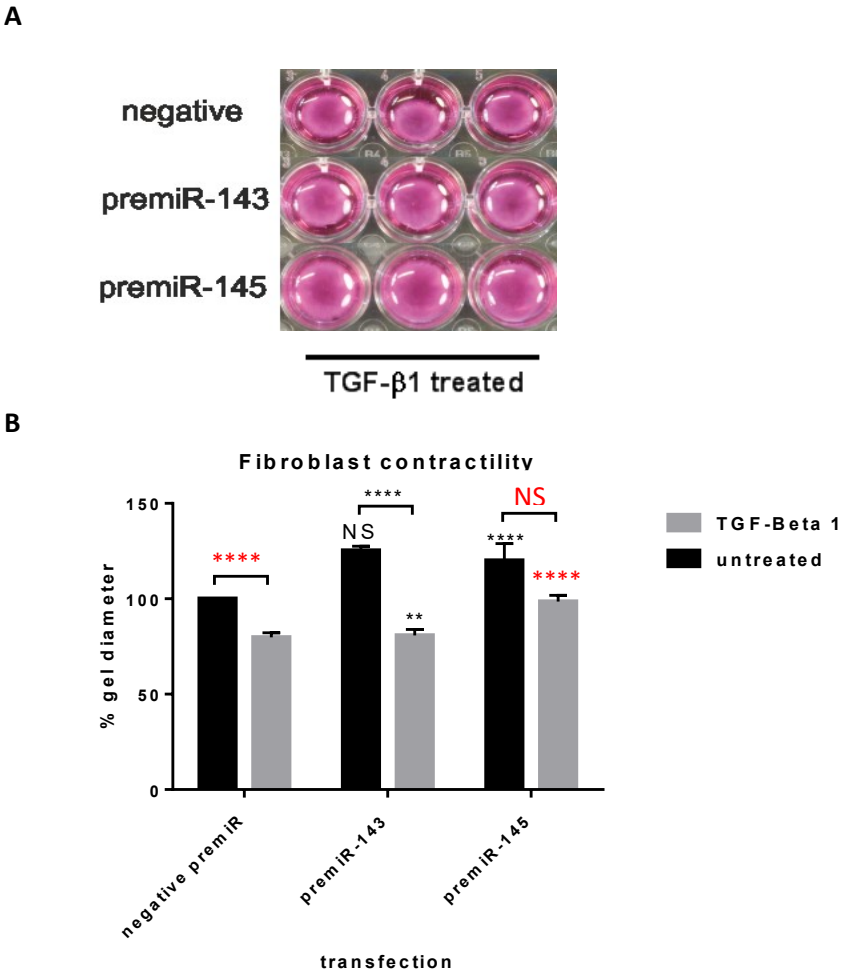

Figure 4.5: miR-145 overexpression prevented TGF-β1 induced myofibroblast contractility. NOFs were transiently transfected with negative premiR, premiR-143 or premiR-145 (50 nM). After 24 h the NOFs were harvested, counted and resuspended in a 1:1 mixture of rat tail collagen 1 (in 0.1 M acetic acid) and DMEM and neutralised with NaOH, at a density 250,000 per 300 µl. The mixture was aliquoted into wells (300 µl/well) and left to set in an incubator at 37 ^{o}C with 5% (v/v) CO_2. After the gels had set, media was added to the wells at 4 h later the media was replaced with serum free media for overnight serum starvation. The gels were detached from the sided of the wells and treated with 5 ng/ml TGF-β1, or serum containing/free media as controls (not shown). Photographs were taken at 0 h, 24 h and 48 h. The level of contraction was assessed at 48 h by measuring the diameter of the gel with ImageJ image analysis software. The figure shows a representative photograph of gels containing transfected NOFs after 48 h TGF-β1 treatment in **A**. The quantified level of contraction is shown in a histogram in **B** as a % of gel contraction compared to negative premiR transfected untreated control. Statistical analysis was performed by a paired two tailed student's t-test, and statistical significance is shown on the figure by ****p<0.0001, **p<0.01, treated premiR-143/5 compared to treated negative premiR. Important significant data is shown in red. N=3, independent experiments. Error bars show the SEM.

premiR (Figure 4.6B). miR-143 overexpression also caused a significant ~0.3 fold decrease in FN1-EDA levels in untreated DENF319 NOFs. miR-145 overexpression was also able to cause a ~0.8 fold downregulation in FN1-EDA levels in untreated DENF319, but not DENF316s. miR-145 overexpression was able to significantly attenuate the TGF-β1 associated elevated FN1-EDA expression, in both NOFs. In DENF316s, miR-145 overexpression reduced the TGF-β1 mediated FN1-EDA expression (~3 fold increase in negative transfected controls) to ~1.6 fold compared to untreated negative transfected FN1-EDA levels. In DENF319s, miR-145 overexpression reduced the TGF-β1 mediated FN1-EDA expression (~1.7 fold increase in negative transfected controls) to ~0.5 fold compared to untreated negative transfected FN1-EDA levels.

Another marker investigated was collagen 1a (COL1A1). Myofibroblasts are known to module their extracellular environment by the elevated secretion of ECM structural molecules and ECM remodelling agents (Kalluri and Zeisberg, 2006). Increased collagen secretion is typical of true myofibroblasts in healing wounds, where it helps to strengthen the wound area. Therefore, the change in COL1A1 mRNA was investigated in NOFs overexpressing miR-143 or miR-145, treated with TGF-β1. Again, patient specific differences were seen in the two NOFs in response to TGF-β1 and in miR-143's effect in the cells (figure 4.7 A and B). In DENF316 TGF-β1 provoked elevated expression of COL1A1 (~2 fold), whereas in DENF319 this was not observed (~0.8 fold). miR-143 overexpression caused a further TGF-β1 mediated elevation in COL1A1 ~4.5 fold increase in DENF316, no difference was seen in DENF319 between TGF-β1 negative transfected NOFs and NOFS overexpressing miR-145 treated. miR-145 overexpression in both untreated and treated NOFs caused a marked, significant downregulation in COL1A1. COL1A1 decreased by ~0.8 and ~0.5 fold in DENF316 and DENF319 respectively, in untreated miR-145 overexpressing NOFs. Similar COL1A1 levels were seen in premiR-145 transfected NOFs treated with TGF-β1, COL1A1 expression decreased from ~0.7 and ~0.8 fold in DENF316 and DENF319 respectively compared to untreated negative transfected NOFs.

Another way myofibroblasts act to reorganise the ECM is by regulating the expression, secretion and activation of proteases, such as MMPs and ADAMs (Kalluri and Zeisberg, 2006). These specifically cleave ECM molecules and receptors, allowing for invasion of cancer cells, ligand release and altered cellular signalling. MMP2, is one such MMP which has been highlighted to be important in promoting paracrine invasion by breaking down the ECM to create a path for the cancer cells to migrate through, and by the releasing of chemokines that have been sequestered in the ECM, promoting migration (Zhang *et al*., 2006). MMP2 has also recently been highlighted to have a role in OSCC (Fuller *et al*., 2012; Hassano *et al*., 2014). The expression of

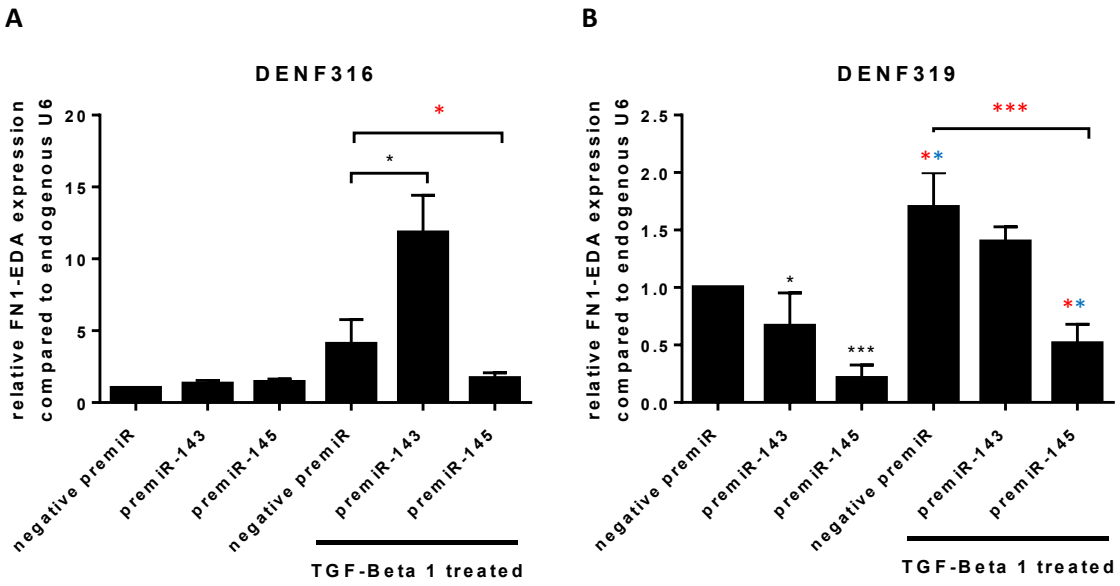

Figure 4.6: miR-145 overexpression attenuated TGF-β1 induced fibronectin 1 (with extra domain A) expression. Two primary NOFs, DENF316 and DENF319 (**A** and **B** respectively), were seeded at 250,00 cells per 6 well and were transiently transfected with premiR-143, premiR-145 or a negative non-targeting premiR (50nM) 24 h prior to treatment with TGF-β1 for 48 h. After treatment, fibroblasts were harvested and the RNA was isolated, quantified and 100 ng was used to generate total cDNA for qRT-PCR analysis using primers designed to amplify FN1-EDA and U6, as an endogenous control. Each bar on the figure represents the mean relative quantification of FN1-EDA transcript levels compared to endogenous U6, for each transfection plus/minus treatment relative to untreated negative premiR. Statistical analysis was performed by a paired two tailed student's t-test, and statistical significance is shown on the figure by *p<0.05, **p<0.01, ***p<0.001. If not indicated by a bar, the black significance asterix are compared to the untreated, negative premiR transfected, negative control. Blue significance asterix indicate significance compared to the untreated counterpart, e.g. premiR-145 transfected, TGF-β1 treated compared with premiR-145 transfected untreated. Bars also indicate statistical comparisons. Important significant data is shown in red. Error bars represent the SEM. N=3, independent experiments.

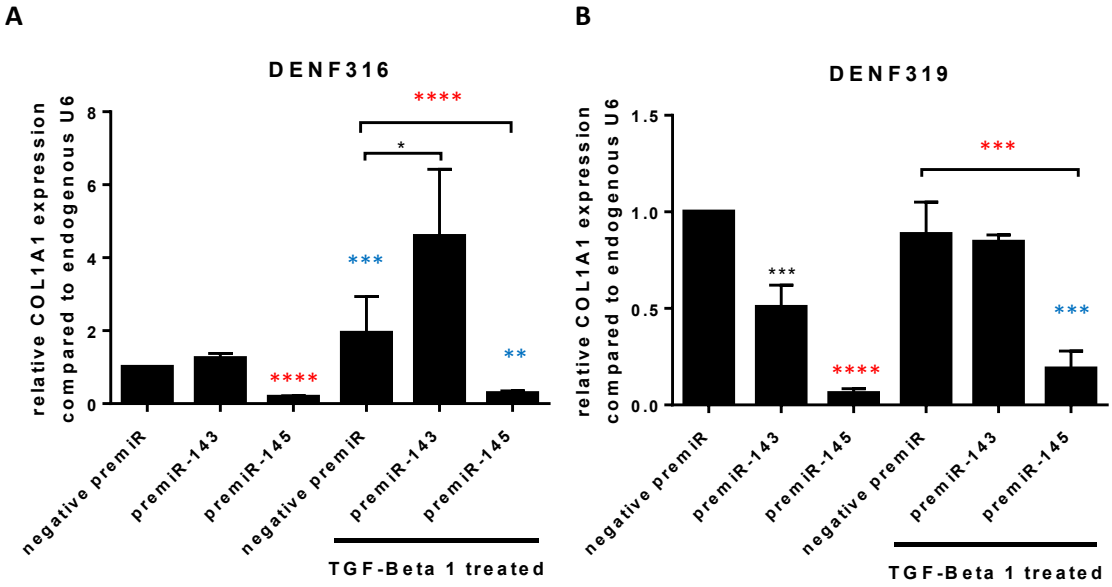

Figure 4.7: miR-145 overexpression inhibited collagen 1a expression. Two primary NOFs, DENF316 and DENF319 (**A** and **B** respectively), were seeded at a density of 250,000 cells per six well and were transiently transfected with premiR-143, premiR-145 or a negative non-targeting premiR (50 nM) for 24 h prior to treatment with TGF-β1 for 48 h. After treatment, fibroblasts were harvested and the RNA was isolated and 100 ng was used to generate cDNA for qRT-PCR analysis using primers designed to amplify COL1A1 and U6, as an endogenous control. Each bar on the figure represents the mean relative quantification of COL1A1 transcript levels compared to endogenous U6, for each transfection plus/minus treatment relative to untreated negative premiR. Statistical analysis was performed by a paired two tailed student's t-test, and statistical significance is shown on the figure by *p<0.05, **p<0.01, ***p<0.001, ****p<0.0001. If not indicated by a bar, the black significance asterix are compared to the untreated, negative premiR transfected, negative control. Blue significance asterix indicate significance compared to the untreated counterpart, e.g. premiR-145 transfected, TGF-β1 treated compared with premiR-145 transfected untreated. Bars also indicate statistical comparisons. Important significant data is shown in red. Error bars represent the SEM. N=3, independent experiments.

MMP2 was investigated in NOFs transfected with premiRs, then TGF-β1 treated. In DENF316 NOFs, induction of the myofibroblast phenotype with TGF-β1 caused a ~2 fold increase in MMP2 expression (figure 4.8), however TGF-β1 treatment caused a significant ~0.5 fold decrease in MMP2 expression. In DENF319 NOFs, overexpression of miR-145 caused a downregulation of MMP2 in both treated and untreated NOFs (figure 4.8B). Overexpression of miR-143 and miR-45 in DENF316 NOFs caused a significant reduction in the TGF-β1 mediated increase in MMP2 (to ~1.4 and 1.3 fold greater than untreated negative control transfected, respectively NOFs).

In the untreated fibroblasts miR-143 and miR-145 overexpression had no effect on MMP2 transcript levels (figure 4.8A). miR-143 overexpression and TGF-β1 treatment in DENF319, separately, were able to decrease MMP2 expression in DENF319 NOFs to ~0.5 fold relative to negative premiR transfected, untreated NOFs (figure 4.8B). miR-145 overexpression was able to downregulate MMP2 levels by ~0.8 fold. miR-143 and miR-145 overexpression were able to further decrease MMP2 in TGF-β1 treated NOFs, which were both decrease by ~0.7 fold, compared to negative transfected, untreated DENF319s.

4.3 *miR-145 attenuated the protumourigenic paracrine effects of oral myofibroblasts*

The presence of myofibroblasts in the tumour stroma is indicative of poor prognosis in many cancers including OSCC (Marsh *et al*., 2011). This is likely to be due to the altered secretome and ECM remodelling capabilities of myofibroblasts, which is postulated to promote the migration and invasion of surrounding transformed cells, creating a more invasive tumour. To investigate whether TGF-β1-induced functional myofibroblasts are able to promote the paracrine migration and invasion of OSCC cells. H357 cells were seeded in the top of a transwell migration chamber with an 8 µM porous membrane, with or without a layer of Matrigel, to analyse migration or invasion respectively. The chambers were placed above conditioned media prepared from fibroblasts transfected with premiRs and then treated with TGF-β1. The assay plates were incubated for 38/ 72 h to allow the cells to migrate/invade. After this time, cells were fixed to the membranes and stained with 0.1% (w/v) crystal violet. Photographs were taken at 40x with a light microscope of 4 representative views, and counted to calculate relative migration or invasion.

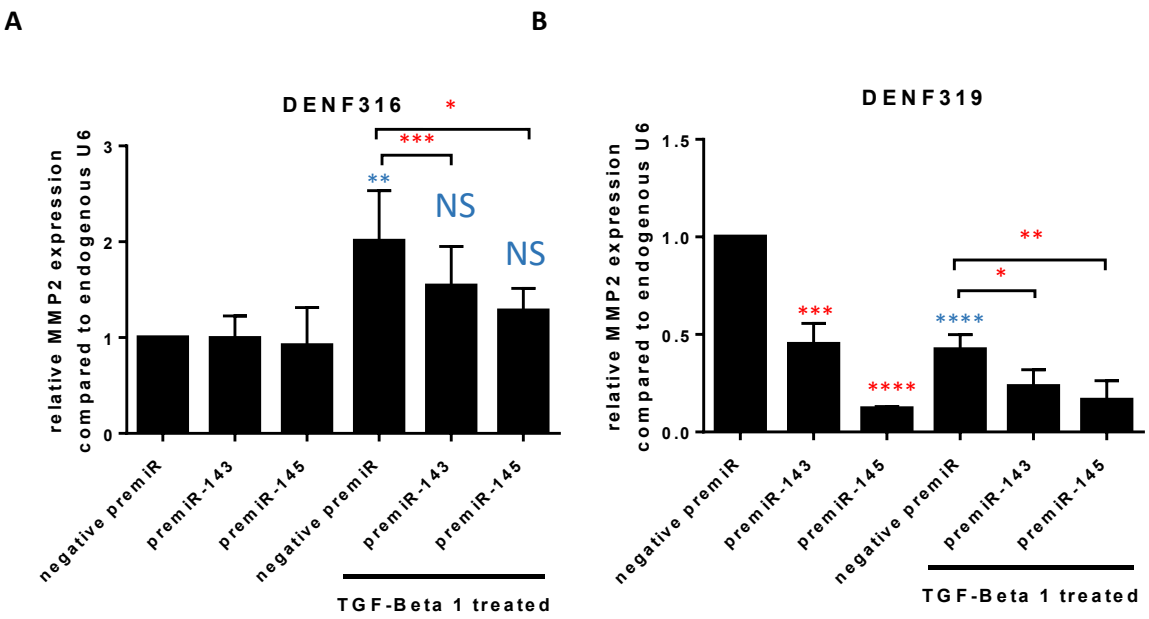

Figure 4.8: MMP2 expression was altered by miR-143 and miR-145 overexpression. Two primary NOFs, DENF316 and DENF319 (**A** and **B** respectively), were seeded at a density of 250,000 cells per six well and were transiently transfected with premiR-143, premiR-145 or a negative non-targeting premiR (50 nM) 24 h prior to treatment with 5 ng/ml TGF-β1 for 48 h. After treatment, fibroblasts were harvested and the RNA was isolated and 100 ng was used to generate total cDNA for qRT-PCR analysis using primers for MMP2 and U6, as an endogenous control. Each bar on the figure represents the mean relative quantification of MMP2 transcript levels compared to endogenous U6, for each transfection plus/minus treatment relative to untreated negative premiR. Statistical analysis was performed by a paired two tailed student's t-test, and statistical significance is shown on the figure by *p<0.05, **p<0.01, ***p<0.001, ****p<0.0001. If not indicated by a bar, the black significance asterix are compared to the untreated, negative premiR transfected, negative control. Blue significance asterix indicate significance compared to the untreated counterpart, e.g. premiR-145 transfected, TGF-β1 treated compared with premiR-145 transfected untreated. Bars also indicate statistical comparisons. Important significant data is shown in red. Error bars represent the SEM. N=3, independent experiments.

Conditioned media from TGF-β1 induced myofibroblasts (DENF316) caused a significant increase (~1.6 fold) in migration (figure 4.9) and invasion (~2.5 fold) of H357 cells (figure 4.10). The overexpression of miR-143 and miR-145 was able to completely inhibit the pro-migratory effect of the TGF-β1 treated NOF-derived conditioned media (figure 4.9). miR-145 overexpression was also able to inhibit the TGF-β1 induced increase in invasion in a dose dependent manner (figure 4.10) in DENF316 NOFs 5 nM premiR-145 reduced invasion to ~2 fold and 50 nM completely inhibited the TGF-β1 induced increase in invasion. However, in DENF319 fibroblasts TGF-β1 induced myofibroblasts conditioned media stimulated less invasion (~0.9 fold) compared to the untreated control (figure 4.11). MiR-145 overexpression caused a significant reduction (~0.6 fold) in the amount of invasion, but there was no difference when NOFs overexpressing miR-145 were treated with TGF-β1.

4.4 *miR-145 was able to rescue the myofibroblast phenotype*

To test whether miR-145 has the potential to be used therapeutically to reverse the myofibroblast phenotype and subsequently reduce the harmful effects of myofibroblasts-like CAFs in the tumour microenvironment or true myofibroblasts in chronic fibrosis, the ability of miR-145 to rescue the myofibroblast phenotype was investigated. An experiment was performed in which the oral myofibroblast phenotype was induced using TGF-β1, and then miR-145 was overexpressed. Two different doses of premiR-145 were used for the transfection and were incubated for 24 h or 48 h to optimise the conditions required for miR-145 to have any effect. NOFs were seeded, serum starved and treated with 5 ng/ml TGF-β1 for 48 h to induce the myofibroblast phenotype and serum free media was used as an untreated control. After treatment, the fibroblasts were transiently transfected with negative premiR (50 nM) or either 5 nM/50 nM premiR-145 to overexpress miR-145, and were left to transfect for either 24 h or 48 h. The fibroblasts were then harvested for molecular analysis to investigate any change in the markers of myofibroblast transdifferentiation.

qRT-PCR analysis of αSMA transcript levels, showed that there was a significant upregulation of αSMA mRNA with TGF-β1 treatment (~34 fold increase at 24 h, ~4 fold at 48 h; figure 4.12). The transfection of the lower dose of premiR-145 (5 nM) caused a further upregulation at both 24 h and 48 h after transfection (~57 fold at 24 h and ~8 fold at 48 h, compared to negative premiR transfected untreated NOFs). The higher dose of premiR-145 (50 nM) reduced the expression of αSMA mRNA in both 24 h and 48 h after transfection (~28 fold at 24 h and ~2 fold at 48 h),

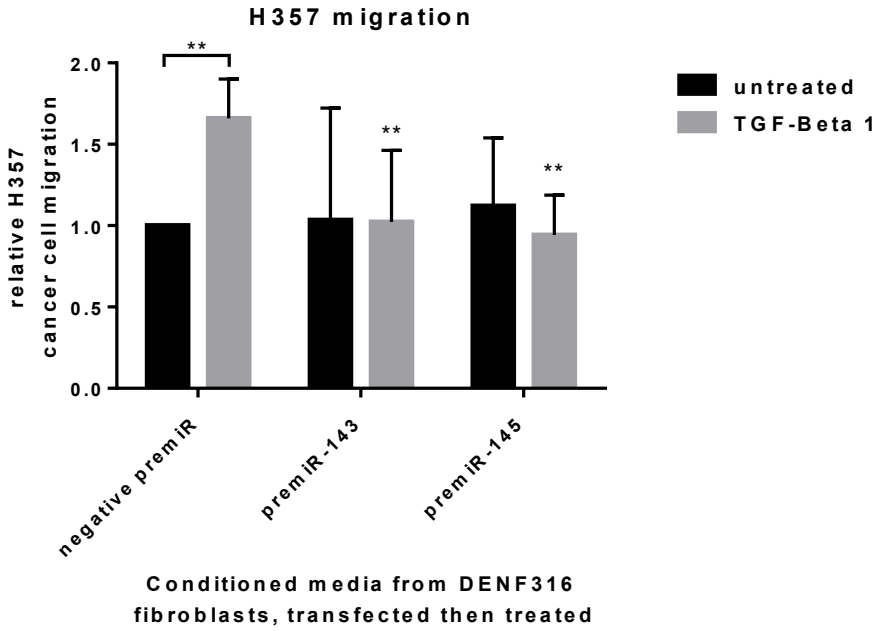

Figure 4.9: Overexpression of miR-143 and miR-145 in NOFs reduced the TGF-β1's effect on paracrine migration of H357 cancer cells. Conditioned media was collected from DENF316 NOFs transfected with negative premiR, premiR-143 or premiR-145 (50 nM) for 24 h then treated with 5 ng/ml TGF-β1 for 48 h or serum free media as a control. The conditioned media was spun at >2500xg to remove cellular debris then placed in the bottom of a transwell migration assay plate. H357 cancer cell line were seeded at 100,000 cells per well into an 8µm porous transwell with 1 mg/ml mitomycin c and allowed to migrate for 38 h. The ability of the conditioned media to promote migration was assessed by methanol fixing cells attached to the membrane after 38 h, staining the cells with 0.1% (w/v) crystal violet, taking photographs at 40x, and calculating the average number of cells in the representative photographs. The figure shows the relative H357 cancer cell migration compared to untreated, negative premiR. Statistical analysis was performed by a paired two tailed student's t-test, and statistical significance is shown on the figure by **p<0.01. The significance is compared to the treated negative premiR, unless indicated by the bar. Error bars represent the SEM. N=3, independent experiments.

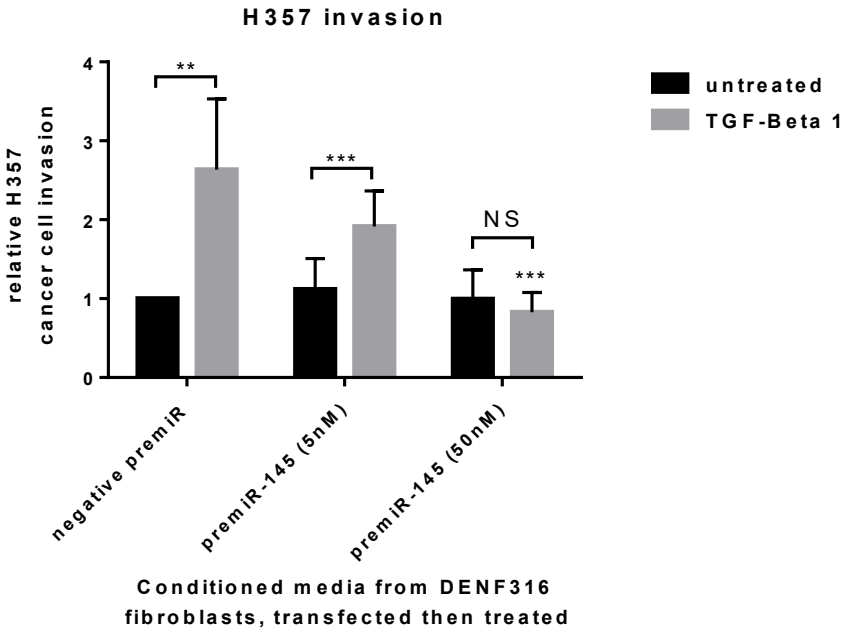

Figure 4.10: Overexpression of miR-145 in DENF316 NOFs attenuated TGF-β1's ability to promote paracrine invasion of H357 cancer cells. Conditioned media was collected from DENF316 NOFs transfected with negative control premiR, premiR-143 or premiR-145 (50 nM) for 24 h then treated with 5 ng/ml TGF-β1 for 48 h or serum free media as a control. The conditioned media was spun at >2500xg to remove cellular debris then placed in the bottom of a transwell migration assay plate. H357 cancer cell line were seeded at 100,000 cells per well into an 8 µm porous Matrigel coated transwell, with 1 mg/ml mitomycin c and allowed to migrate for 38 h. The ability of the conditioned media to promote invasion was assessed by methanol fixing cells attached to the underside of the transwell membrane after 38 h, staining the cells with 0.1% (w/v) crystal violet, taking photographs at 40x, and calculating the average number of cells in the representative photographs. The figure shows the relative H357 cancer cell invasion compared to untreated, negative premiR. Statistical analysis was performed by a paired two tailed student's t-test, and statistical significance is shown on the figure by **p<0.01, ***p<0.001. If not indicated by a bar, the significance is compared to the treated negative premiR. Error bars represent the SEM. N=3, independent experiments.

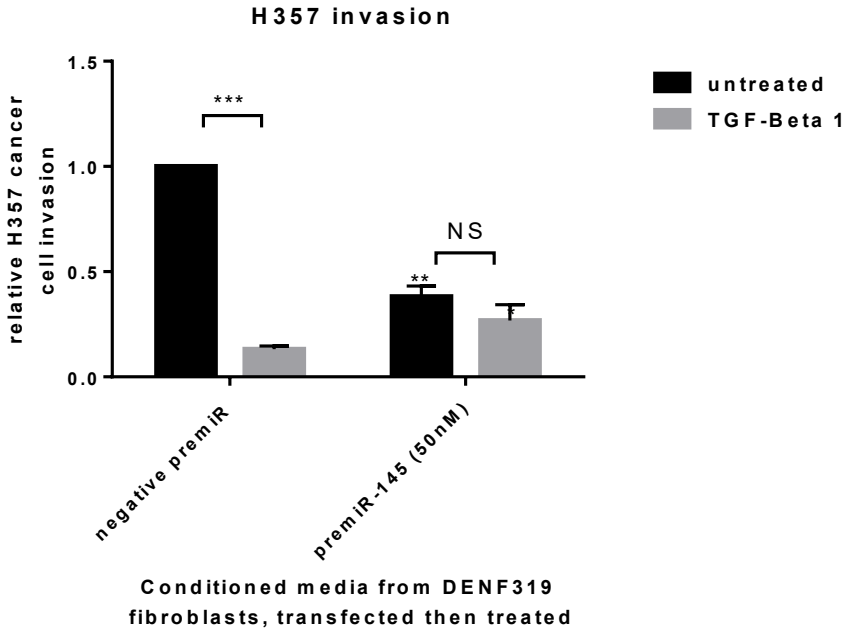

Figure 4.11 TGF-β1 reduced the amount paracrine invasion of H357 cancer cells in DENF319 NOFs. Conditioned media was collected from DENF319 NOFs transfected with negative premiR, premiR-143 or premiR-145 (50 nM) for 24 h then treated with 5 ng/ml TGF-β1 for 48 h or serum free media as a control. The conditioned media was spun at >2500xg to remove cellular debris then placed in the bottom of a transwell migration assay plate. H357 cancer cell line were seeded at 100,000 cells per well into an 8 µm porous Matrigel coated transwell, with 1 mg/ml mitomycin c and allowed to migrate for 38 h. The ability of the conditioned media to promote invasion was assessed by methanol fixing cells attached to the underside of the transwell membrane after 38 h, staining the cells with 0.1% (w/v) crystal violet, taking photographs at 40x, and calculating the average number of cells in the representative photographs. The figure shows the relative H357 cancer cell invasion compared to untreated, negative premiR. Statistical analysis was performed by a paired two tailed student's t-test, and statistical significance is shown on the figure by **p<0.01, ***p<0.001. If not indicated by a bar, the significance is compared to the untreated negative premiR. Error bars represent the SEM. N=3, independent experiments.

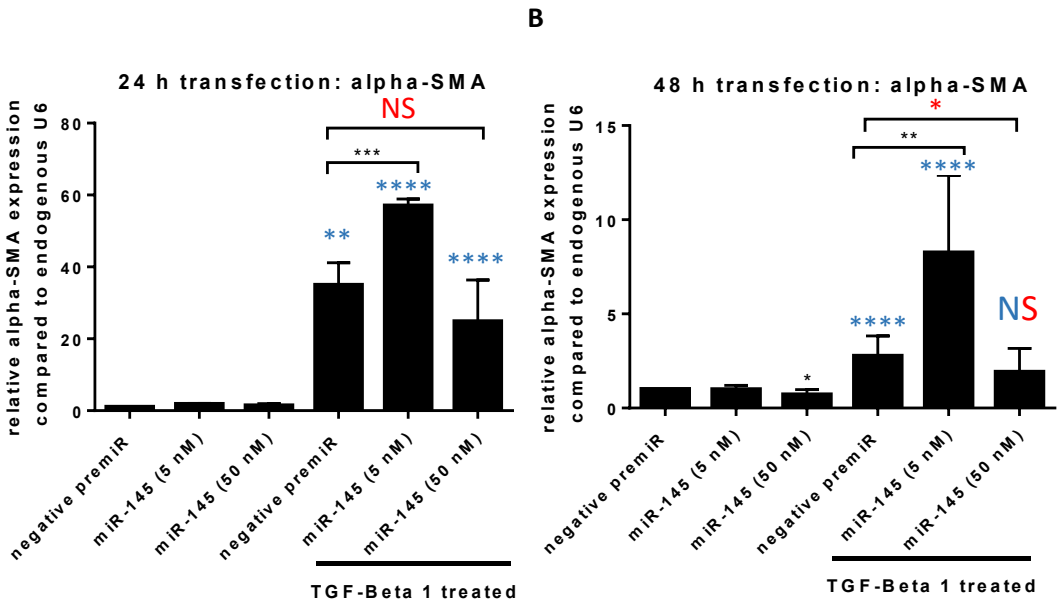

Figure 4.12: miR-145 overexpression (50 nM) reduced αSMA transcript levels in TGF-β1 induced myofibroblasts. DENF316 NOFs were treated with 5 ng/ml TGF-β1 or serum free media, then transiently transfected with 5 nM premiR-145, 50 nM premiR-145 or a negative non-targeting premiR. The transfection was left for either 24 h or 48 h before being harvested. RNA was isolated and 100 ng was used to generate total cDNA for qRT-PCR analysis using primers for αSMA and U6, as an endogenous control. Each bar on the figure represents the mean relative quantification of αSMA transcript levels compared to endogenous U6, for each transfection plus/minus treatment relative to untreated negative premiR. Figure **A** shows the relative αSMA transcript levels in samples left for 24 h to transfect and **B** shows samples left for 48 h to transfect. Statistical analysis was performed by a paired two tailed student's t-test, and statistical significance is shown on the figure by *p<0.05, **p<0.01, ***p<0.001, ****p<0.0001. If not indicated by a bar, the black significance asterix are compared to the untreated, negative premiR transfected, negative control. Blue significance asterix indicate significance compared to the untreated counterpart, e.g. premiR-145 transfected, TGF-β1 treated compared with premiR-145 transfected untreated. Bars also indicate statistical comparisons. Important significant data is shown in red. Error bars represent the SEM. N=3, independent experiments.

however, this trend only was significantly different from the negative premiR transfected TGF-β1 treated NOFs in the 48 h after transfection (figure 4.12B). At 48 h after transfection 50 nM premiR-145 was able to rescue the TGF-β1 induced αSMA expression as there was no significant difference in αSMA levels between untreated 50 nM premiR-145 transfected and TGF-β1 treated, 50 nM premiR-145 transfected. In the other NOF tested, DENF319, 48 h after transfection, there was a ~13 fold increase in αSMA in TGF-β1 treated NOFs, this was reduced to ~3 fold when transfected with 50 nM premiR-145 (Figure 4.13A). Therefore, miR-145 was able to markedly reverse the TGF-β1 induced myofibroblast increase in αSMA mRNA.

The same samples taken at 48 h after transfection were used to isolate total protein lysates and immunoblotting was performed to assess αSMA protein levels. αSMA protein levels were increased in NOFs induced to be myofibroblasts by TGF-β1, the TGF-β1 increase was quantified to be ~2 fold greater than untreated controls. miR-145 (50 nM) was able to slightly reduce the amount of αSMA protein, to ~1.5 fold (figure 4.13 B and C). The change in αSMA protein levels was small compared to the dramatic change in mRNA expression perhaps reflecting αSMA reported long half-life.

Next, the effect of the overexpression of miR-145 on the presence of αSMA-positive stress fibres in oral myofibroblasts was assessed. NOFs were seeded on coverslips and induced to transdifferentiate to myofibroblasts using 5 ng/ml TGF-β1, and were then transiently transfected with premiR-145 (5 nM or 50 nM) or a negative premiR for 48 h. The coverslips were then removed, methanol fixed, cells permeabilised and used for immunocytochemistry for αSMA stress fibres using a FITC-conjugated αSMA antibody. NOFs treated, then transfected with either negative premiR or the lower dose of premiR-145 (5 nM) stained brightly for stress fibres compared to their corresponding controls (figure 4.14A). When quantified, premiR-145 (5 nM) transfected induced myofibroblasts had a significant increase (~2.5 fold) in the amount of total fluorescence per cell, however, although negative premiR transfected induced myofibroblast increase (also ~2.5 fold) in fluorescence did not reach significance, it was clear from the images that there was an induction of stress fibre formation. There was a reduction in the amount of total fluorescence and width of stress fibres when TGF-β1 induced myofibroblasts were transfected with the higher dose of premiR-145 (50 nM) (figure 4.14). The data shown here was obtained using DENF319 NOFs but similar results were obtained using DENF316s.

The most well-characterised marker of myofibroblast phenotype, αSMA, was partially reduced on overexpression of miR-145. But to more fully investigate the effect of miR-145 on induced myofibroblasts, it was necessary to analyse the effect on other markers of myofibroblast,

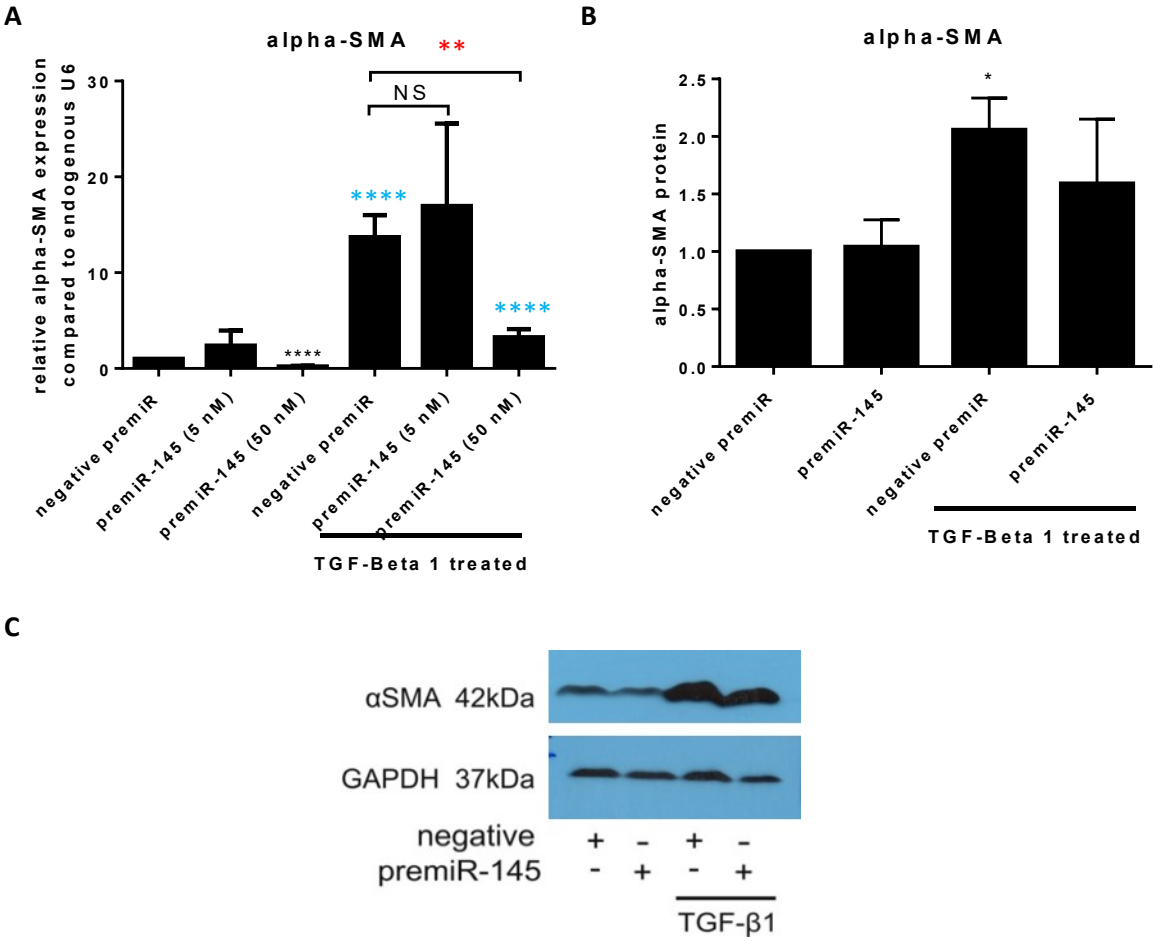

Figure 4.13: miR-145 significantly reduced TGF-β1 induced αSMA transcript levels. DENF319 NOFs were treated with 5 ng/ml TGF-β1 or serum free media, then transiently transfected with 5 nM premiR-145, 50 nM premiR-145 or a negative non-targeting premiR. The transfection was left for 48 h before being harvested. RNA was isolated and 100 ng was used to generate total cDNA for qRT-PCR analysis using primers for αSMA and U6, as an endogenous control. Total protein lysates were prepared my resuspending cell pellets in RIPA protein lysis buffer and quantifying using a BCA assay. 30 ug was loading on 3-8 tris-acetate SDS-PAGE gel, then transferred to a nitrocellulose membrane for immunoblotting using antibodies raised to human αSMA and GAPDH as a loading control. Each bar on the figure **A** represents the mean relative quantification of αSMA transcript levels compared to endogenous U6, for each transfection plus/minus treatment relative to untreated negative premiR. **B** shows the quantified amount of protein in each sample and **C** shows a representative immunoblot. Statistical analysis was performed by a paired two tailed student's t-test, and statistical significance is shown on the figure by *p<0.05, **p<0.01, ***p<0.001, ****p<0.0001. If not indicated by a bar, the black significance asterix are compared to the untreated, negative premiR transfected, negative control. Blue significance asterix indicate significance compared to the untreated counterpart, e.g. premiR-145 transfected, TGF-β1 treated compared with premiR-145 transfected untreated. Bars also indicate statistical comparisons. Important significant data is shown in red. Error bars represent the SEM. N=3, independent experiments.

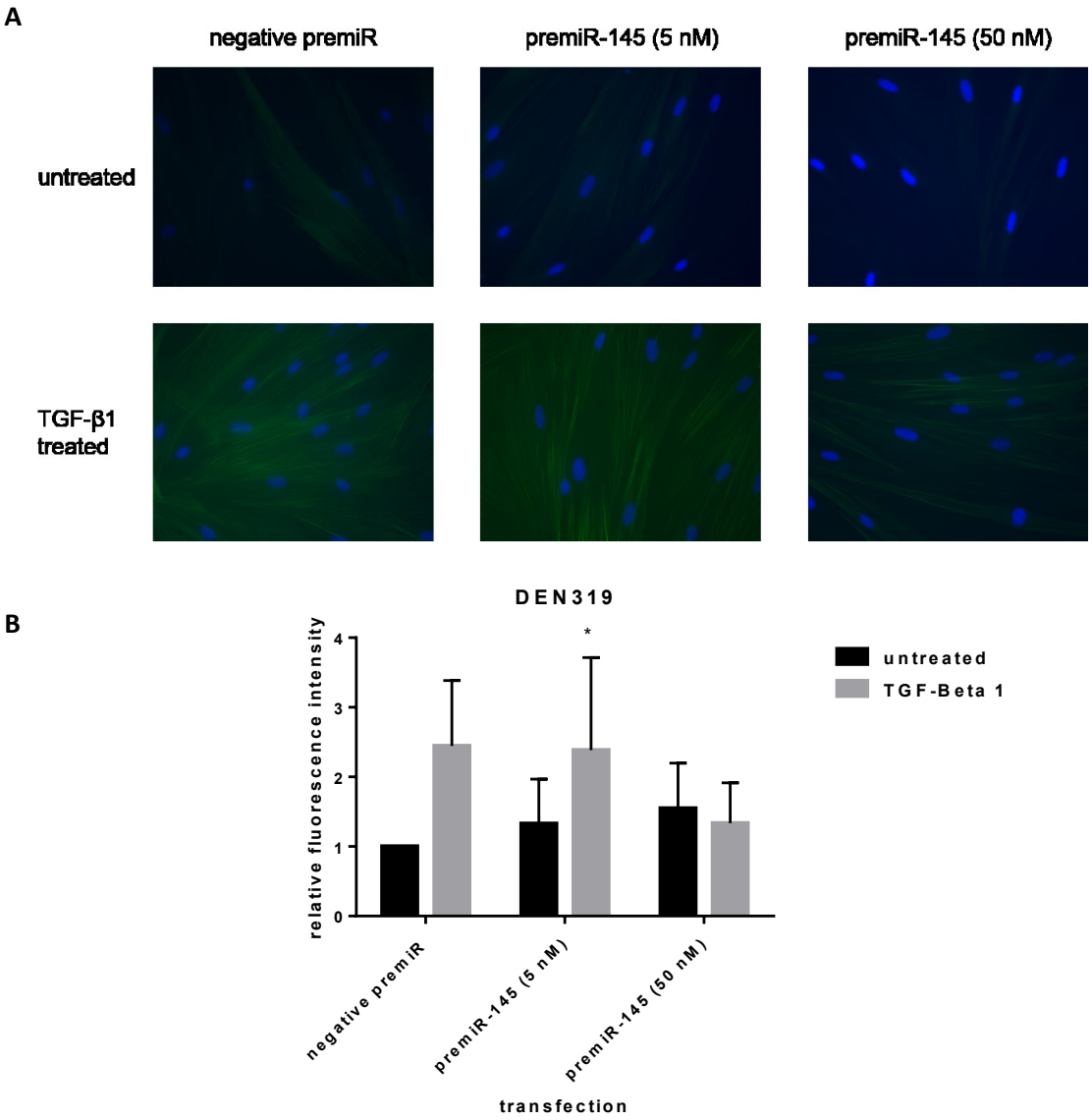

Figure 4.14: miR-145 overexpression reduced αSMA stress fibre formation. NOFs were seeded onto coverslips overnight, treated with 5 ng/ml TGF-β1 for 48 h, or serum free media, then were transiently transfected with negative premiR, or premiR-145 (at two doses, 5 nM or 50 nM). The coverslips were washed in PBS, before being fixed in 100% methanol for 10 min, they were then permeablised using 4 mM sodium deoxycholate for 10 min, and blocked using 2.5% (w/v) BSA in PBS for 30 min before incubation with a primary FITC-conjugated αSMA antibody at 4 ^{o}C overnight. The coverslips were then washed in PBS before mounting on microscope slides using DAPI containing mounting medium. Fluorescent images were taken using a fluorescent light microscope, using Pro-plus 7 imaging software at 40x magnification. Representative pictures are shown in **A.** The amount of fluorescence intensity per cell was quantified using Image J, and displayed in **B** as the mean relative fluorescent intensity for DENF319. Statistical analysis was performed by a paired two tailed student's t-test, and statistical significance is shown on the figure by *p<0.05, premiR-145 (5 nM) treated compared to treated. N=3, independent experiments. Error bars show the SEM.

namely COL1A1 and FN1-EDA. Each myofibroblast marker assessed had a greater fold change in the treated NOFs at 24 h than 48 h (figure 4.12, 15, 17). DENF316s were treated with TGF-β1 then transfected with miR-145 (5 nM or 50 nM) or negative premiR for 24 h or 48 h, and COL1A1 and FN1-EDA transcript levels were assessed via qRT-PCR. At 24 h after transfection there was an increase in COL1A1 in treated NOFs transfected with a low doses of premiR-145 (5 nM) (~3.3 fold increase), but no significant change in negative premiR transfected NOFs (~1.3 fold increase) (figure 4.15). There was also no change in COL1A1 levels in TGF-β1 induced myofibroblasts 48 h after transfection in DENF316. miR-145 at the highest dose (50 nM) was able to significantly decrease COL1A1 mRNA levels in untreated NOFs at 24 h and 48 h after transfection, by ~0.5 fold in DENF316s and ~0.9 fold in DENF319s. In DENF319 NOFs TGF-β1 caused a significant upregulation of COL1A1 marker at 48 h (~1.7 fold) when transfected with negative premiR after TGF-β1 treatment. TGF-β1 treated NOFs transfected with the low dose of premiR-145 (5 nM) transfection showed a similar level of COL1A1 (~1.7 fold increase), but when transfected with the high dose there was a significant attenuation of the COL1A1 expression (~1 fold; figure 4.16). miR-145 transfected at a high dose was also able to downregulate COL1A1 mRNA levels in untreated NOFs in DENF319s (~0.9 fold decrease).

The other myofibroblast molecular marker assessed was FN1-EDA. At 24 h after transfection of premiR-145 at the highest dose (50 nM) there was a significant inhibition (~2 fold increase) of the increase in FN1-EDA compared to treated, negative premiR transfected (~3 fold increase). Treated NOFs transfected with 5 nM premiR-145, also had a significant increase in FN1-EDA expression at 24 h after transfection (~7 fold) compared to untreated miR-145 (5 nM) (figure 4.17). However, at 48 h after transfection both in NOFs (figure 4.17 and 4.18), the highest dose of miR-145 (50 nM) was not able to significantly reduce FN1-EDA expression compared to the negative premiR, treated control (~3 and ~4 fold increases, respectively).

Finally, to confirm miR-145 was overexpressed in a dose dependant manner in these rescue experiments, qRT-PCR was performed to assess the levels of mature miR-145 in treated then transfected NOFs. RNA isolated from the experiments was used to generate specific miR-145 and RNU 48 cDNA, the used in a qRT-PCR reaction using primers specific for miR-145 and RNU 48. In DENF316, 24 h after transfection the lower dose of premiR-145 produced a ~25 fold overexpression of the mature miRNA; this falls to ~8 fold overexpression at 48 h after transfection. The higher dose of premiR-145 (50 nM) caused an overexpression of ~55 fold after 24 h which had fallen to ~35 and ~20 fold, untreated and treated respectively (figure 4.19). In

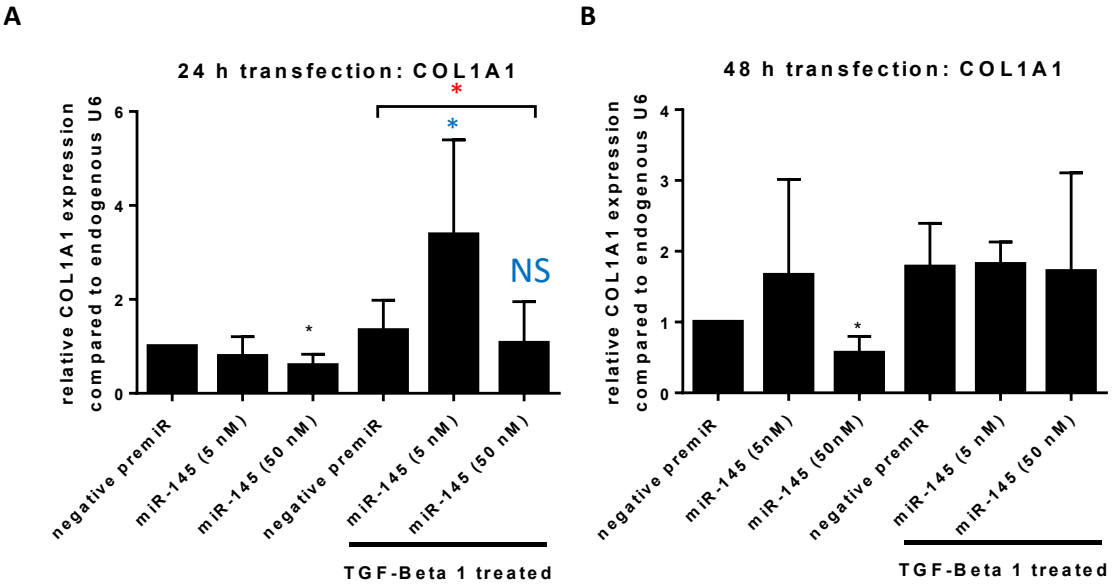

Figure 4.15: miR-145 overexpression in TGF-β1 induced myofibroblasts reduced COL1A1 expression at 24 h, but not at 48 h after transfection in DENF316 NOFs. DENF316 NOFs were treated with 5 ng/ml TGF-β1 or serum free media, then transiently transfected with 5 nM premiR-145, 50 nM premiR-145 or a negative non-targeting premiR. The transfection was left for either 24 h or 48 h before being harvested. RNA was isolated and used to generate total cDNA for qRT-PCR analysis using primers for COL1A1 and U6, as an endogenous control. Each bar on the figure represents the mean relative quantification of COL1A1 transcript levels compared to endogenous U6, for each transfection plus/minus treatment relative to untreated negative premiR. Figure **A** shows the relative COL1A1 transcript levels in samples left for 24 h to transfect and **B** shows samples left for 48 h to transfect. Statistical analysis was performed by a paired two tailed student's t-test, and statistical significance is shown on the figure by *p<0.05. If not indicated by a bar, the black significance asterix are compared to the untreated, negative premiR transfected, negative control. Blue significance asterix indicate significance compared to the untreated counterpart, e.g. premiR-145 transfected, TGF-β1 treated compared with premiR-145 transfected untreated. Bars also indicate statistical comparisons. Important significant data is shown in red. Error bars represent the SEM. N=3, independent experiments.

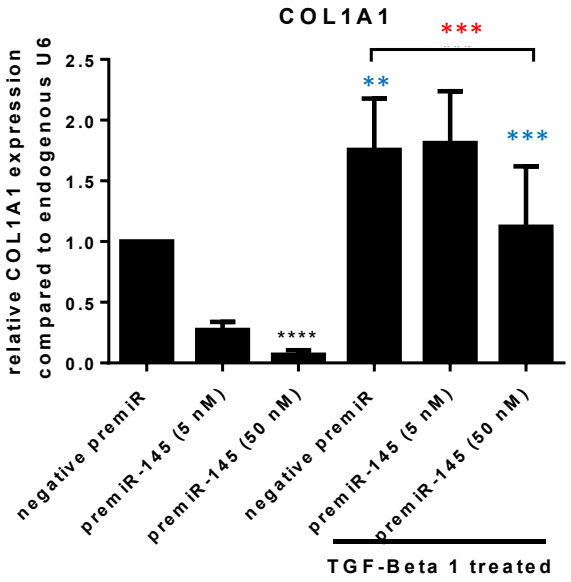

Figure 4.16: miR-145 overexpression in TGF-β1 induced myofibroblasts reduced COL1A1 expression at 48 h after transfection in DENF319 NOFs. DENF319 NOFs were treated with 5 ng/ml TGF-β1 or serum free media, then transiently transfected with 5 nM premiR-145, 50 nM premiR-145 or a negative non-targeting premiR. The transfection was left for 48 h before being harvested. RNA was isolated and 100 ng was used to generate total cDNA for qRT-PCR analysis using primers for COL1A1 and U6, as an endogenous control. Each bar on the figure represents the mean relative quantification of COL1A1 transcript levels compared to endogenous U6, for each transfection plus/minus treatment relative to untreated negative premiR. Statistical analysis was performed by a paired two tailed student's t-test, and statistical significance is shown on the figure by *p<0.05, **p<0.01, ***p<0.001, ****p<0.0001. If not indicated by a bar, the black significance asterix are compared to the untreated, negative premiR transfected, negative control. Blue significance asterix indicate significance compared to the untreated counterpart, e.g. premiR-145 transfected, TGF-β1 treated compared with premiR-145 transfected untreated. Bars also indicate statistical comparisons. Important significant data is shown in red. Error bars represent the SEM. N=3, independent experiments.

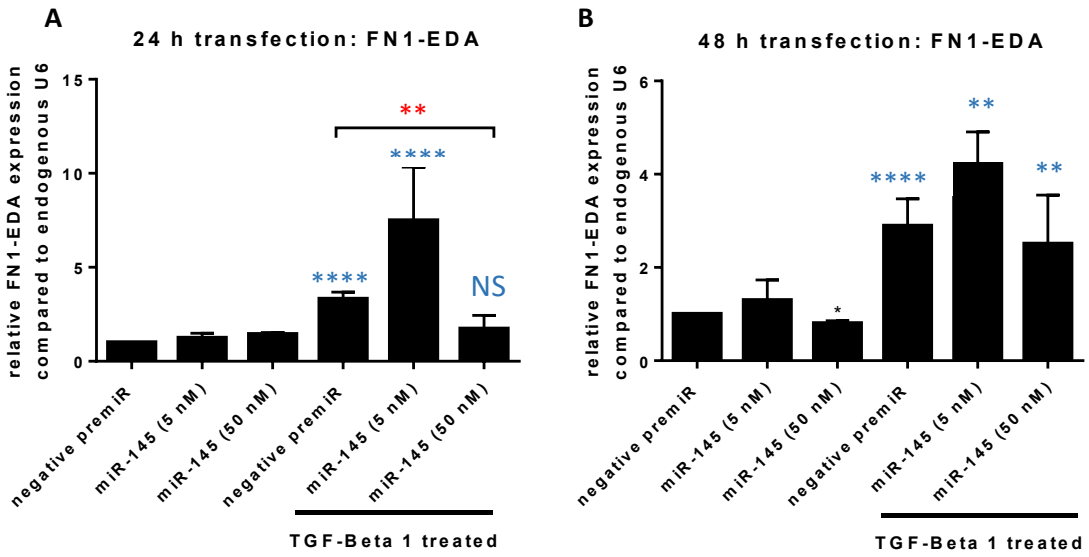

Figure 4.17: miR-145 overexpression in TGF-β1 induced myofibroblasts reduced FN1-EDA expression at 24 h, but not 48 h after transfection in DENF316. DENF316 NOFs were treated with 5 ng/ml TGF-β1 or serum free media, then transiently transfected with 5 nM premiR-145, 50 nM premiR-145 or a negative non-targeting premiR. The transfection was left for either 24 h or 48 h before being harvested. RNA was isolated and 100 ng was used to generate total cDNA for qRT-PCR analysis using primers for FN1-EDA and U6, as an endogenous control. Each bar on the figure represents the mean relative quantification of FN1-EDA transcript levels compared to endogenous U6, for each transfection plus/minus treatment relative to untreated negative premiR. Figure **A** shows the relative FN1-EDA transcript levels in samples left for 24 h to transfect and **B** shows samples left for 48 h to transfect. Statistical analysis was performed by a paired two tailed student's t-test, and statistical significance is shown on the figure by *p<0.05. If not indicated by a bar, the black significance asterix are compared to the untreated, negative premiR transfected, negative control. Blue significance asterix indicate significance compared to the untreated counterpart, e.g. premiR-145 transfected, TGF-β1 treated compared with premiR-145 transfected untreated. Bars also indicate statistical comparisons. Important significant data is shown in red. Error bars represent the SEM. N=3, independent experiments.

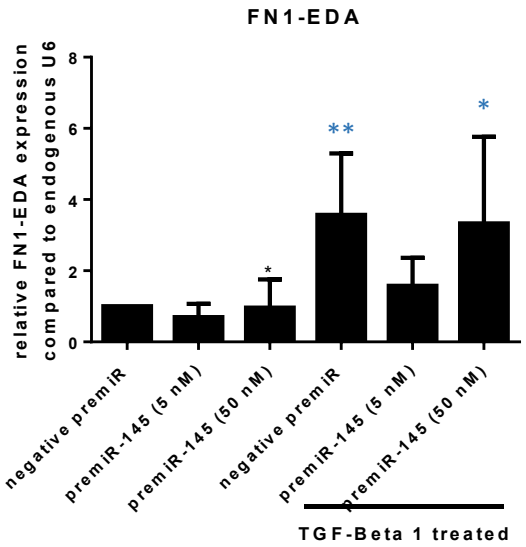

Figure 4.18: miR-145 overexpression did not reduce FN1-EDA expression in TGF-β1 induced oral myofibroblasts. DENF319 NOFs were treated with 5 ng/ml TGF-β1 or serum free media, then transiently transfected with 5 nM premiR-145, 50 nM premiR-145 or a negative non-targeting premiR. The transfection was left for 48 h before being harvested. RNA was isolated and 100 ng was used to generate total cDNA for qRT-PCR analysis using primers for FN1-EDA and U6, as an endogenous control. Each bar on the figure represents the mean relative quantification of FN1-EDA transcript levels compared to endogenous U6, for each transfection plus/minus treatment relative to untreated negative premiR. Statistical analysis was performed by a paired two tailed student's t-test, and statistical significance is shown on the figure by *p<0.05, **p<0.01, ***p<0.001, ****p<0.0001. If not indicated by a bar, the black significance asterix are compared to the untreated, negative premiR transfected, negative control. Blue significance asterix indicate significance compared to the untreated counterpart, e.g. premiR-145 transfected, TGF-β1 treated compared with premiR-145 transfected untreated. Bars also indicate statistical comparisons. Important significant data is shown in red. Error bars represent the SEM. N=3, independent experiments.

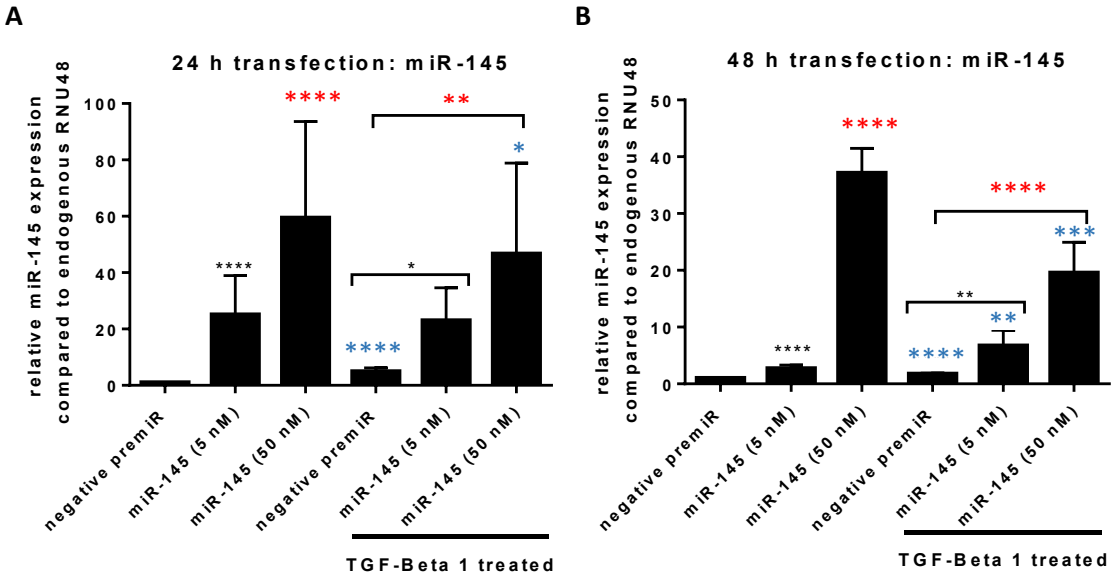

Figure 4.19: Validation of the overexpression of miR-145 using premiR-145 in DENF316 NOFs. DENF316 NOFs were treated with 5 ng/ml TGF-β1 or serum free media, then transiently transfected with 5 nM premiR-145, 50 nM premiR-145 or a negative non-targeting premiR. The transfection was left for either 24 h or 48 h before being harvested. RNA was isolated and 100 ng was used to generate specific cDNA for RNU 48 and miR-145 using specific primers, this cDNA was then used in qRT-PCR analysis using primers for miR-145 and RNU 48, as an endogenous control. Each bar on the figure represents the mean relative quantification of mature miR-145 transcript levels for compared to endogenous U6, each transfection plus/minus treatment relative to untreated negative premiR. Figure **A** shows the relative FN1-EDA transcript levels in samples left for 24 h to transfect and **B** shows samples left for 48 h to transfect. Statistical analysis was performed by a paired two tailed student's t-test, and statistical significance is shown on the figure by *p<0.05, **p<0.01, ***p<0.001, ****p<0.0001. If not indicated by a bar, the black significance asterix are compared to the untreated, negative premiR transfected, negative control. Blue significance asterix indicate significance compared to the untreated counterpart, e.g. premiR-145 transfected, TGF-β1 treated compared with premiR-145 transfected untreated. Bars also indicate statistical comparisons. Important significant data is shown in red. Error bars represent the SEM. N=3, independent experiments.

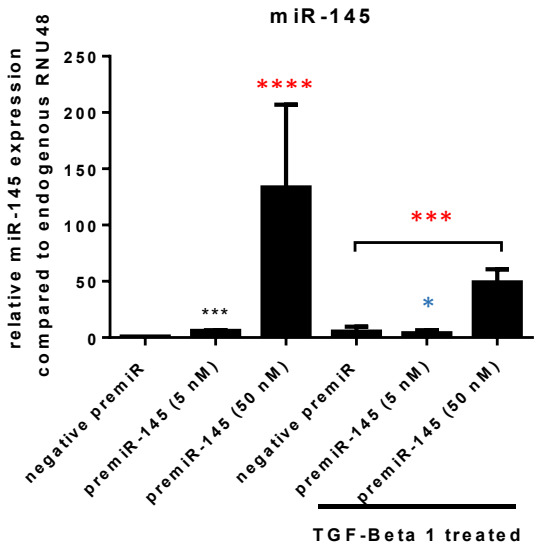

Figure 4.20: Validation of the overexpression of miR-145 using premiR in DENF319 NOFs. DENF319 NOFs were treated with 5 ng/ml TGF-β1 or serum free media, then transiently transfected with 5 nM premiR-145, 50 nM premiR-145 or a negative non-targeting premiR. The transfection was left for 48 h before being harvested. RNA was isolated and 100 ng was used to generate specific miR-145 and RNU 48 cDNA for qRT-PCR analysis using primers for miR-145 and RNU 48, as an endogenous control. Each bar on the figure represents the mean relative quantification of miR-145 transcript levels compared to endogenous RNU 48, for each transfection plus/minus treatment relative to untreated negative premiR. Statistical analysis was performed by a paired two tailed student's t-test, and statistical significance is shown on the figure by *p<0.05, **p<0.01, ***p<0.001, ****p<0.0001. If not indicated by a bar, the black significance asterix are compared to the untreated, negative premiR transfected, negative control. Blue significance asterix indicate significance compared to the untreated counterpart, e.g. premiR-145 transfected, TGF-β1 treated compared with premiR-145 transfected untreated. Bars also indicate statistical comparisons. Important significant data is shown in red. Error bars represent the SEM. N=3, independent experiments.

DENF319 premiR-145 (5 nM) transfection was only able to cause a small overexpression (~5 fold) of mature miR-145 in untreated NOFs, whereas 50 nM caused a ~139 and ~50 fold overexpression of miR-145 in untreated and treated DENF319 respectively (figure 4.20) 48 h after transfection.

To fully investigate the role of miR-145 in the myofibroblast transdifferentiation, an attempt to knock-down miR-145 was made using an anti-sense anti-miR-145 to inhibit mature miR-145 via RNAi. NOFs were transiently transfected with antimiR-145 at 3 different concentrations in 0.5 nM, 5 nM and 50 nM, with a mock (water) control for 48 h. The fibroblasts were then harvested, RNA isolated and used to prepare miR-145 and RNU 48 specific cDNA for use in qRT-PCR. qPCR revealed that the antimiR-145 oligonucleotide was not able to downregulate mature miR-145 levels at either concentration tested (figure 4.21).

4.5 *miR-145 partially reversed the pro-tumourigenic effects of oral myofibroblasts*

Transwell paracrine migration and invasion assays were used to assess miR-145's ability to effect the paracrine effects of myofibroblast. Conditioned media was collected from NOFs treated with 5 ng/ml TGF-β1 for 48 h to induce myofibroblast differentiation, then transiently transfected with negative premiR, or premiR-145 (5 nM or 50 nM). This conditioned media was placed in the bottom of a transwell migration/invasion assay, with an 8 µM porous membraned transwell with or without a Matrigel layer (migration/invasion respectively) placed on top of the media. H357 cells were seeded in the transwell and allowed to migrate/invade through towards the conditioned media for 38 h/72 h. The migrated cells were then methanol fixed to the membrane and stained with crystal violet to visualise. Representative pictures were taken with a light microscope at 40x and the number of cells migrated were counted using ImageJ software.

Media from TGF-β1-treated NOFs promoted the migration of the H357s cells 1.5 fold more than untreated controls (figure 4.22). In DENF316 NOFs, the overexpression of miR-145 (highest dose) was able to significantly inhibit the effect of TGF-β1 (figure 4.22A), however in DENF319 neither 5 nM nor 50 nM premiR-145 was able to reverse the effect of TGF-β1 on the fibroblasts' ability to stimulate cancer cell migration (figure 4.22B) and all treated conditions stimulated ~1.5 fold more migration than the untreated control. miR-145 overexpression in untreated DENF316 NOFs caused an increase (~1.4 fold) in cancer cell migration, although this trend did not reach significance.

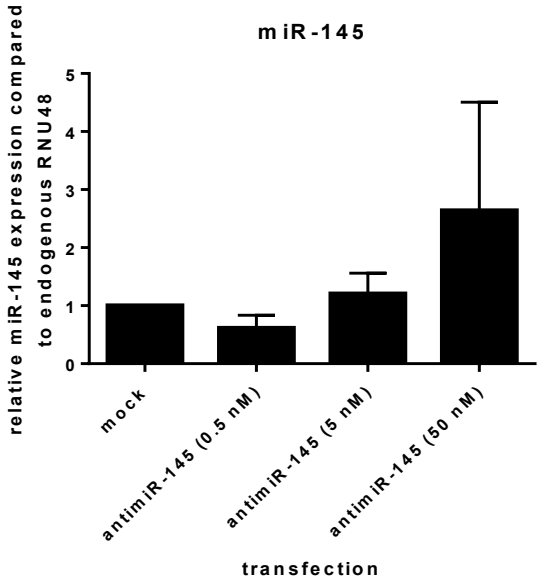

Figure 4.21: antimiR-145 failed to knock-down mature miR-145 levels in DENF316 NOFs. NOFs were transiently transfected with 0 nM, 0.5 nM, 5 nM, 50 nM antimiR-145 for 48 h. RNA was isolated and 10 ng used to generate specific cDNA for RNU 48 and miR-145 using gene specific Taqman primers, this cDNA was then used in qRT-PCR analysis using primers for miR-145 and RNU 48, as an endogenous control. Each bar on the figure represents the mean relative quantification of mature miR-145 transcript levels compared to endogenous RNU 48, for each transfection plus/minus treatment relative to untreated negative premiR. Error bars represent the SEM. N=3, independent experiments.

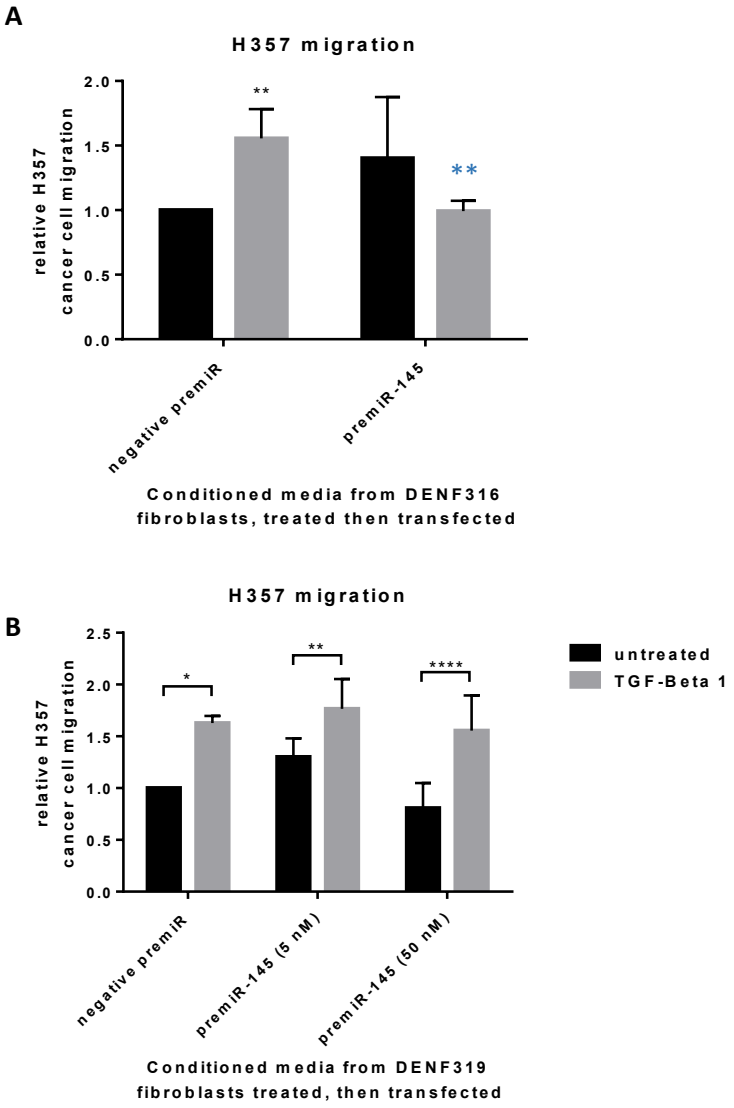

Figure 4.22: miR-145 reversed TGF-β1's paracrine pro-migratory effect on H357 cancer cell migration in DENF316 NOFs, not DENF319s. Conditioned media was collected from DENF316 or DENF319 NOFs (**A** and **B** respectively) were treated with 5 ng/ml TGF-β1 for 48 h or serum free media as a control, then transfected with negative premiR, or premiR-145 (5 nM or 50 nM) for 24 h then. The conditioned media was spun at >2500xg to remove cellular debris then placed in the bottom of a transwell migration assay plate. H357 cancer cell line were seeded at 100,000 cells per well into an 8 µm porous transwell with 1 mg/ml mitomycin c and allowed to migrate for 38 h. The ability of the conditioned media to promote migration was assessed by methanol fixing cells attached to the membrane after 38 h, staining the cells with 0.1% (w/v) crystal violet, taking photographs at 40x, and calculating the average number of cells in the representative photographs. The figure shows the relative H357 cancer cell migration. Statistical analysis was performed by a paired two tailed student's t-test, and statistical significance is shown on the figure by *p<0.05, **p<0.01, ***p<0.001, ****p<0.0001. If not indicated by a bar, the black significance asterix are compared to the untreated, negative premiR transfected and blue significance asterix are compared to the TGF-β1 treated, negative transfected. Bars also indicate statistical comparisons. Error bars represent the SEM. N=3, independent experiments.

TGF-β1-treated NOFs were unable to cause a significant change in invasion when the conditioned media from treated, then transfected NOFs was used in the invasion assays. In DENF316, TGF-β1 treated NOF-derived conditioned media caused a slight, but not significant increase (~1.5 fold) in H357 invasion (figure 4.23A) whereas in DENF319 there was a slight decrease (~0.2 fold decrease) in invasion (figure 4.23B). Again, miR-145 overexpression had opposing effects in the two cultures tested. In DENF316, premiR-145 transfection in untreated NOFs caused an increase (~2.5 fold) in invasion (not significant; figure 4.23A), whereas in DENF319 premiR-145 (50 nM) also caused a significant reduction (~0.75) fold in cancer cell invasion in untreated NOFs and both doses caused a further decrease in invasion in treated DENF319s (figure 4.23B).

4.6 ***Mir-145 effect on cancer associated fibroblasts.***

To assess miR-145s effect on fibroblasts isolated from OSCCs, referred to as CAFs, miR-145 was transiently overexpressed in 4 different CAFs and myofibroblasts molecular markers were assessed. qRT-PCR revealed that miR-145 overexpression in 3 out of 4 of the CAFs (BICR-3, BICR-59 and BICR-63) tested caused a reduction of the myofibroblasts markers αSMA, COL1A1 and FN1-EDA (figure 4.24). BICR-3, BICR-59 and BICR-63 each had a ~0.6 fold decrease in αSMA when transfected with premiR-145 (figure 4.24A) compared to CAFs transfected with negative non targeted premiR. COL1A1 transcript levels were reduced in the 3 CAFs overexpressing miR-145 by ~0.92 ~0.94, and ~0.5 fold in BICR-59, BICR-63 and BICR-3 respectively (figure 4.24B). FN1-EDA transcript levels were also decreased in these 3 miR-145 overexpressing CAFs by ~0.8 fold compared to negative control transfected cells (figure 4.24C). In BICR-70 primary CAFs, the miR-145 overexpression caused a ~0.25 fold reduction in COL1A1 transcript levels, however αSMA and FN1-EDA increased on average by ~8 fold and ~7 fold respectively (figure 4.24).

A similar effect of miR-145 reducing the markers of myofibroblast markers expression was seen in NOFs. Also, miR-145 was able to prevent TGF-β1 inducing the myofibroblasts phenotype in NOFs. Therefore, to assess whether miR-145 had a similar effect on preventing TGF-β1 effects in CAFs, the transfection was repeated, then TGF-β1 treatment experiment assessing molecular markers via qRT-PCR, immunoblotting and immunocytochemistry. TGF-β1 was able to cause an increase in markers of myofibroblasts markers αSMA, COL1A1 and FN1-EDA (figure 4.25, 4.28 and 4.29) in the 4 CAFs tested. Like with the NOFs, TGF-β1 treatment produced a different magnitude of response from each of the CAFs. TGF-β1 caused αSMA transcript levels to increase

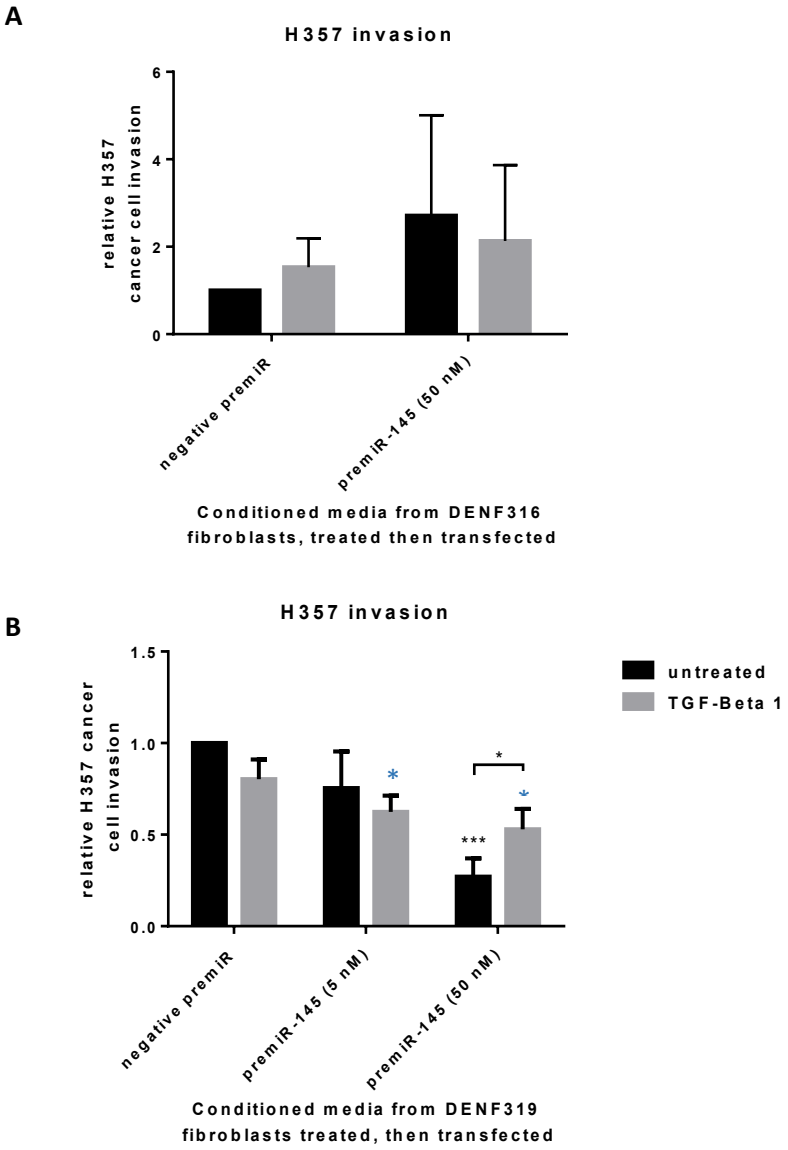

Figure 4.23: miR-145 decreased invasion in DENF319 not DENF316 NOFs. Conditioned media was collected from DENF316 or DENF319 NOFs (**A** and **B** respectively) treated with 5 ng/ml TGF-β1 for 48 h or serum free media as a control, then transfected with negative premiR, premiR-145 (5 nM or 50 nM) for 48 h. The conditioned media was spun at >2500xg to remove cellular debris then placed in the bottom of a transwell invasion assay plate. H357 cancer cell line were seeded at 100,000 cells per well into a 8 µm porous Matrigel coated transwell, with 1 mg/ml mitomycin c and allowed to migrate for 38 h. The ability of the conditioned media to promote invasion was assessed by methanol fixing cells attached to the underside of the transwell membrane after 38 h, staining the cells with 0.1% (w/v) crystal violet, taking photographs at 40x, and calculating the average number of cells in the representative photographs. The figure shows the relative H357 cancer cell invasion compared to untreated, negative premiR. Statistical analysis was performed by a paired two tailed student's t-test, and statistical significance is shown on the figure by **p<0.01, ***p<0.001. If not indicated by a bar, the black significance asterix are compared to the untreated, negative premiR transfected and blue significance asterix are compared to the TGF-β1 treated, negative transfected. Bars also indicate statistical comparisons. Error bars represent the SEM. N=3, independent experiments.

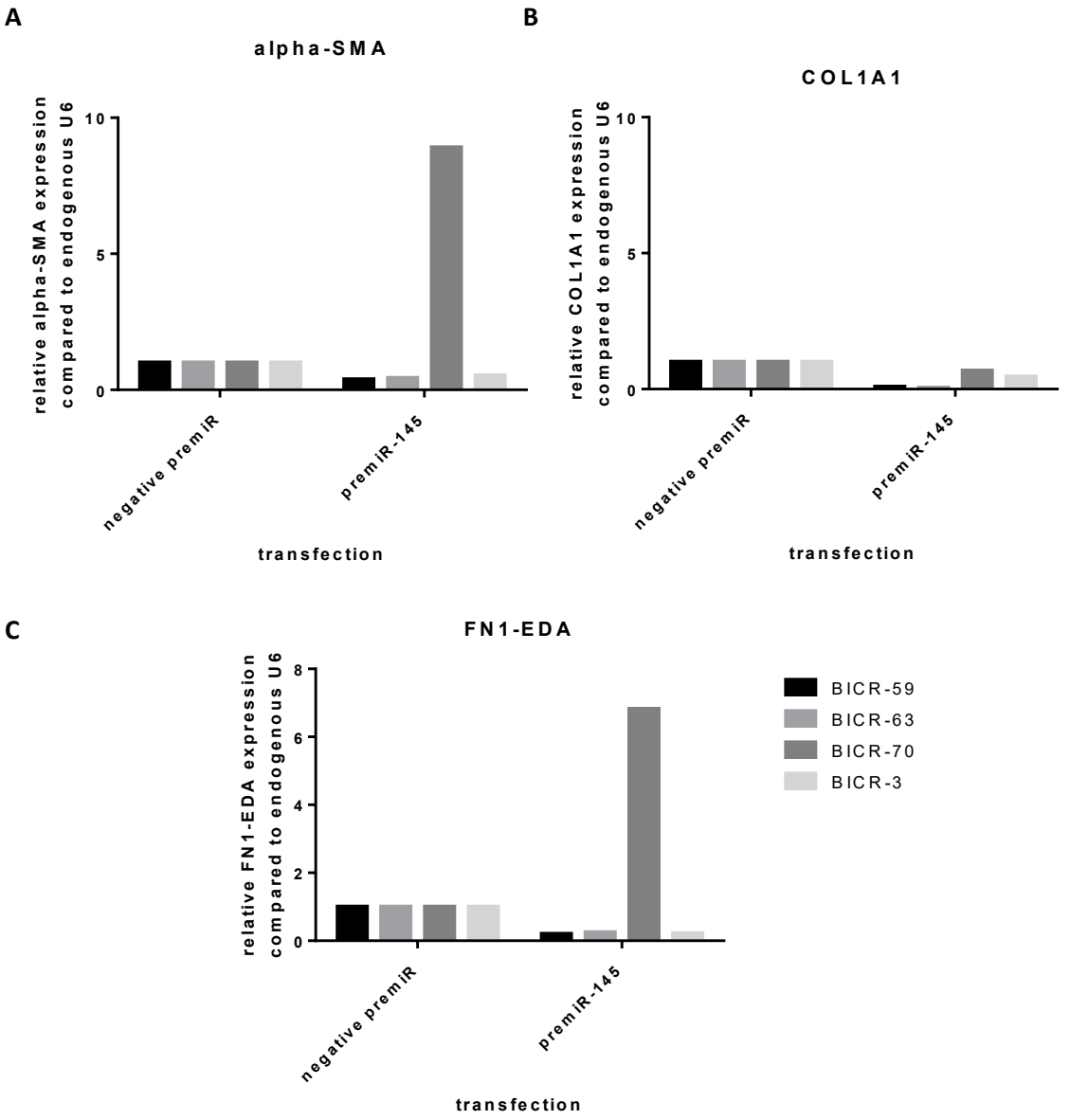

Figure 4.24: miR-145 overexpression reduced the expression of αSMA, COL1A1 and FN1-EDA myofibroblast markers in CAFs. Primary CAFs BICR-3, BICR-59, BICR-63 and BICR 70 were transiently transfected with premiR-145 (50 nM) or a negative non-targeting premiR 24 h, they were then left in serum free media for a further 48 h before harvesting. The RNA was isolated and 100 ng was used to generate total cDNA for qRT-PCR analysis using primers designed to amplify αSMA, FN1-EDA, COL1A1 and U6, as an endogenous control. Each bar on the figure represents the mean relative quantification of αSMA (**A**), COL1A1 (**B**) and FN1-EDA (**C**) transcript levels compared to endogenous U6, for each transfection plus/minus treatment relative to untreated negative premiR. N=2, independent experiments per CAF.

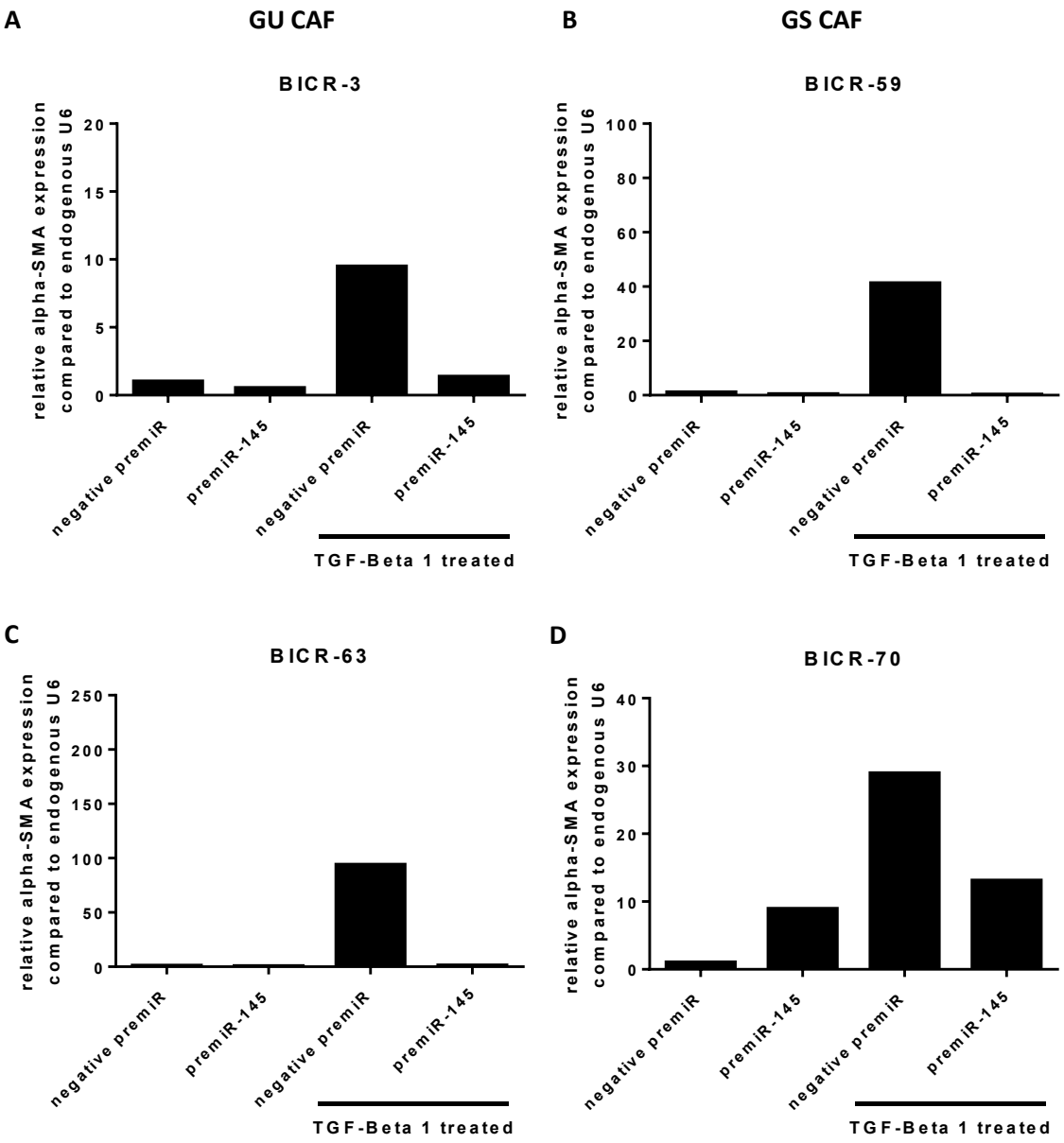

Figure 4.25: miR-145 overexpression prevented TGF-β1 stimulated increase in αSMA mRNA levels in CAFs. Primary CAFs BICR-3 (**A**), BICR-59 (**B**), BICR-63 (**C**) and BICR 70 (**D**) were transiently transfected with premiR-145 (50 nM) or a negative non-targeting premiR 24 h prior to the treatment with 5 ng/ml TGF-β1 or serum free media as a control. The RNA was isolated and 100 ng was used to generate total cDNA for qRT-PCR analysis using primers designed to amplify αSMA and U6, as an endogenous control. Each bar on the figure represents the mean relative quantification of αSMA transcript levels compared to endogenous U6, for each transfection plus/minus treatment relative to untreated negative premiR. N=2, independent experiments per CAF.

by ~10, ~40, ~100, ~30 fold increases in BICR-3, BICR-59, BICR-63 and BICR-70 respectively (figure 4.25). In each CAF tested, overexpression of miR-145 prior to TGF-β1 treatment was able to reduce the TGF-β1 increase in myofibroblast marker expression. Overexpression in BICR-3, BICR-59 and BICR-63 CAFs was able to completely prevent any induction in αSMA in response to TGF-β1, the αSMA transcript levels were ~1.4 fold, ~0.4 fold, and ~1.3 fold compared to negative transfected, untreated CAFs. BICR-70 CAFs that were transfected with premiR-145 on the other hand, only partially reduced the TGF-β1 stimulated increase in αSMA transcript levels, from ~30 fold to ~12.4 fold (figure 4.25D). Similar effects of miR-145 were observed in αSMA at the protein level (figure 4.26). Immunoblotting revealed that CAFs treated with TGF-β1 had a significantly higher αSMA protein expression, quantified to be ~5 fold higher by densitometry. This increase in αSMA was prevented in CAFs that were overexpressing miR-145, where the detectable protein was ~1.5 fold higher than untreated, negative premiR transfected controls.

Similar effects of miR-145 were observed in αSMA at the protein level (figure 4.26). Immunoblotting revealed that CAFs treated with TGF-β1 had a significantly higher αSMA protein expression, quantified to be ~5 fold higher by densitometry. This increase in αSMA was prevented in CAFs that were using a fluorescently tagged antibody to αSMA, αSMA stress fibres were visualised in CAFs that were transfected then treated with TGF-β1. TGF-β1 was able to cause a marked increase in αSMA staining and stress fibre formation in each of the CAFs that were treated. The increase in fluorescence was quantified to be ~5 fold, ~2 fold, and ~8 fold than untreated endogenous fluorescence in BICR-3, BICR-59, and BICR-63 CAFs respectively (figure 4.27). microRNA-145 caused a small reduction in TGF-β1 induced stress fibre formation and a reduction in total quantified fluorescence to ~4 fold, ~1.75 fold and ~2.5 fold in BICR-3, BICR-59 and BICR-63 CAFs respectively. Overexpression of microRNA-145, without TGF-β1 also caused a small increase in fluorescence intensity (~2.5 fold, ~1.7 fold and ~1.25 fold in BICR-3, BIR-59 and BICR-63 CAFs), but this was not accompanied by a visual increase in stress fibre formation. It is worth noting that miR-145 only partially inhibited TGF-β1 induced αSMA fibre formation in CAFs, compared to it being able to almost completely block the process in NOFs (figure 4.4).

In response to TGF-β1, 3 out of 4 of the CAFs tested (BICR-59, BICR-63 and BICR-70) had an increase in COL1A1 expression by ~2.6 fold, ~3.4 fold and 4.2 fold increase in BICR-3, BICR-59, BICR-63 and BICR-70 respectively (figure 4.28). Only BICR-3 CAFs no change in COL1A1 transcript levels relative to untreated controls (figure 4.28A). The overexpression of miR-145 was able to inhibit the TGF-β1 induced increase in COL1A1, the COL1A1 levels in CAFs overexpressing miR-

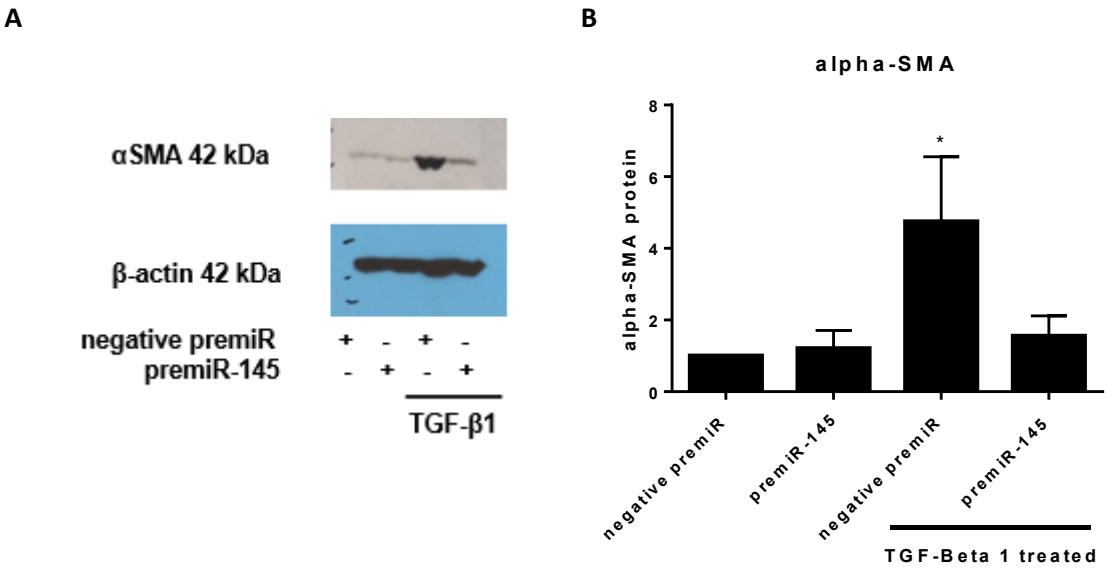

Figure 4.26: miR-145 overexpression prevented TGF-β1 induced αSMA increase in protein expression in oral CAFs. BICR-59 (shown here), BICR-63 and BICR-70 CAFs were transiently transfected with premiR-145 (50 nM) or negative non-targeting premiR-145 for 24 h prior to 5 ng/ml TGF-β1 treatment for 48 h. Total protein lysates were isolated, 20 µg was resolved on a 3–8% (w/v) tris-acetate gel and transferred to nitrocellulose membrane for immunoblotting. Antibodies raised to human αSMA and GAPDH as a loading control, were used to assess the amount of αSMA in samples (**A**), the amount detected was quantified using Image J and shown in **B**. N=3, independent experiments for BICR-59, N=1 for BICR-63 and BICR-70. SEM represents SEM. Statistical analysis was performed by a paired two tailed student's t-test, and statistical significance is shown on the figure by *p<0.05, compared to untreated, negative premiR transfected control.

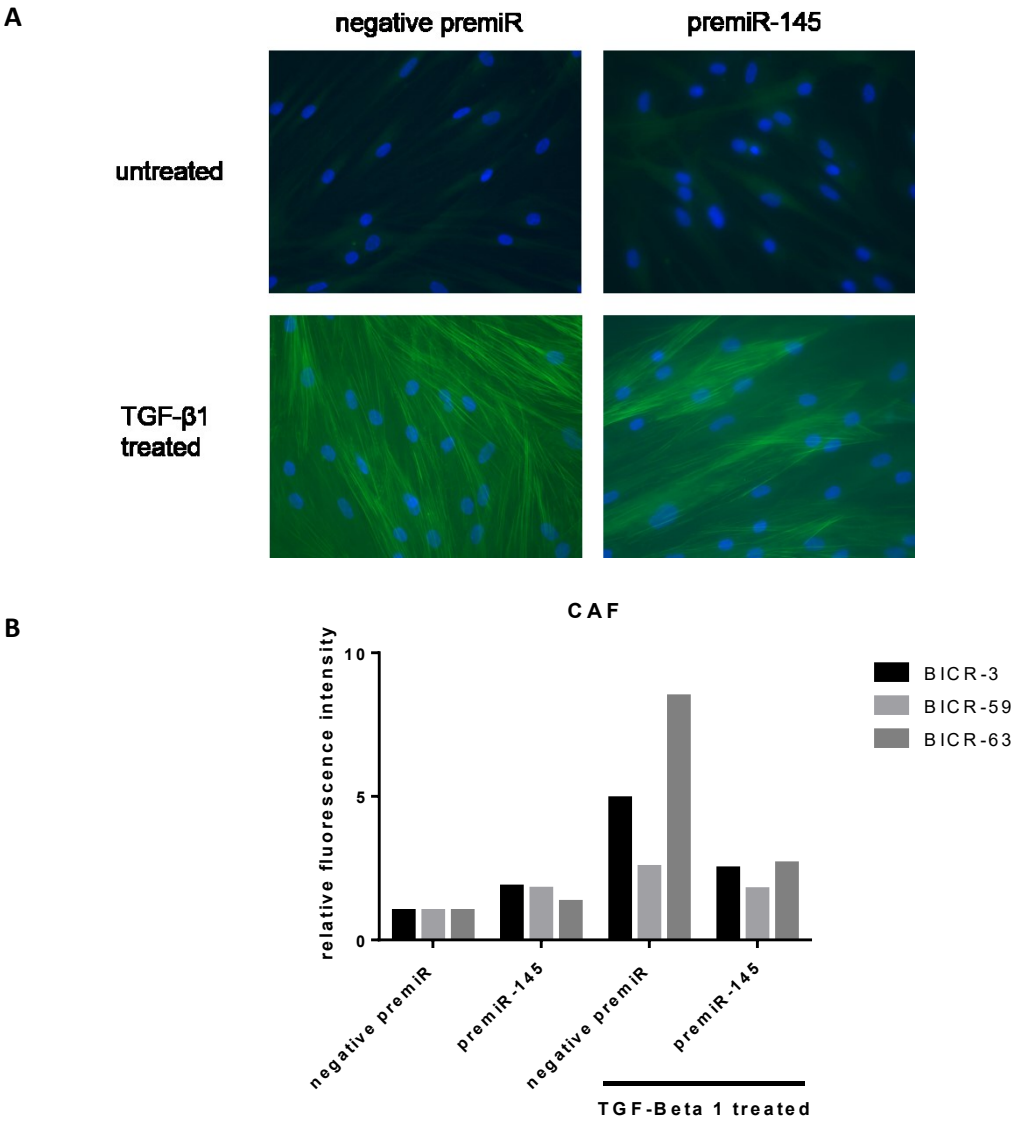

Figure 4.27: miR-145 overexpression reduced αSMA stress fibre formation in CAFs. CAFs were seeded onto coverslips overnight, treated with 5 ng/ml TGF-β1 for 48 h, or serum free media, then were transiently transfected with negative premiR, or premiR-145 (50 nM). The coverslips were washed in PBS, before being fixed in 100% methanol for 10 min, they were then permeablised using 4 mM sodium deoxycholate for 10 min, and blocked using 2.5% (w/v) BSA in PBS for 30 min before incubation with a primary FITC-conjugated αSMA antibody at 4 ^{o}C overnight. The coverslips were then washed in PBS before mounting on microscope slides using DAPI containing mounting medium. Fluorescent images were taken using a fluorescent light microscope, using Pro-plus 7 imaging software at 40x magnification. Representative pictures from BICR-63 are shown in **A.** The amount of fluorescence intensity per cell was quantified using Image J, and displayed in **B** as the mean relative fluorescent intensity for BICR-3, BICR-59 and BICR-63. N=2, independent experiments per CAF.

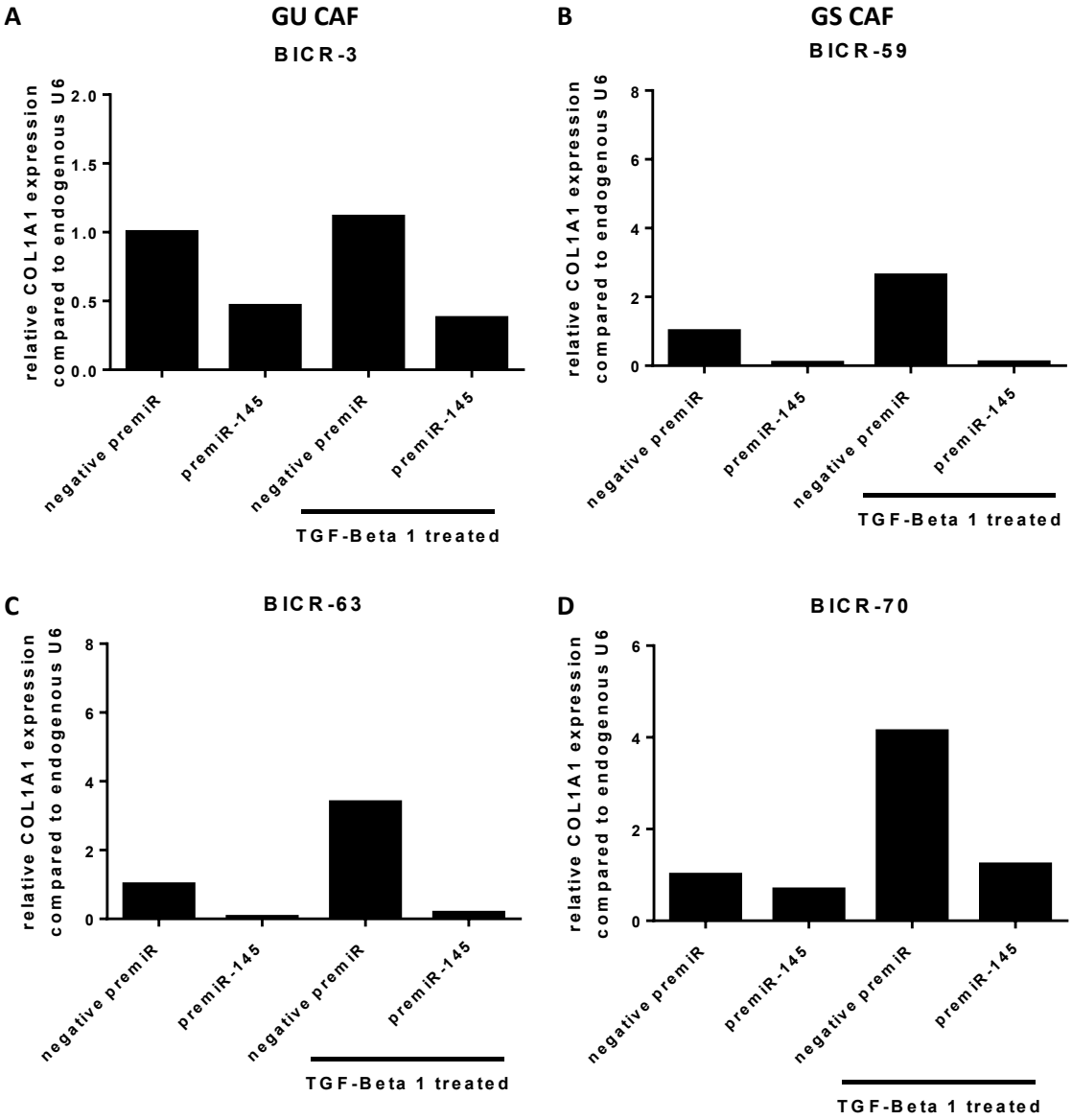

Figure 4.28: miR-145 overexpression prevented TGF-β1 stimulation of COL1A1 expression in CAFs. Primary CAFs BICR-3 (**A**), BICR-59 (**B**), BICR-63 (**C**) and BICR 70 (**D**) were transiently transfected with premiR-145 (50 nM) or a negative non-targeting premiR 24 h prior to the treatment with 5 ng/ml TGF-β1 or serum free media as a control. The RNA was isolated and used to generate cDNA for qRT-PCR analysis using primers designed to amplify COL1A1 and U6, as an endogenous control. Each bar on the figure represents the mean relative quantification of COL1A1 transcript levels compared to endogenous U6, for each transfection plus/minus treatment relative to untreated negative premiR. N=2, independent experiments per CAF.

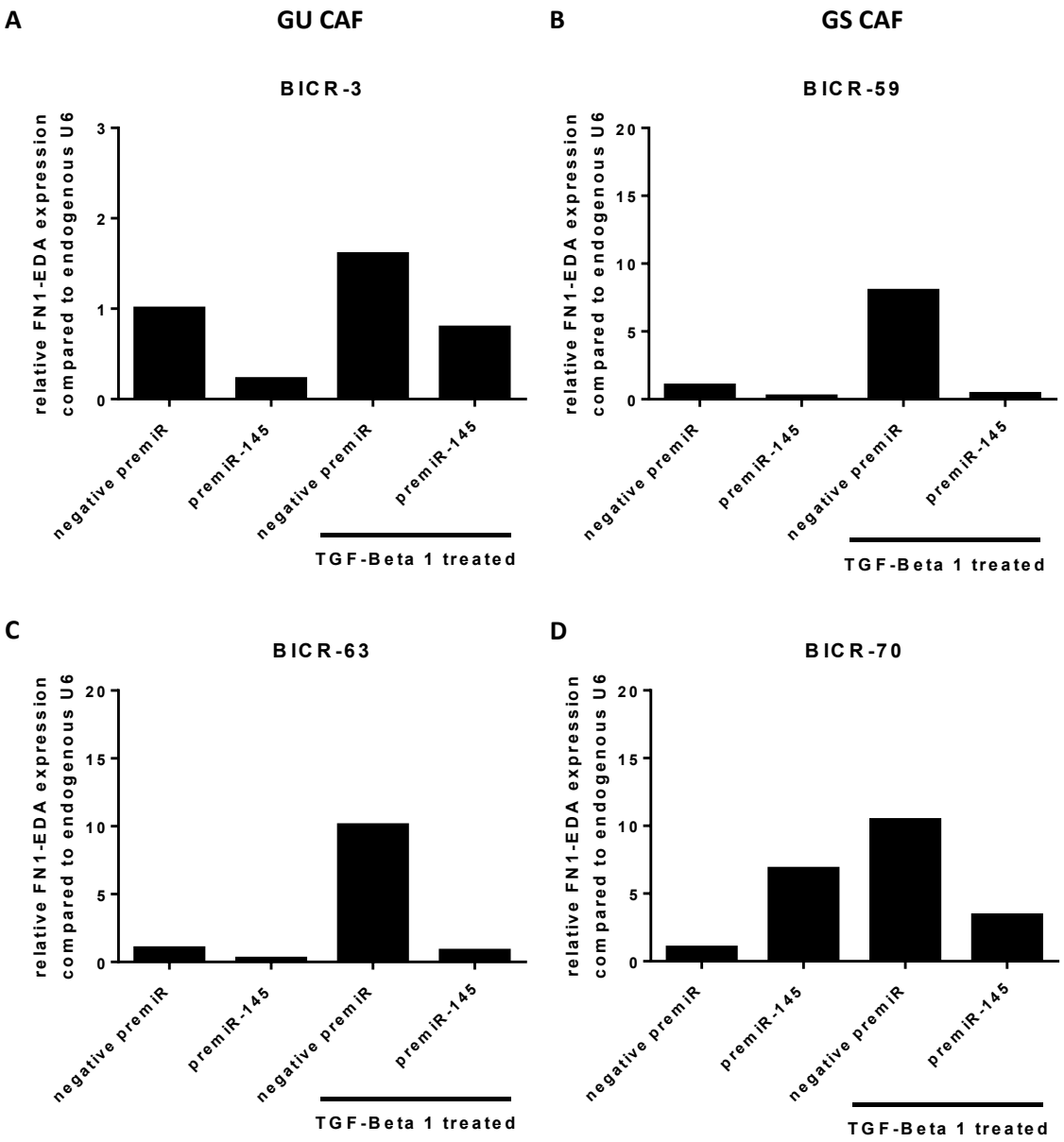

Figure 4.29: miR-145 overexpression prevented TGF-β1 stimulation of FN1-EDA expression in CAFs. Primary CAFs BICR-3 (**A**), BICR-59 (**B**), BICR-63 (**C**) and BICR 70 (**D**) were transiently transfected with premiR-145 (50 nM) or a negative non-targeting premiR 24 h prior to the treatment with 5 ng/ml TGF-β1 or serum free media. The RNA was isolated and used to generate cDNA for qRT-PCR analysis using primers designed to amplify FN1-EDA and U6, as an endogenous control. Each bar on the figure represents the mean relative quantification of FN1-EDA transcript levels compared to endogenous U6, for each transfection plus/minus treatment relative to untreated negative premiR. N=2, independent experiments per CAF.

145 were ~0.4 fold, ~0.9 fold, ~0.2 fold, and ~1.2 fold compared to negative transfected, untreated BICR-3, BICR-59, BICR-63 and BICR70 CAFs respectively.

The final myofibroblasts marker assessed by qRT-PCR was FN1-EDA, this also was significantly increased in response to TGF-β1 treatment in 3 out of the 4 CAFs tested (BICR-59, BICR-63 and BICR-70), by ~8 fold, ~10 fold and ~10.5 fold compared to untreated CAFs (figure 4.29). In BICR-3 CAFs, TGF-β1 increased FN1-EDA transcript levels by ~1.5 fold compared to untreated, although this was not found to be significant (figure 4.29A). Again, miR-145 prevented the TGF-β1 stimulated FN1-EDA expression in 3 out of four of the CAFs (BICR-59, BICR-63, and BICR-70), as CAFs overexpressing miR-145 which were TGF-β1 treated had ~0.4 fold, ~0.9 fold, and ~3.4 fold compared to untreated, negatively transfected BICR-59, BICR-63 and BICR-70 CAFs respectively. However, microRNA-145 overexpression of BICR-3 CAFs did not change the TGF-β1 effect on FN1-EDA expression, both negative transfected and premiR-145 transfected CAFs had a ~1.5 fold increase in FN1-EDA expression when treated with TGF-β1.

TGF-β1 treated NOFs produced conditioned media which was able to stimulate the paracrine migration of oral cancer cells, miR-145 was able to inhibit these pro-tumourigenic effects of the TGF-β1 on NOFs. To investigate whether TGF-β1, and microRNA-145 were able to have similar effects in CAFs as NOFs, conditioned media was collected from CAFs that were transiently transfected with premiR-145 prior to treatment with TGF-β1 or serum free media as a control and used in a transwell oral cancer migration assay. The effect of miR-145 on the CAF's ability to stimulate paracrine migration varied in the different CAFs tested, in BICR-59 CAFs there was no difference migration in CAFS overexpressing miR-145, in BICR-63 CAFs miR-145 overexpression there was a ~1.25 fold increase in paracrine migration (figure 4.30). On the other hand, in BICR-70 and MCA CAFs there overexpression of miR-145 caused a decrease in paracrine migration, by ~0.5 fold and ~0.3 fold respectively. In each of the 4 CAFs tested, TGF-β1 treatment decreased the CAFs ability to stimulate paracrine migration by ~0.4 fold, ~0.1 fold, ~0.2 fold and ~0.3 fold in BICR-59, BICR-63, BICR-70 and MCA CAFs respectively. In the conditioned media from CAFs that were overexpressing miR-145 and treated with TGF-β1, it appeared that miR-145 had no effect on preventing TGF-β1 effect. The amount of paracrine migration in these cells, was similar to that of the conditioned media from negative transfected, TGF-β1 treated CAFs. However, there was a significant ~1.25 fold increase in paracrine migration in BICR-59 CAFs overexpressing miR-145 and TGF-β1 treated, compared to miR-145 overexpressing, untreated BICR-59 CAFs conditioned media. Overall, miR-145 had no clear effect on preventing the CAFs' paracrine migration of oral cancer cells.

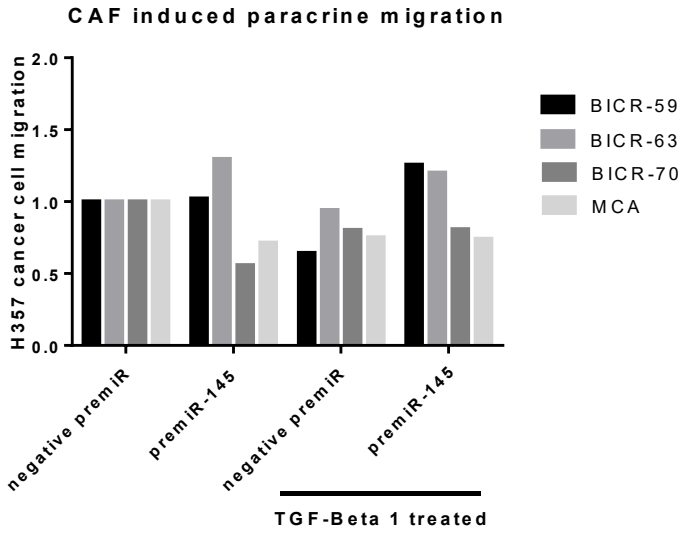

Figure 4.30: TGF-β1 treatment in CAFs did not stimulate the paracrine migration of oral cancer cells. Conditioned media was collected from primary CAFs BICR-59, BICR-63, BICR 70 and MCA which were transiently transfected with premiR-145 (50 nM) or a negative non-targeting premiR 24 h prior to the treatment with 5 ng/ml TGF-β1 or serum free media as a control. The conditioned media was spun at >2500xg to remove cellular debris then placed in the bottom of a transwell migration assay plate. H357 cancer cell line were seeded at 100,000 cells per well into an 8 µm porous transwell with 1 mg/ml mitomycin c and allowed to migrate for 38 h. The ability of the conditioned media to promote migration was assessed by methanol fixing cells attached to the membrane after 38 h, staining the cells with 0.1% (w/v) crystal violet, taking photographs at 40x, and calculating the average number of cells in the representative photographs. The figure shows the relative H357 cancer cell migration compared to untreated, negative premiR. N=2, independent experiments per CAF.

4.7 ***Summary***

Results showed that gain of function of miR-145 was able to inhibit and reverse TGF-β1 mediated myofibroblasts transdifferentiation in NOFs. Unfortunately, no loss of function experiments were successfully performed. miR-145 was also able to reduce myofibroblast markers in non-treated CAFs and inhibit TGF-β1 induced myofibroblasts markers. miR-145 was also able inhibit and reverse TGF-β1 mediated paracrine migration of cancer cells when overexpressed in NOFs. However, the effect of TGF-β1 in NOFs effect on paracrine invasion was less clear as different NOFs had different responses. The chapter successfully identified a role for miR-145 in oral myofibroblast transdifferentiation.

Chapter 5: The role of proteoglycan versican in stromal oral fibroblasts.

5.1 *Aims and objectives*

This results chapter aimed to investigate the role of versican in the myofibroblast transdifferentiation of oral fibroblasts. Specifically, the work objectives were to assess which versican isoforms are expressed in normal oral fibroblasts and oral CAFs, as well as elucidating the effect of TGF-β1 treatment on versican expression. The work in this chapter also aimed to investigate the effect of miR-143 and miR-145 overexpression on versican expression. Using a versican siRNA, the work planned to examine the effect of versican in the myofibroblast phenotype in CAFs and TGF-β1 induced oral myofibroblasts. Versican's effect on cancer cell paracrine migration was also established. In addition, work aimed to determine the regulation of versican in the tumour microenvironment by investigating the expression of metalloproteases, ADAMTS-1 and -4, which cleave versican in induced myofibroblasts and CAFs, compared to NOFs, and identifying the presence of the truncated form of versican in these cells.

5.2 *TGF-β1 induced the expression of proteoglycan versican in normal oral fibroblasts.*

The extracellular proteoglycan versican has been reported to be play important roles in cancer including migration, adhesion and proliferation (Ricciardelli *et al*., 2009) and is associated with poor prognosis in OSCC (Pukkila *et al*., 2006), amongst other carcinomas. It is mainly expressed by fibroblasts and CAFs are reported to express it at high levels. Versican is reported to be necessary for myofibroblast transdifferentiation in dermal fibroblasts (Hattori *et al*., 2012). TGF-β1, a known inducer of myofibroblast differentiation, is known to upregulate the expression of many extracellular matrix components including versican in many different fibroblasts (Yeung *et al*., 2013).

Here, the effect of TGF-β1 on versican expression in human gingival fibroblasts (NOFs). NOFs (DENF319) were treated with 5 ng/ml TGF-β1 for 24 h, 48 h or 72 h, or with serum free media as a negative control. After the indicated times, the NOFs were harvested, RNA extracted and used to generate total cDNA, and total protein lysates were also generated. qRT-PCR was performed using primers to amplify versican V0, V1, V2 and V3 isoforms and U6 as a reference gene. Versican V2 and V3 isoforms were considered to be not expressed in these NOFS as their CT values were above 35. V2 CT value was undetermined and V3 average CT value was 38.3. The relative transcript levels of the expressed versican isoforms, V0 and V1, in treated NOFs were compared to the untreated NOFs at the relevant timepoint. Both versican isoforms were upregulated in response to TGF-β1 stimulation, V0 was unchanged after 24 h, but was then

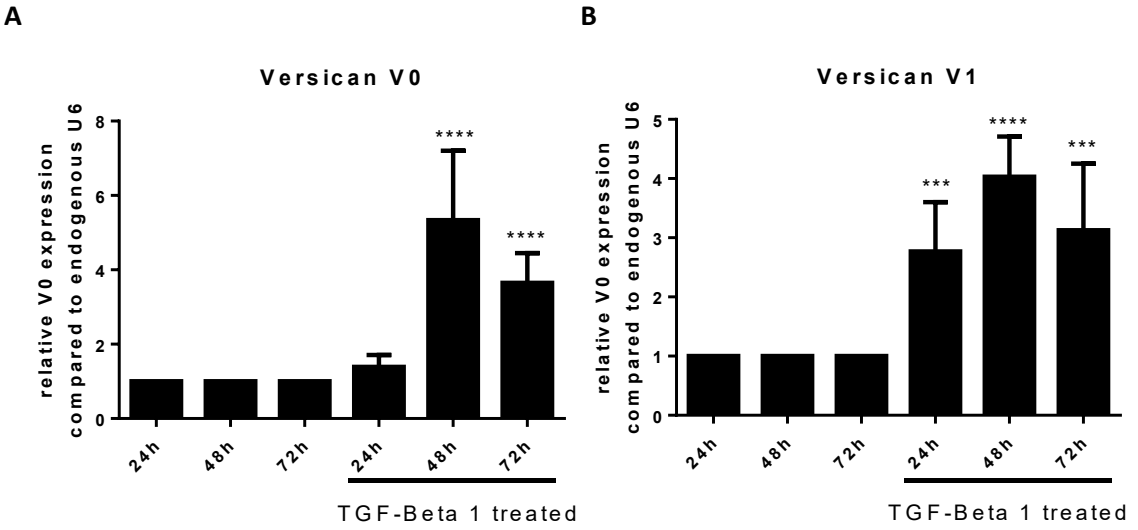

Figure 5.1: TGF-β1 induced versican expression in oral fibroblasts. DENF319 NOFs were seeded, serum starved and treated with 5 ng/ml TGF-β1, or serum free media as a control for 24 h, 48 h and 72 h. After treatment fibroblasts were harvested, RNA isolated and used in a total cDNA preparation. qRT-PCR was performed with the cDNA with primers to amplify V0 and V1 versican isoforms and U6 as a reference gene. Each bar on the figure represents the mean relative quantification of V0 (A) and V1 (B) transcript levels compared to endogenous U6, for each treatment relative to the relevant untreated timepoint. Statistical analysis was performed by a paired two tailed student's t-test, and statistical significance is shown on the figure by ***p<0.001, ****p<0.0001. The significance is compared to the untreated equivalent transfection. Error bars represent the SEM. N=3, independent experiments.

significantly increased by ~6 fold after 48 h, then by ~4 fold after 72 h (figure 5.1). V1 isoform was significantly different at each timepoint by ~3 fold, ~4 fold and ~3 fold respectively. For both isoforms 48 h stimulation was the peak response, which corresponds with the length of TGF-β1 treatment used to induce myofibroblast transdifferentiation in NOFs.

The change in versican protein levels on TGF-β1 treatment were assessed by immunoblotting. Total protein lysates were generated from the fibroblasts treated with TGF-β1 for 24 h, 48 h and 72 h. Protein lysates were resolved on a gradient gel, then transferred to a nitrocellulose membrane for immunoblotting using antibodies raised to human versican, αSMA and β-actin as a loading control. αSMA was used as a positive control to ensure TGF-β1 was stimulating these NOFs to become myofibroblastic. Immunoblotting for versican produced a ladder of bands of variable molecular weights due to its different sized isoforms and the differentially chondroitin sulphate side chains (figure 5.2). Attempts to remove the chondroitin sulphate chains to produce a uniform band were unsuccessful due to non-specific protein degradation occurring during incubation with chondroitinase (data not shown). There was an increase in versican in the protein levels on TGF-β1 treatment compared to untreated NOFs, especially after 48 h and 72 h (Figure 5.2A), this correlated with a slight increase in αSMA protein expression in these fibroblasts. Untreated 48 h NOFs appeared to have more versican protein then other untreated NOFs.

As a 48 h, 5 ng/ml TGF-β1 treatment was used throughout this study to induce the myofibroblast phenotype versican protein levels were also assessed in NOFs treated for 48 h. TGF-β1 treatment caused a clear increase in versican protein levels in all but one repeat, and again this correlated with the increase in αSMA (figure 5.2B). Image J was used to quantify the change in αSMA, TGF-β1 caused a ~1.3 fold increase in versican protein expression (figure 5.2C).

In chapter 4, the NOFs used varied in their response to TGF-β1, as determined by the variable αSMA expression. The versican response to TGF-β1 was also tested in these NOFs. Only some of the NOFs examined had significantly increased versican V0 and V1 transcript levels (figure 5.3). TGF-β1 treated DENF319 and OF26 NOFs had a significantly higher V0 expression (~3 fold and 2.5 fold higher respectively), than their untreated counterparts. DENF008 had a ~3 fold higher expression of V0 when treated with TGF-β1 but this was not a significant change. There was no difference in V0 levels in DENF316 treated NOFs, however there was around a ~1.8 fold increase in versican V1 expression in these NOFs. This fold increase in versican V1 was similar to that seen in DENF008, however this was not found to be significant. There was a significant induction (~2.5 fold increase) of V1 expression on TGF-β1 treatment in DENF319. There was no change in V0

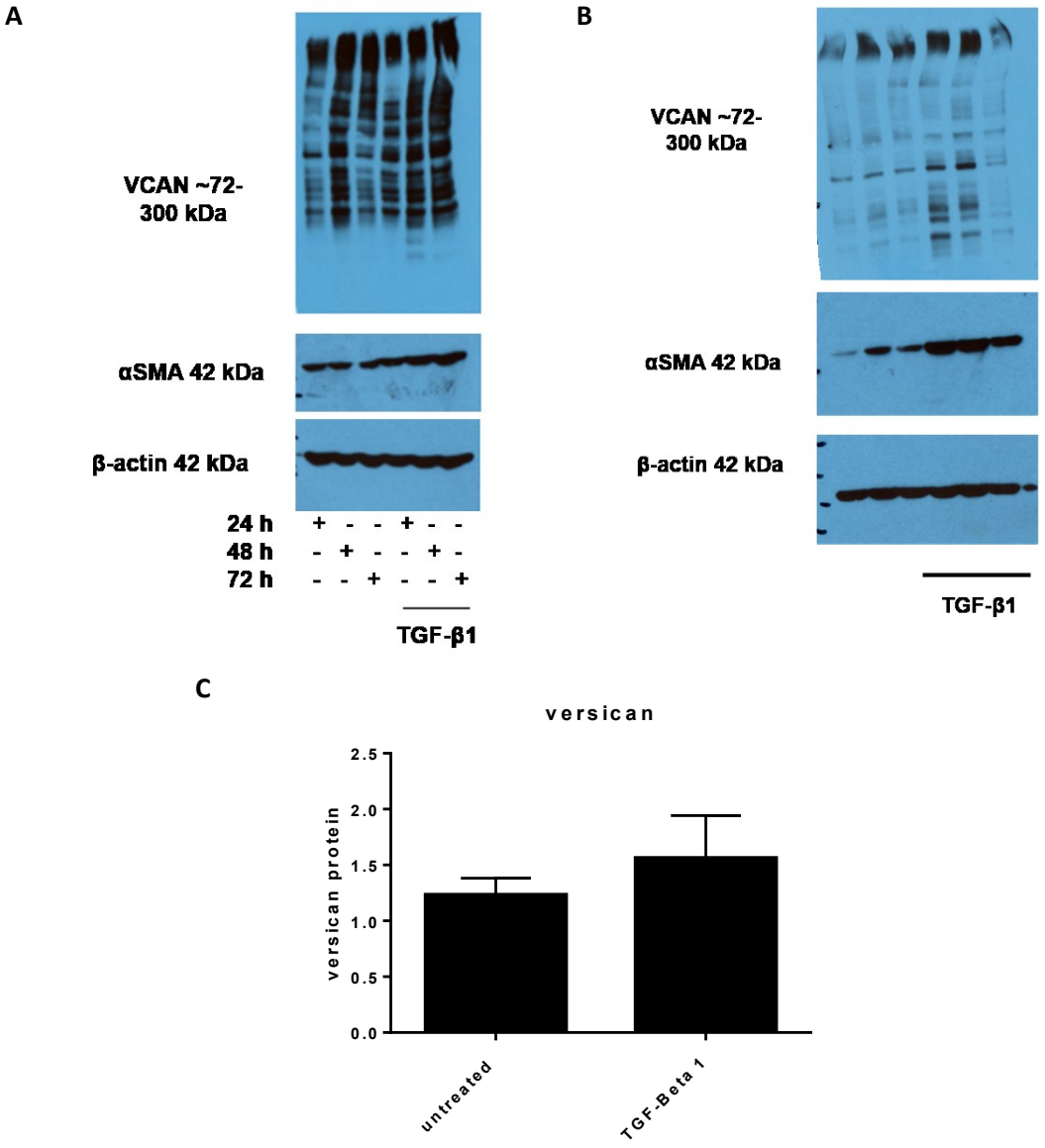

Figure 5.2: TGF-β1 treatment caused a non-significant increase versican protein levels in normal oral fibroblasts. NOFs (DENF319) were treated with 5 ng/ml TGF-β1 for 24 h, 48 h or 72 h or with serum free media as an endogenous control. Each time duration of the TGF-β1 or serum free media is indicated by the + on the figure. (**A**). Or were treated with 5 ng/ml TGF-β1 for 48h in **B**. The NOFs were then harvested, and total protein lysates were generated. **C** Protein (20 µg) was resolved on a 3–8% (w/v) tris acetate gradient gels, before being transferred to nitrocellulose membranes for immunoblotting. Antibodies raised against human versican and αSMA were used to assess relative protein levels, and β-actin was used as a loading control. Blots shown are representative. N=3, independent experiments (**A**). N=3, technical repeats (**B and C**).

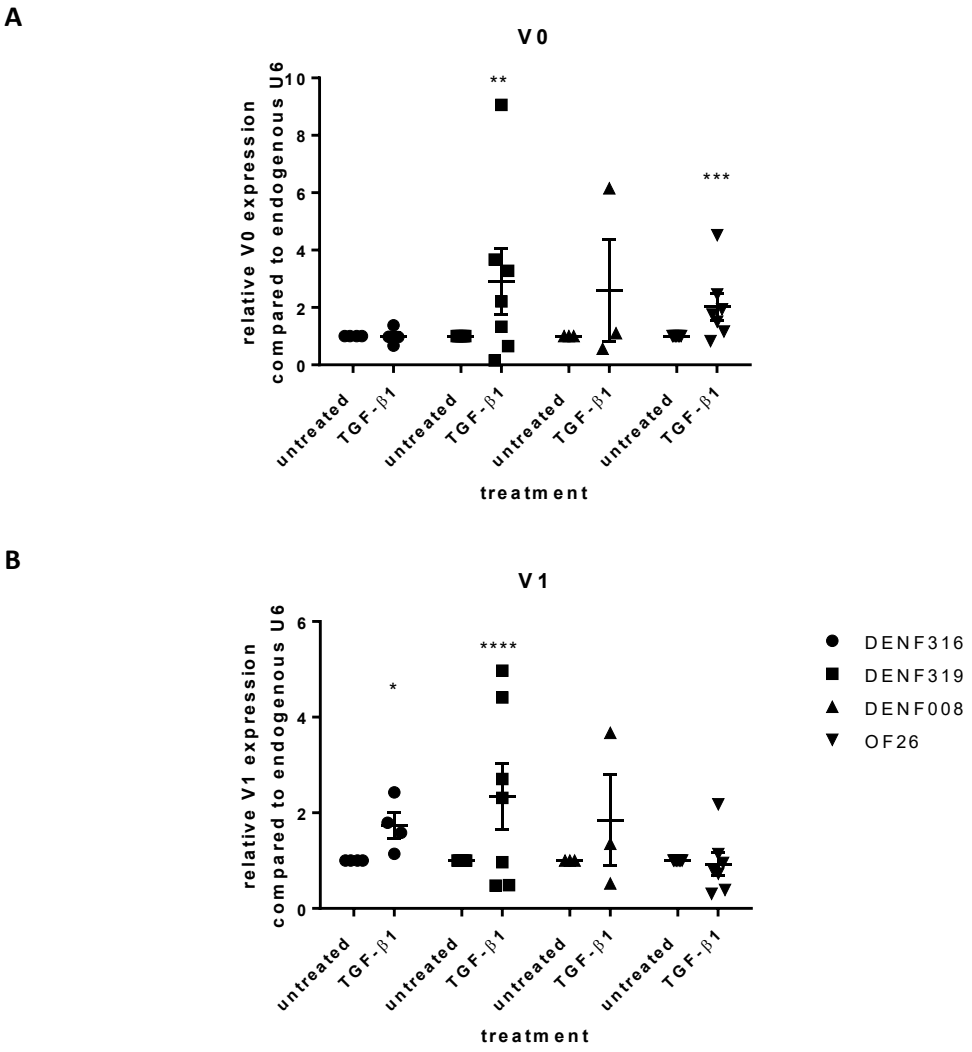

Figure 5.3: TGF-β1 had a variable effect on versican expression in NOFs. DENF316, DENF319, DENF008 and OF26 were seeded, serum starved and treated with 5 ng/ml TGF-β1, or serum free media as a control for 48 h. After treatment fibroblasts were harvested, RNA isolated and used in a total cDNA preparation. qRT-PCR was performed with the cDNA with primers to amplify V0 and V1 versican isoforms and U6 as a reference gene. Each dot on the figure represents the relative quantification of V0 (**A**) and V1 (**B**) transcript levels compared to endogenous U6, for each treatment relative to untreated, the line represents the mean relative difference. Statistical analysis was performed by a paired two tailed student's t-test, and statistical significance is shown on the figure by ***p<0.001, ****p<0.0001. The significance is compared to the untreated equivalent transfection. Error bars represent the SEM. N=3-7, independent experiment.

versican in OF26 NOFs on TGF-β1. Overall, there was a variable but general increase in the two versican isoforms tested.

5.3 *The expression of versican in oral cancer associated fibroblasts was lower than that of normal oral fibroblasts.*

Versican is reported to be found at higher levels within the tumour microenvironment of many tumours including breast, prostate, lung, colorectal, and oral (reviewed in Ricciardelli *et al.*, 2009). It is known to be expressed in high levels in CAFs (Yeung *et al*., 2013). V0 and V1 isoforms expression was therefore investigated in fibroblasts isolated from OSCC compared to NOFs. The CAF cohort included 10 fibroblasts taken from genetically stable and unstable tumours. The genetically stability of the tumours was judged based on the presence/absence of inactivating mutations in P53 and P16INKA and the presence/absence of loss of heterozygosity and copy number alteration mutations in these OSCCs (Lim *et al*., 2011). CAFs were isolated and kindly provided by Prof. Erik Parkinson. qRT-PCR was used to investigate the endogenous levels of versican V0 and V1 in these CAFs. The CAF population was compared to normal fibroblasts from the same institution (BICR NOFs) and normal fibroblasts collected from the School of Clinical Dentistry, Sheffield, collectively. Surprisingly, versican V0 was found to have a significantly (Mann-Whitney test) lower level of expression in the CAF population compared to the NOFs (figure 5.4A), whereas there was no difference in versican V1 (figure 5.4B).

When the expression of versican from CAFs isolated from genetically stable and unstable CAFS were compared to BICR NOFs and NOFs isolated in the School of Dentistry in Sheffield. NOFs from Sheffield had much higher levels (significant by a multiple comparison ANOVA) of versican V0 than BICR NOFs, and CAFs from genetically stable and unstable OSCCs (figure 5.5A). However, BICR NOFs and the CAFs expression were a similar of V0 transcript. For V1 versican, CAFs from genetically stable OSCCs had the highest level of expression comparatively to both NOFs and CAFs from genetically unstable OSCCs, however this was not significant (figure 5.5B). As the CAF cohort was small, it is unknown if this data is representative of the CAF gene profile.

The expression of versican at protein level was also investigated in the CAFs. Total protein from NOFs and CAFs was resolved on a gel and transferred to a nitrocellulose membrane for immunoblotting. A human full-length polyclonal versican antibody was used to detect versican protein in the screen, and a β-actin antibody was used as a loading control. As versican has different isoforms of different molecular weights and each protein has a varying number of

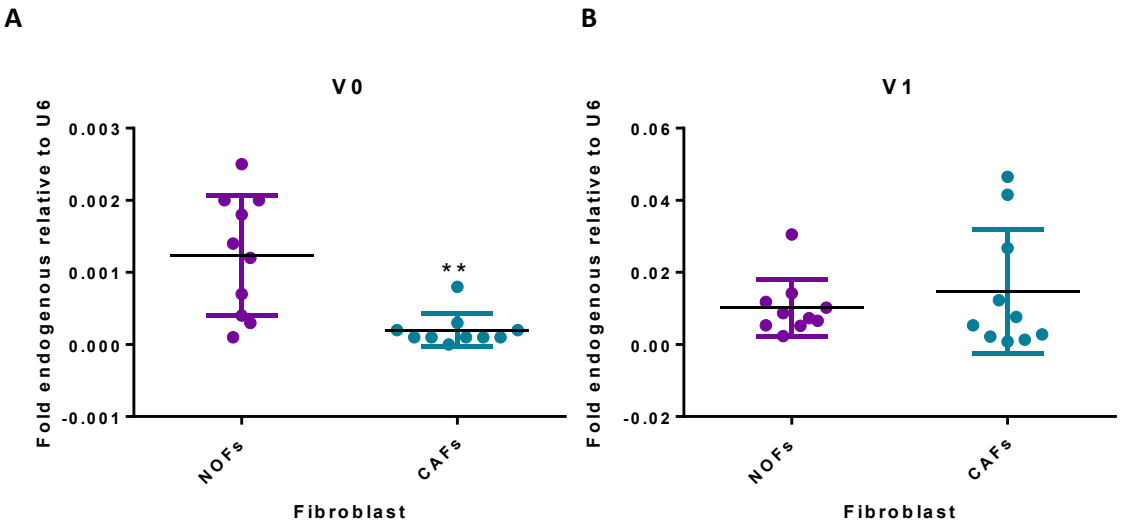

Figure 5.4: versican V0 was downregulated in OSCC CAFs. Fibroblasts isolated from OSCC, CAFs (10), and NOFs (10) were grown, RNA was isolated and used to generate cDNA for qRT-PCR analysis using primers designed to amplify V0, V1 versican and U6, as an endogenous control. The fold endogenous change of target versican V0 (**A**) or versican V1 (**B**), compared to reference gene U6 is plotted on each graph, each dot representing a different NOF/CAF. The line represents the mean fold endogenous for each set of fibroblasts. Statistical analysis was performed by Mann-Whitney test, and statistical significance is shown on the figure by **p<0.01. Error bars display the SD.

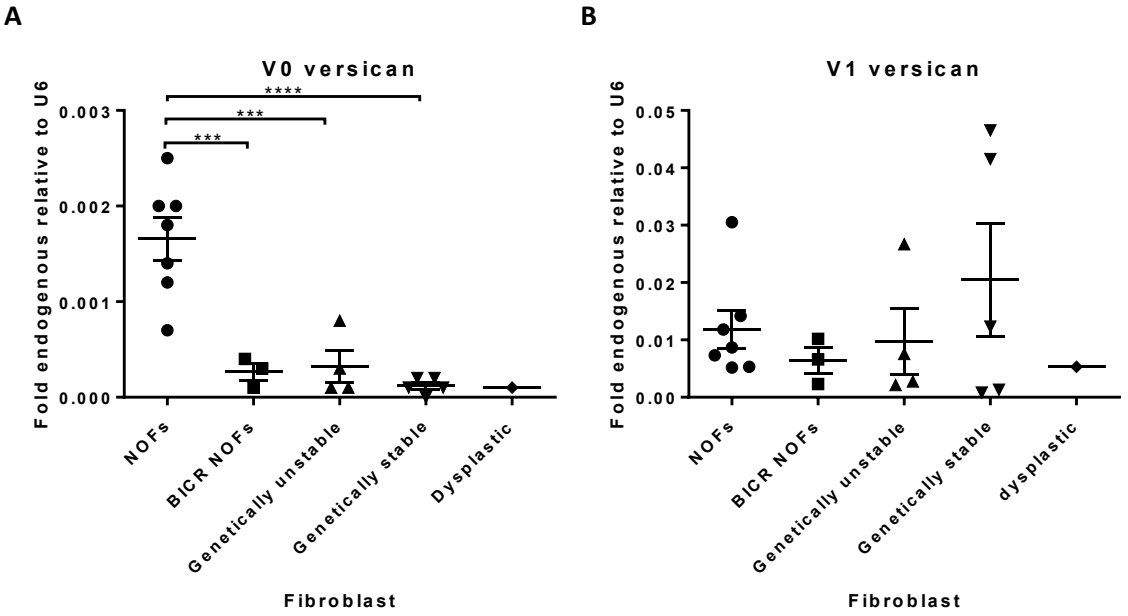

Figure 5.5: A subset of NOFs had a higher versican V0 expression than in OSCC CAFs. CAFs isolated from genetically stable OSCCs (N=5), unstable OSCCs (N=5), oral dysplasia (N=1), normal gingiva (BICR NOFs; N=3) all originally from Prof Ken Parkinson and NOFs (from Sheffield; N=7) were cultured. RNA was isolated and 100 ng was used to generate cDNA for qRT-PCR analysis using primers designed to amplify V0, V1 versican and U6, as an endogenous control. The fold endogenous change of target versican V0 (**A**) or versican V1 (**B**), compared to reference gene U6 is plotted on each graph, each dot representing a different NOF/CAF. The line represents the mean fold endogenous for each set of fibroblasts. Statistical analysis was performed by multiple ANOVA, and statistical significance is shown on the figure by **p<0.01, ***p<0.001. Error bars display the SEM.

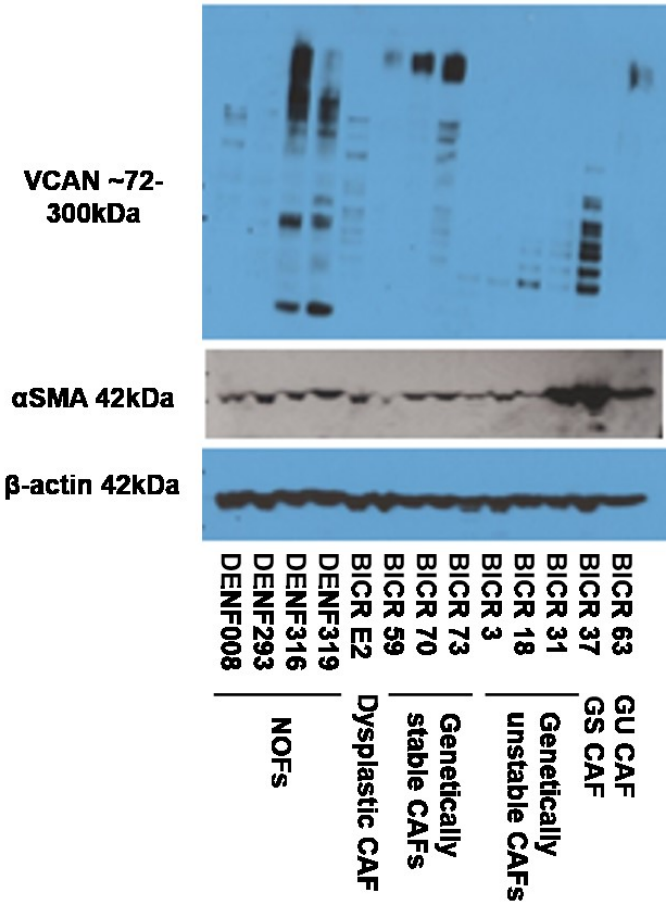

Figure 5.6: There was no clear pattern of versican protein expression in the different subsets of NOFs and oral CAFS tested. CAFs isolated from genetically stable tumours. CAFs isolated from genetically stable OSCCs (N=4), unstable OSCCs (N=4), oral dysplasia (N=1), all originally from Prof Erik Parkinson and NOFs (from Sheffield; N=4) were cultured. Total protein lysates (20 µg) were resolved on 3–8% (w/v) tris acetate gels and transferred onto nitrocellulose membranes for immunoblotting. A polyclonal anti-human full length versican antibody and a monoclonal anti-human αSMA antibody was used to detect versican and αSMA levels in this CAF/NOF screen. β-actin was used as a loading control. N=1.

chondroitin sulphate side chains attached, immunoblotting produced a ladder of bands of different sizes, with varying molecular weights from 72kDa - >300kDa (figure 5.6). Generally, there was no clear pattern seen, however, there seemed to be a greater amount of protein detected in NOFs tested than the CAFs. There was also a greater amount of protein detected in CAFs taken from genetically stable OSCCs compared to CAFs from unstable OSCCs, which was perhaps consistent with the slight increase in V1 versican transcript levels (Figure 5.5B). The pattern of the bands was also different between the NOF and the CAF population with the NOFs having more bands of varying sizes, whereas CAFs tended to have detectable bands at higher molecular weights >250kDa. αSMA is shown as for a comparison, (shown previously; figure 3.8). However, there was no apparent correlation between high αSMA expressing CAFs and versican isoform expression tested by Pearsons correlation (αSMA vs V0 R= 0.474 p=0.197 and αSMA vs V1 R=0.01 p=0.981).

5.4 *miR-145 regulated the expression of proteoglycan versican.*

Studies in smooth muscle cells have shown that versican is a functional target of miR-143 (Wang *et al*., 2010) and that myocardin fine-tunes the smooth muscle phenotype by downregulating the ECM, specifically versican through miR-143 binding to its 3'UTR. miR-145 was not found to have an effect on versican in these cells, as miR-145 was not found to bind to versican's 3'UTR, therefore presumed not to regulate versican. Versican has been suggested to be necessary for the myofibroblast transdifferentiation in dermal fibroblasts (Hattori *et al*., 2012), its potential regulation by the miR-143/145 cluster was investigated. NOFs were transiently transfected with premiR-143, premiR-145 or a negative non-targeting premiR, before being treated with TGF-β1 for 48 h to induce myofibroblast transdifferentiation. Fibroblasts were harvested, and RNA and protein was extracted for molecular analysis of versican expression via qRT-PCR and immunoblotting.

Total cDNA was prepared to investigate V0 and V1 versican isoform levels in two transfected then TGF-β1 treated fibroblasts (DENF316 and DENF319). In both NOFs (DENF316 and DENF319) overexpression of miR-145 caused a marked downregulation of versican V0 in untreated (~0.98 and 0.91 fold) and treated (~0.91 and 0.97 fold decrease) NOFs (figure 5.7). Overexpression of miR-143 was only able to cause a downregulation of versican V0 in some instances and this was smaller than the downregulation by miR-145, in treated DENF316s (~0.5 fold; figure 5.7A) and untreated DENF319s (~0.7 fold; figure 5.7B). TGF-β1 did not cause an increase in V0 in this experiment in either NOFs, again reflecting the variable response to TGF-β1 seen in figure 5.3.

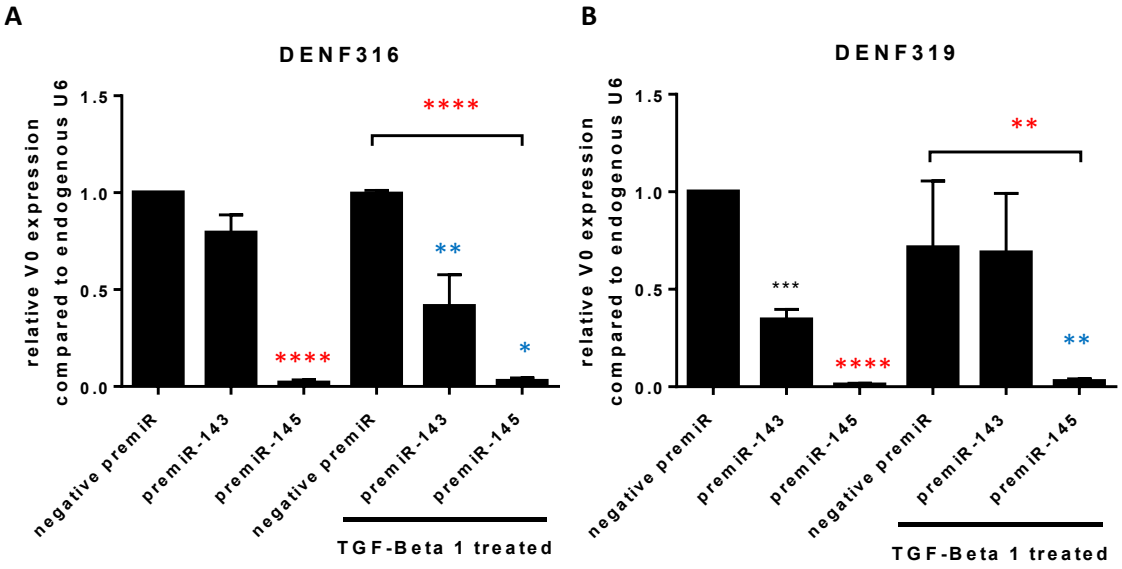

Figure 5.7: miR-145 overexpression downregulated versican V0 transcript levels. Two primary NOFs, DENF316 and DENF319 (**A** and **B** respectively), were transiently transfected with premiR-143, premiR-145 (50 nM) or a negative non-targeting premiR 24 h prior to treatment with TGF-β1 for 48 h. After treatment, fibroblasts were harvested and the RNA was isolated and used to generate cDNA for qRT-PCR analysis using primers designed to amplify versican V0 and U6, as an endogenous control. Each bar on the figure represents the mean relative quantification of V0 transcript levels compared to endogenous U6, for each transfection plus/minus treatment relative to untreated negative premiR. Statistical analysis was performed by a paired two tailed student's t-test, and statistical significance is shown on the figure by *p<0.05, **p<0.01, ***p<0.001. If not indicated by a bar, the black significance asterix are compared to the untreated, negative premiR transfected, negative control. Blue significance asterix indicate significance compared to the untreated counterpart, e.g. premiR-143 transfected, TGF-β1 treated compared with premiR-143 transfected untreated. Bars also indicate statistical comparisons. Red asterix indicate important significant data. Error bars represent the SEM. N=3, independent experiments.

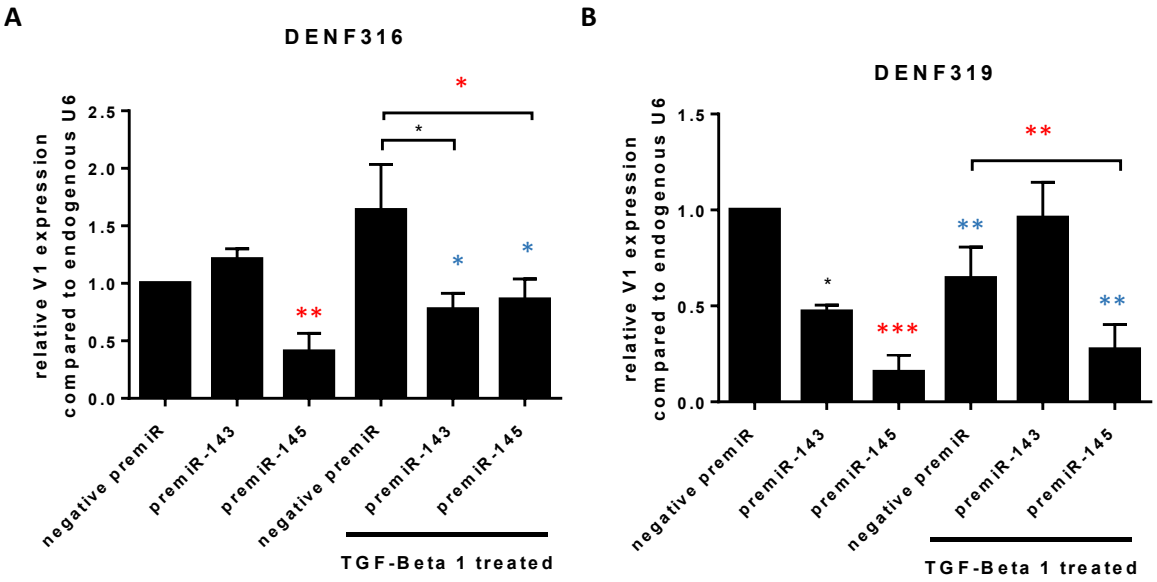

Figure 5.8: miR-145 overexpression downregulated versican V1 transcript levels. Two primary NOFs, DENF316 and DENF319 (**A** and **B** respectively), were transiently transfected with premiR-143, premiR-145 or a negative non-targeting premiR (50 nM) 24 h prior to treatment with TGF-β1 for 48 h. After treatment, fibroblasts were harvested and the RNA was isolated and used to generate cDNA for qRT-PCR analysis using primers designed to amplify versican V1 and U6, as an endogenous control. Each bar on the figure represents the mean relative quantification of V1 transcript levels compared to endogenous U6, for each transfection plus/minus treatment relative to untreated negative premiR. Statistical analysis was performed by a paired two tailed student's t-test, and statistical significance is shown on the figure by *p<0.05, **p<0.01. If not indicated by a bar, the black significance asterix are compared to the untreated, negative premiR transfected, negative control. Blue significance asterix indicate significance compared to the untreated counterpart, e.g. premiR-143 transfected, TGF-β1 treated compared with premiR-143 transfected untreated. Bars also indicate statistical comparisons. Red asterix indicate important significant data. Error bars represent the SEM. N=3, independent experiments.

On investigating versican V1 transcript levels in these cells, miR-145 was able to cause a significant downregulation of V1 (figure 5.8) but this was not as marked as the downregulation seen in the V0 isoform (figure 5.7). In DENF316, overexpression of miR-145 caused a ~0.6 fold decrease in V1 versican transcript levels in untreated NOFs and ~0.2 fold decrease in TGF-β1 treated NOFs (figure 5.8A), and in DENF319 V1 versican levels were downregulated by ~0.9 fold in untreated cells and ~0.7 fold in TGF-β1 treated DENF319s (figure 5.8B). Again, miR-143 overexpression was only able to cause the significant downregulation of versican V1 in TGF-β1 treated DENF316s (~0.3 fold reduction) and untreated DENF319s (~0.5 fold reduction). As with the V0 isoform, TGF-β1 failed did not stimulate an increase in V1 versican expression in this experiment.

The overexpression of miR-145 was also able to cause an almost complete reduction in detected versican protein levels shown by immunoblotting (figure 5.9). Protein lysates from NOFs overexpressing miR-145 were compared to lysates from NOFs overexpressing miR-143 and with NOFs with depleted versican levels, using a versican targeting siRNA. NOFs (OF26) were transiently transfected with premiR-145, premiR-143, negative premiR, antimiR-145, negative siRNA and versican siRNA for 24 h prior to treatment with TGF-β1 for 48 h. Total protein lysates were resolved on a gel and transferred to a nitrocellulose membrane for immunoblotting with a versican antibody and GAPDH antibody as a loading control. NOFs overexpressing miR-143 had no difference in versican protein levels compared to negative premiR transfected controls (figure 5.9). On the other hand, NOFs overexpressing miR-145 had almost undetectable levels of versican protein, and this was comparable to the level of versican protein in NOF where versican was knocked down using a targeted siRNA. AntimiR-145 was unable to knock down miR-145 levels (as seen in Chapter 4; figure 2.22), so its effect on versican will be ignored in this figure (figure 5.9).

To fully assess the role of the versican regulation in NOFs, the ability of miR-145 to rescue the TGF-β1 stimulated increase in versican protein levels was tested. NOFs were treated with TGF-β1 for 48 h to induce oral myofibroblasts, then were transiently transfected with miR-145 (5 nM or 50 nM) for 48 h to allow its downstream effects. NOFs were harvested, RNA and protein were extracted to assess versican expression via qRT-PCR and immunoblotting. Total cDNA was generated and versican V0 and V1 primers were used in a qRT-PCR reaction. Overexpression of miR-145 at both the doses used (5 and 50 nM) was able to cause a significant reduction of versican V0 (~0.7 fold and ~0.9 fold reduction; figure 5.10A) and V1 (~0.99 and ~0.97 fold reduction; figure 5.10B) in untreated NOFs. miR-145 overexpression was also able to cause a

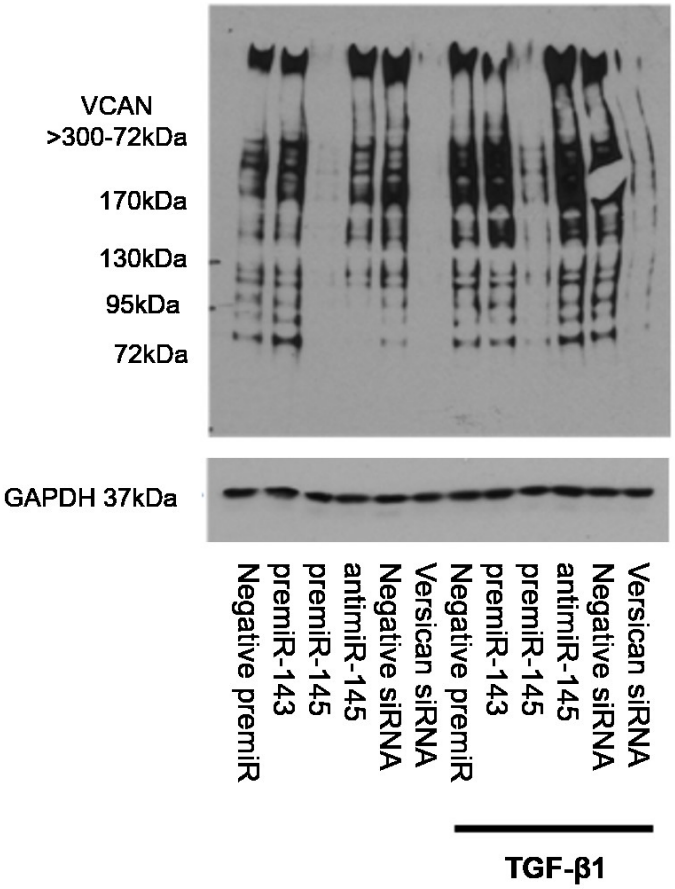

Figure 5.9: Overexpression of miR-145, not miR-143, caused a marked downregulation of versican protein expression. Primary NOFs (OF26), were transiently transfected with premiR-143, premiR-145 or a negative non-targeting premiR, antimiR-145, versican siRNA or negative non targeting siRNA (50 nM) for 24 h prior to treatment with 5 ng/ml TGF-β1 for 48 h. After treatment, fibroblasts were harvested and protein lysates were generated. Total protein lysates (20 µg) were resolved on 3–8% (w/v) tris acetate gels and transferred onto nitrocellulose membranes for immunoblotting. A polyclonal anti-human full length versican antibody was used to detect versican protein levels in the transfected then treated NOFs. GAPDH was used as a loading control. N=3, independent experiments.

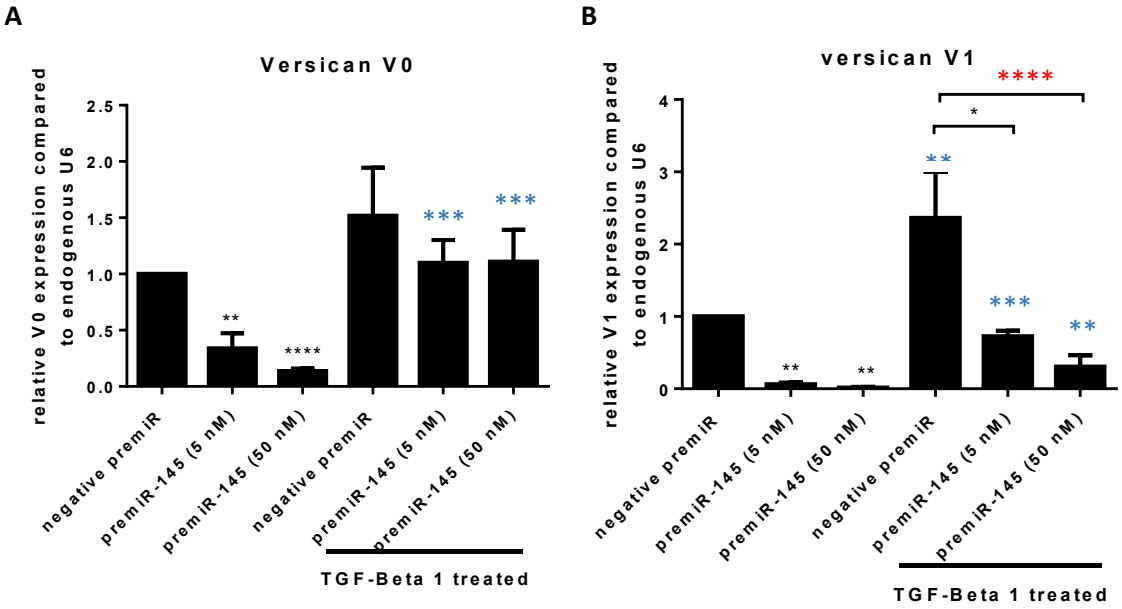

Figure 5.10: miR-145 overexpression reduced versican V1 expression in TGF-β1 induced myofibroblasts. DENF319 NOFs were treated with 5 ng/ml TGF-β1 or serum free media, then transiently transfected with 5 nM premiR-145, 50 nM premiR-145 or a negative non-targeting premiR. The transfection was left for 48 h before being harvested. RNA was isolated and used to generate total cDNA for qRT-PCR analysis using primers for versican V0 and V1, and U6, as an endogenous control. Each bar on the figure represents the mean relative quantification of V0 (A) and V1 (B) transcript levels compared to endogenous U6, for each transfection plus/minus treatment relative to untreated negative premiR. Statistical analysis was performed by a paired two tailed student's t-test, and statistical significance is shown on the figure by *p<0.05, **p<0.01, ***p<0.001 and ****p<0.0001. If not indicated by a bar, the black significance asterix are compared to the untreated, negative premiR transfected, negative control. Blue significance asterix indicate significance compared to the untreated counterpart, e.g. premiR-145 transfected, TGF-β1 treated compared with premiR-145 transfected untreated. Bars also indicate statistical comparisons. Important significant data is shown in red. Error bars represent the SEM. N=3, independent experiments.

downregulation of versican V1 in induced myofibroblasts, 5 nM overexpression caused a downregulation by ~0.3 fold and 50 nM caused a further downregulation by ~0.7 fold (figure 5.10B). The expression of versican V0, however, was not significantly reduced in induced myofibroblast when transfected with miR-145 at the 5 nM dose or 50 nM dose (figure 5.10A). TGF-β1-induced myofibroblasts had an increased V1 isoform expression than untreated controls. Assessing the protein levels in TGF-β1 treated, then transfected NOFs by immunoblotting revealed that miR-145 was able to reverse the increase in versican protein expression in TGF-β1 induced oral myofibroblasts (figure 5.11). miR-145 transfected after TGF-β1 treatment, had a greatly reduced effect on versican protein levels than miR-145 transfected before TGF-β1 treatment (figure 5.9).

5.5 *Versican knock-down had a small effect on oral myofibroblast transdifferentiation.*

Versican has been shown to be pivotal in the dermal myofibroblast transdifferentiation (Hattori *et al*., 2010). Due to miR-145's ability to inhibit oral myofibroblast transdifferentiation, and markedly reduce versican levels, it was hypothesised that miR-145 controls oral myofibroblast transdifferentiation through its regulation of versican. To test this hypothesis, versican loss of function experiments were performed. A versican targeting siRNA was used to transiently deplete NOFs of versican to see any effect on the TGF-β1 induced myofibroblasts transdifferentiation. Two different NOFs (DENF316 and DENF319) were transiently transfected with versican siRNA or negative siRNA for 24 h prior to TGF-β1 treatment, or serum free media for 48 h. Fibroblasts were harvested, RNA and protein lysates extracted and used to assess myofibroblast markers and versican expression for validation of the knock-down via qRT-PCR and immunoblotting and immunocytochemistry.

The versican knock-down was shown to be efficient as both versican V0 and V1 isoforms were significantly decreased. Both versican V0 (figure 5.12) and V1 (figure 5.13) expression was reduced by ≤0.9 fold compared to negative siRNA transfected NOFs (both for DENF316 and DENF319).

To assess the effect of versican depletion on the myofibroblast phenotype, myofibroblast marker αSMA was assessed by qRT-PCR, immunoblotting and immunocytochemistry. The knockdown of versican levels was able to significantly dampen the increase in αSMA transcript expression in response to TGF-β1 in DENF316, ~40 fold increase in αSMA in versican depleted

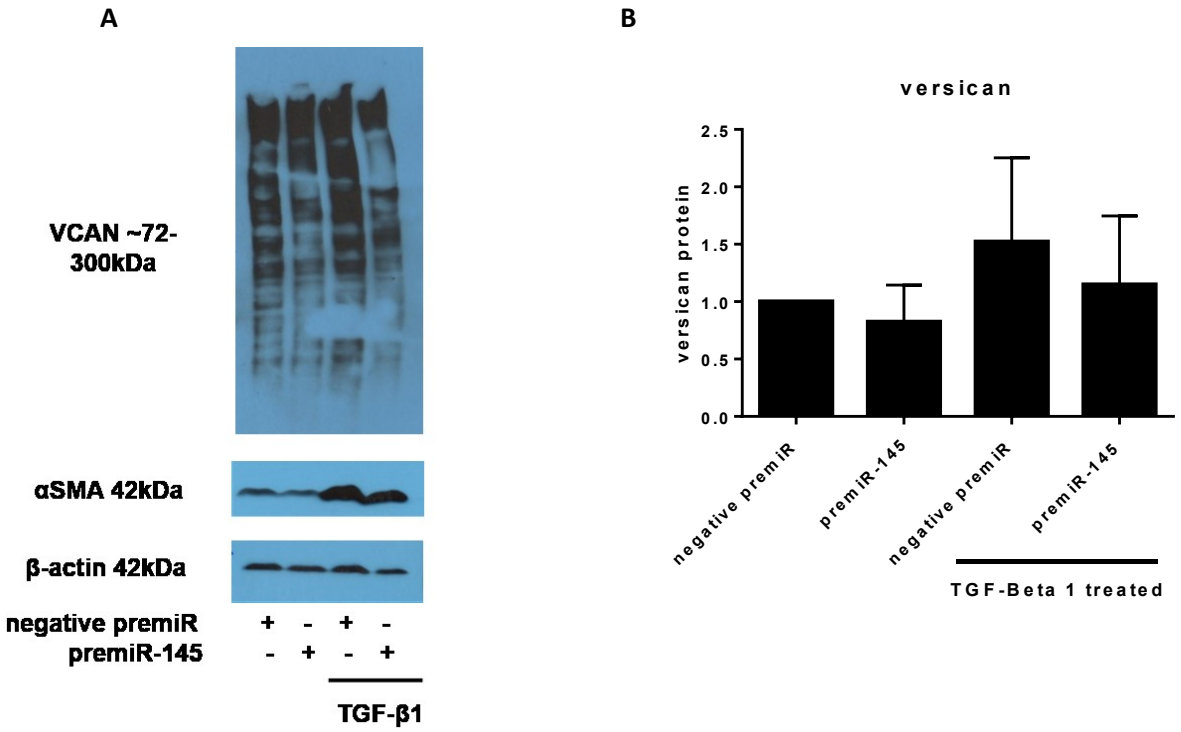

Figure 5.11: miR-145 overexpression reduced versican protein levels in induced oral myofibroblasts. DENF316 NOFs were treated with 5 ng/ml TGF-β1 or serum free media, then transiently transfected with 5 nM premiR-145, 50 nM premiR-145 or a negative non-targeting premiR. The transfection was left for 48 h before being harvested. Total protein lysates (20 µg) were resolved on 3–8% (w/v) tris acetate gels and transferred onto nitrocellulose membranes for immunoblotting. A polyclonal anti-human full length versican antibody and a monoclonal anti-human αSMA antibody was used to detect versican and αSMA protein levels in the TGF-β1 treated then transfected NOFs. B-actin was used as a loading control. Figure **A** shows is a representative blot, **B** shows the quantified amount of protein determined by densitometry. The error bars represent SEM. N=3, independent experiments.

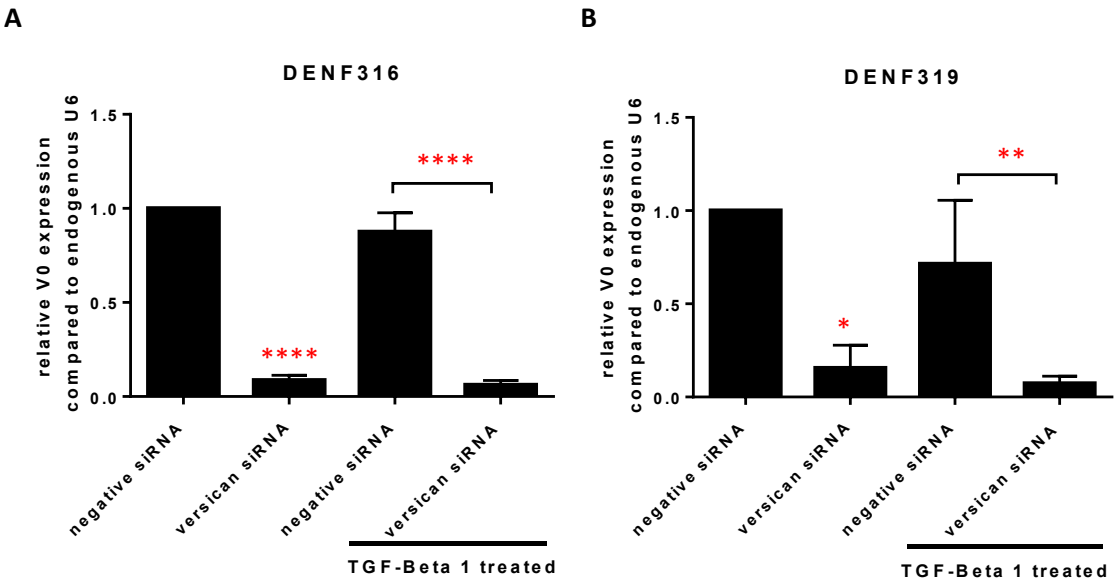

Figure 5.12: Versican siRNA knocked down versican V0 transcript levels in normal oral fibroblasts. Two NOFs, DENF316 (A) and DENF319 (B) were transiently transfected with a versican targeting siRNA or a negative non targeting siRNA (50 nM) as a control for 24 h, prior to 5 ng/ml TGF-β1 treatment for 48 h. RNA was isolated and used to generate total cDNA for qRT-PCR analysis using primers for versican V0 and U6, as an endogenous control. Each bar on the figure represents the mean relative quantification of versican V0 transcript levels compared to endogenous U6, for each transfection plus/minus treatment relative to untreated negative premiR. Statistical analysis was performed by a paired two tailed student's t-test, and statistical significance is shown on the figure by *p<0.05, **p<0.01, ****p<0.0001. If not indicated by a bar, the significance is compared to the untreated equivalent transfection, or negative siRNA in the case of the untreated versican siRNA. Red asterix indicate important significant data. Error bars represent the SEM. N=3, independent experiments for each NOF.

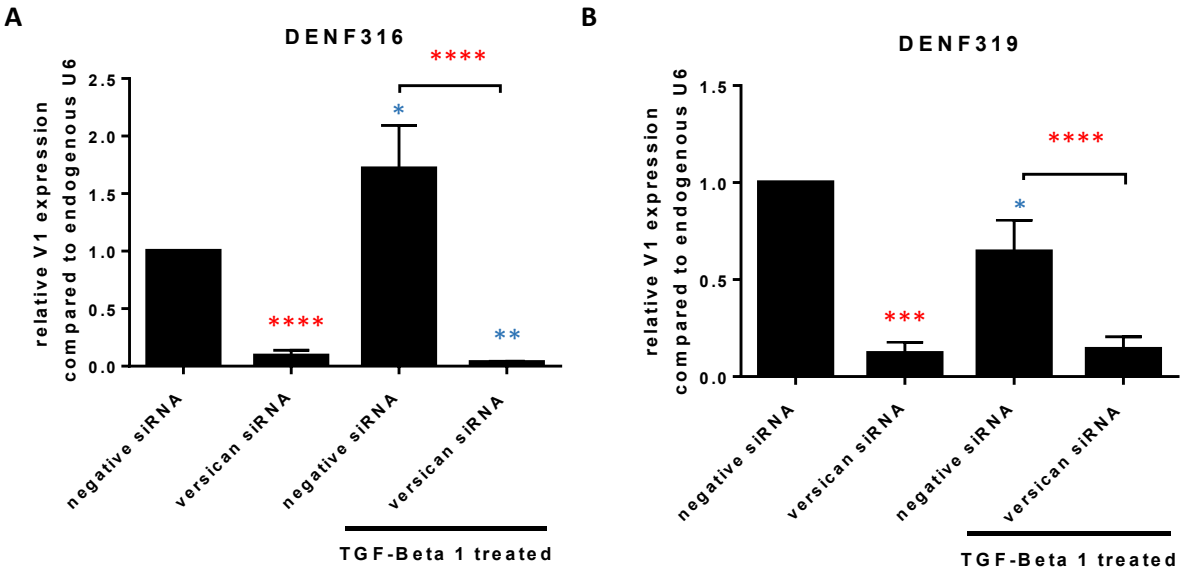

Figure 5.13: Versican siRNA knocked down versican V1 transcript levels in normal oral fibroblasts. Two NOFs, DENF316 (A) and DENF319 (B) were transiently transfected with a versican targeting siRNA or a negative non targeting siRNA (50 nM) as a control for 24 h, prior to 5 ng/ml TGF-β1 treatment for 48 h. RNA was isolated and used to generate total cDNA for qRT-PCR analysis using primers for versican V1 and U6, as an endogenous control. Each bar on the figure represents the mean relative quantification of versican V1 transcript levels compared to endogenous U6, for each transfection plus/minus treatment relative to untreated negative premiR. Statistical analysis was performed by a paired two tailed student's t-test, and statistical significance is shown on the figure by *p<0.05, **p<0.01, ***p<0.001, ****p<0.0001. If not indicated by a bar, the black significance asterix are compared to the untreated, negative premiR transfected, negative control. Blue significance asterix indicate significance compared to the untreated counterpart, e.g. premiR-145 transfected, TGF-β1 treated compared with premiR-145 transfected untreated. Bars also indicate statistical comparisons. Important significant data is shown in red. Error bars represent the SEM. N=3, independent experiments.

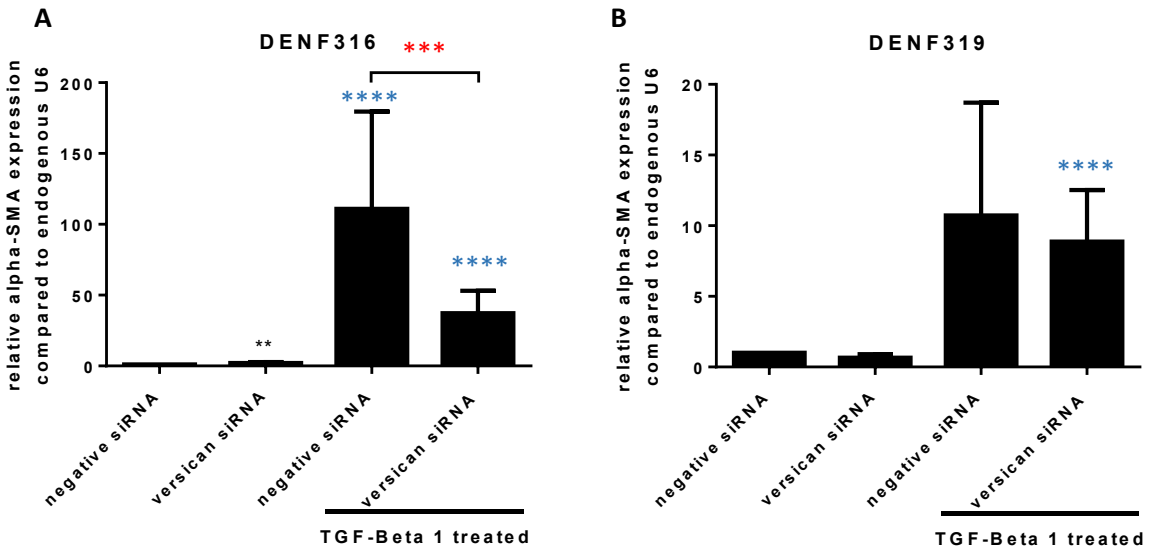

Figure 5.14: Versican knock-down in DENF316 NOFs reduced the TGF-β1 induced increase in αSMA transcript levels, but not in DENF319s. Two NOFs, DENF316 (A) and DENF319 (B) were transiently transfected with a versican targeting siRNA or a negative non targeting siRNA (50 nM) as a control for 24 h, prior to 5 ng/ml TGF-β1 treatment for 48 h. RNA was isolated and used to generate total cDNA for qRT-PCR analysis using primers for αSMA and U6, as an endogenous control. Each bar on the figure represents the mean relative quantification of αSMA transcript levels compared to endogenous U6, for each transfection plus/minus treatment relative to untreated negative premiR. Statistical analysis was performed by a paired two tailed student's t-test, and statistical significance is shown on the figure by *p<0.05, **p<0.01, ***p<0.001, ****p<0.0001. If not indicated by a bar, the black significance asterix are compared to the untreated, negative siRNA transfected, negative control. Blue significance asterix indicate significance compared to the untreated counterpart, e.g. premiR-145 transfected, TGF-β1 treated compared with premiR-145 transfected untreated. Bars also indicate statistical comparisons. Important significant data is shown in red. Error bars represent the SEM. N=3, independent experiments.

NOFs compared to ~100 fold in negative siRNA controls (figure 5.14A). However, in DENF319 NOFs there was no difference versican depleted NOFs αSMA expression in response to TGF-β1, both around ~10 fold increase in αSMA expression (figure 5.14B). The effect on the induction of αSMA protein levels was assessed by an immunoblot. There was no difference between the amount of protein detected in versican depleted NOFs and negative siRNA when treated with TGF-β1 (figure 5.15). The experiment was performed in both DENF316 and DENF319 in triplicate, these immunoblots quantified by densitometry and shown in figure 5.15B. TGF-β1 treatment caused an increase in αSMA in all transfections; negative premiR, premiR-143, premiR-145, antimiR-145, versican siRNA by ~8, ~12, ~6, ~13 and ~9 fold respectively. All these TGF-β1 mediated increases in αSMA protein were found to be statistically significant apart from antimiR-145, which will be ignored due to it not effectively knocking down miR-145 levels. The TGF-β1 mediated increase in αSMA was reduced in NOFs overexpressing miR-145, however this wasn't statistically significant using the densitometry data.

Immunocytochemistry revealed that versican knock-down in NOFs had no effect on TGF-β1 ability to induce αSMA stress fibres which are typical of myofibroblasts. NOFs were seeded onto coverslips before being transfected, then TGF-β1 treated. Fibroblasts on coverslips were fixed, permeabilised and incubated with a FITC conjugated αSMA antibody, visualised on a fluorescent light microscope and quantification of fluorescence was measured. There was no visible or quantified difference between NOFs transfected with versican siRNA or negative siRNA in their responses to TGF-β1 (figure 5.16).

The expression of other myofibroblast phenotypic markers COL1A1 and FN1-EDA were determined by qRT-PCR. A similar pattern of expression was seen in DENF316 NOFs to αSMA expression, NOFs with endogenous levels of versican and knocked down versican NOFs on TGF-β1 stimulated αSMA stress fibres (figure 5.16). Versican knock-down prevented some induction of the markers of myofibroblasts phenotype (figure 5.17). In DENF319, however, differences between the response of versican knock-down NOFs and negative siRNA transfected NOFs to TGF-β1 was not seen. For DENF316 NOFs versican reduced the TGF-β1 induction of COL1A1 expression from ~4.5 fold (negative siRNA, TGF-β1 treated DENF316s) to ~1.5 fold (still significantly different to untreated controls; figure 5.17A), and FN1-EDA from ~12 fold to ~7 fold (figure 5.18A). For DENF319s TGF-β1 treatment did not cause a significant increase in COL1A1 expression, versican knock-down in untreated NOFs caused a significant reduction in COL1A transcript levels, by ~0.5 fold (figure 5.17B), FN1-EDA transcript levels increased to ~1.7 fold on

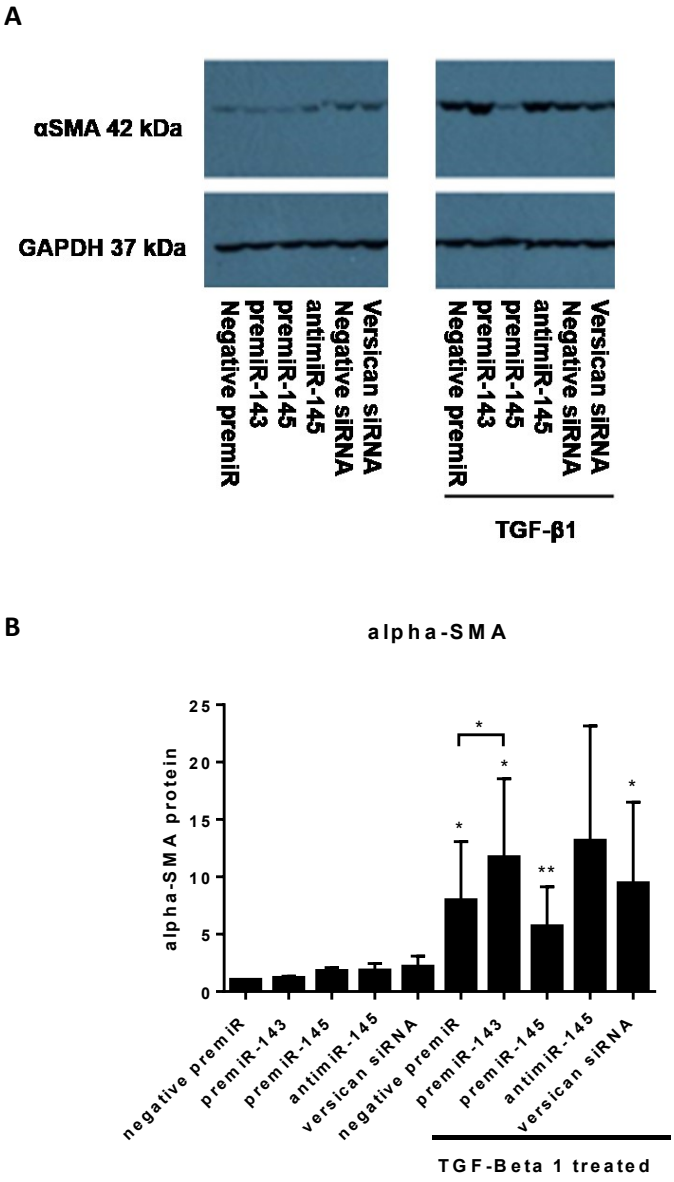

Figure 5.15: Versican knock-down had no effect on TGF-β1 induced increase in αSMA protein levels in oral fibroblasts. Two NOFs, DENF316 (shown in **A**) and DENF319, were transiently transfected with negative premiR, premiR-143, premiR-145, antimiR-145, negative control siRNA, or versican siRNA (50 nM) for 24 h prior to treatment with 5 ng/ml TGF-β1 or serum free media. Total protein lysates (20 µg) were resolved on 3–8% (w/v) tris acetate gels and transferred onto nitrocellulose membranes for immunoblotting. A monoclonal anti-human αSMA antibody was used to detect αSMA protein levels in the transfected then treated NOFs. GAPDH was used as a loading control. Figure **A** shows a representative DENF316 blot. Densitometry was performed using image J for both DENF316 and DENF319 in triplicate and shown in **B**. Statistical analysis was performed by a paired two tailed student's t-test, and statistical significance is shown on the figure by *p<0.05, **p<0.01. If not indicated by a bar, the significance is compared to the untreated equivalent transfection. N=3, independent experiments for both NOFs.

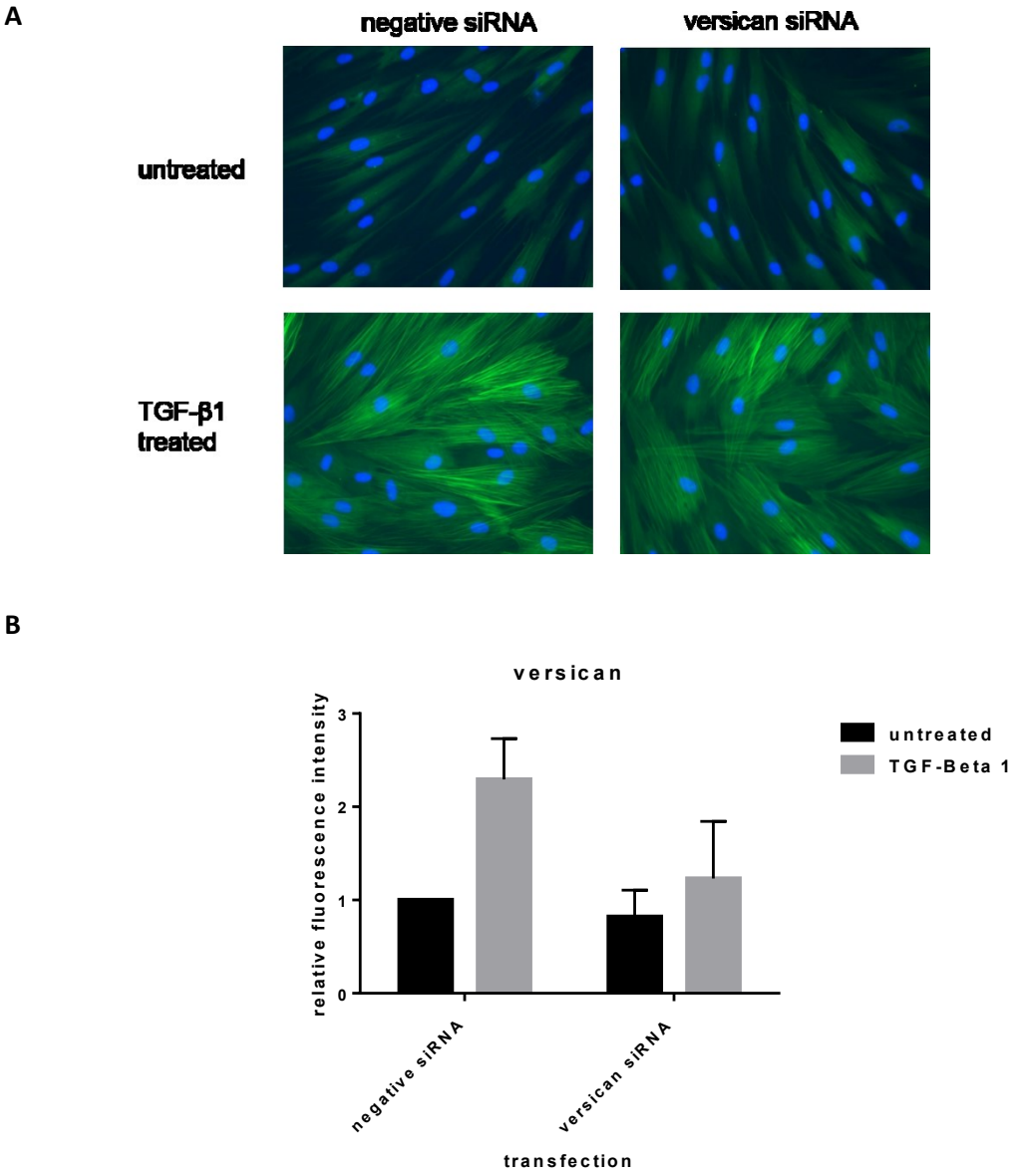

Figure 5.16: Versican knock-down had no effect on TGF-β1 stimulated αSMA stress fibre formation. NOFs (DENF316) were seeded onto coverslips overnight, transiently transfected with negative siRNA, or versican siRNA (50 nM) 24 h prior to being treated with 5 ng/ml TGF-β1 for 48 h. The coverslips were washed in PBS, before being fixed in 100% methanol for 10 min, they were then permeablised using 4 mM sodium deoxycholate for 10 min, and blocked using 2.5% (w/v) BSA in PBS for 30 min before incubation with a primary FITC-conjugated αSMA antibody at 4 ^{o}C overnight. The coverslips were then washed in PBS before mounting on microscope slides using DAPI containing mounting medium. Fluorescent images were taken using a microscope, using Pro-plus 7 imaging software at 40x magnification. Representative pictures are shown in **A.** The amount of fluorescence intensity per cell was quantified using Image J, and displayed in **B** as the mean relative fluorescent intensity for HDF283. Statistical analysis was performed by a paired two tailed student's t-test, and statistical significance is shown on the figure by *p<0.05, negative premiR treated compared to treated. Error bars show the SEM. N=3, independent experiments.

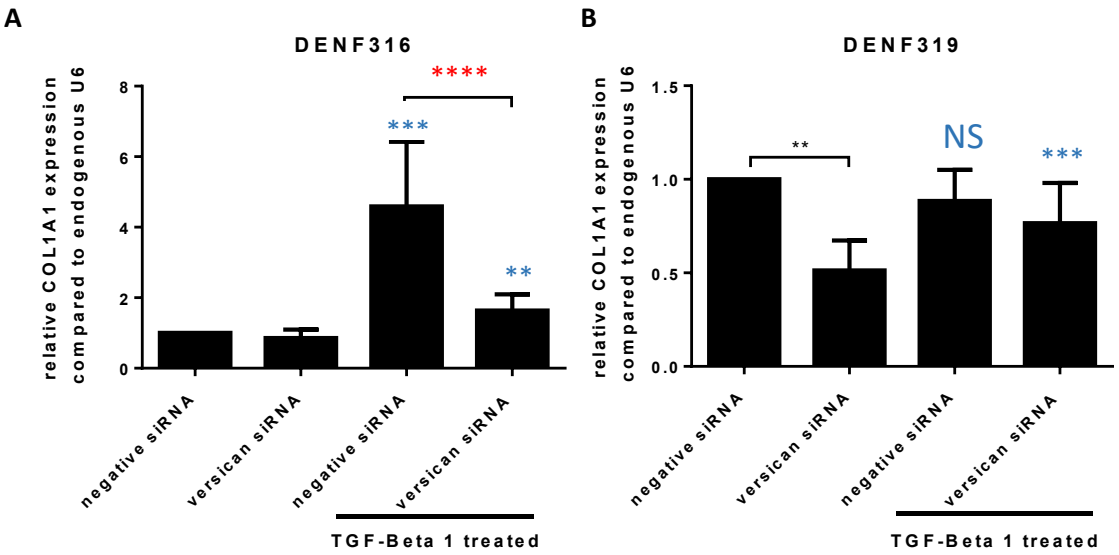

Figure 5.17: Versican knock-down in DENF316 NOFs reduced the TGF-β1 induced increase in COL1A1 transcript levels, and decreased COL1A1 transcript levels in DENF319. Two NOFs, DENF316 (A) and DENF319 (B) were transiently transfected with a versican targeting siRNA or a negative non-targeting siRNA (50 nM) as a control for 24 h, prior to 5 ng/ml TGF-β1 treatment for 48 h. RNA was isolated and used to generate total cDNA for qRT-PCR analysis using primers for COL1A1 and U6, as an endogenous control. Each bar on the figure represents the mean relative quantification of COL1A1 transcript levels compared to endogenous U6, for each transfection plus/minus treatment relative to untreated negative premiR. Statistical analysis was performed by a paired two tailed student's t-test, and statistical significance is shown on the figure by **p<0.01, ***p<0.001, ****p<0.0001. If not indicated by a bar, the black significance asterix are compared to the untreated, negative premiR transfected, negative control. Blue significance asterix indicate significance compared to the untreated counterpart, e.g. premiR-145 transfected, TGF-β1 treated compared with premiR-145 transfected untreated. Bars also indicate statistical comparisons. Important significant data is shown in red. Error bars represent the SEM. N=3, independent experiments.

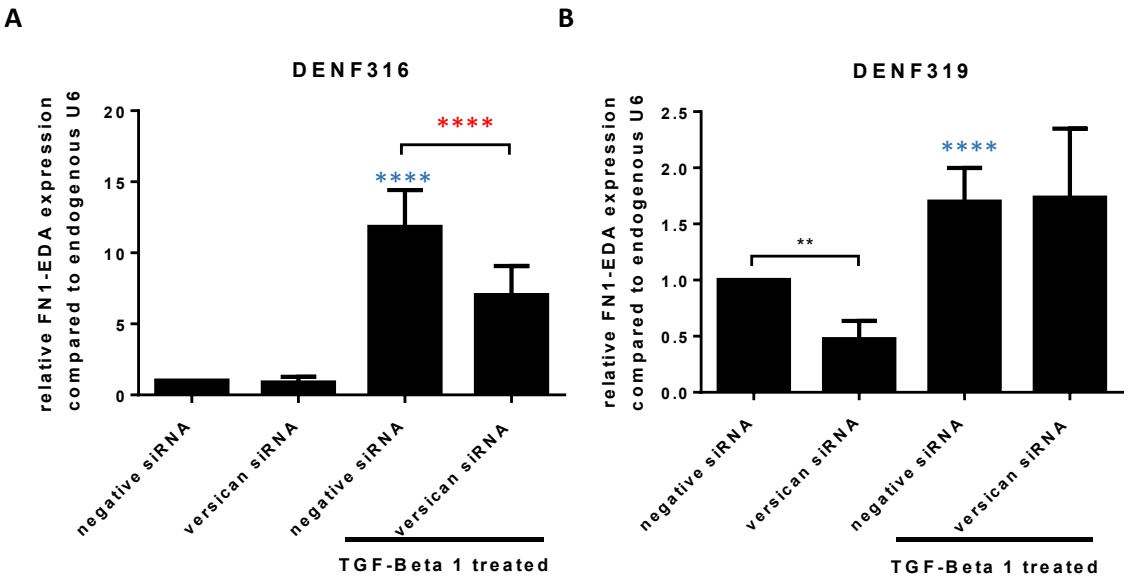

Figure 5.18: Versican knock-down in DENF316 NOFs reduced the TGF-β1 induced increase in FN1-EDA transcript levels, but not in DENF319s. Two NOFs, DENF316 (A) and DENF319 (B) were transiently transfected with a versican targeting siRNA or a negative non-targeting siRNA (50 nM) as a control for 24 h, prior to 5 ng/ml TGF-β1 treatment for 48 h. RNA was isolated and used to generate total cDNA for qRT-PCR analysis using primers for FN1-EDA and U6, as an endogenous control. Each bar on the figure represents the mean relative quantification of FN1-EDA transcript levels compared to endogenous U6, for each transfection plus/minus treatment relative to untreated negative premiR. Statistical analysis was performed by a paired two tailed student's t-test, and statistical significance is shown on the figure by *p<0.05, **p<0.01, ***p<0.001, ****p<0.0001. If not indicated by a bar, the black significance asterix are compared to the untreated, negative premiR transfected, negative control. Blue significance asterix indicate significance compared to the untreated counterpart, e.g. premiR-145 transfected, TGF-β1 treated compared with premiR-145 transfected untreated. Bars also indicate statistical comparisons. Important significant data is shown in red. Error bars represent the SEM. N=3, independent experiments.

TGF-β1, this was unchanged in NOFs were versican was knocked down (figure 5.18B). Versican knock-down did cause a significant reduction in FN1-EDA transcript levels in untreated NOFs.

One of versican's well characterised roles in the tumour microenvironment is to stimulate cancer cell migration (Riccidarelli *et al*., 2009). Versican's effect on stimulating paracrine cancer cell migration was also assessed by a transwell migration assay. Conditioned media was collected from NOFs transfected with negative siRNA, or versican siRNA, then TGF-β1 treated and used in the bottom of a transwell migration assay to stimulate an oral cancer cell migration. H357 cell line was seeded into the top of a transwell chamber and allowed to migrate through an 8μm porous membrane for 38 h. The membranes were then methanol fixed and stained with 0.1% (w/v) crystal violet and imaged using a light microscope at 40x magnification to count and assess relative migration. In this particular experiment conditioned media from TGF-β1 treated NOFs was unable to stimulate paracrine migration, and conditioned media from versican knocked down NOFs had a significant reduction in cancer cell migration of around ~0.3 fold in both untreated and treated samples (figure 5.19).

5.6 ***The effect of versican in CAFs.***

Versican is known to have important roles in ovarian CAFs (Yeung *et al*., 2013), and has been reported to be responsible for dermal myofibroblasts transdifferentiation (Hattori *et al*., 2011). In addition, this chapter has described data which can lead to the hypothesis that versican plays a role in oral CAFs. To list a few, versican V0 is downregulated in the CAF cohort used in this study (figure 5.4), TGF-β1 induced oral myofibroblasts have a significantly upregulated expression of versican (figure 5.1), miR-145 regulates versican expression in NOFs (figure 5.7) and versican knock-down in NOFs appeared to have some effect on the myofibroblasts markers expression. Therefore, the potential role of versican in oral CAFs was investigated.

As miR-145 was able to prevent TGF-β1 effects in CAFs and versican knock-down was able to dampen the TGF-β1 mediated effects in one of the two NOFs tested; the effect of miR-145 overexpression on versican expression was investigated by immunoblotting in CAFs (figure 5.20). As with the NOFs, TGF-β1 treatment in CAFs led to an increase in versican protein expression, quantified to be ~3.5 fold higher than endogenous levels. CAFs overexpressing miR-145 inhibited this increase. CAFs overexpressing miR-145 had a marked reduction in versican protein levels, however densitometry using all the repeats failed to show a difference between negative control transfected CAFs and CAFs overexpressing miR-145.

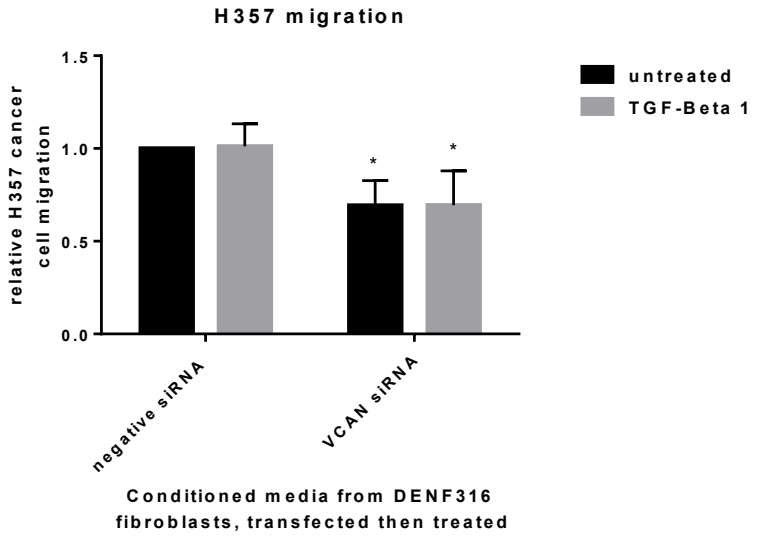

Figure 5.19: Versican knock-down in oral fibroblasts attenuated their ability to stimulate the paracrine migration of cancer cells. Conditioned media was collected from DENF316 NOFs transfected with negative siRNA or versican siRNA (50 nM) for 24 h then treated with 5 ng/ml TGF-β1 for 48 h or serum free media as a control. The conditioned media was spun at >2500xg to remove cellular debris then placed in the bottom of a transwell migration assay plate. H357 cancer cell line were seeded at 100,000 cells per well into an 8 µm porous transwell with 1 mg/ml mitomycin c and allowed to migrate for 38h. The ability of the conditioned media to promote migration was assessed by methanol fixing cells attached to the membrane after 38 h, staining the cells with 0.1% (w/v) crystal violet, taking photographs at 40x, and calculating the average number of cells in the representative photographs. The figure shows the relative H357 cancer cell migration compared to untreated, negative premiR. Statistical analysis was performed by a paired two tailed student's t-test, and statistical significance is shown on the figure by **p<0.01. The significance is compared to the treated negative premiR. Error bars represent the SEM. N=3, independent experiments.

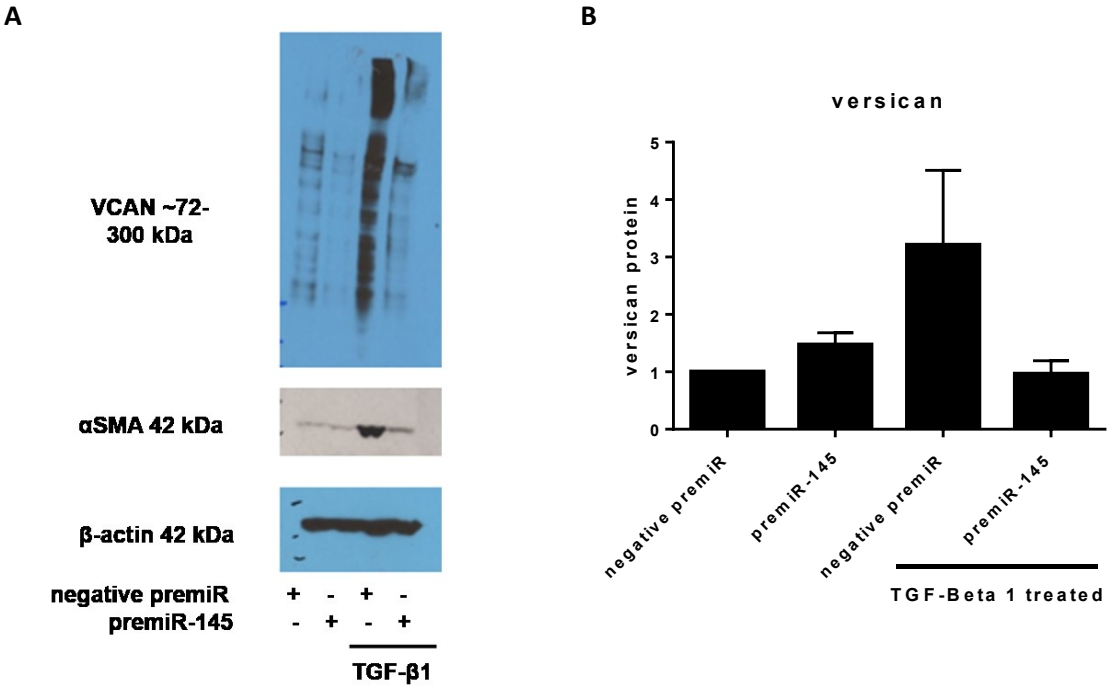

Figure 5.20: miR-145 prevented TGF-β1 increase in versican expression in CAFs. BICR-59 CAFs were transiently transfected with premiR-145 (50 nM) or a negative non-targeting premiR 24 h prior to the treatment with 5 ng/ml TGF-β1 or serum free media as a control. Total protein (20 µg) was resolved on a 3–8% (w/v) tris acetate gel and transferred to nitrocellulose for immunoblotting. A polyclonal versican antibody and a β-actin antibody was used as a control, to detect versican levels in these samples. The immunoblot shown in A is a representative blot. The detectable differences were quantified by densitometry using Image J. Error bars represent the SEM. N=3, independent experiments.

As miR-145 appears to regulate versican in CAFs as well as NOFs, versican may be able to mediate some of miR-145's anti-myofibroblast effects in CAFs. To test this, versican levels were knocked down using a versican targeting siRNA in CAFs, to investigate any effect on the *in vitro* phenotype and the TGF-β1 induced phenotype.

The effect of versican knock-down in CAFs on myofibroblasts markers αSMA, COL1A1 and FN1-EDA was assessed by qRT-PCR. There was a ~6 fold increase in αSMA in CAFs treated with TGF-β1. Versican knock-down was able to dampen the increase (to ~3.5 fold increase). Versican siRNA transfected CAFs had a ~0.85 fold decrease in αSMA transcript levels compared to negative siRNA transfected CAFs (figure 5.21A). Versican knock-down in CAFs caused a ~0.7 fold decrease in COL1A1 expression, and TGF-β1 caused no difference in COL1A1 in these CAFs (~1.1 fold compared to negative siRNA transfected CAFs) (figure 5.21B). TGF-β1 treated versican knocked down CAFs had a small ~2 fold increase in COL1A1 transcript levels compared to versican knocked down untreated cells. Versican knock-down also resulted in a ~0.9 fold decrease in FN1-EDA transcript levels (figure 5.21C). TGF-β1 induces a ~2 fold increase in FN1-EDA expression, which is prevented if transfected with versican siRNA beforehand.

The effect of versican knock-down on αSMA protein expression in CAFs was assessed by immunoblotting and immunocytochemistry. Immunoblotting revealed that versican knock-down had no effect on αSMA expression either in untreated CAFs or TGF-β1 treated CAFs (figure 5.22). Densitometry of these blots revealed there was a slight decrease in the TGF-β1 induced αSMA expression from ~2.5 fold to ~1.75 fold compared to untreated and negative siRNA transfected CAFs (figure 5.22B). Immunoblotting with a versican antibody was used to validate that versican levels were decreased in CAFs transfected with a versican targeting siRNA. Versican siRNA was able to decrease versican levels on average by ~0.5 fold in these CAFs (figure 5.23). Immunocytochemistry using a FITC-tagged αSMA antibody was used to visualise the αSMA stress fibres associated with the myofibroblast phenotype. TGF-β1 was able to induce αSMA stress fibres in both versican knocked down CAFs and negative siRNA transfected CAFs to similar levels, the fluorescence in both TGF-β1 treated CAFs was quantified to be ~5.5 fold higher compared to untreated (figure 5.24).

The effect of versican in CAFs to promote the paracrine migration of cancer cells was also investigated using conditioned media from MCA and MC15 CAFs. CAFs were transiently transfected with versican siRNA or negative siRNA (figure 5.25A), then treated with TGF-β1 (figure 5.25B). After treatment the conditioned media was collected and used in a transwell paracrine migration assay assessing H357 cells migration through the conditioned media.

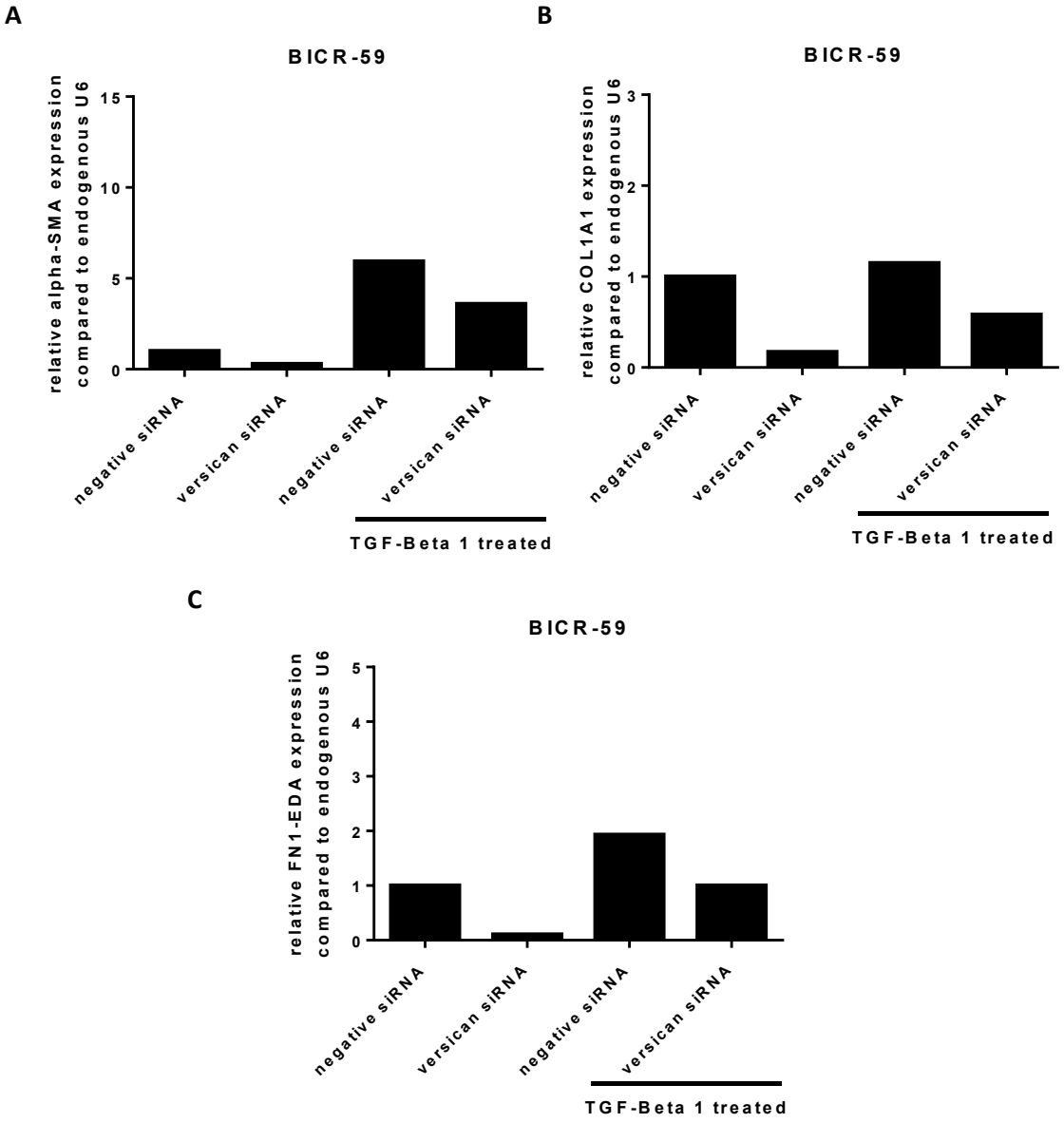

Figure 5.21: Versican knock-down in CAFs dampened the TGF-β1 induced myofibroblast markers αSMA, COL1A1 and FN1-EDA. CAFs (BICR-59s) were transiently transfected with versican siRNA (50 nM) or a negative non-targeting siRNA 24 h prior to treatment with 5 ng/ml TGF-β1 for 48 h. After treatment, fibroblasts were harvested and the RNA was isolated and used to generate cDNA for qRT-PCR analysis using primers designed to amplify αSMA, COL1A1, FN1-EDA and U6, as an endogenous control. Each bar on the figure represents the mean relative quantification of αSMA (**A**), COL1A (**B**) and FN1-EDA (**C**) transcript levels compared to endogenous U6, for each transfection plus/minus treatment relative to untreated negative siRNA. N=2, independent experiments for each CAF.

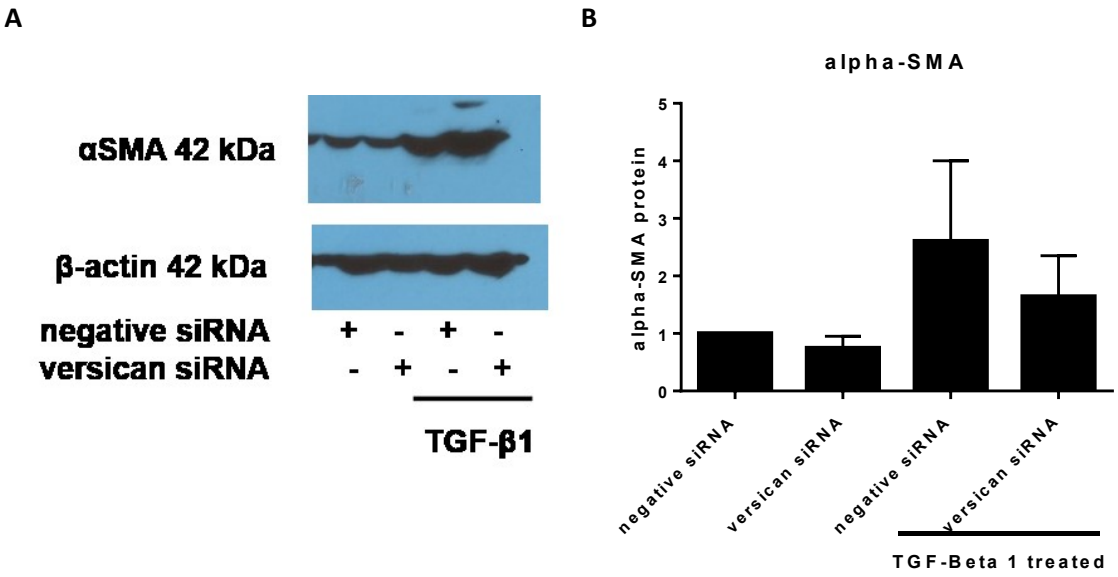

Figure 5.22: Versican knock-down in CAFs had no effect on TGF-β1 induced αSMA protein expression. CAFs were transiently transfected with versican siRNA (50 nM) or a negative non-targeting siRNA (50 nM) 24 h prior to treatment with 5 ng/ml TGF-β1 for 48 h. Total protein lysates (20 µg) were resolved on a 3-8% (w/v) tris acetate SDS PAGE gel and transferred to a nitrocellulose membrane for immunoblotting. A monoclonal αSMA antibody and a monoclonal β-actin antibody used to assess αSMA protein levels in these samples. Figure A shows a representative blot of BICR-63, densitometry was performed using image J for all CAFs tested shown in B. Error bars represent SEM. N=1 for each BICR-3, BICR-63, BICR-70 CAF.

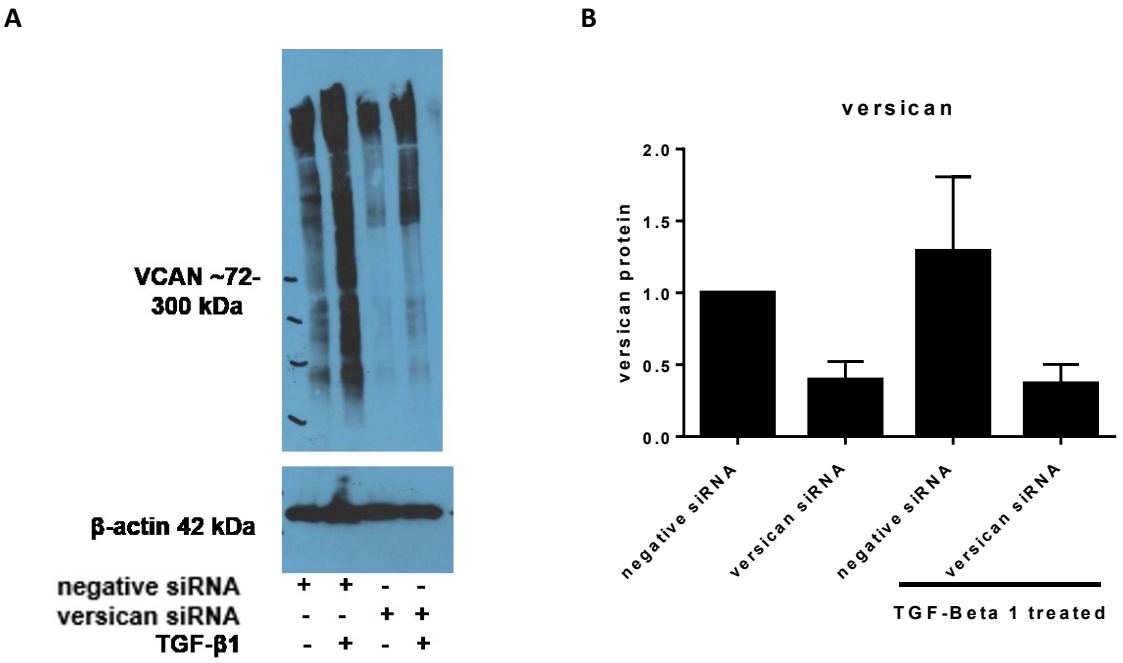

Figure 5.23: Versican siRNA knocked down versican levels in CAFs. CAFs were transiently transfected with versican siRNA (50 nM) or a negative non-targeting siRNA 24 h prior to treatment with 5 ng/ml TGF-β1 for 48 h. Total protein lysates (20 µg) were resolved on a 3–8% (w/v) tris acetate gel and transferred to a nitrocellulose membrane for immunoblotting. A polyclonal versican antibody and a monoclonal β-actin antibody used to assess versican protein levels in these samples. Figure A shows a representative blot of BICR-3, densitometry was performed using image J for all CAFs tested shown in B. Error bars represent SEM. N=1 for each BICR-3, BICR-63, BICR-70 CAF.

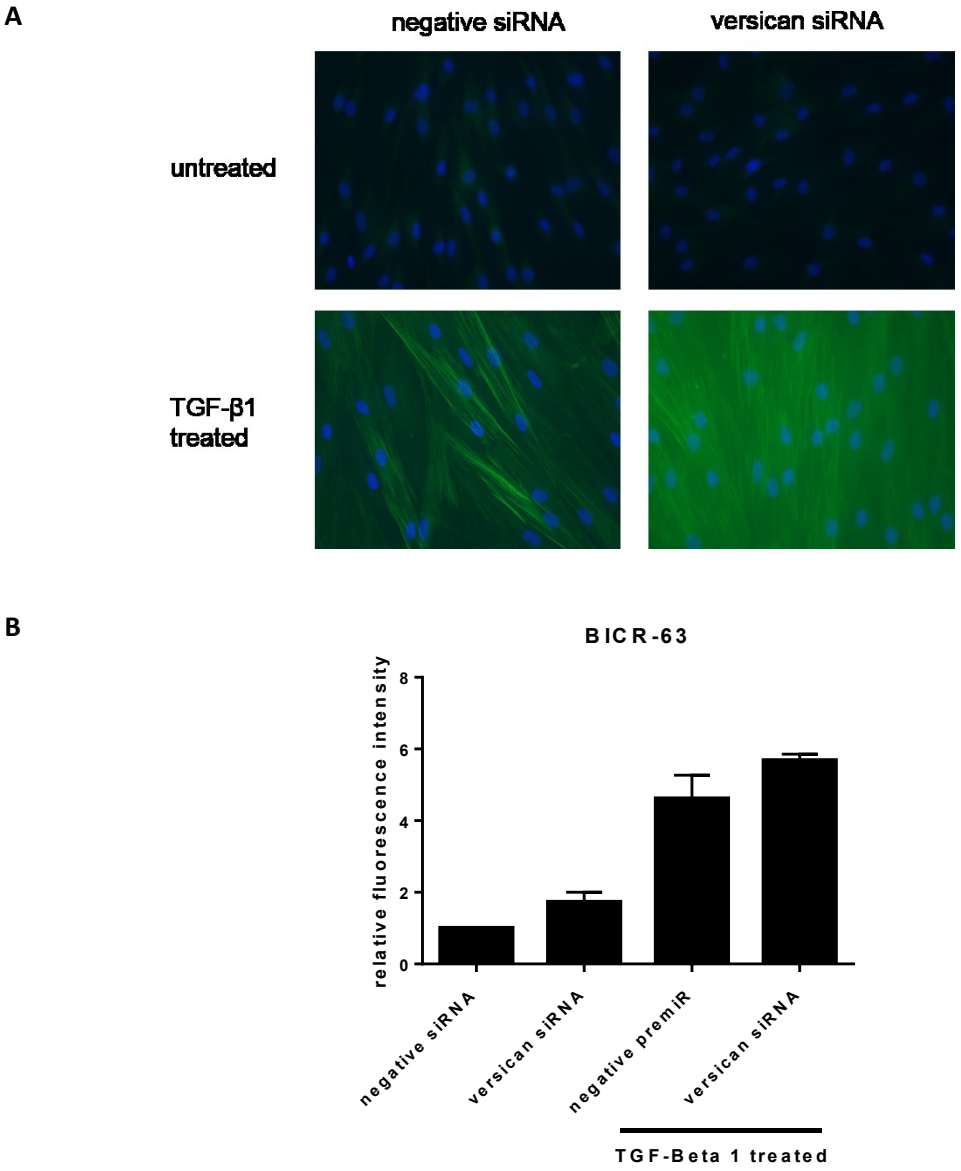

Figure 5.24: Versican knock-down in CAFs had no effect on TGF-β1 induced αSMA stress fibre formation. CAFs (BICR-63, shown here, and BICR-70) were seeded onto coverslips overnight, transiently transfected with negative siRNA, or versican siRNA (50 nM) 24 h prior to being treated with 5 ng/ml TGF-β1 for 48 h. The coverslips were washed in PBS, before being fixed in 100% methanol for 10 min, they were then permeablised using 4 mM sodium deoxycholate for 10 min, and blocked using 2.5% (w/v) BSA in PBS for 30 min before incubation with a primary FITC-conjugated αSMA antibody at 4 ^{o}C overnight. The coverslips were then washed in PBS before mounting on microscope slides using DAPI containing mounting medium. Fluorescent images were taken using a microscope, using Pro-plus 7 imaging software at 40x magnification. Representative pictures are shown in **A.** The amount of fluorescence intensity per cell was quantified using Image J, and displayed in **B** as the mean relative fluorescent intensity for HDF283. Error bars show the SEM. N=2, independent experiments for each CAF.

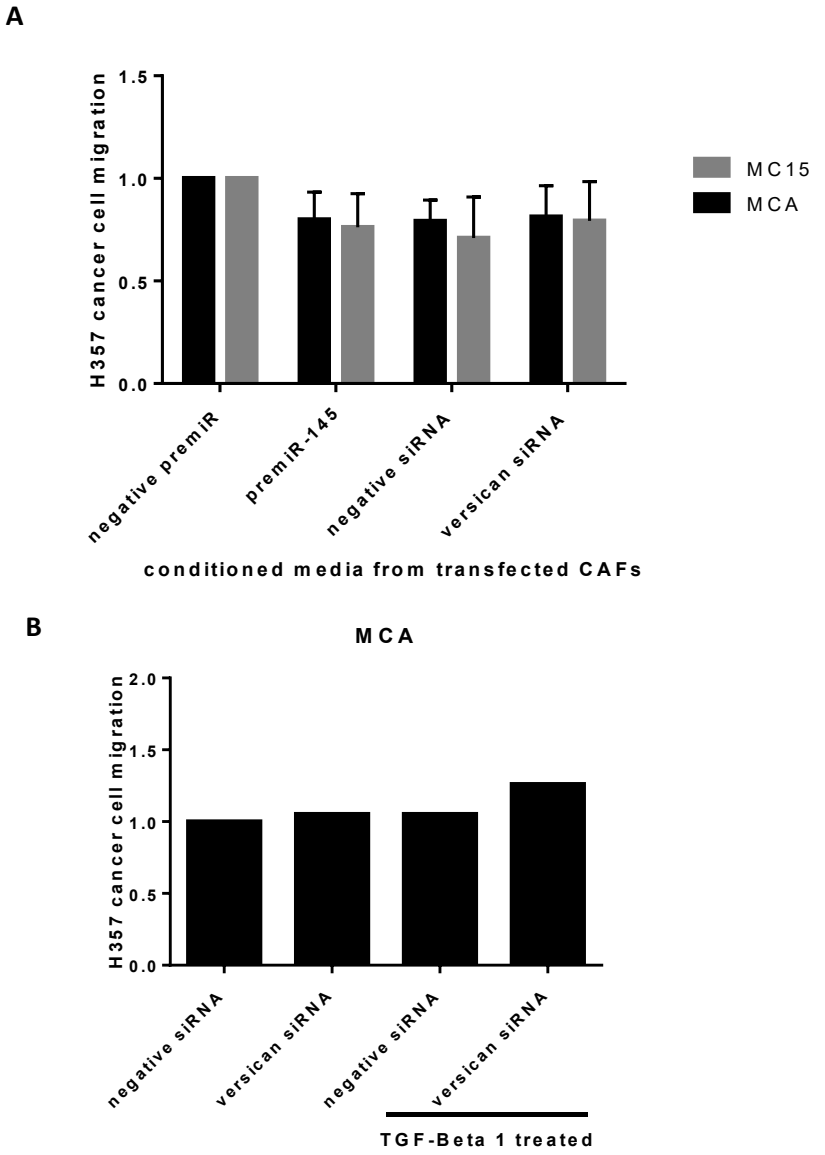

Figure 5.25: Versican knock-down in CAFs had no effect on normal or TGF-β1 stimulated paracrine oral cancer cell H357 migration. Primary CAFs (MCA and MC15), were transiently transfected with premiR-145 (50 nM) or versican siRNA or non-targeting control premiR/ siRNA (50 nM) for 24 h (A). MCA CAFs were also transiently transfected with versican siRNA or a non-targeting siRNA for 24 h prior to treatment with TGF-β1 (5 ng/ml) for 48 h (B). After treatment (A) or transfection (B), fibroblasts, conditioned media was collected for used in a transwell migration assay H357 were seeded in the transwell and allowed to migrate for 38 h through an 8 µm porous membrane to conditioned media. The membranes were methanol fixed and stained with 0.1% (w/v) crystal violet to visualise and count the cells. The figures shows the relative migration of H357 cancer cells compared to negative premiR transfected and untreated control. The error bars represent SEM. (A) N=3, independent experiments for each CAF. (B) N=2, independent experiments.

Versican knock-down in CAFs appeared to have no effect on stimulating H357 migration in either MCA or MC15 CAFs (figure 5.25A). Treatment of TGF-β1 had no effect on MCA ability to promote H357 migration (figure 5.25B). This was compared to the effect of miR-145 overexpression in the CAFs, in figure 5.25A, which was able to reduce the paracrine migration of H357s cells in both of the CAFs tested, however this trend did not reach statistical significance. By comparing the migration of CAFs transfected with negative premiR and negative siRNA in MCA and MC15 it highlights that the negative siRNA, used as a control, has some non-specific effects. Conditioned media from negative siRNA transfected CAFs had a reduced ability to stimulate paracrine migration compared to negative premiR transfected CAFs (figure 5.25A). This may explain why versican had no effect on migration in this assay.

The data described above suggests that versican knockdown reduced the expression of myofibroblast markers and has a small reduction on TGF-β1 induced expression of αSMA and FN1-EDA. The protein data however suggests that versican has little effect on CAF TGF-β1 induced αSMA expression and stress fibre formation. It is worthy of note that the qRT-PCR versican siRNA experiments were performed in BICR-59 CAFs only, whereas different combinations of CAFs (BICR-63, BICR-3 and BICR-70) were used in the immunoblotting and immunocytochemistry experiments and MCA and MC15 CAFs were used in the paracrine migration studies. The used of different CAFs could explain why versican had a variable effect on the overall CAF phenotype. CAFs are a heterogeneous population with many distinct phenotypes within the tumour microenvironment, the effect of versican knock-down may vary somewhat from CAF to CAF, therefore it would be beneficial to repeat this experiment in many different primary CAFs and ensure there are a substantial number of repeats for each CAF.

5.7 ***Examining the proteolytic cleavage of versican in oral myofibroblasts.***

Versican can be regulated and processed by proteases in the extracellular environment resulting in products different functional cleaved domains which can function independently. Versican can undergo catabolism by a select number of secreted peptidases belonging to the ADAMTS protease family (Riccidarelli *et al*., 2009). In the study aforementioned by Hattori *et al*., 2010, an ADAMTS5 knockout mouse, responsible for versican degradation in the extracellular environment, was able to cause the transdifferentiation of normal dermal fibroblasts to myofibroblasts. TIMPs inhibitors have also been shown to be responsible for CAF production (Shimaoda *et al*., 2014), perhaps this is through their regulation of versican. Some of the products that result from the proteolytic cleavage of versican can have specific roles within

cancers. For example, the globular domains, G1 and G3, of versican are reported to have several roles in cell proliferation and cell proliferation (Ricciadarelli *et al*., 2009). ADAMTS-1 and ADAMTS4, the expression of which is reported to be elevated in malignant prostates (Sandy *et al*., 2001), has been identified as responsible for the proteolytic cleavage of versican at the Glu441-Ala442 bond. This cleaved form of versican has a suggested role in promoting invasion in prostate tumours and was found to be associated poor prognosis (Arslan *et al*., 2007). Therefore, an aim was to find investigate the proteolytic cleavage of versican in OSCC.

In order to find evidence for the processing of versican, the expression of ADAMTS-1 and ADAMTS-4 were assessed in NOFs treated with TGF-β1. NOFs were treated with TGF-β1 for 24 h, 48 h and 72 h, then were harvested, RNA extracted and used to generate total cDNA for qRT-PCR to assess the transcript levels of ADAMTS-1 and ADAMTS-4. TGF-β1 caused an increase in expression of both ADAMTSs (figure 5.26). ADAMTS-1 expression increased by ~4 fold after 24 h of TGF-β1 treatment compared to untreated control, at 48 h and 72 h the ADAMTS-1 transcript levels were around ~3 fold greater than controls (figure 5.26A). After 24 h of TGF-β1 caused a ~12 fold increase in ADAMTS-4 transcript levels, this increased decreased to ~5 fold greater than untreated controls and after 72 h of TGF-β1 treatment, this had further decreased to ~1.5 fold greater expression than controls (figure 5.26B).

Next, there was an investigation into whether these ADAMTSs were able to function to cleave pericellular versican at the Glu441-Ala442 bond, as previously published. An antibody raised against this ADAMTS mediated cleaved form of versican, referred to as truncated versican, and was used to assess expression of cleaved versican in NOFs treated with TGF-β1. Total protein lysates were prepared from NOFs treated with 24 h, 48 h, and 72 h TGF-β1 or untreated controlled, were resolved on a gel and transferred to a nitrocellulose membrane for use in immunoblotting. Faint bands at ~65 kDa corresponding to the size of the truncated versican was detected in lysates from untreated NOFs (figure 5.27). Interestingly, no bands were detected in TGF-β1 treated NOFs. This data requires further confirmation due to problems with detecting any immunoreactivity in subsequent repeats of this experiment.

The expression of ADAMTS-1 and ADAMTS-4 was also investigated in the previously described CAF cohort compared to NOFs. 10 CAFs from genetically stable and unstable OSCCs were grown and RNA isolated for cDNA generation and compared to 10 NOFs. qRT-PCR was used to assess the transcript levels of the ADAMTS. There was no difference in ADAMTS-1 and ADAMTS-4 expression in CAFs compared to NOFs (figure 5.28). There was also no difference in the expression of either ADAMTSs in different subsets of CAFs (figure 5.29).

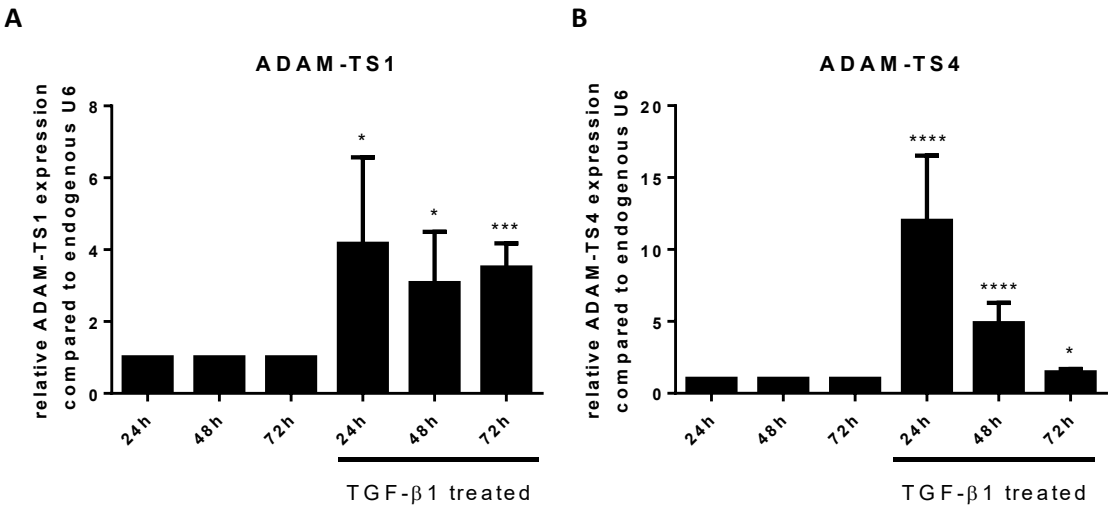

Figure 5.26: TGF-β1 induced ADAMTS-1 and ADAMTS-4 expression in oral fibroblasts. DENF319 NOFs were seeded, serum starved and treated with 5 ng/ml TGF-β1, or serum free media as a control for 24 h, 48 h and 72 h. After treatment fibroblasts were harvested, RNA isolated and used in a total cDNA preparation. qRT-PCR was performed with the cDNA with primers to amplify ADAMTS-1 and ADAMTS-4 isoforms and U6 as a reference gene. Each bar on the figure represents the mean relative quantification of ADAMTS-1 (A) and ADAMTS-4 (B) transcript levels compared to endogenous U6, for each treatment relative to the relevant untreated timepoint. Statistical analysis was performed by a paired two tailed student's t-test, and statistical significance is shown on the figure by ***p<0.001, ****p<0.0001. The significance is compared to the untreated equivalent transfection. Error bars represent the SEM. N=3, independent experiments.

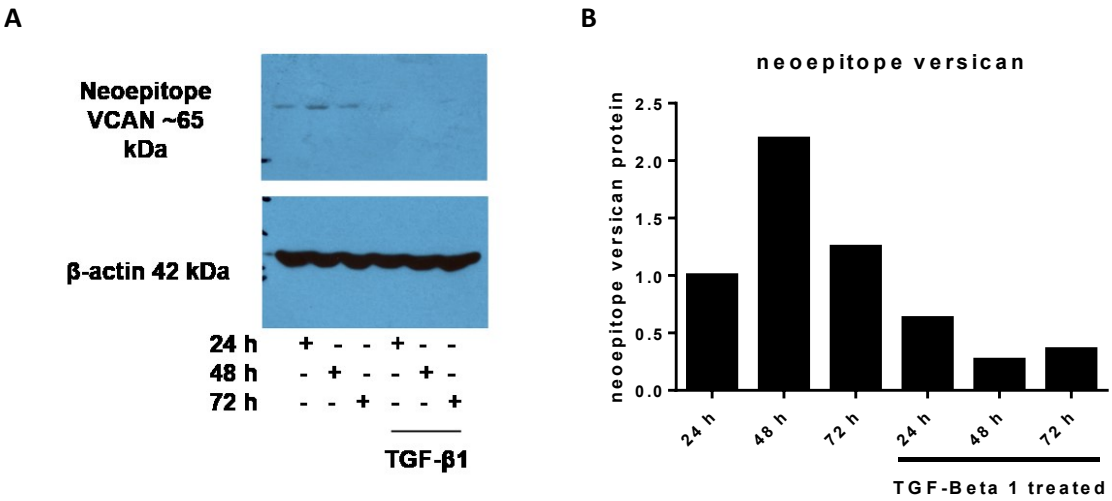

Figure 5.27: Truncated versican was detected in NOFs but not TGF-β1 treated NOFs. NOFs (DENF319) were treated with 5 ng/ml TGF-β1 for 24 h, 48 h or 72 h, or with serum free media as an endogenous control. The NOFs were then harvested, and total protein lysates were generated. Protein (20 µg) was resolved on a 3–8% (w/v) tris-acetate gradient gels, before being transferred to nitrocellulose membranes for immunoblotting. Antibodies raised against human the truncated versican, produced from ADAMTS-1 and -4 cleavage was used to assess relative protein levels, and β-actin was used as a loading control. The figure shows the immunoblot and the quantified amount of detectable protein by densitometry is shown in **B**. N=1.

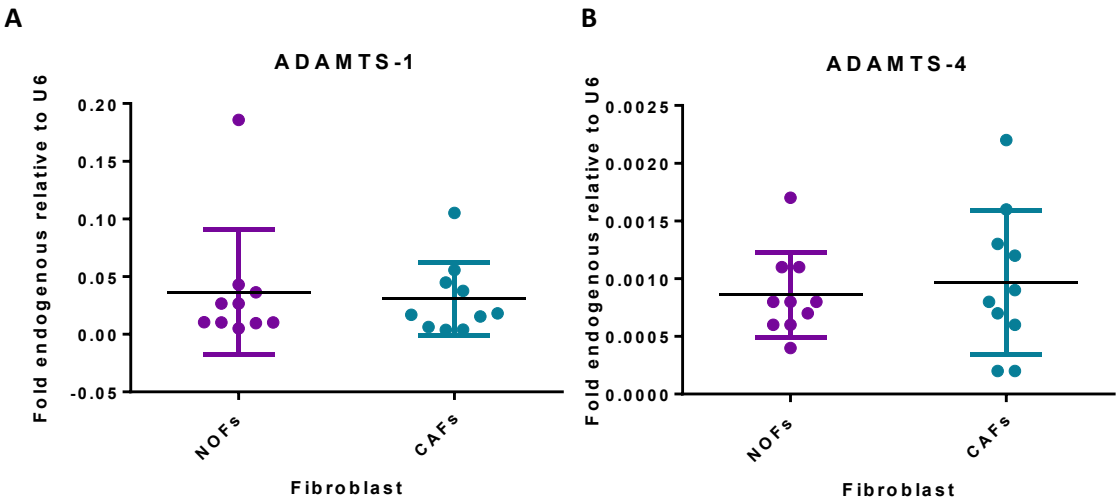

Figure 5.28: There was no difference between ADAMTS-1 and ADAMTS-4 expression between NOFs and CAFs. Fibroblasts isolated from OSCC, CAFs (10), and NOFs (10) were grown, RNA was isolated and used to generate cDNA for qRT-PCR analysis using primers designed to amplify ADAMTS-1, ADAMTS-4 and U6, as an endogenous control. The fold endogenous change of target ADAMTS-1 (**A**) or ADAMTS-4 (**B**), compared to reference gene U6 is plotted on each graph, each dot representing a different NOF/CAF. The line represents the mean fold endogenous for each set of fibroblasts. Error bars display the SD.

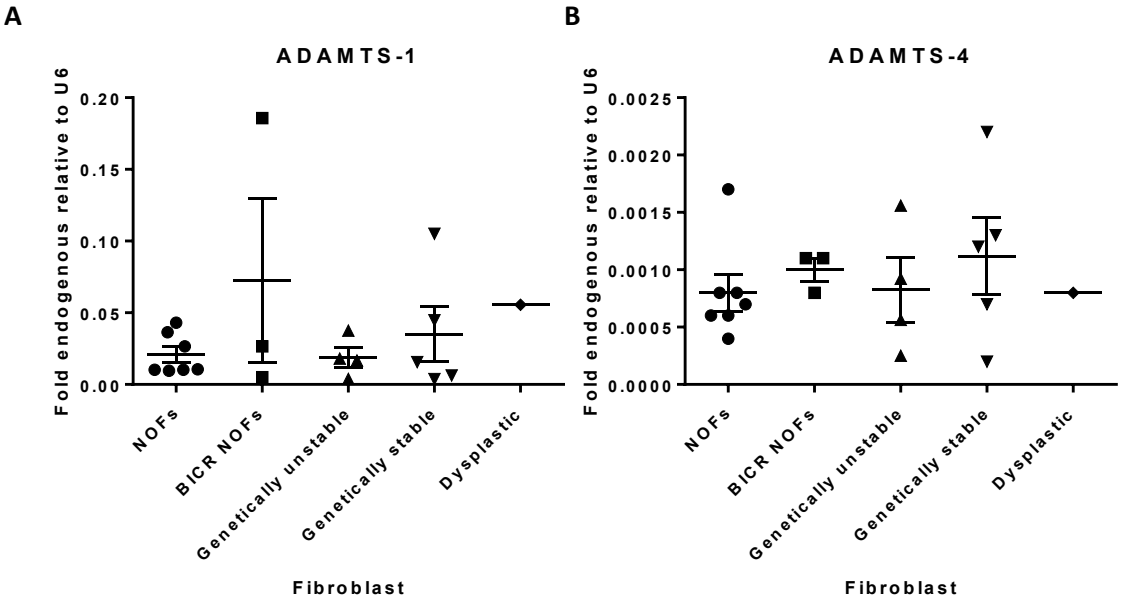

Figure 5.29: There was no difference in ADAMTS-1 and ADAMTS-4 expression in CAFs isolated from different genetically stable OSCCs. CAFs isolated from genetically stable OSCCs (N=5), unstable OSCCs (N=5), oral dysplasia (N=1), normal gingiva (BICR NOFs; N=3) all originally from Prof Ken Parkinson and NOFs (from Sheffield; N=7) were cultured. RNA was isolated and used to generate cDNA for qRT-PCR analysis using primers designed to amplify V0, V1 versican and U6, as an endogenous control. The fold endogenous change of target versican V0 (**A**) or versican V1 (**B**), compared to reference gene U6 is plotted on each graph, each dot representing a different NOF/CAF. The line represents the mean fold endogenous for each set of fibroblasts. Statistical analysis was performed by multiple ANOVA, and statistical significance is shown on the figure by **p<0.01, ***p<0.001. Error bars display the SEM.

5.8 ***Summary***

Results from this chapter showed that versican has a small effect on oral myofibroblast transdifferentiation and promoting paracrine migration. The results outlined in this chapter showed that NOFs express two isoforms, V0 and V1, which were both upregulated in response to TGF-β1. The expression of V0 versican was lower in CAFs than NOFs, whereas there was no significant difference in V1 versican expression. The expression miR-145 and not miR-143, negatively regulates versican expression. Versican depletion in 1 out of 2 NOFs and CAFs dampened the TGF-β1 induced myofibroblast markers, but had no effect on αSMA protein, stress fibre formation. Versican depletion in NOFs, but not CAFs, significantly inhibited cancer cell paracrine migration. The effect of versican on TGF-β1 induced myofibroblast paracrine migration was not able to be determined due to the negative non-targeting siRNA prevented TGF-β1 from increasing paracrine migration. The expression of ADAMTS-1 and ADAMTS-4, known to cleave versican, were shown to be elevated with TGF-β1 treatment, and experiments assessing the amount of cleaved versican showed that there was more in untreated NOFs than TGF-β1, however there were insufficient n numbers.

Chapter 6: Examination of the mechanism of the regulation of oral myofibroblast transdifferentiation by miR-145

6.1 *Aims and objectives*

The aim of this results chapter was to investigate the molecular mechanisms by which miR-145 regulates myofibroblast transdifferentiation. In an attempt to confirm published targets and identify novel ones, the objectives were to determine the effect of miR-145 on the expression smooth muscle transcript factors myocardin, myocardin related transcription factors (MRTFs) and myocardin inhibitors Krüppel like factor 4 (KLF4) and KLF5, in addition to assessing the expression of putative targets Sox-9, TGF-β Receptor II, and connective tissue growth factor (CTGF). The effect of MRTF-B on myofibroblast transdifferentiation was also assessed by a loss of function experiment. To further investigate how miR-145 regulates versican transcript levels, versican's promoter region was cloned and used in a dual luciferase reporter assay to assess whether the regulation involves the promoter, and bioinformatics was used to identify any putative binding sites. Finally, the effect of miR-145 on ADAMTS-1 and -4s was assessed, to further understand how miR-145 the controls versican expression and influences the myofibroblast phenotype.

6.2 *miR-145 effect on myofibroblast markers*

Data discussed in chapter 4 provided some evidence for miR-145 regulating the myofibroblast markers tested in untreated fibroblast, miR-145 downregulated αSMA (figure 4.3), and FN1-EDA (figure 4.6) in DENF319, and COL1A1 in both NOFs (figure 4.7). To investigate the potential targets of miR-145 an overexpression dose response was performed. NOFs (DENF316) were transiently transfected with 0, 0.5, 5, 50 nM premiR-145 for 48 h, the NOFs were then harvested for qRT-PCR analysis of the myofibroblast markers. The premiR dose response caused an overexpression of miR-145 of ~2 fold in 0.5 nM transfections, ~11 fold in 5 nM transfections, and ~15 fold in 50 nM transfections compared to mock transfected control (figure 6.1A). Unlike previous data in figure 4.3, miR-145 overexpression at the highest dose (50 nM) caused no difference in αSMA, whereas 5 nM overexpression caused a small increase in αSMA (~1.5 fold; figure 6.1B). This dose (5 nM) also caused an ~1.7 fold increase in COL1A1 levels, however 0.5 and 50 nM did not cause a significant change in COL1A levels in these cells (figure 6.2A). Overexpression of miR-145 did not have an effect on FN1-EDA levels at any dose (figure 6.2B).

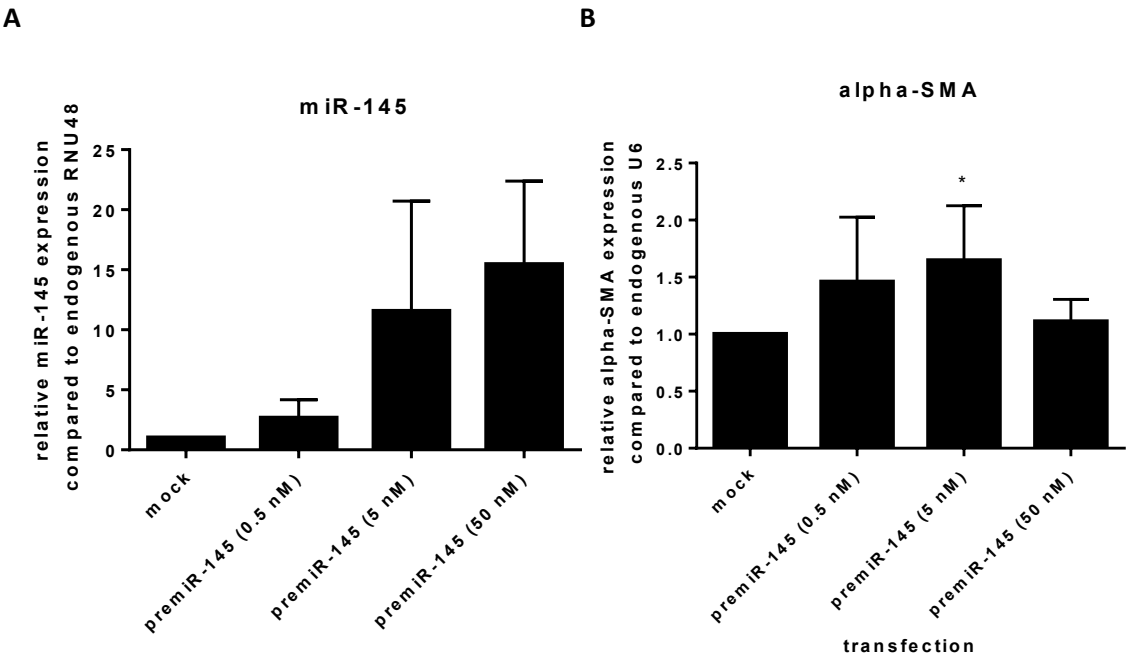

Figure 6.1: Overexpression of miR-145 by 5 nM premiR-145 transfection, caused a small increase αSMA. DENF316 NOFs were transiently transfected with premiR-145 0.5 nM, 5 nM or 50 nM or a mock (water) for 48 h. Fibroblasts were harvested and the RNA was isolated and used to generate cDNA for qRT-PCR analysis using primers designed to amplify miR-145 and RNU 48 and αSMA and U6, as an endogenous control. Each bar on the figure represents the mean relative quantification of miR-145 (**A**) and αSMA (**B**) transcript levels compared to endogenous RNU 48 and U6 respectively, for each transfection plus/minus treatment relative to untreated negative premiR. Statistical analysis was performed by a paired two tailed student's t-test, and statistical significance is shown on the figure by *$p<0.05$. If not indicated by a bar, the significance is compared to the untreated equivalent transfection, or negative premiR in the case of the untreated premiRs. Error bars represent the SEM. N=3, independent experiments.

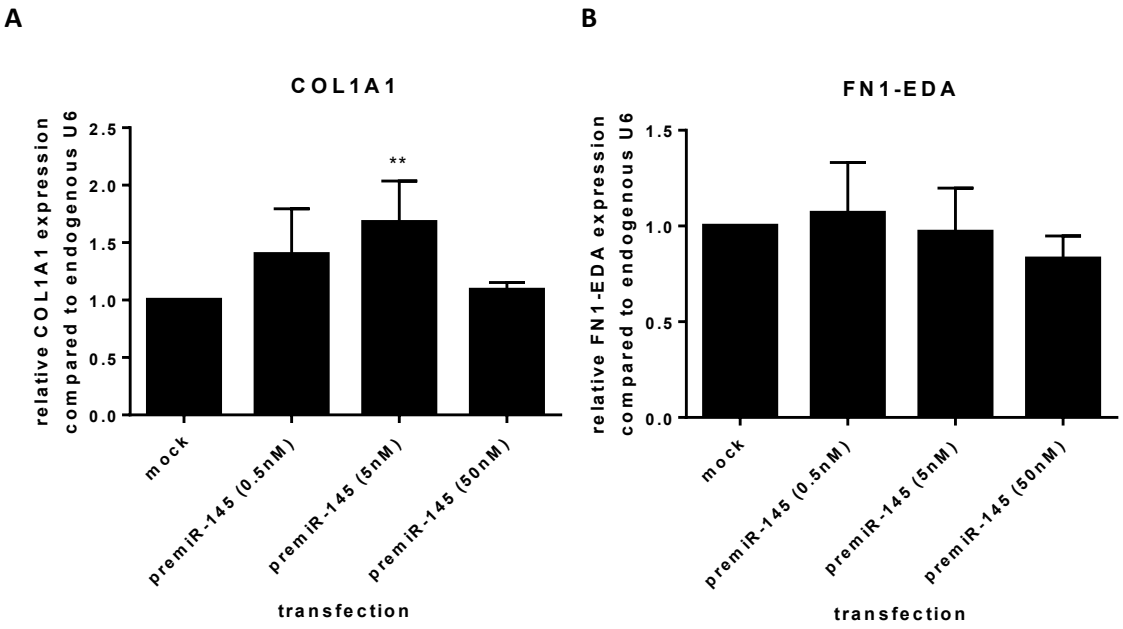

Figure 6.2: Overexpression of miR-145 by 5 nM premiR-145 transfection, caused a small increase COL1A1. DENF316 NOFs were transiently transfected with premiR-145 0.5 nM, 5 nM or 50 nM or a mock (water) for 48 h. Fibroblasts were harvested and the RNA was isolated and used to generate cDNA for qRT-PCR analysis using primers designed to amplify COL1A1, FN1-EDA and U6, as an endogenous control. Each bar on the figure represents the mean relative quantification of COL1A1 (**A**) and FN1-EDA (**B**) transcript levels compared to endogenous U6, for each transfection plus/minus treatment relative to untreated negative premiR. Statistical analysis was performed by a paired two tailed student's t-test, and statistical significance is shown on the figure by *p<0.05, ***p<0.001 and ****p<0.0001. If not indicated by a bar, the significance is compared to the untreated equivalent transfection, or negative premiR in the case of the untreated premiRs. Error bars represent the SEM. N=3, independent experiments.

6.3 *miR-145 effect on chondrogenic transcription factor Sox-9*

miR-145 has been previously shown to directly target chondrogenesis master regulator Sox-9 (Yang *et al*., 2011). This also has been shown to play a role in stromal epithelial interactions in HNSCC (Yu *et al.,* 2013). Consequently, the effect of miR-145 overexpression, and TGF-β1 treatment on sox-9 expression was studied to investigate if miR-145 regulates myofibroblast transdifferentiation through sox-9 regulation. NOFS (OF26) were transiently transfected with premiR-145 or negative non-targeting premiR then treated with TGF-β1 for 48 h to induce myofibroblasts. Both miR-145 overexpression and TGF-β1 treatment were able to downregulate sox-9 transcript levels (by ~0.3 fold and ~0.4 fold respectively; figure 6.3). Combined miR-145 overexpression, then TGF-β1 treatment caused significantly less downregulation by ~0.25 fold.

6.4 *miR-145 effect on smooth muscle transcription factors*

The data outlined in chapter 4 showed that miR-145 prevents TGF-β1 mediated αSMA expression. This is the opposite of how miR-143 and miR-145 are known to 'master regulate' smooth muscle differentiation by mediating TGF-β1 regulated key transcription factors which control the smooth muscle phenotype and αSMA expression. Specifically, miR-145 is documented to target KLF4 (Cordes *et al*., 2009), which can then regulate myocardin to induce CArG box transcriptional activation, including αSMA. miR-145 has also been reported to target myocardin related transcription factor-B MRTF-B (Xin *et al*., 2009) which are known to co-activate the CARG box to allow downstream smooth muscle gene expression. This seems to be opposed to what is suggested by our data in oral fibroblasts, that miR-145 expression represses αSMA expression.

To further delineate miR-145 mechanism of negatively regulating TGF-β1 mediated αSMA expression in oral fibroblasts, the effect of miR-145 and TGF-β1 on these smooth muscle transcription factors, myocardin, myocardin related transcription factors (MRTFs) and transcription factors KLF4/5, which known to regulate myocardin. NOFs (OF26) were transiently transfected with premiR-145 for 24 h, then treated with 5 ng/ml TGF-β1 for 48 h, subsequently these fibroblasts were used for qRT-PCR analysis investigating the gene expression of the above transcription factors.

In untreated NOFs there was no detectable expression of myocardin, however when miR-145 was overexpressed in these NOFs there was detectable expression (figure 6.4). The same occurred when the NOFs were treated with TGF-β1, and there was further induction (not

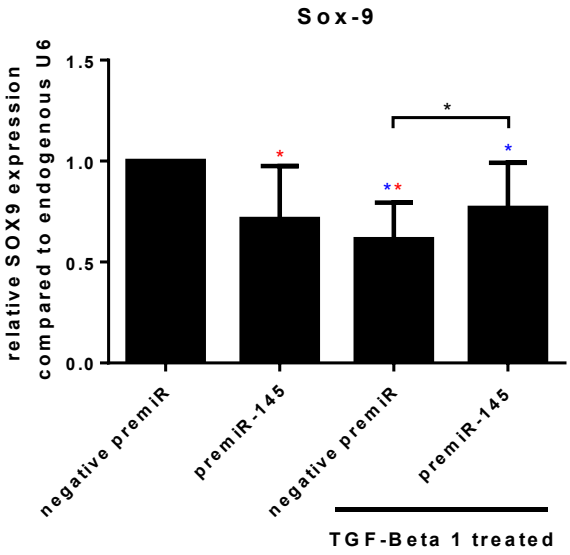

Figure 6.3: miR-145 and TGF-β1 treatment downregulated Sox-9 expression in NOFs. OF26 NOFs were transiently transfected with premiR-145 or a negative non-targeting premiR 24 h prior to treatment with TGF-β1 for 48 h. After treatment, fibroblasts were harvested and the RNA was isolated and used to generate cDNA for qRT-PCR analysis using primers designed to amplify sox-9 and U6, as an endogenous control. In figure B, each bar shows the fold endogenous of sox-9 relative to U6. Statistical analysis was performed by a paired two tailed student's t-test, and statistical significance is shown on the figure by *p<0.05 and **p<0.01. If not indicated by a bar, the black significance asterix are compared to the untreated, negative premiR transfected, negative control. Blue significance asterix indicate significance compared to the untreated counterpart, e.g. premiR-145 transfected, TGF-β1 treated compared with premiR-145 transfected untreated. Bars also indicate statistical comparisons. Important significant data is shown in red. Error bars represent the SEM. N=5, independent experiments.

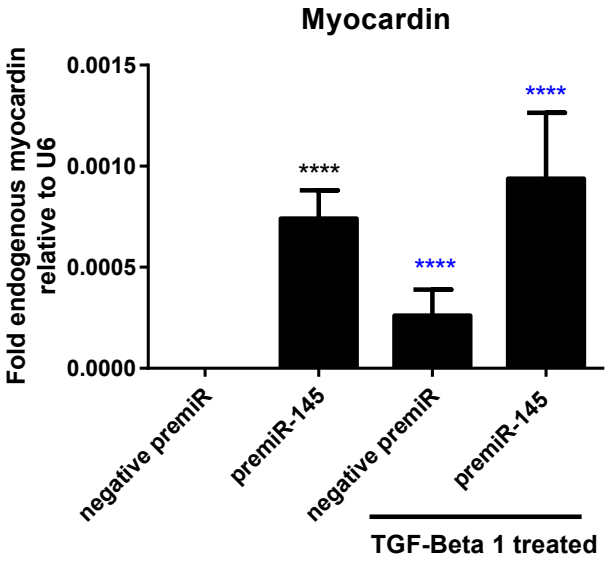

Figure 6.4: miR-145 and TGF-β1, both induced the expression of myocardin in NOFs. OF26 NOFs were transiently transfected with premiR-145 or a negative non-targeting premiR 24 h prior to treatment with TGF-β1 for 48 h. After treatment, fibroblasts were harvested and the RNA was isolated and used to generate cDNA for qRT-PCR analysis using primers designed to amplify myocardin and U6, as an endogenous control. In figure B, each bar shows the fold endogenous of myocardin relative to U6. Statistical analysis was performed by a paired two tailed student's t-test, and statistical significance is shown on the figure by ****p<0.0001. The black significance asterix are compared to the untreated, negative premiR transfected, negative control. Blue significance asterix indicate significance compared to the untreated counterpart, e.g. premiR-145 transfected, TGF-β1 treated compared with premiR-145 transfected untreated. Bars also indicate statistical comparisons. Error bars represent the SEM. N=5, independent experiments.

significant) of expression when cells were overexpressing miR-145 and TGF-β1 treated. This suggests that miR-145 may block the inhibition of myocardin, which led to the investigation of the effect of miR-145 on the known inhibitors of myocardin function KLF4 and KLF5.

TGF-β1 treatment decreased KLF4 transcript levels by 0.4 fold, however this was not found to be significant (figure 6.5A). The overexpression of miR-145, had no effect on KLF4 transcript levels, however when NOFs overexpressing miR-145 were treated with TGF-β1 there was a significant 0.5 fold decrease in KLF4 transcripts. TGF-β1 treatment increased the expression of KLF5 expression by ~2.75 fold (figure 6.5B), overexpression of miR-145 prior to this treatment prevented the TGF-β1 mediated increase in KLF5 expression.

The expression of MRTF-A and B were also examined. Although miR-145 and TGF-β1 had no effect on MRTF-A expression, NOFs overexpressing miR-145 and treated with TGF-β1 had half the MRTF-A transcript levels compared to control NOFs (figure 6.6A). Overexpression of miR-145 downregulated MRTF-B transcript levels by ~0.3 fold (figure 6.6B). TGF-β1 caused a 0.4 fold decrease in MRTF-B. NOFS both overexpressing miR-145 and treated with TGF-β1 showed further downregulation of MRTF-B, reduced by ~0.6 fold compared to control NOFs.

6.5 ***MRTF-B effect on myofibroblast transdifferentiation.***

MRTF-B (and MRTF-A) is also been reported to be involved with myofibroblast transdifferentiation in rat embryonic fibroblasts (Crider *et al*., 2011). The bioinformatical database TargetScan revealed that there are 4 putative miR-145 binding sites in MRTF-B 3'UTR. miR-143 has one predicted binding site in MRTF-B 3'UTR. Combined with the data in figure 6.6B it was hypothesised that miR-145 regulates oral myofibroblast transdifferentiation by the direct regulation of MRTF-B. To investigate this further, the expression of MRTF-B was examined in two NOFs overexpressing miR-143 or miR-145, then treated with TGF-β1. In DENF316, overexpression of miR-145 did not decrease MRTF-B transcript levels but increased them by ~2.7 fold (figure 6.7A), miR-143 also caused an increase in MRTF-B expression by ~1.6 fold compared to controls. TGF-β1 had no effect on MRTF-B in these NOFs, but damped the mir-145 mediated increase in MRTF-B levels (~1.3 fold increase), and miR-143 overexpressing NOFs treated with TGF-β1 had a reduction MRTF-B by 0.6 fold compared to control NOFs. In DENF319, overexpression of miR-145 resulted in a decrease in MRTF-B expression by ~0.75 fold compared to control NOFs in TGF-β1 treated and untreated NOFs, however these trends were not statistically significant (figure 6.7B). Similarly, miR-143 overexpression caused a decrease in

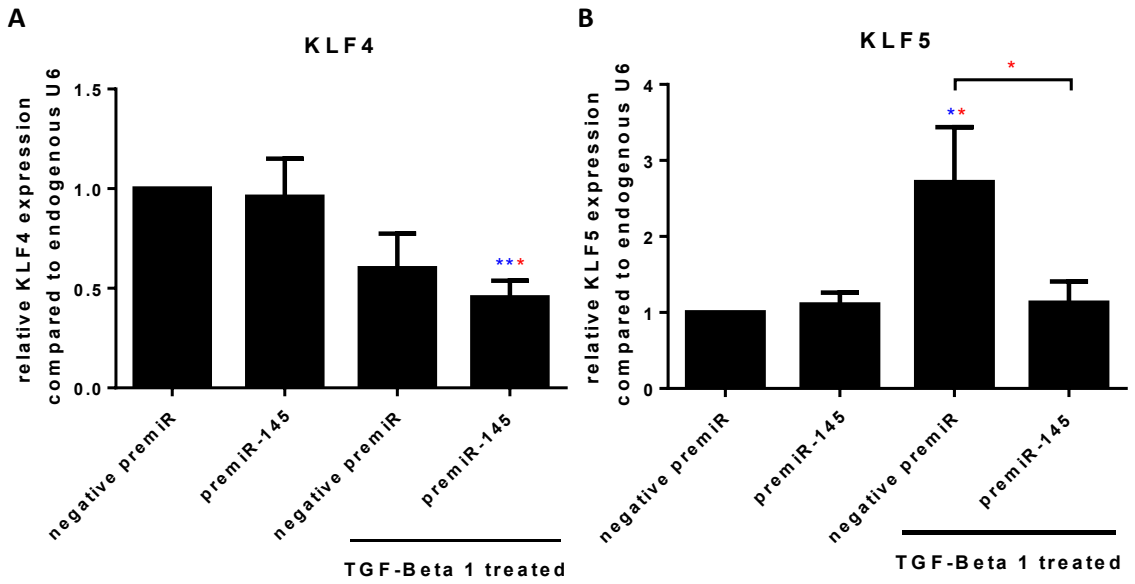

Figure 6.5: miR-145 overexpression combined with TGF-β1 treatment resulted in the downregulation of KLF4 and miR-145 inhibited TGF-β1 mediated increased KLF5 expression. OF26 NOFs were transiently transfected with premiR-145 or a negative non-targeting premiR (50 nM) 24 h prior to treatment with TGF-β1 for 48 h. After treatment, fibroblasts were harvested and the RNA was isolated and used to generate cDNA for qRT-PCR analysis using primers designed to amplify KLF4, KLF5 and U6, as an endogenous control. Each bar on the figure represents the mean relative quantification of KLF4 (**A**) and KLF5 (**B**) transcript levels compared to endogenous U6, for each transfection plus/minus treatment relative to untreated negative premiR. Statistical analysis was performed by a paired two tailed student's t-test, and statistical significance is shown on the figure by *p<0.05, **p<0.01, or ***p<0.001. If not indicated by a bar, the black significance asterix are compared to the untreated, negative premiR transfected, negative control. Blue significance asterix indicate significance compared to the untreated counterpart, e.g. premiR-145 transfected, TGF-β1 treated compared with premiR-145 transfected untreated. Bars also indicate statistical comparisons. Important significant data is shown in red. Error bars represent the SEM. N=5, independent experiments.

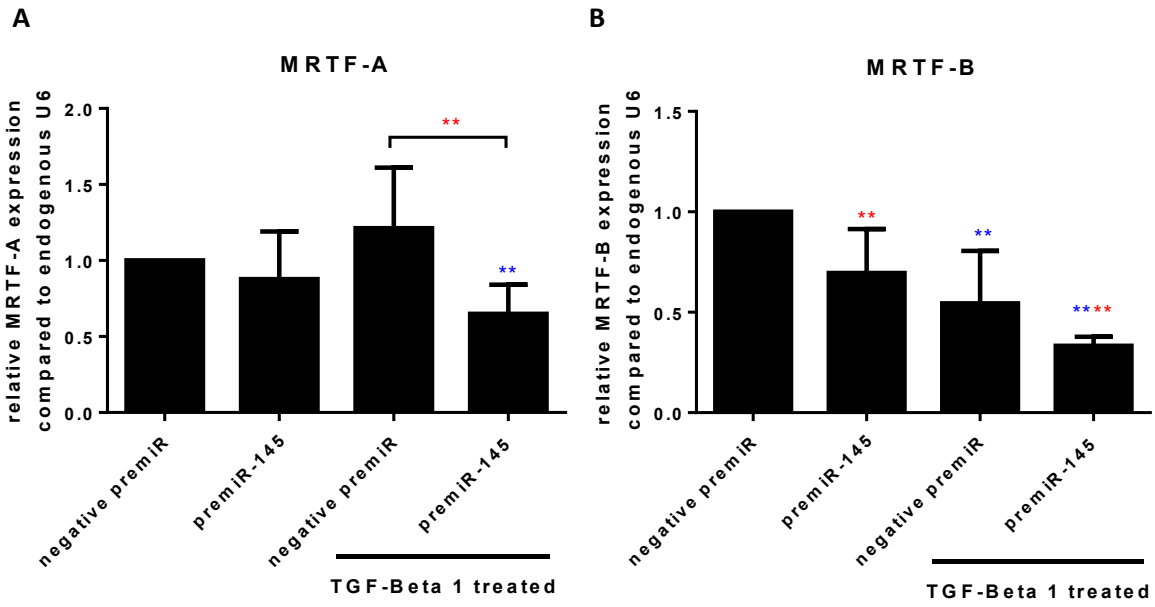

Figure 6.6: miR-145 overexpression combined with TGF-β1 treatment resulted in the downregulation of both MRTF-A and MRTF-B, also MRTF-B was downregulated by miR-145 and TGF-β1 treatment. OF26 NOFs were transiently transfected with premiR-145 or a negative non-targeting premiR (50 nM) 24 h prior to treatment with TGF-β1 for 48 h. After treatment, fibroblasts were harvested and the RNA was isolated and used to generate cDNA for qRT-PCR analysis using primers designed to amplify MRTF-A, MRTF-B and U6, as an endogenous control. Each bar on the figure represents the mean relative quantification of MRTF-A (**A**) and MRTF-B (**B**) transcript levels compared to endogenous U6, for each transfection plus/minus treatment relative to untreated negative premiR. Statistical analysis was performed by a paired two tailed student's t-test, and statistical significance is shown on the figure by **p<0.01, or ****p<0.0001. If not indicated by a bar, the black significance asterix are compared to the untreated, negative premiR transfected, negative control. Blue significance asterix indicate significance compared to the untreated counterpart, e.g. premiR-145 transfected, TGF-β1 treated compared with premiR-145 transfected untreated. Bars also indicate statistical comparisons. Important significant data is shown in red. Error bars represent the SEM. N=5, independent experiments.

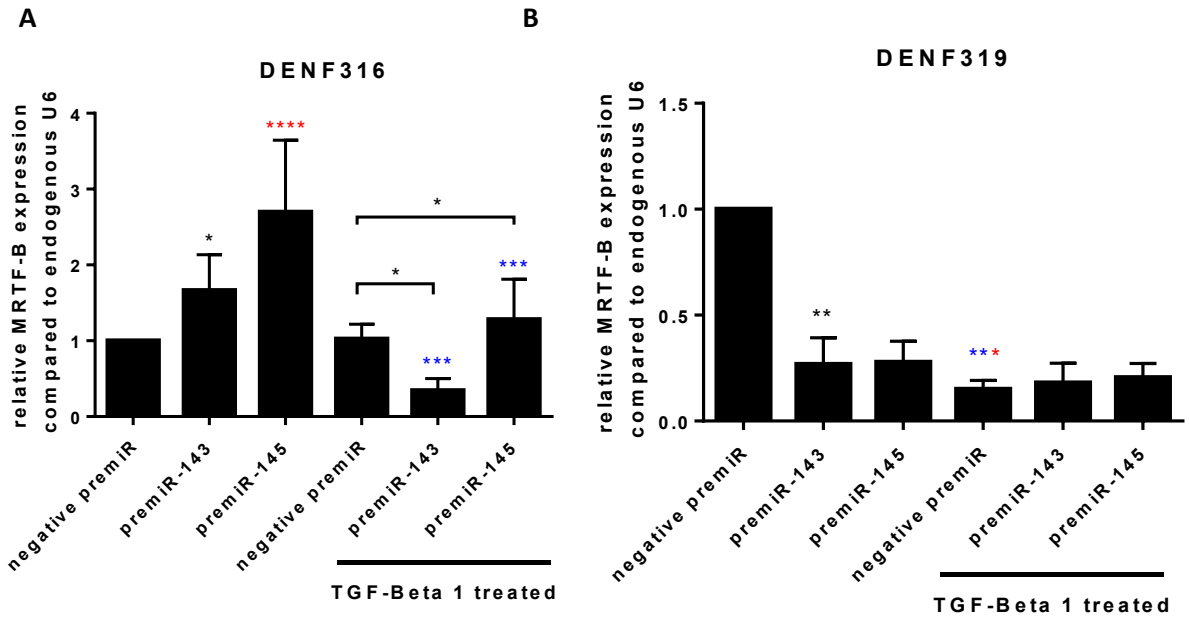

Figure 6.7: miR-145 overexpression caused an increase in MRTF-B expression in DENF316s NOFs and a trend in a decrease in MRTF-B DENF319 NOFs. Two primary NOFs, DENF316 and DENF319 (**A** and **B** respectively), were transiently transfected with premiR-143, premiR-145 or a negative non-targeting premiR (50 nM) 24 h prior to treatment with TGF-β1 for 48 h. After treatment, fibroblasts were harvested and the RNA was isolated and used to generate cDNA for qRT-PCR analysis using primers designed to amplify MRTF-B and U6, as an endogenous control. Each bar on the figure represents the mean relative quantification of MRTF-B transcript levels compared to endogenous U6, for each transfection plus/minus treatment relative to untreated negative premiR. Statistical analysis was performed by a paired two tailed student's t-test, and statistical significance is shown on the figure by *p<0.05, **p<0.01, ***p<0.001, or ****p<0.0001. If not indicated by a bar, the black significance asterix are compared to the untreated, negative premiR transfected, negative control. Blue significance asterix indicate significance compared to the untreated counterpart, e.g. premiR-145 transfected, TGF-β1 treated compared with premiR-145 transfected untreated. Bars also indicate statistical comparisons. Important significant data is shown in red. Error bars represent the SEM. N=3, independent experiments.

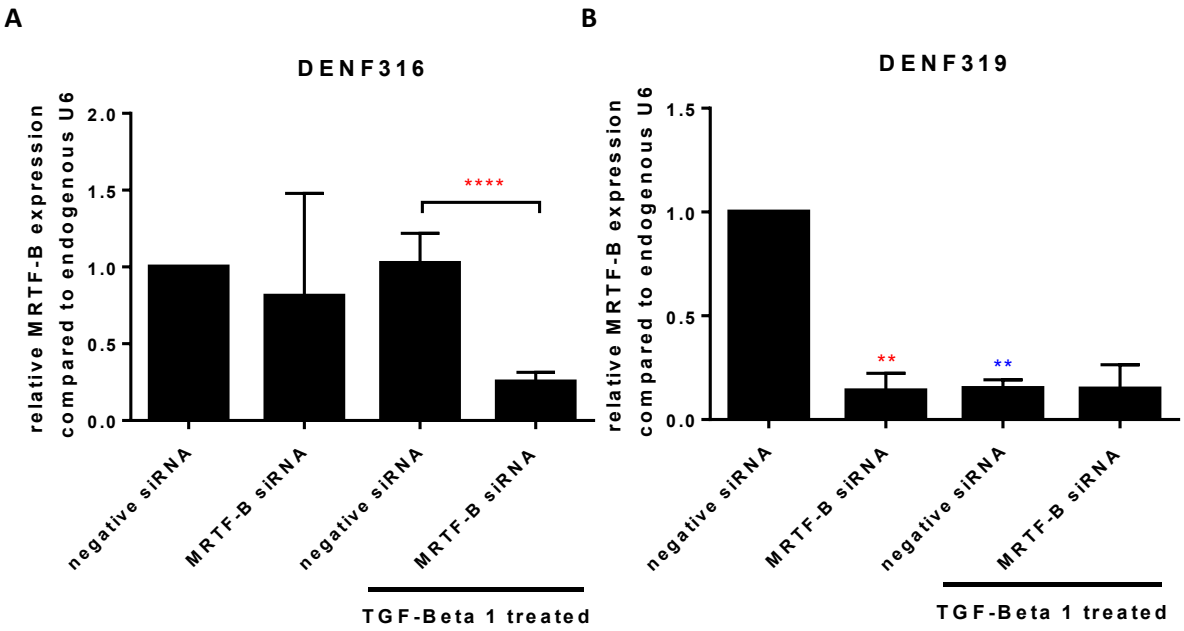

Figure 6.8: A MRTF-B targeting siRNA was knocked down MRTF-B transcript levels. Two NOFs, DENF316 and DENF319 (**A** and **B,** respectively) were transiently transfected with a MRTF-B targeting siRNA or a negative non- targeting siRNA (50 nM) for 24 h prior to TGF-β1 (5 ng/ml) treatment for 48 h. Fibroblasts were harvested and the RNA was isolated and used to generate cDNA for qRT-PCR analysis using primers designed to amplify MRTF-B and U6, as an endogenous control. Each bar on the figure represents the mean relative quantification of MRTF-B transcript levels compared to endogenous U6, for each transfection plus/minus treatment relative to untreated negative premiR. Statistical analysis was performed by a paired two tailed student's t-test, and statistical significance is shown on the figure by *p<0.05, **p<0.01 and ****p<0.0001. If not indicated by a bar, the black significance asterix are compared to the untreated, negative premiR transfected, negative control. Blue significance asterix indicate significance compared to the untreated counterpart, e.g. premiR-145 transfected, TGF-β1 treated compared with premiR-145 transfected untreated. Bars also indicate statistical comparisons. Important significant data is shown in red. Error bars represent the SEM. N=3, independent experiments.

MRTF-B expression by ~ 0.7 fold compared to control NOFs, in both TGF-β1 treated and untreated DENF319s. MRTF-B transcript levels were also reduced in DENF319s treated with TGF-β1, by ~0.8 fold. The expression patterns of DENF319 were similar to that of OF26 described above.

To assess if MRTF-B plays an important role in oral myofibroblast transdifferentiation, a MRTF-B targeting siRNA was used to deplete NOFs of MRTF-B transcript levels before inducing myofibroblasts transdifferentiation with TGF-β1 treatment. DENF316 NOFs transiently transfected with MRTF-B siRNA did not on average show decreased MRTF-B levels, as MRTF-B were reduced by ~0.3 fold compared to control NOFs, which was not significantly different to negative control siRNA NOFs (figure 6.8A). However, DENF316 transfected with MRTF-B siRNA and treated with TGF-β1 had knocked down MRTF-B levels (~0.7 fold reduced from control NOFs). DENF319s transfected with MRTF-B siRNA had significantly reduced MRTF-B levels by ~0.8 fold, this was similar to the reduction produced by TGF-β1 treatment (figure 6.8B).

Using the same cDNA the effect on MRTF-B depletion on the acquisition of the myofibroblasts phenotype was assessed by qRT-PCR analysis for myofibroblast markers. In DENF316s, TGF-β1 treatment induced αSMA expression to ~105 fold greater than untreated NOF controls, MRTF-B depletion reduced the TGF-β1 mediated αSMA to ~30 fold (figure 6.9A). However, in DENF319, MRTF-B knock-down had no effect on the response to TGF-β1, both negative and MRTFB siRNA transfected NOFS treated with TGF-β1 had a ~11 fold increase in αSMA transcript levels (figure 6.9B). COL1A1 expression showed a similar pattern of expression, MRTF-B knock-down was able to reduce a TGF-β1 mediated increase in COL1A levels (to ~2 fold increase compared to ~4.5 increase in negative siRNA TGF-β1 treated NOFs) in DENF316 NOFs only (figure 6.10A). In DENF319 NOFs TGF-β1 treatment alone did not cause an increase in COL1A1 expression, but MRTF-B knock-down and TGF-β1 increased COL1A1 expression to ~1.5 fold compared to control NOFs (figure 6.10B). MRTF-B knock-down alone resulted in a 0.4 fold reduction in COL1A1 transcript levels in DENF319s. Finally, FN1-EDA expression followed a similar trend. MRTF-B knock-down was able to reduce TGF-β1 increase in FN1-EDA expression from ~12 fold to ~7 fold, although these trends did not reach statistical significance. Whereas, in DENF319 MRTF-B knock-down increase TGF-β1 mediated FN1-EDA expression from ~1.8 fold to ~3 fold (figure 6.11), and MRTF-B knock-down alone caused a ~0.4 fold decrease in FN1-EDA, compared to DENF319 NOF controls.

Immunoblotting and immunocytochemistry were also used to assess MRTF-B knock-down's effect on αSMA protein expression. Immunoblotting revealed that MRTF-B knock-down had no

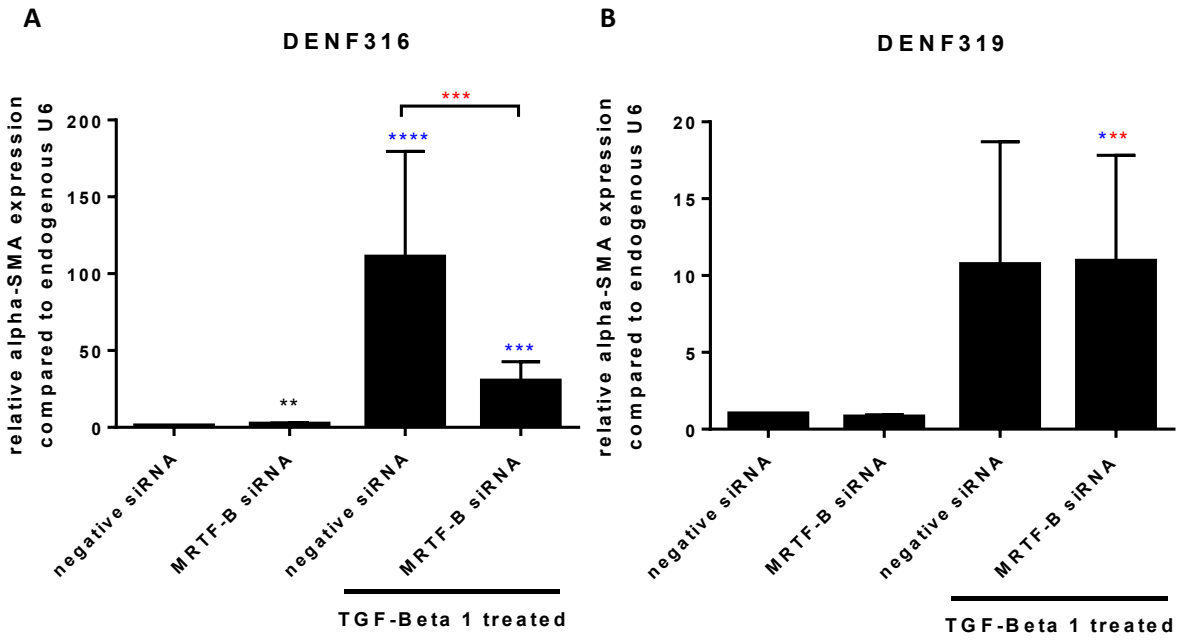

Figure 6.9: MRTF-B knock-down reduced TGF-β1 mediated αSMA expression in DENF316 NOFs not DENF319. Two NOFs, DENF316 and DENF319 (**A** and **B,** respectively) were transiently transfected with a MRTF-B targeting siRNA or a negative non-targeting siRNA (50 nM) for 24 h prior to TGF-β1 (5 ng/ml) treatment for 48 h. Fibroblasts were harvested and the RNA was isolated and used to generate cDNA for qRT-PCR analysis using primers designed to amplify αSMA and U6, as an endogenous control. Each bar on the figure represents the mean relative quantification of αSMA transcript levels compared to endogenous U6, for each transfection plus/minus treatment relative to untreated negative premiR. Statistical analysis was performed by a paired two tailed student's t-test, and statistical significance is shown on the figure by *p<0.05, **p<0.01, ***p<0.001 and ****p<0.0001. If not indicated by a bar, the black significance asterix are compared to the untreated, negative premiR transfected, negative control. Blue significance asterix indicate significance compared to the untreated counterpart, e.g. premiR-145 transfected, TGF-β1 treated compared with premiR-145 transfected untreated. Bars also indicate statistical comparisons. Important significant data is shown in red. Error bars represent the SEM. N=3, independent experiments.

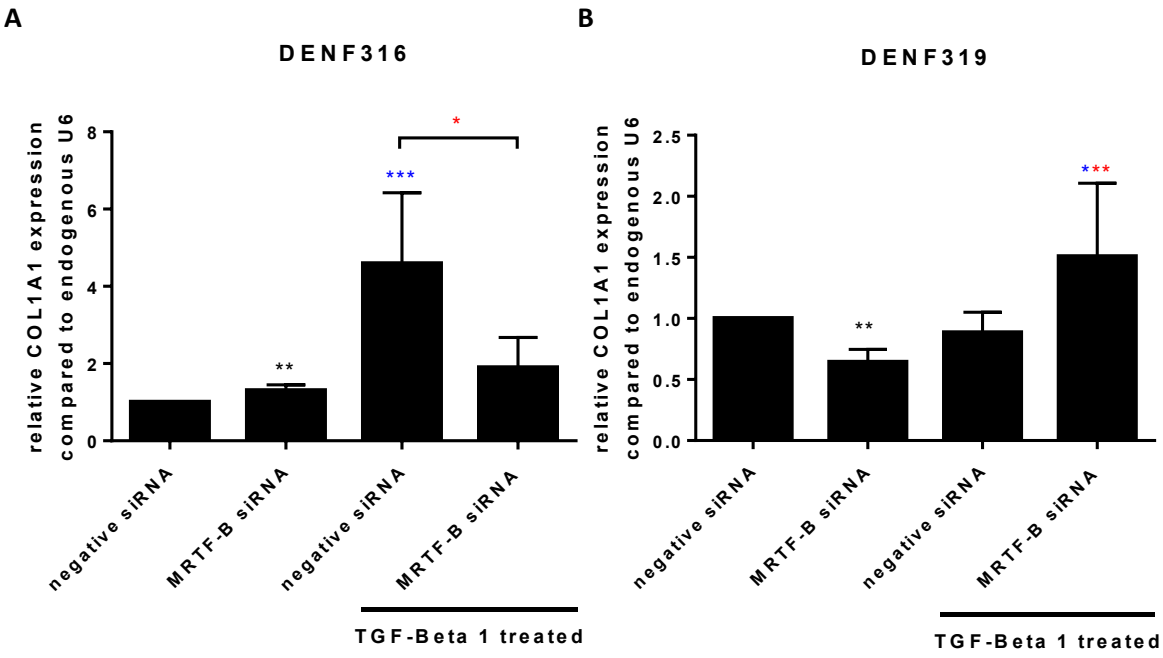

Figure 6.10: MRTF-B knock-down reduced TGF-β1 mediated COL1A1 expression in DENF316 NOFs not DENF319. Two NOFs, DENF316 and DENF319 (**A** and **B,** respectively) were transiently transfected with a MRTF-B targeting siRNA or a negative non-targeting siRNA (50 nM) for 24 h prior to TGF-β1 (5 ng/ml) treatment for 48 h. Fibroblasts were harvested and the RNA was isolated and used to generate cDNA for qRT-PCR analysis using primers designed to amplify COL1A1 and U6, as an endogenous control. Each bar on the figure represents the mean relative quantification of COL1A1 transcript levels compared to endogenous U6, for each transfection plus/minus treatment relative to untreated negative premiR. Statistical analysis was performed by a paired two tailed student's t-test, and statistical significance is shown on the figure by *p<0.05, **p<0.01, and ***p<0.001. If not indicated by a bar, the black significance asterix are compared to the untreated, negative premiR transfected, negative control. Blue significance asterix indicate significance compared to the untreated counterpart, e.g. premiR-145 transfected, TGF-β1 treated compared with premiR-145 transfected untreated. Bars also indicate statistical comparisons. Important significant data is shown in red. Error bars represent the SEM. N=3, independent experiments.

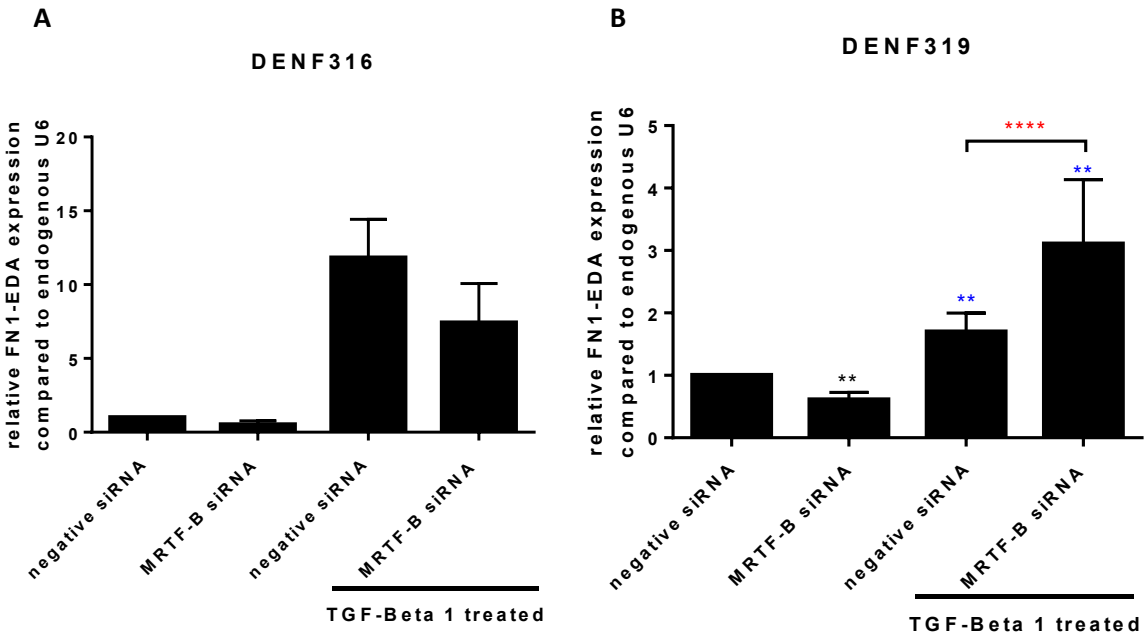

Figure 6.11: MRTF-B knock-down reduced TGF-β1 mediated FN1-EDA expression in DENF316 NOFs, and increased TGF-β1 mediated FN1-EDA expression in DENF319. Two NOFs, DENF316 and DENF319 (**A** and **B,** respectively) were transiently transfected with a MRTF-B targeting siRNA or a negative non- targeting siRNA (50 nM) for 24 h prior to TGF-β1 (5 ng/ml) treatment for 48 h. Fibroblasts were harvested and the RNA was isolated and used to generate cDNA for qRT-PCR analysis using primers designed to amplify FN1-EDA and U6, as an endogenous control. Each bar on the figure represents the mean relative quantification of FN1-EDA transcript levels compared to endogenous U6, for each transfection plus/minus treatment relative to untreated negative premiR. Statistical analysis was performed by a paired two tailed student's t-test, and statistical significance is shown on the figure by **p<0.01, and ****p<0.0001. If not indicated by a bar, the black significance asterix are compared to the untreated, negative premiR transfected, negative control. Blue significance asterix indicate significance compared to the untreated counterpart, e.g. premiR-145 transfected, TGF-β1 treated compared with premiR-145 transfected untreated. Bars also indicate statistical comparisons. Important significant data is shown in red. Error bars represent the SEM. N=3, independent experiments.

effect on TGF-β1 mediated increase in αSMA protein expression (figure 6.12), which was also quantified by densitometry (figure 6.12B). In addition, immunocytochemistry using a FITC-conjugated αSMA antibody showed that there was no difference in TGF-β1 mediated αSMA stress fibre assembly in MRTF-B knocked down NOFs, however quantification of fluorescence showed a small not significant decrease in the amount of total fluorescence (figure 6.13). Bigger n numbers were needed for this experiment.

6.6 ***Other miR-145 possible targets***

Connective Tissue Growth Factor (CTGF) has a complex relationship with tumour progression; it has been reported to both promote and inhibit tumour progression (Jacobson & Cunningham, 2012). In OSCC, it prevents tumour growth and invasion (Chuang *et al*., 2011; Moritani *et al*., 2003; Yang *et al*., 2012). In other tumours such as breast, CTGF has been shown to promote tumour growth (Chien *et al.*, 2011). It has also been shown to be required for myofibroblast transdifferentiation (Garrett et al., 2004) and is a reported to be a direct target of miR-145 (Lee et al., 2013). Therefore, the effect of miR-145 overexpression on CTGF was investigated in oral fibroblasts. In an overexpression dose response 5 nM dose of premiR-145 was the only one to cause a significant downregulation of CTGF transcript levels (by ~0.5 fold; figure 6.14A). miR-145 overexpression (50 nM) did not cause a downregulation in CTGF expression in DENF316, it caused a ~3 fold increase, but it caused a ~0.5 fold downregulation in DENF319s (figure 6.14 B and C).

miR-143 overexpression alone caused a similar trend, in DENF316s miR-143 overexpression resulted in a ~6 fold upregulation of CTGF, but in DENF319 it caused a ~0.5 fold decrease in CTGF levels. TGF-β1 caused a large upregulation of CTGF in both DENF316 and DENF319, but like with other myofibroblast markers there were different degrees of activation in the NOFs, ~78 fold and ~15 fold respectively. miR-145 was able to reduce this TGF-β1 mediated CTGF expression in DENF316s to ~14 fold compared to ~78 fold in negatively transfected TGF-β1 mediated CTGF expression (figure 6.14A). miR-143 was also able to reduce TGF-β1 mediate to ~48 fold, however this was not found to be a significant change compared to TGF-β1 treated, negative premiR transfected DENF316s. Both miR-143 and miR-145 overexpression were able to reduce the TGF-β1 mediated increase in CTGF expression in DENF319s, miR-143 overexpressing, TGF-β1 treated NOFs had ~10 fold CTGF expression and miR-145 overexpressing TGF-β1 treated NOFs had ~5 fold CTGF expression, compared to untreated DENF319 controls (figure 6.14C).

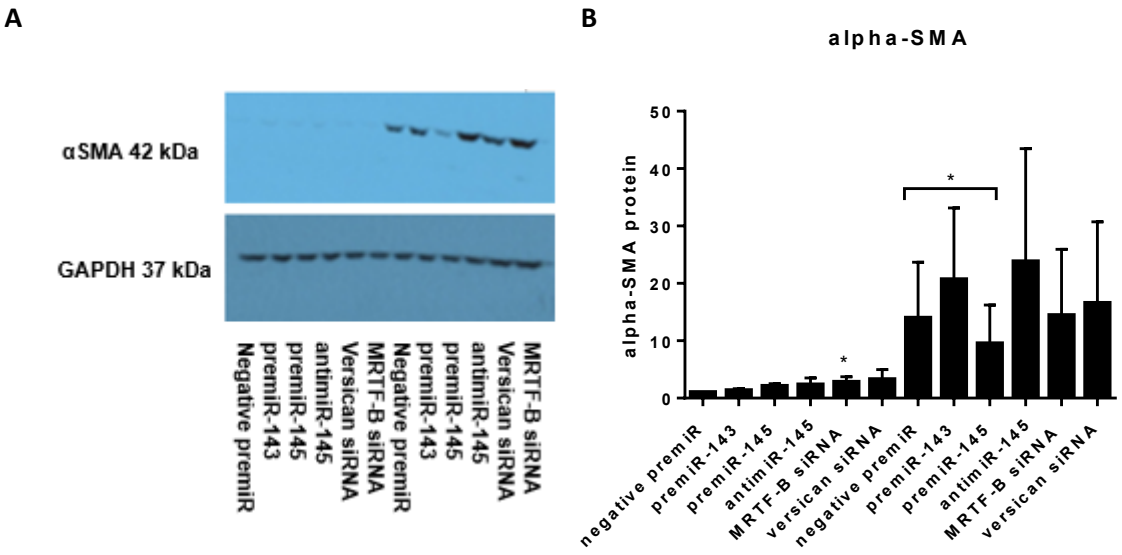

Figure 6.12: MRTF-B knock-down did not reduce TGF-β1 induced αSMA protein expression. Two NOFs, DENF316 (shown here) and DENF319, were transiently transfected with negative premiR, premiR-143, premiR-145, antimiR-145, negative control siRNA, MRTF-B siRNA or versican siRNA (50 nM) for 24 h prior to treatment with 5 ng/ml TGF-β1 or serum free media. Total protein lysates (20 µg) were resolved on 3–8% (w/v) tris acetate gels and transferred onto nitrocellulose membranes for immunoblotting. A monoclonal anti-human αSMA antibody was used to detect αSMA protein levels in the transfected then treated NOFs. GAPDH was used as a loading control. Figure A shows a representative DENF316 blot. Densitometry was performed using image J for DENF316 in triplicate and shown in B. Statistical analysis was performed by a paired two tailed student's t-test, and statistical significance is shown on the figure by *p<0.05. If not indicated by a bar, the significance is compared to the untreated equivalent transfection. N=3, independent experiments for both NOFs.

A

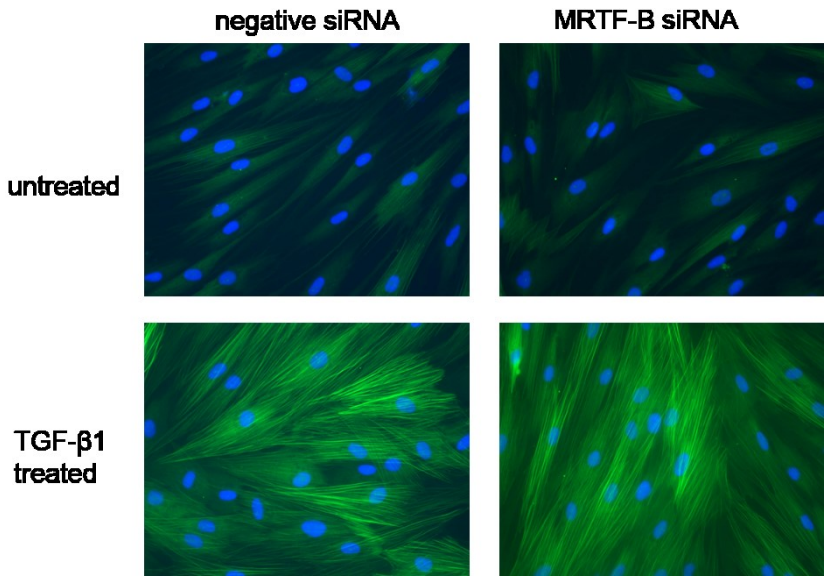

B

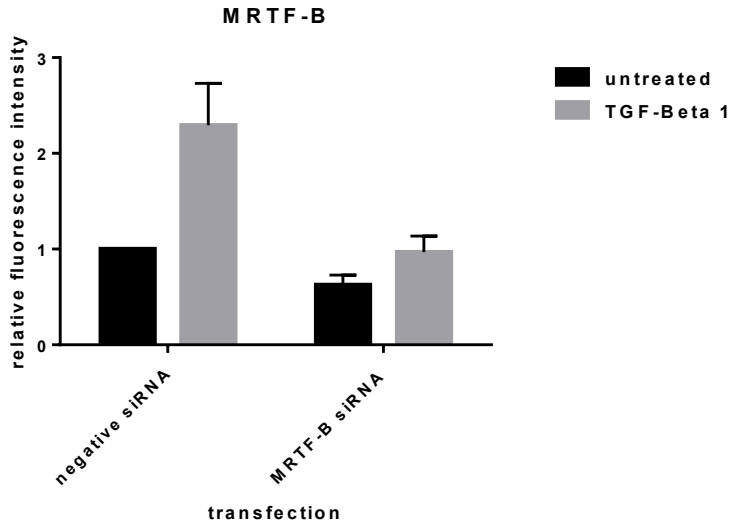

Figure 6.13: MRTF-B knock-down decreased the total αSMA-FITC fluorescence, but there was no observed effect on TGF-β1 induced αSMA stress fibres. NOFs (DENF316) were seeded onto coverslips overnight, transiently transfected with negative siRNA, or MRTF-B siRNA (50 nM) 24 h prior to being treated with 5 ng/ml TGF-β1 for 48 h. The coverslips were washed in PBS, before being fixed in 100% methanol for 10 min, they were then permeablised using 4 mM sodium deoxycholate for 10 min, and blocked using 2.5% (w/v) BSA in PBS for 30 min before incubation with a primary FITC-conjugated αSMA antibody at 4 ^{o}C overnight. The coverslips were then washed in PBS before mounting on microscope slides using DAPI containing mounting medium. Fluorescent images were taken using a microscope, using Pro-plus 7 imaging software at 40x magnification. Representative pictures are shown in **A.** The amount of fluorescence intensity per cell was quantified using Image J, and displayed in **B** as the mean relative fluorescent intensity for NOFs negative premiR treated compared to treated. Error bars show the SEM. N=2, independent experiments.

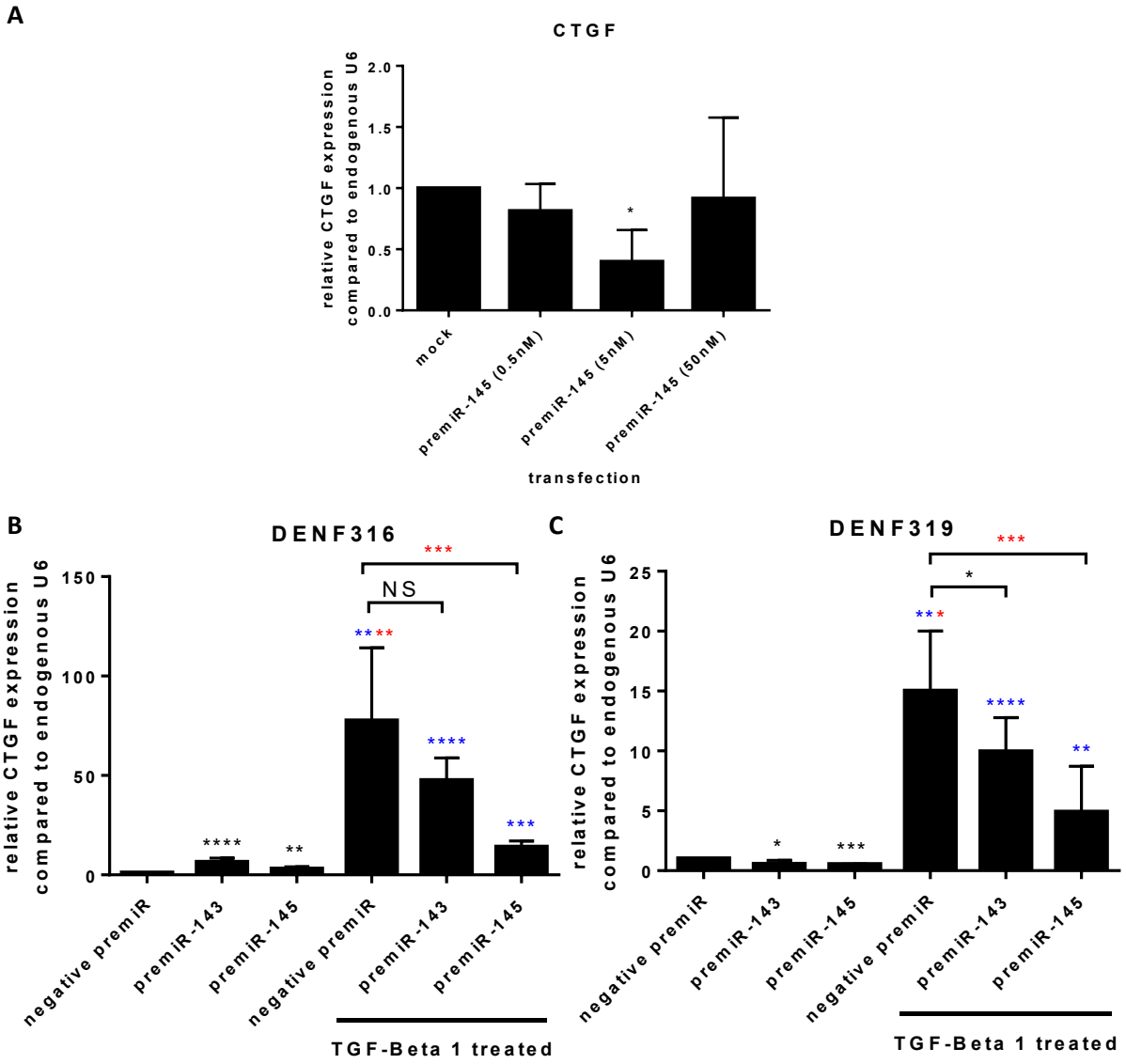

Figure 6.14: miR-145 reduced TGF-β1 induced CTGF expression. DENF316 NOFs were transiently transfected with premiR-145 0.5 nM, 5 nM or 50 nM or a mock (water) for 48 h (A). Two primary NOFs, DENF316 and DENF319 (**B** and **C** respectively), were transiently transfected with 50 nM premiR-143, premiR-145 or a negative non-targeting premiR (50 nM) 24 h prior to treatment with TGF-β1 for 48 h. Fibroblasts were harvested and the RNA was isolated and used to generate cDNA for qRT-PCR analysis using primers designed to amplify CTGF and U6, as an endogenous control. Each bar on the figure represents the mean relative quantification of CTGF transcript levels compared to endogenous U6, for each transfection plus/minus treatment relative to untreated negative premiR. Statistical analysis was performed by a paired two tailed student's t-test, and statistical significance is shown on the figure by *p<0.05, **p<0.01, ***p<0.001, or ****p<0.0001. If not indicated by a bar, the black significance asterix are compared to the untreated, negative premiR transfected, negative control. Blue significance asterix indicate significance compared to the untreated counterpart, e.g. premiR-145 transfected, TGF-β1 treated compared with premiR-145 transfected untreated. Bars also indicate statistical comparisons. Important significant data is shown in red. Error bars represent the SEM. N=3, independent experiments.

DIANA miR-Path pathway analysis software highlighted miR-145 as targeting several parts of the TGF-β1 pathway, including smad4, smad4, smad5 and TGF-β R II. A recent paper validated TGF-β RII as a direct target of miR-145 (Zhao et al., 2014). To investigate whether miR-145 may regulate oral myofibroblast transdifferentiation through the regulation of TGF-β R II, the expression was assessed by qRT-PCR. Overexpression of miR-145, caused a 0.5 fold decrease in TGF-β RII (figure 6.15). Interestingly, TGF-β1 treatment itself caused a 0.5 fold decrease in TGF-β RII and combined miR-145 overexpression and TGF-β RII resulted in a similar amount of downregulation of TGF-β R II.

6.7 *miR-145 regulation of versican*

In chapter 5, miR-145 was shown to negatively regulate versican expression. An overexpression dose response was used to shown miR-145 dose dependent regulation of V0 and V1 versican isoforms (figure 6.16). V0 expression reduced by 0.4 and 0.6 fold in 5 nM and 50 nM premiR-145 doses respectively (figure 6.16A). V1 expression reduced by ~0.4 and 0.5 fold in 5 nM and 50 nM premiR-145 respectively (figure 6.16B).

miR-143 has been shown to directly target versican (Wang *et al*., 2010), in this study miR-145 did not bind the versican 3'UTR. Bioinformatic databases also do not show predicted binding for miR-145 in the 3'UTR. Therefore, miR-145 is not thought to directly target versican. To investigate if this regulation was brought about through regulation of the activity of the versican promoter by miR-145, the promoter region of versican was cloned into the pGL3 basic luciferase reporter vector and used in a dual luciferase reporter (DLR) assay. The pGL3 basic vector contains the firefly luciferase gene to monitor transcriptional activity, it lacks any eukaryote regulatory elements, therefore making it ideal to insert a promoter upstream of the luciferase gene. The DLR was optimised by co-transfecting the BICR16 cell line, a OSCC cell line known to endogenously express versican, with different ratios of Renilla control vector with empty pGL3-basic or the versican promoter construct (VCANp-pGL3b) (1:5, 1:10, 1:50, 1:100) to achieve a read-out relative Renilla: Luciferase ratio of around 1, (figure 6.17A), a ratio of 1:10 appeared to give the nearest read out to 1, therefore was used in the DLR assay. BICR16 cells were co transfected with Renilla: VCANp-Luc (1:10) and negative premiR, premiR-143, premiR-145 or antimiR-145 for 48 h. The cells were then lysed and lysates were used to assess the luciferase activity of the VCANp-luc construct using a dual luciferase assay. There was no significant difference in promoter activity between any of the transfection conditions (figure 6.17B).

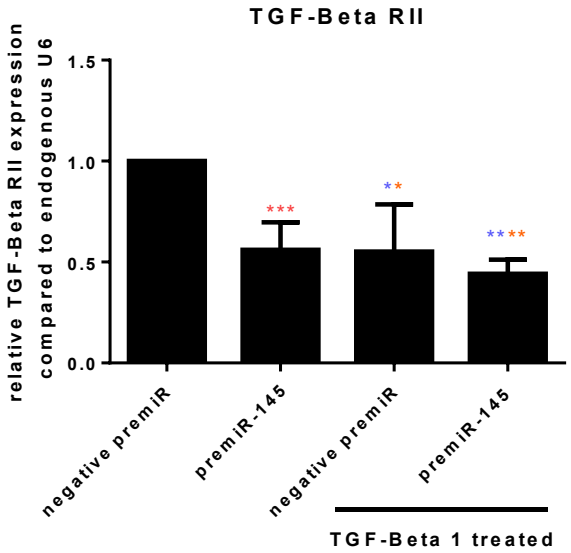

Figure 6.15 miR-145 and TGF-β1 downregulated TGF-β Receptor II expression in normal oral fibroblasts. OF26 NOFs were transiently transfected with premiR-145 or a negative non-targeting premiR (50 nM) 24 h prior to treatment with TGF-β1 for 48 h. After treatment, fibroblasts were harvested and the RNA was isolated and used to generate cDNA for qRT-PCR analysis using primers designed to amplify TGF-βRII and U6, as an endogenous control. Each bar on the figure represents the mean relative quantification of TGF-βRII transcript levels compared to endogenous U6, for each transfection plus/minus treatment relative to untreated negative premiR. Statistical analysis was performed by a paired two tailed student's t-test, and statistical significance is shown on the figure by **p<0.01, ***p<0.001 or ****p<0.0001. If not indicated by a bar, the black significance asterix are compared to the untreated, negative premiR transfected, negative control. Blue significance asterix indicate significance compared to the untreated counterpart, e.g. premiR-145 transfected, TGF-β1 treated compared with premiR-145 transfected untreated. Bars also indicate statistical comparisons. Important significant data is shown in red. Error bars represent the SEM. N=5, independent experiments.

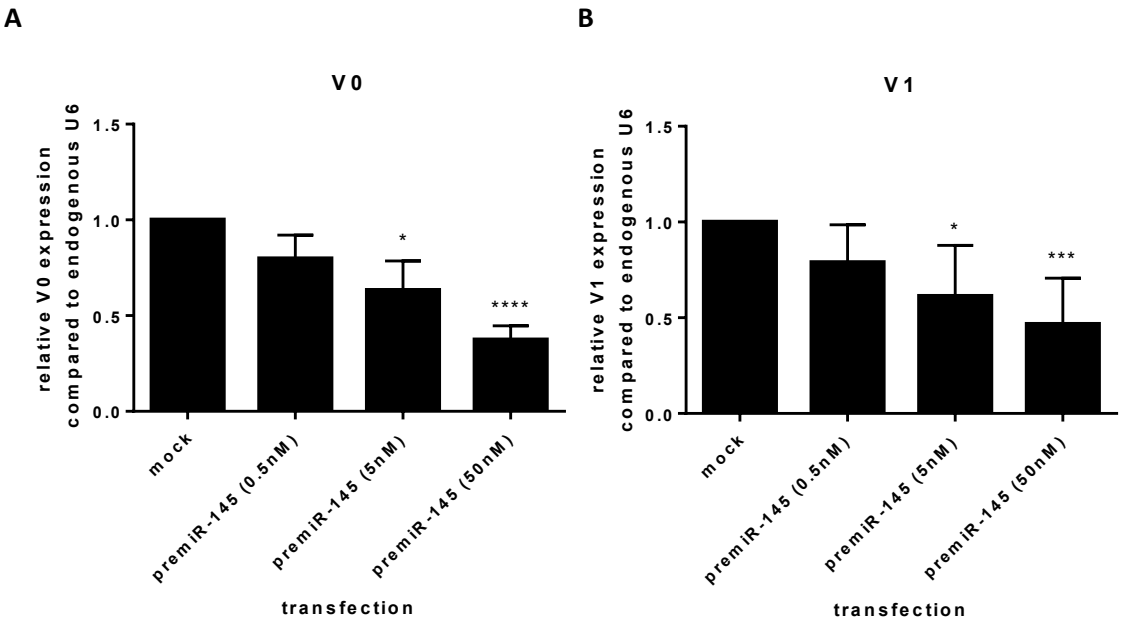

Figure 6.16: miR-145 negatively regulated versican in a dose dependent manner. DENF316 NOFs were transiently transfected with premiR-145 0.5 nM, 5 nM or 50 nM or a mock (water) for 48 h. Fibroblasts were harvested and the RNA was isolated and used to generate cDNA for qRT-PCR analysis using primers designed to amplify versican V0, V1 and U6, as an endogenous control. Each bar on the figure represents the mean relative quantification of versican V0 (**A**) and versican V1 (**B**) transcript levels compared to endogenous U6, for each transfection plus/minus treatment relative to untreated negative premiR. Statistical analysis was performed by a paired two tailed student's t-test, and statistical significance is shown on the figure by *p<0.05, ***p<0.001, and ****p<0.0001. If not indicated by a bar, the significance is compared to the untreated equivalent transfection, or negative premiR in the case of the untreated premiRs. Error bars represent the SEM. N=3, independent experiments.

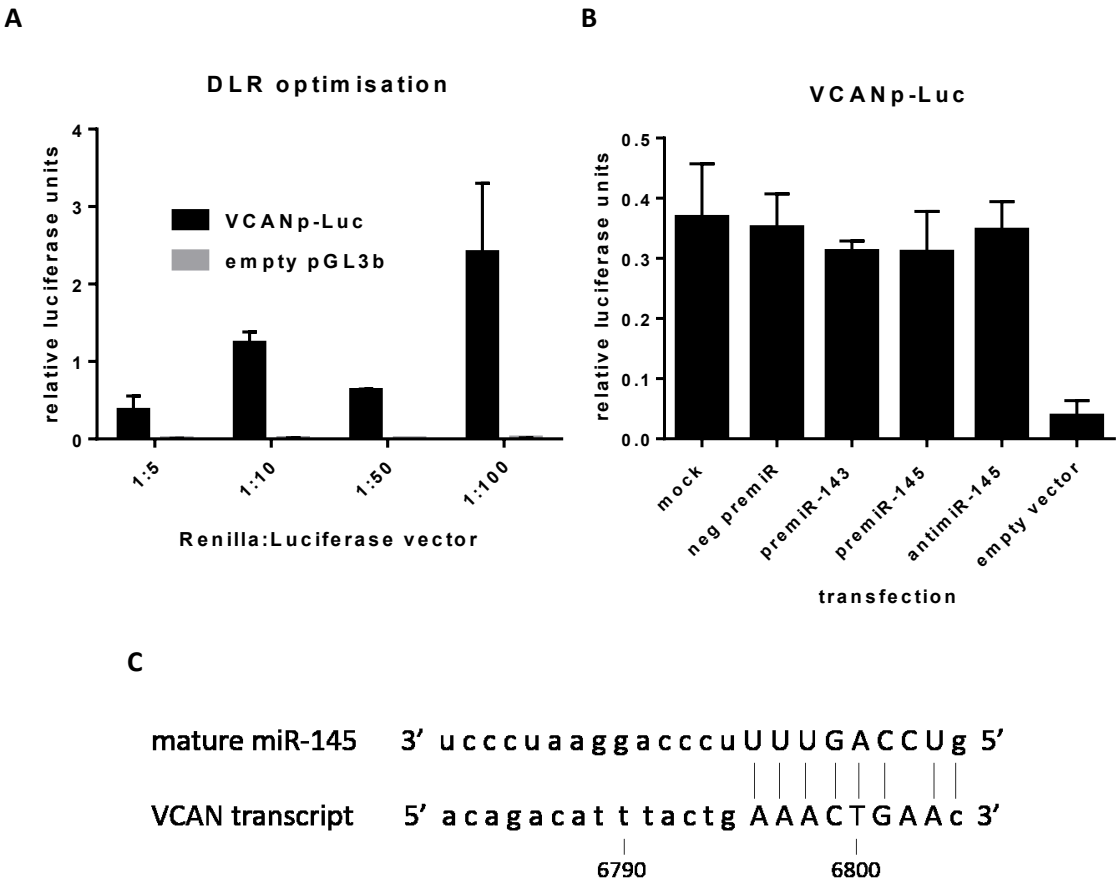

Figure 6.17: miR-145 had no effect on the promoter activity of versican. Optimisation (**A**). BICR16 cell line was co-transfected with VCANp-Luc (pGL3-basic luciferase reporter vector containing the versican promoter region), or empty pGL3 basic vector (0.5, 1, 5, or 10 µg) with Renilla plasmid control (0.1 µg) for 48 h. To examine the transcriptional effect miR-145 has on the versican gene (**B**). BICR16 cells were transfected with VCANp-Luc (1 µg) and Renilla (0.1 µg), were also co-transfected with mock (water), negative non-targeting premiR, premiR-143, premiR-145, or antimiR-145 (50 nM). Cells were lysed using passive lysis buffer and Renilla and Firefly Luciferase activity was measured using a dual-luciferase reporter assay kit using a Glowmax microplate luminometer. Firefly luciferase levels were normalised to Renilla luciferase and plotted on the figure as relative luciferase units. Error bars represent SEM. N=3. **C** shows an alignment of the mature miR-145 sequence with versican mRNA transcript, miR-145's seed sequence and putative binding site is highlighted in capitals. Alignment was performed using multalin online software using the versican mRNA transcript 1 sequence and the complementary miR-145 seed sequence. N=3, independent experiments.

Bioinformatic software were used to further investigate miR-145s regulation of versican. A promoter and miRNA interaction online database confirmed that there was no putative binding site for miR-145 within the versican promoter (Piriyapongsa *et al*., 2014). The presence of miR-145 binding sites within the coding region of versican was investigated using alignment online software multalin (Corpet, 1988). The miR-145 complementary seed sequence was aligned to versican's mRNA transcript variant 1 sequence obtained from the NCBI database. A putative binding site was identified in an exon region of versican's sequence (6796-6805), in which 7 out of 8 nucleotides within the miR-145 seed sequence complemented the transcript sequence (figure 6.17C).

The control of versican proteolytic cleavage by ADAMTS-1 and -4 may also be important, as cleaved versican may promote invasion in OSCC, like in prostate cancers (Carmela Ricciardelli *et al*., 2009). The effect of miR-145 on ADAMTS-1 and -4 was investigated. Overexpression of miR-145 resulted in a ~0.4 fold downregulation of ADAMTS-1, in both untreated and TGF-β1 treated NOFs (figure 6.18A). TGF-β1 caused a ~3 fold increase in ADAMTS-1 and a ~4 fold increase in ADAM TS-4 compared to untreated controls (figure 6.18 A and B). Overexpression of miR-145 caused a ~0.5 fold decrease in ADAMTS-4 transcript levels, overexpression of miR-145 prevented the TGF-β1 mediated increase of ADAMTS-4 to ~1.3 fold (figure 6.18B).

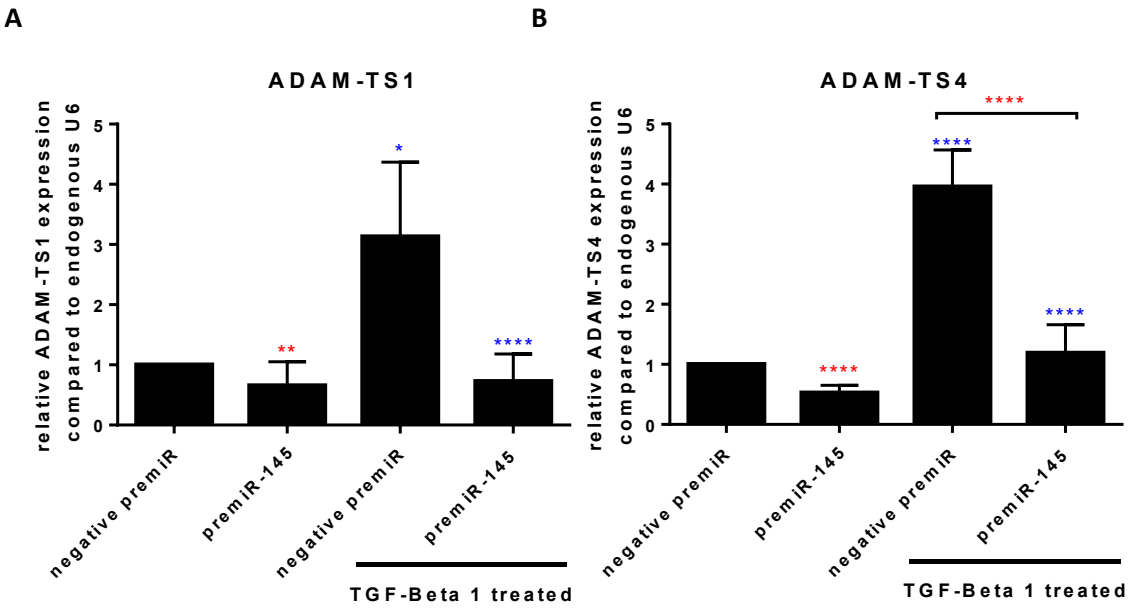

Figure 6.18: miR-145 overexpression downregulated ADAMTS-1 and -4 expression and prevented TGF-β1 mediated ADAMTS-1 and -4 increase. DENF316 NOFs were transiently transfected with premiR-145 0.5 nM, 5 nM or 50 nM or a mock (water) for 48 h. Fibroblasts were harvested and the RNA was isolated and used to generate cDNA for qRT-PCR analysis using primers designed to amplify ADAMTS-1, ADAMTS-4 and U6, as an endogenous control. Each bar on the figure represents the mean relative quantification of ADAMTS-1 (**A**) and ADAMTS-4 (**B**) transcript levels compared to endogenous U6, for each transfection plus/minus treatment relative to untreated negative premiR. Statistical analysis was performed by a paired two tailed student's t-test, and statistical significance is shown on the figure by *p<0.05, **p<0.01 and ****p<0.0001. If not indicated by a bar, the black significance asterix are compared to the untreated, negative premiR transfected, negative control. Blue significance asterix indicate significance compared to the untreated counterpart, e.g. premiR-145 transfected, TGF-β1 treated compared with premiR-145 transfected untreated. Bars also indicate statistical comparisons. Important significant data is shown in red. Error bars represent the SEM. N=3, independent experiments.

6.8 ***Summary***

Data outlined in this chapter showed that miR-145 significantly regulates the expression of several transcription factors, growth factors and ECM components that have been published to be involved in the regulation of the myofibroblast phenotype. Data showed that both TGF-β1 treatment and miR-145 overexpression independently downregulated MRTF-B, Sox-9 and TGF-βR II and the combined treatment of TGF-β1 and miR-145 resulted in the downregulation of KLF4 and MRTF-A. miR-145 was able to inhibit TGF-β1 mediated increase in KLF5 expression. miR-145 caused the downregulation of CTGF, and prevented TGF-β1 mediated increase in expression. Both TGF-β1 and miR-145 induced the neo-expression of myocardin.

Data from this chapter confirmed that miR-145 negatively regulates versican as a miR-145 dose response showed a step-wise reduction in the expression of both versican isoforms. In the investigation into the nature of this regulation, it was found that miR-145 had no effect on the versican promoter region, however a putative miR-145 binding site for versican was identified in versican's coding region. Data also showed that miR-145 downregulates the expression of ADAMTS-1 and -4, metalloproteases that can proteolytically cleave versican, in NOFs, and prevents the TGF-β1 mediated increase in their expression.

Chapter 7: The role of miR-145 in the acquisition of the dermal myofibroblast phenotype.

7.1 *Aims and objectives*

The overall aim of this results chapter was to establish whether miR-145 had similar effects on dermal myofibroblast transdifferentiation as observed in oral fibroblasts. Therefore, the objectives were to characterise the TGF-β1 mediated dermal myofibroblast transdifferentiation and perform miR-145 gain of function experiments to determine whether miR-145 was able to prevent and rescue dermal myofibroblast formation. The effect of versican on TGF-β1 induced dermal myofibroblasts was also assessed.

7.2 *TGF-β1 treatment induced myofibroblast transdifferentiation in normal dermal fibroblasts.*

The data outlined in chapter 4 showed that TGF-β1 was able to induce the myofibroblast phenotype in normal oral fibroblasts, however TGF-β1 treatment induced a variable level of response from different primary oral fibroblasts. TGF-β1 is known to cause myofibroblast transdifferentiation in many fibroblasts of different origins including dermal (Hinz., 2010). In our study, dermal fibroblasts were used to compare miR-145 effects in oral fibroblast to a well characterised fibroblast. First, the effect of TGF-β1 treatment on dermal fibroblasts was investigated. Three different human dermal fibroblasts (HDFs) were used in this investigation: promocell HDF, HDF283, and HDF286. Each were grown and treated 5 ng/ml TGF-β1 for 48 h. After treatment the fibroblasts were harvested and RNA isolated. qRT-PCR was used to analyse the αSMA, versican V0 and V1 and miR-145 expression.

In all dermal fibroblasts tested, the TGF-β1 treatment stimulated an increase in the main myofibroblast marker αSMA (figure 7.1). Each HDF had a similar level of increase in expression, around ~15-20 fold compared to the respective untreated HDF. TGF-β1 had a more variable effect on mature miR-145 expression in different dermal fibroblasts. TGF-β1 treatment was able to cause an increase (~3.5 fold) in miR-145 in promocell HDFs (figure 7.2), although there was a small increase in miR-145 expression in HDF286 or HDF283, this was not significant.

Unlike in oral fibroblasts (figure 5.3), TGF-β1 consistently caused an increase in versican V0 and V1 expression for each HDF analysed (figure 7.3). In HDF283s, there was only a small increase (~3.5 fold) in versican V0 isoform expression in response to TGF-β1, whereas HDF283s had the biggest increase (~10 fold) in V1 versican expression in response to TGF-β1, but this result is likely due an outlier in the data set. Both HDF286 and promocell HDFs had a similar increase in V1 versican isoform levels (~3.5 fold) however V0 levels were increased by ~22 fold in promocell

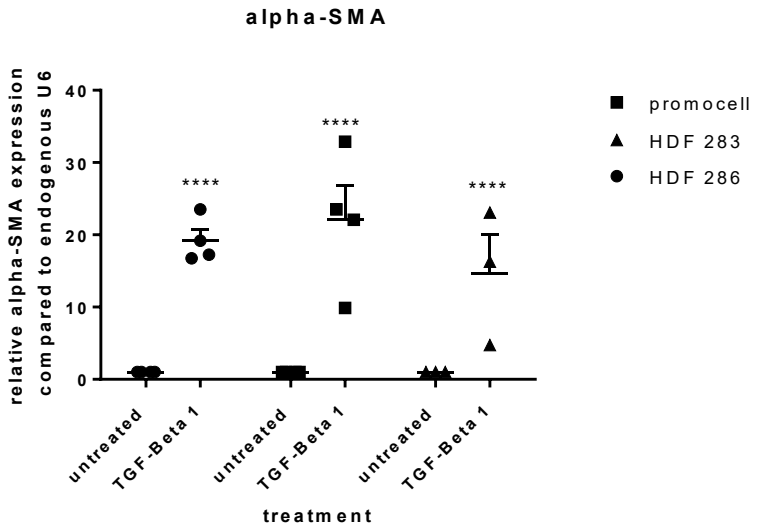

Figure 7.1: TGF-β1 effect on αSMA transcript levels was similar in different human dermal fibroblasts. Different HDFs, promocell HDF, HDF283, and HDF286 were treated 5 ng/ml TGF-β1 for 48 h. After treatment the fibroblasts were harvested and RNA isolated and used to generate total cDNA for qRT-PCR analysis using primers for αSMA and U6, as an endogenous control. Each dot on the dot plot represents a single repeat of the experiment showing the relative quantification of αSMA transcript levels compared to U6, for each TGF-β1 treatment relative to untreated control. The mean quantification was shown by the horizontal bar. Statistical analysis was performed by a paired two tailed student's t-test, and statistical significance is shown on the figure by ****$p<0.0001$. Error bars represent the SEM. N=3, independent experiments.

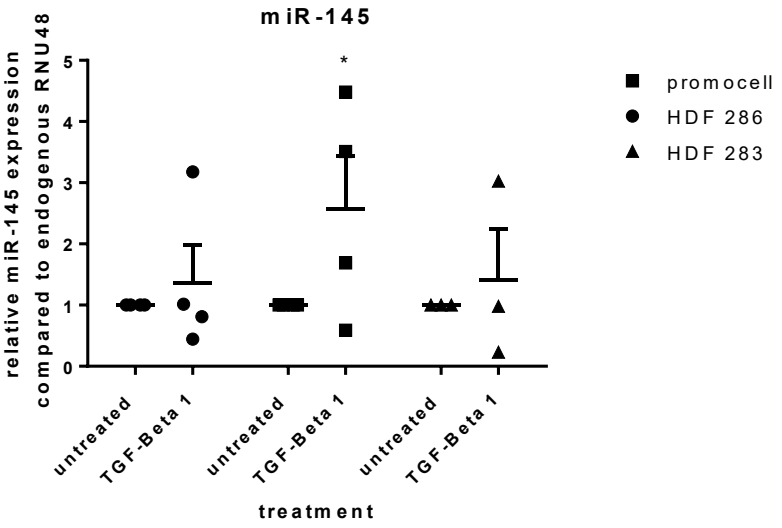

Figure 7.2: TGF-β1 caused an increase in miR-145 levels in HDF286 dermal fibroblasts. Different HDFs, promocell HDF, HDF283, and HDF286 were treated 5 ng/ml TGF-β1 for 48 h. After treatment the fibroblasts were harvested and RNA isolated and used to generate specific miR-145 and RNU48 cDNA and used for qRT-PCR analysis using primers for miR-145 and RNU 48, as an endogenous control. Each dot on the dot plot represents a single repeat of the experiment showing the relative quantification of miR-145 transcript levels compared to RNU 48, for each TGF-β1 treatment relative to untreated control. The mean quantification was shown by the horizontal bar. Statistical analysis was performed by a paired two tailed student's t-test, and statistical significance is shown on the figure by *$p<0.05$. Error bars represent the SEM. N=3, independent experiments.

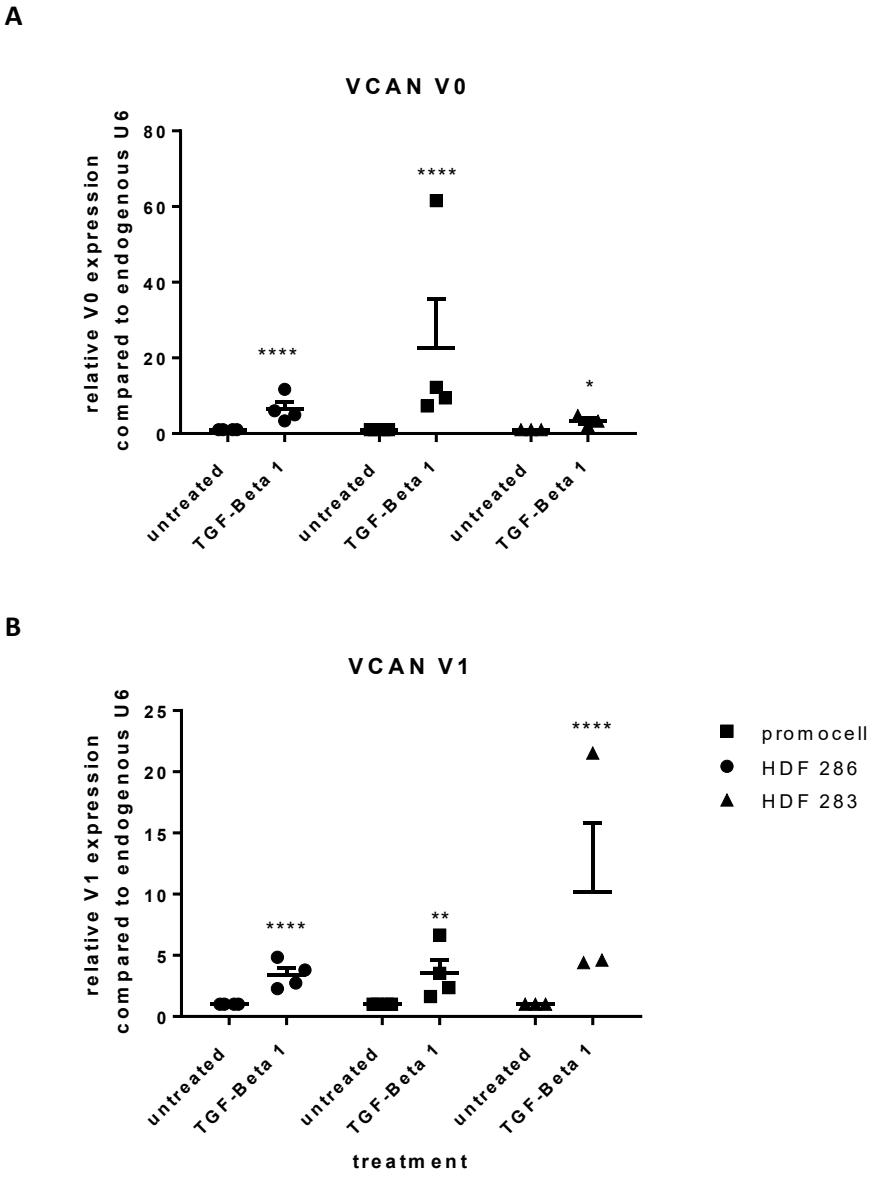

Figure 7.3: TGF-β1 increased the expression of versican V0 and V1 in human dermal fibroblasts. Different HDFs, promocell HDF, HDF283, and HDF286 were treated 5 ng/ml TGF-β1 for 48 h. After treatment the fibroblasts were harvested and RNA isolated and used to generate total cDNA for qRT-PCR analysis using primers for versican V0 and V1 and U6, as an endogenous control. Each dot on the dot plot represents a single repeat of the experiment showing the relative quantification of versican V0 (**A**) and V1 (**B**) transcript levels compared to U6, for each TGF-β1 treatment relative to untreated control. The mean quantification was shown by the horizontal bar. Statistical analysis was performed by a paired two tailed student's t-test, and statistical significance is shown on the figure by *p<0.05, **p<0.001, ***p<0.0001 and ****p<0.0001. Error bars represent the SEM. N=3, independent experiments.

HDFs compared to ~6.5 fold in HDF286s, showing some variability in response to TGF-β1 treatment.

7.3 *miR-145 inhibited myofibroblast transdifferentiation in normal dermal fibroblasts*

The data presented in chapter 4 showed that miR-145 was able to inhibit the TGF-β1 induced myofibroblast transdifferentiation of NOFs. This anti-fibrotic role of miR-145 has been the opposite of that suggested by published data from studies in pulmonary and cardiac fibrosis (Yang *et al*., 2013, Wang *et al*., 2014). However, a recently published study showed an anti-fibrotic effect of miR-145 in vascular smooth muscle cells (Zhao *et al*., 2014). To further investigate miR-145's effect on myofibroblasts of a different cellular origin, human dermal fibroblasts were used. miR-145 is reported to be downregulated in scleroderma (Zhu *et al*., 2013), an autoimmune skin fibrotic disorder, therefore it can be hypothesised that miR-145 my play an anti-fibrotic role in human dermal fibroblasts (HDFs) also.

To investigate if miR-145 plays a role in TGF-β1 induced dermal myofibroblasts, the experiments performed in the NOFs were repeated in the HDFs. Normal HDFs (HDF286 and Promocell HDF) were cultured, seeded, and transfected with negative premiR, premiR-145 (50nM) or a nuclease free water control, mock, for 24 h. Subsequently the fibroblasts were treated with TGF-β1 for 48 h. Fibroblasts were then harvested, and total RNA and protein were isolated to molecularly assess myofibroblast markers. qRT-PCR was used to assess the transcript levels of αSMA, COL1A1 and FN1-EDA. The expression of αSMA was also evaluated via immunoblotting and immunocytochemistry. The results outlined below are from HDF286s but are representative of other HDFs tested.

Firstly, αSMA, the main marker of myofibroblast phenotype was assessed. TGF-β1 induced a ~20 fold increase in αSMA transcript levels in mock transfected HDF, and ~13 fold increase in negative premiR transfected HDF (figure 7.4A). However, transfected with premiR-145 prior to the treatment of TGF-β1 had no significant increase in αSMA, ~2 fold compared to mock, untreated control. Immunoblotting revealed that HDF overexpressing miR-145 also inhibited the TGF-β1 associated increase in αSMA protein levels (figure 7.4 B and C). Therefore, like in oral fibroblasts, miR-145 was able to inhibit the TGF-β1 induced increase in αSMA expression in dermal fibroblasts.

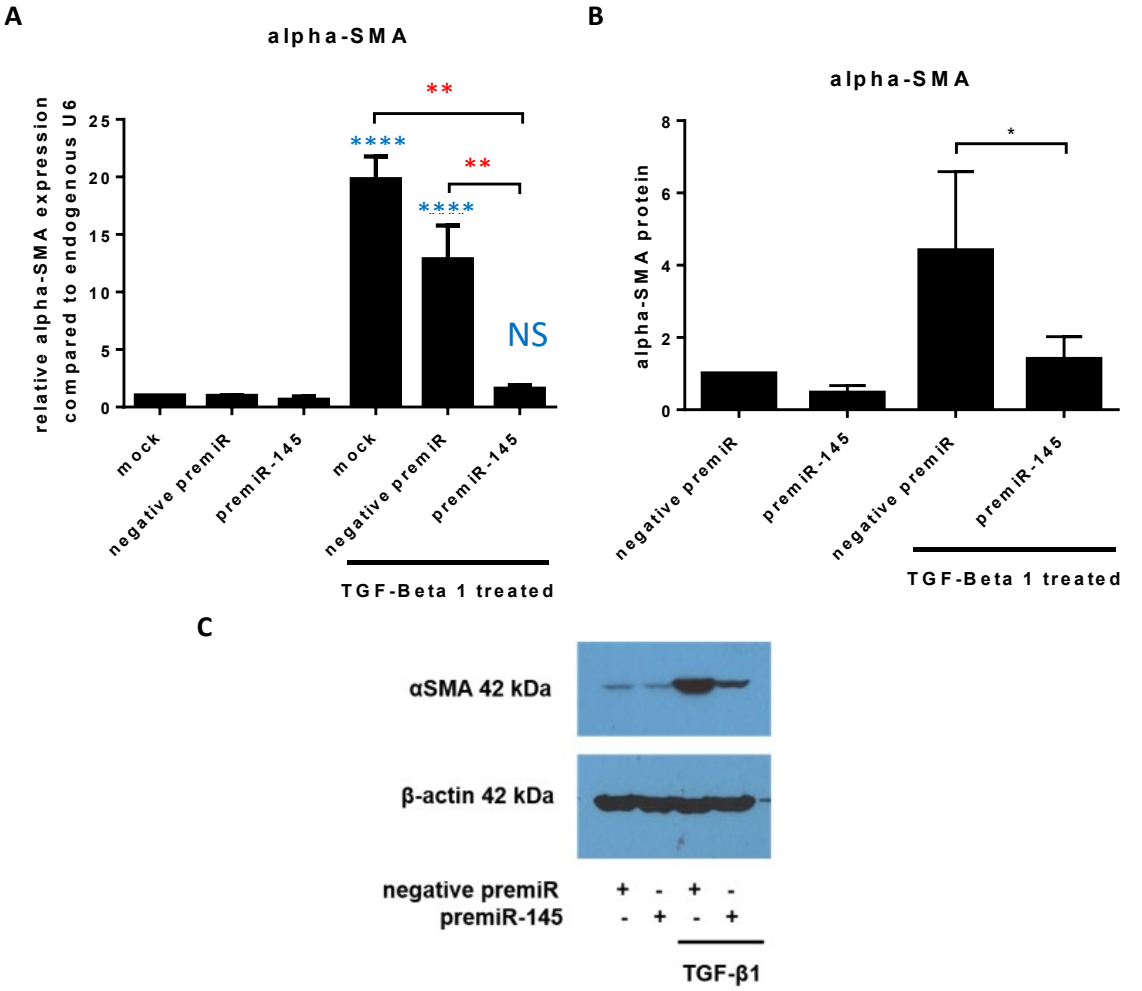

Figure 7.4: miR-145 overexpression attenuated TGF-β1 induced α smooth muscle actin expression in human dermal fibroblasts. Two primary HDF, HDF286 (**A**) and Promocell (**B** and **C**), were transiently transfected with mock (nuclease free water), a negative non-targeting premiR or premiR-145 (50 nM) 24 h prior to treatment with 5 ng/ml TGF-β1 for 48 h. After treatment, fibroblasts were harvested and the RNA was isolated and used to generate cDNA for qRT-PCR analysis using primers designed to amplify αSMA and U6, as an endogenous control. Each bar on the figure represents the mean relative quantification of αSMA transcript levels compared to endogenous U6, for each transfection plus/minus treatment relative to untreated negative premiR (**A**). **B** and **C** Total protein lysate (20 µg) was run on a 3–8% (w/v) tris acetate gradient gel and transferred to a nitrocellulose membrane and immunoblotted for αSMA and GAPDH as the loading control. Protein changes were quantified by densitometry using Image J and are shown in figure **B**, relative to GAPDH. Figure **C** shows a representative blot. Statistical analysis was performed by a paired two tailed student's t-test, and statistical significance is shown on the figure by *p<0.05, **p<0.01, ***p<0.001, ****p<0.0001. If not indicated by a bar, the black significance asterix are compared to the untreated, negative premiR transfected, negative control. Blue significance asterix indicate significance compared to the untreated counterpart, e.g. premiR-145 transfected, TGF-β1 treated compared with premiR-145 transfected untreated. Bars also indicate statistical comparisons. Important significant data is shown in red. Error bars represent the SEM. N=3, independent experiments.

MiR-145's effect on αSMA stress fibre formation was assessed via immunocytochemistry. HDF were seeded on coverslips, then transfected and treated as above. After treatment the coverslips were washed, fixed, permeablised and incubated with a FITC-conjugated αSMA antibody. TGF-β1 caused an increase in bright αSMA stress fibres, which are typical of myofibroblasts, in mock and negative premiR transfected HDFs (figure 7.5A). This increase in fluorescence was calculated to be ~3 fold (not significant) and ~4 fold (significant) (figure 7.5B) in mock and negative premiR transfected treated HDFs respectively. Overexpression of miR-145 slightly decreased the increase in total fluorescence (figure 7.5B), which increased by ~2 fold but visually completely inhibited this TGF-β1 increase in αSMA stress fibre formation (figure 7.5A).

The changes in myofibroblast markers COL1A1 and FN1-EDA were also assessed by qRT-PCR. TGF-β1 was able to increase the expression of both COL1A and FN1-EDA in mock (~2.5 fold and ~4 fold) and negative premiR transfected (~4.5 and ~6.5 fold) HDFs (figure 7.6), although the increase in COL1A for mock (~2.5 fold), treated HDFs was not significant (figure 7.6A). The overexpression of miR-145 caused an inhibition of the TGF-β1 associated increase in both these markers (~0.4 fold for COL1A and ~0.8 fold for FN1-EDA) and also caused a significant decrease in untreated HDFs (~0.1 and ~0.5 fold for COL1A and FN1-EDA respectively). Interestingly, the transfection of negative premiR induced an increase in both the markers of myofibroblasts.

Lastly, the ability of premiR-145 transfection to overexpress mature miR-145 levels was validated by qRT-PCR. Specific miR-145 and RNU 48 cDNA was generated using specially designed miR-145 and RNU 48 stem loop primers. This cDNA was used in qRT-PCR reactions using miR-145 and RNU 48 Taqman probes. Mature levels of miR-145 were increased by an average of ~30 and ~60 fold in untreated and treated HDFs respectively (figure 7.7). Negative premiR transfected cells had a significantly lower levels (~0.3 fold) of miR-145 than mock controls, in untreated cells. TGF-β1 caused a significant increase in miR-145 levels (~2.5 fold, compared to negative premiR, untreated control) in negative premiR transfected HDFs, which is consistent with the data in Figure 7.2, however mock transfected cells did not have a significantly altered expression of miR-145 when treated with TGF-β1.

7.4 *The effect of versican in the dermal myofibroblasts transdifferentiation.*

miR-145 regulated versican expression in oral fibroblasts (Chapter 6). As versican has been implicated in being important in the dermal myofibroblast transdifferentiation (Hattori *et al*., 2011), an investigation was carried out as to whether miR-145 regulates the myofibroblast

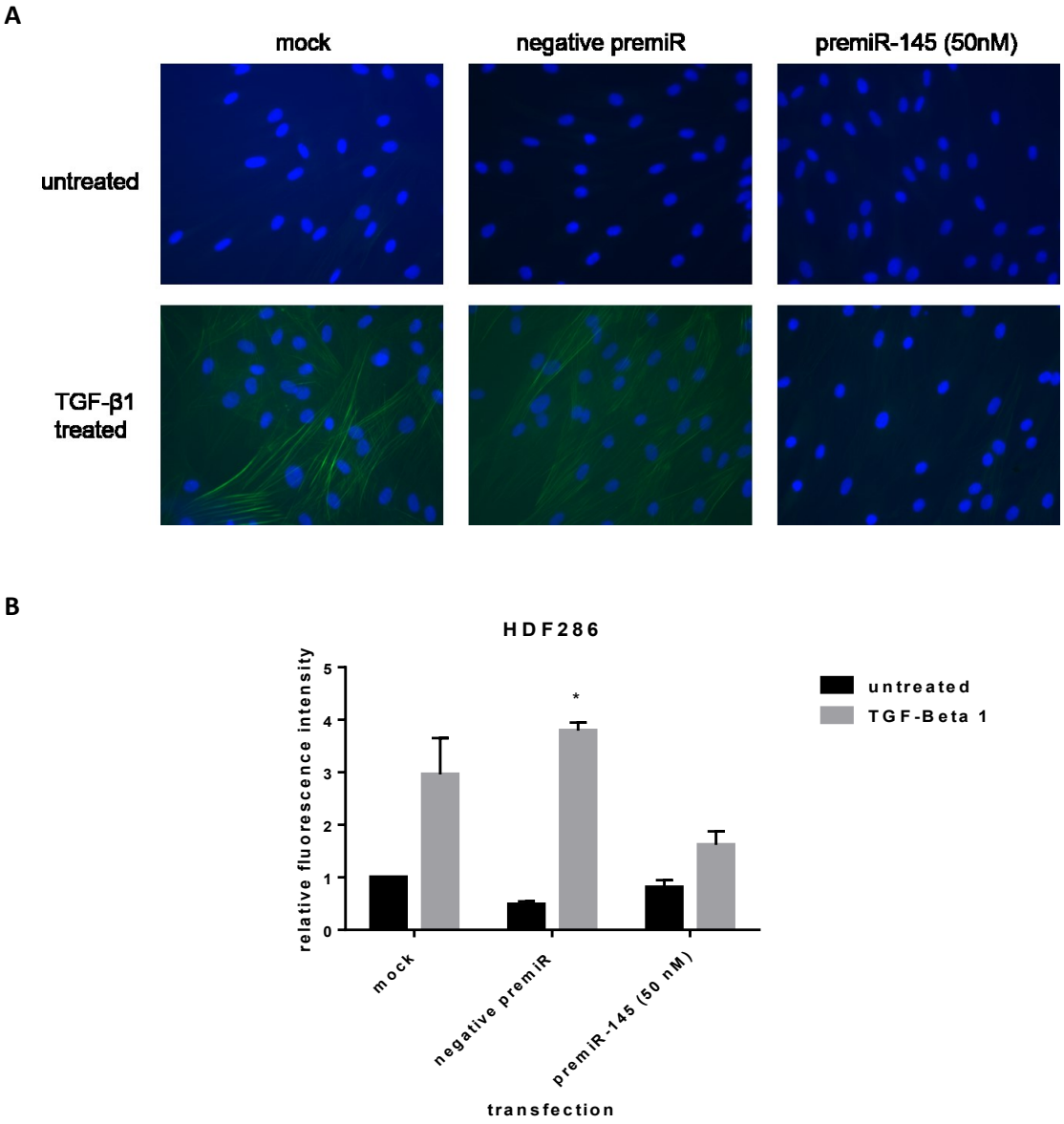

Figure 7.5: miR-145 overexpression prevented αSMA stress fibre formation in human dermal fibroblasts. HDF286 were seeded onto coverslips overnight, transiently transfected with mock (nuclease free water) negative premiR, or premiR-145 (50nM) 24 h prior to being treated with 5 ng/ml TGF-β1 for 48 h. The coverslips were washed in PBS, before being fixed in 100% methanol for 10 min, they were then permeablised using 4 mM sodium deoxycholate for 10 min, and blocked using 2.5% (w/v) BSA in PBS for 30 min before incubation with a primary FITC-conjugated αSMA antibody at 4°C overnight. The coverslips were then washed in PBS before mounting on microscope slides using DAPI containing mounting medium. Fluorescent images were taken using a microscope, using Pro-plus 7 imaging software at 40x magnification. Representative pictures are shown in **A.** The amount of fluorescence intensity per cell was quantified using Image J, and displayed in **B** as the mean relative fluorescent intensity for HDF286. Statistical analysis was performed by a paired two tailed student's t-test, and statistical significance is shown on the figure by *p<0.05, negative premiR treated compared to treated. Error bars show the SEM. N=3, independent experiments.

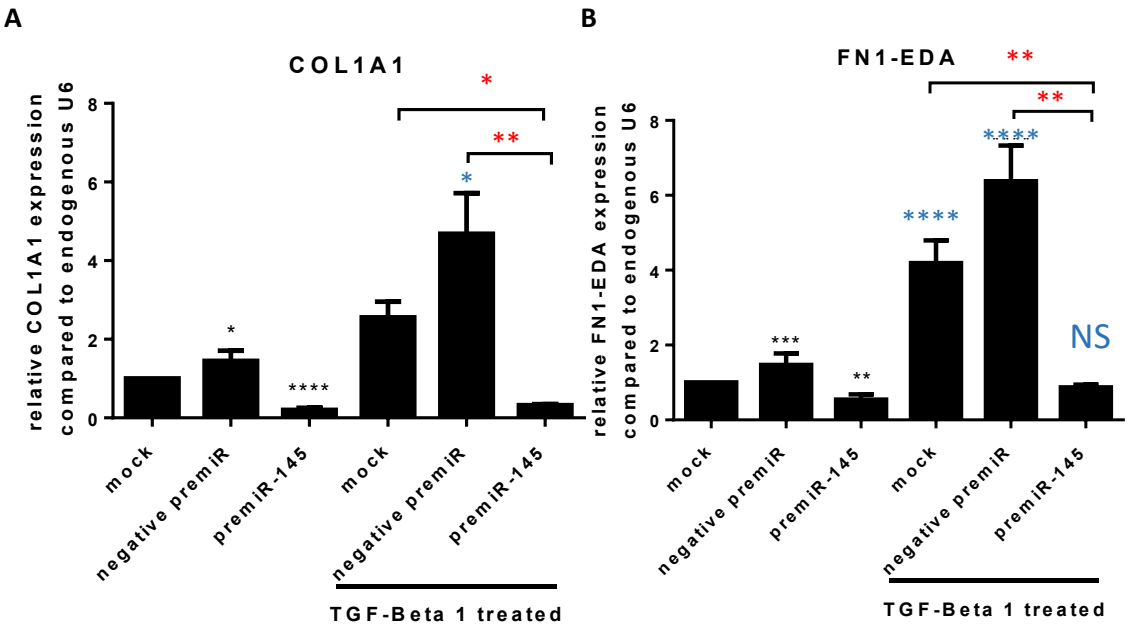

Figure 7.6: miR-145 overexpression attenuated TGF-β1 induced collagen 1a and fibronectin 1 (with extra domain A) expression in normal dermal fibroblasts. Two primary HDFs, HDF286 (data shown here) and Promocell HDF (data not shown), were transiently transfected with mock (nuclease free water), a negative non-targeting premiR or premiR-145 (50 nM) 24 h prior to treatment with TGF-β1 for 48 h. After treatment, fibroblasts were harvested and the RNA was isolated and used to generate cDNA for qRT-PCR analysis using primers designed to amplify COL1A1, FN1-EDA and U6, as an endogenous control. Each bar on the figure represents the mean relative quantification of COL1A1 (**A**) and FN1-EDA (**B**) transcript levels compared to endogenous U6, for each transfection plus/minus treatment relative to untreated negative premiR. Statistical analysis was performed by a paired two tailed student's t-test, and statistical significance is shown on the figure by *p<0.05, **p<0.01, ***p<0.001, ****p<0.0001. If not indicated by a bar, the black significance asterix are compared to the untreated, negative premiR transfected, negative control. Blue significance asterix indicate significance compared to the untreated counterpart, e.g. premiR-145 transfected, TGF-β1 treated compared with premiR-145 transfected untreated. Bars also indicate statistical comparisons. Important significant data is shown in red. Error bars represent the SEM. N=3, independent experiments.

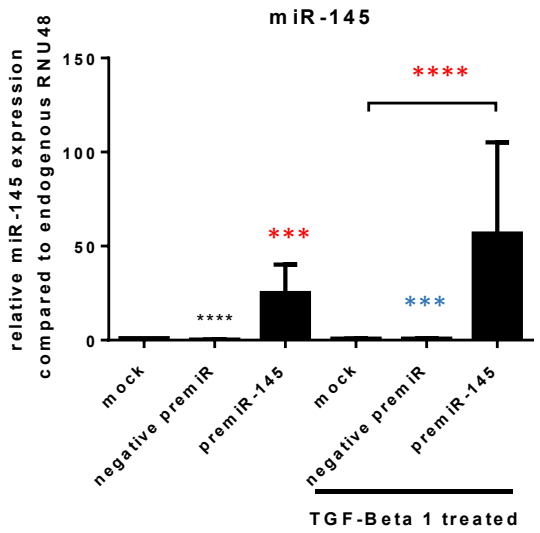

Figure 7.7: PremiR-145 transfection resulted in the overexpression of mature miR-145 in human dermal fibroblasts. Two primary HDFs, HDF286 (shown here) and Promocell HDFs, were transiently transfected with mock (nuclease water), a negative non-targeting premiR or premiR-145 (50 nM) for 24 h prior to treatment with 5 ng/ml TGF-β1 for 48 h. After treatment, fibroblasts were harvested and the RNA was isolated and used to generate specific miR-145 and RNU 48 cDNA for qRT-PCR analysis using primers for miR-145 and RNU 48, as an endogenous control. Each bar on the figure represents the mean relative quantification of miR-145 transcript levels compared to endogenous RNU 48, for each transfection plus/minus treatment relative to untreated negative premiR. Statistical analysis was performed by a paired two tailed student's t-test, and statistical significance is shown on the figure by ***p<0.001, and ****p<0.0001. If not indicated by a bar, the black significance asterix are compared to the untreated, negative premiR transfected, negative control. Blue significance asterix indicate significance compared to the untreated counterpart, e.g. premiR-145 transfected, TGF-β1 treated compared with premiR-145 transfected untreated. Bars also indicate statistical comparisons. Important significant data is shown in red. Error bars represent the SEM. N=3, independent experiments.

phenotype by the regulation of versican in HDF. miR-145's effect on versican expression was assessed by qRT-PCR using the total cDNA preps from fibroblasts transfected with negative premiR, premiR-145 or a mock control, before TGF-β treatment to induce dermal myofibroblasts. Two isoforms of versican V0 and V1 transcript levels were assessed. TGF-β1 induced dermal myofibroblast had an elevated expression of both V0 (~5 fold) and V1 (~3 fold) in both negative premiR and mock transfected HDFs (figure 7.8). MiR-145 overexpressing HDFs expressed significantly lower levels of V0 (~0.1 fold, figure 7.8A) and V1 (~0.6 fold, figure 7.8B) versican transcript in untreated HDFs. TGF-β1 treatment in HDFs overexpressing miR-145 was only able to prevent the increase of V0 versican isoform expression (figure 7.8A) and not V1 (figure 7.8B), which were not significantly different from the treated controls. Compared to mock transfected, negative premiR transfected HDFs had a significantly lower expression of both isoforms (~0.5 fold). Again, demonstrating that the negative non-targeting premiR apparently has some effect on these HDFs.

Versican expression was also measured by immunoblotting. Total protein lysates were isolated from HDFs transfected with premiR-145 or negative premiR control and then treated. Protein (20 μg) was resolved on a tris acetate 3–8% (w/v) gradient gel and transferred to a nitrocellulose membrane for immunoblotting using a full length versican antibody. TGF-β1 treatment in negative premiR transfected HDFs had a large increase in versican protein levels, quantified to increase by ~2 fold (figure 7.9). The overexpression of miR-145 before TGF-β1 treatment prevented this increase in versican protein.

To investigate whether miR-145 ability to inhibit dermal myofibroblast transdifferentiation was due to the regulation of V0 versican isoform, a versican targeting siRNA was used to perform a loss of function experiment in HDF. HDFs were seeded and transfected with either versican or a non-targeting negative siRNA, prior to TGF-β1 treatment to induce the dermal myofibroblast phenotype. Myofibroblast marker αSMA expression was assessed by qRT-PCR, immunoblotting and immunohistochemistry. The expression of versican isoforms and other myofibroblasts markers COL1A1 and FN1-EDA were assessed via qRT-PCR.

To assess the efficacy of the versican knock-down, V0 and V1 isoform transcript levels were assessed by qRT-PCR. The versican siRNA was able to decrease versican V0 transcript levels to ~0.35 fold (figure 7.10A) and versican V1 transcript levels to ~0.3 fold (figure 7.10B). As seen in figure 7.4, TGF-β1 treatment was able to increase versican V0 and V1 expression. Here, TGF-β1 increased versican V0 expression by ~10 fold, and V1 isoform by ~3.5 fold, this is reduced to ~2 fold and ~1 fold respectively in HDFs where versican is knocked down. Therefore, the knock-

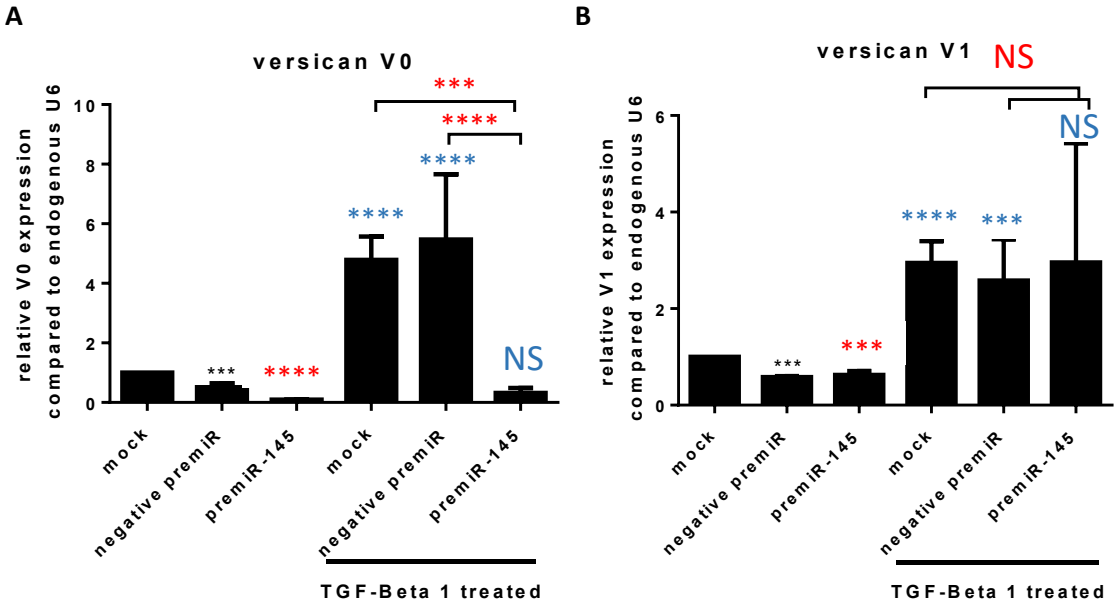

Figure 7.8: miR-145 downregulated V0 and V1 expression in human dermal fibroblasts, and attenuated the TGF-β1 associated increase in V0, but not in V1 versican transcript levels. Two primary HDFs, HDF286 (data shown here) and Promocell HDF (data not shown), were transiently transfected with mock (nuclease free water), a negative non-targeting premiR or premiR-145 (50 nM) 24 h prior to treatment with TGF-β1 for 48 h. After treatment, fibroblasts were harvested and the RNA was isolated and used to generate cDNA for qRT-PCR analysis using primers designed to amplify V0 and V1 versican isoforms and U6, as an endogenous control. Each bar on the figure represents the mean relative quantification of versican V0 (**A**) and versican V1 (**B**) transcript levels compared to endogenous U6, for each transfection plus/minus treatment relative to untreated negative premiR. Statistical analysis was performed by a paired two tailed student's t-test, and statistical significance is shown on the figure by *p<0.05, **p<0.01, ***p<0.001, ****p<0.0001. If not indicated by a bar, the black significance asterix are compared to the untreated, negative premiR transfected, negative control. Blue significance asterix indicate significance compared to the untreated counterpart, e.g. premiR-145 transfected, TGF-β1 treated compared with premiR-145 transfected untreated. Bars also indicate statistical comparisons. Important significant data is shown in red. Error bars represent the SEM. N=3, independent experiments.

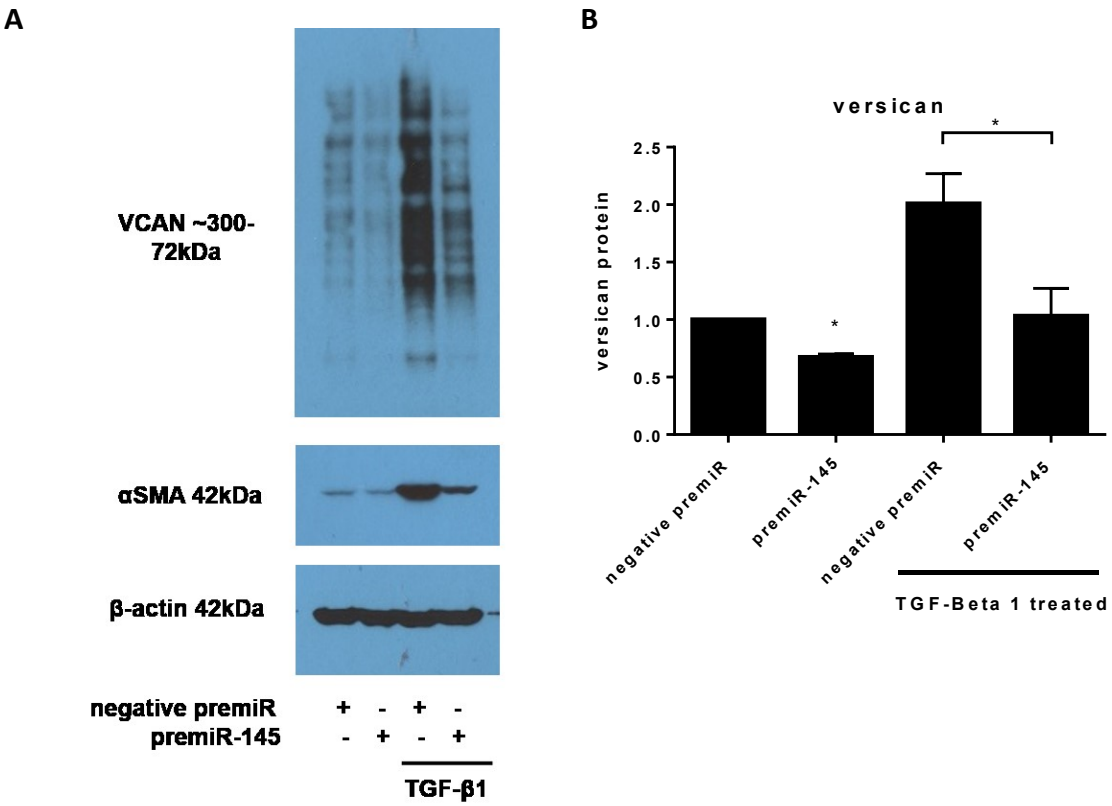

Figure 7.9: miR-145 overexpression attenuated TGF-β1 induced versican protein expression in human dermal fibroblasts. Two primary HDF, HDF286 (data not shown) and Promocell (shown here), were transiently transfected with a negative non-targeting premiR or premiR-145 (50 nM) 24 h prior to treatment with 5 ng/ml TGF-β1 for 48 h. After treatment, fibroblasts were harvested and total protein lysates were prepared. Protein lysate (20 µg) was run on a 3–8% (w/v) tris acetate gradient gel and transferred to a nitrocellulose membrane and immunoblotted for versican, αSMA and β-actin as the loading control. Protein changes were quantified by densitometry using Image J and are shown in figure **B**, relative to GAPDH. Figure **A** shows a representative blot. Statistical analysis was performed by a paired two tailed student's t-test, and statistical significance is shown on the figure by *$p<0.05$. N=3, independent experiments for each NOF.

down adequately prevented the TGF-β1 increase in both isoforms, and was able to knock-down endogenous versican levels.

Hattori *et al*., (2011) showed that the knock-down of versican in HDFs resulted in the inhibition of the myofibroblast transdifferentiation. To investigate whether the transient knock-down of versican could affect the myofibroblast phenotype, and therefore could be a mechanism by which miR-145 regulates the myofibroblast transdifferentiation, αSMA expression was assessed in HDFs transfected with versican siRNA, then treated with TGF-β1. αSMA transcript levels were elevated by ~15 fold in HDFs transfected with negative siRNA were treated with TGF-β1 (figure 7.11). This increase in αSMA was further elevated (~21 fold) in HDFs were versican levels were knocked-down, but this was not statistically significantly.

The effect of versican knock-down on the αSMA stress fibre formation was assessed using immunocytochemistry. HDFs were seeded onto coverslips, they were then transient transfected with versican siRNA or negative siRNA, prior to treatment with TGF-β1 for 48 h. The coverslips were washed, fixed, permeablised and after blocking, were then incubated with a FITC-conjugated αSMA antibody. TGF-β1 induced αSMA stress fibre formation typical of myofibroblasts in HDFs transfected with negative siRNA, when versican was knocked down in HDFs, it had no effect on TGF-β1's ability to induce αSMA stress fibres (figure 7.12).

The effect of versican's knock-down on the effect of TGF-β1 to induce other markers of myofibroblast phenotype, COL1A1 and FN1-EDA. HDFs with knocked down versican levels had a slightly reduced elevation of COL1A1 expression with TGF-β1 treatment (~2 fold, compared to ~3 fold in negative premiR transfected, then treated) (figure 7.13A). The TGF-β1 induced FN1-EDA expression was reduced to ~5 fold from ~7 fold compared to negative siRNA HDF (figure 7.13B). However, these effects were not significant, therefore versican knock-down was not able to effect the acquisition of the dermal myofibroblast transdifferentiation.

7.5 *miR-145 was able to partially rescue the dermal myofibroblast transdifferentiation.*

The data presented in this chapter has outlined miR-145 to have an anti-fibrotic role in dermal fibroblasts, in addition to oral fibroblasts (Chapter 4). Overexpression of miR-145 was able to prevent TGF-β1 dermal myofibroblast transdifferentiation. Again, to see whether this is therapeutically relevant, miR-145 was introduced into induced dermal myofibroblasts to assess whether it is able to reverse the myofibroblast phenotype. HDFs were treated with TGF-β1 for

A B

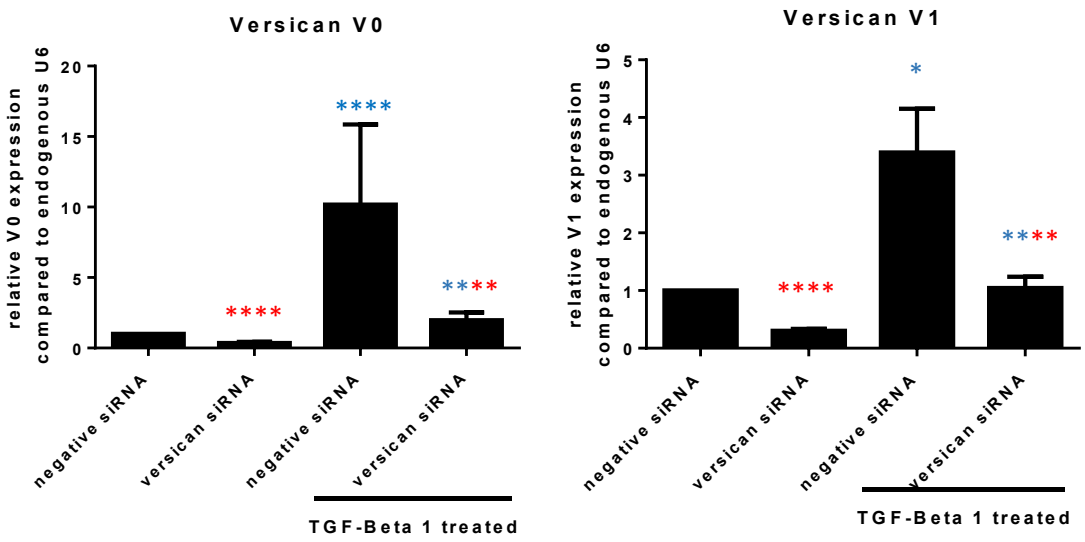

Figure 7.10: Versican siRNA reduced V0 and V1 isoform transcript levels. Two primary HDFs, HDF286 (data shown here) and HDF283 (data not shown), were transiently transfected with mock (nuclease free water), a negative non-targeting siRNA or versican siRNA (50 nM) 24 h prior to treatment with TGF-β1 for 48 h. After treatment, fibroblasts were harvested and the RNA was isolated and used to generate cDNA for qRT-PCR analysis using primers designed to amplify V0 and V1 versican isoforms and U6, as an endogenous control. Each bar on the figure represents the mean relative quantification of versican V0 (**A**) and versican V1 (**B**) transcript levels compared to endogenous U6, for each transfection plus/minus treatment relative to untreated negative premiR. Statistical analysis was performed by a paired two tailed student's t-test, and statistical significance is shown on the figure by *p<0.05, ***p<0.001, ****p<0.0001. If not indicated by a bar, the black significance asterix are compared to the untreated, negative premiR transfected, negative control. Blue significance asterix indicate significance compared to the untreated counterpart, e.g. premiR-145 transfected, TGF-β1 treated compared with premiR-145 transfected untreated. Bars also indicate statistical comparisons. Important significant data is shown in red. Error bars represent the SEM. N=3, independent experiments.

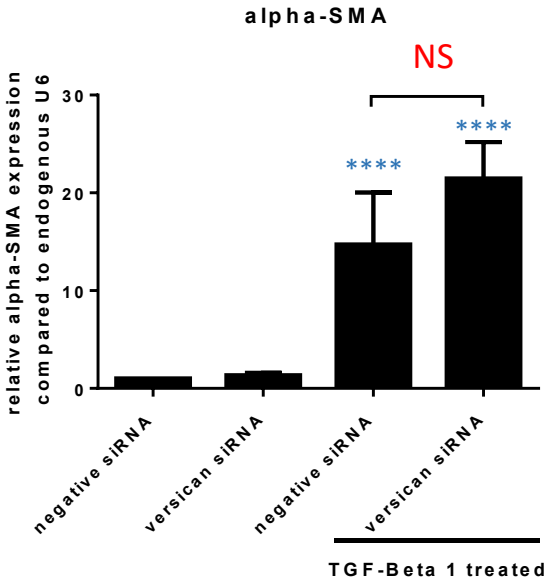

Figure 7.11: Versican siRNA had no effect on TGF-β1 induced αSMA expression. Two primary HDFs, HDF286 (data shown here) and HDF283 (data not shown), were transiently transfected with mock (nuclease free water), a negative non-targeting siRNA or versican siRNA (50 nM) 24 h prior to treatment with TGF-β1 for 48 h. After treatment, fibroblasts were harvested and the RNA was isolated and used to generate cDNA for qRT-PCR analysis using primers designed to amplify αSMA and U6, as an endogenous control. Each bar on the figure represents the mean relative quantification of αSMA (**A**) transcript levels compared to endogenous U6, for each transfection plus/minus treatment relative to untreated negative premiR. Statistical analysis was performed by a paired two tailed student's t-test, and statistical significance is shown on the figure by *p<0.05, ***p<0.001, ****p<0.0001. If not indicated by a bar, the black significance asterix are compared to the untreated, negative premiR transfected, negative control. Blue significance asterix indicate significance compared to the untreated counterpart, e.g. premiR-145 transfected, TGF-β1 treated compared with premiR-145 transfected untreated. Bars also indicate statistical comparisons. Important significant data is shown in red. Error bars represent the SEM. N=3, independent experiments.

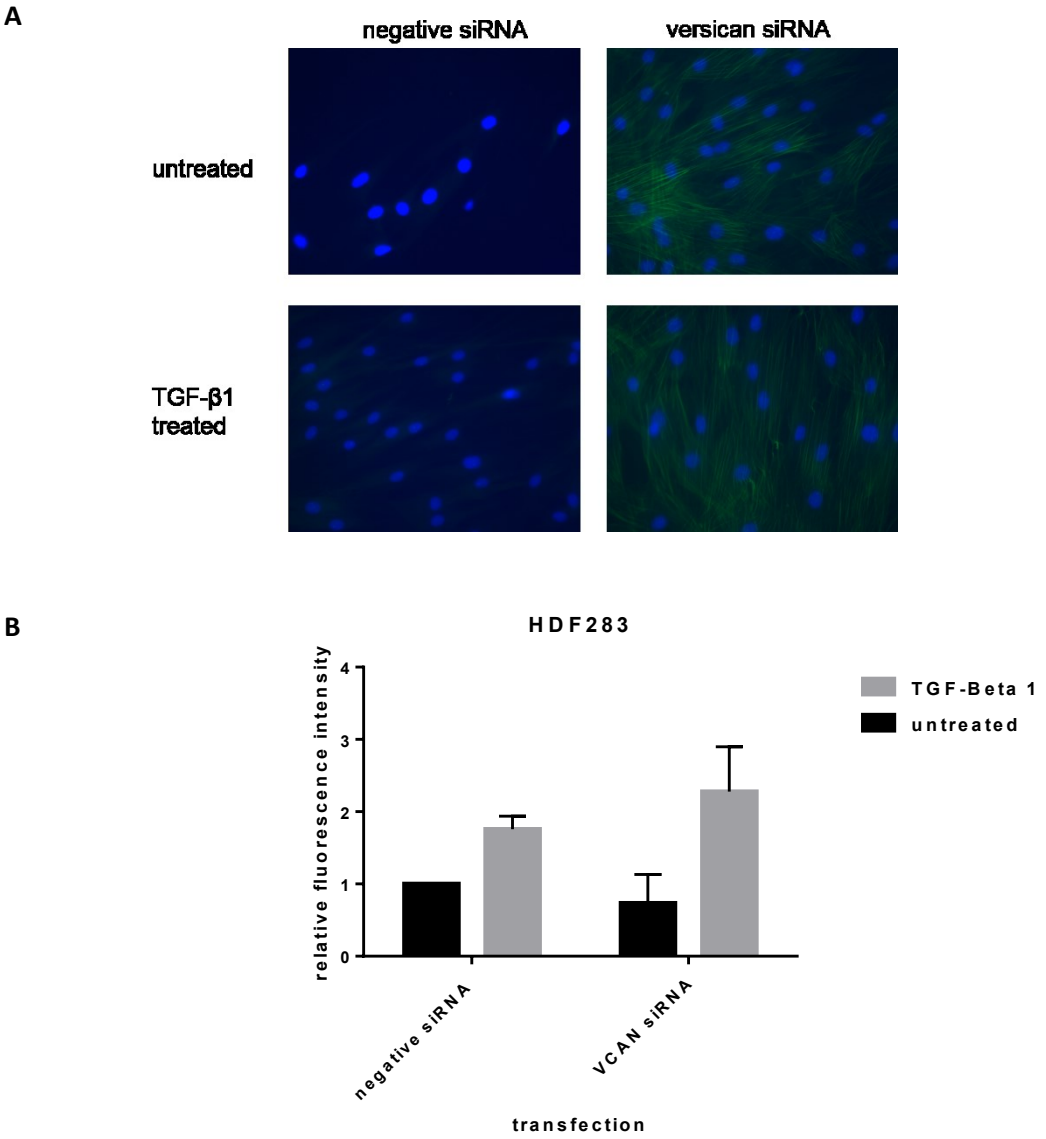

Figure 7.12: Versican knock-down had no effect on TGF-β1 induced αSMA stress fibre formation in human dermal fibroblasts. HDFs were seeded onto coverslips overnight, transiently transfected with negative siRNA, or versican siRNA (50 nM) 24 h prior to being treated with 5 ng/ml TGF-β1 for 48 h. The coverslips were washed in PBS, before being fixed in 100% methanol for 10 min, they were then permeablised using 4 mM sodium deoxycholate for 10 min, and blocked using 2.5% (w/v) BSA in PBS for 30 min before incubation with a primary FITC-conjugated αSMA antibody at 4 °C overnight. The coverslips were then washed in PBS before mounting on microscope slides using DAPI containing mounting medium. Fluorescent images were taken using a microscope, using Pro-plus 7 imaging software at 40x magnification. Representative pictures are shown in **A.** The amount of fluorescence intensity per cell was quantified using Image J, and displayed in **B** as the mean relative fluorescent intensity for HDF283. Statistical analysis was performed by a paired two tailed student's t-test, and statistical significance is shown on the figure by *p<0.05, negative premiR treated compared to treated. N=3, independent experiments. Error bars show the SEM. N=2, independent experiments for each HDF286 and HDF283.

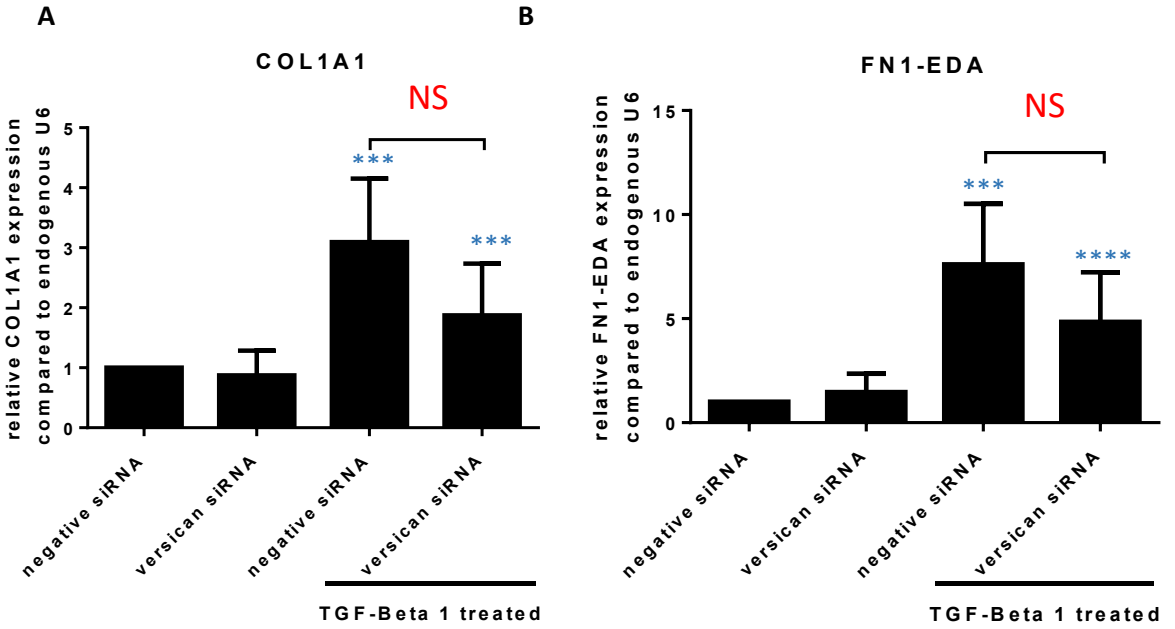

Figure 7.13: Versican siRNA had no effect on the TGF-β1 induced COL1A1 and FN1-EDA expression. Two primary HDFs, HDF286 (data shown here) and HDF283 (data not shown), were transiently transfected with mock (nuclease free water), a negative non-targeting siRNA or versican siRNA (50 nM) 24 h prior to treatment with TGF-β1 for 48 h. After treatment, fibroblasts were harvested and the RNA was isolated and used to generate cDNA for qRT-PCR analysis using primers designed to amplify COL1A1, FN1-EDA and U6, as an endogenous control. Each bar on the figure represents the mean relative quantification of COL1A1 (**A**) and FN1-EDA (**B**) transcript levels compared to endogenous U6, for each transfection plus/minus treatment relative to untreated negative premiR. Statistical analysis was performed by a paired two tailed student's t-test, and statistical significance is shown on the figure by *p<0.05, ***p<0.001, ****p<0.0001. If not indicated by a bar, the black significance asterix are compared to the untreated, negative premiR transfected, negative control. Blue significance asterix indicate significance compared to the untreated counterpart, e.g. premiR-145 transfected, TGF-β1 treated compared with premiR-145 transfected untreated. Bars also indicate statistical comparisons. Important significant data is shown in red. Error bars represent the SEM. N=3, independent experiments.

48 h, before being transiently transfected with negative premiR, or a low (5 nM) or high (50 nM) dose of premiR-145 for 48 h. The fibroblasts were then harvested to analyse their molecular markers of myofibroblast phenotype via qRT-PCR, immunoblotting and immunocytochemistry.

Induced dermal myofibroblasts, transiently transfected with a negative premiR had an elevated αSMA mRNA expression of ~20 fold above untreated HDFs (figure 7.14A). Transfection of TGF-β1 induced dermal myofibroblasts with the high dose of premiR-145 (50 nM) was significantly able to completely reduce αSMA transcript levels, to the same level as the untreated control.

Transfection of the lower dose of premiR-145 (5 nM), slightly reduced αSMA transcript levels to ~15 fold, however this was not significant. In untreated HDFs controls, both of the doses of premiR-145 were able to downregulate αSMA mRNA levels by ~0.2 fold, this was not previously seen in HDFs transfected, then treated (figure 7.4). Similar to oral fibroblasts, premiR-145 (50 nM) transfection was able to slightly reduce the TGF-β1 induced myofibroblast elevated αSMA protein levels (figure 7.14B).

The myofibroblast associated αSMA stress fibres were visualised by immunocytochemistry using a FITC-conjugated αSMA antibody. HDFs were seeded on coverslips before treating them with TGF-β1 to induce dermal myofibroblasts, and transfecting with negative premiR, or premiR-145 (5nM or 50nM). The coverslips were fixed, permeabilised and incubated with the FITC-conjugated αSMA antibody. Induced myofibroblasts transfected with negative premiR or premiR (5 nM) displayed striking αSMA stress fibres, typical of myofibroblasts, and had an increase in fluorescence ~2.5 fold above untreated controls (figure 7.15). Transfection of the higher dose of premiR-145 (50 nM) resulted in a decrease in total fluorescence (not significant), and no visible change in the amount of αSMA stress fibres.

The ability of miR-145 to effect myofibroblasts markers COL1A1 and FN1EDA, post myofibroblast induction was investigated by qRT-PCR. Both genes saw a dose dependent reduction in expression in untreated HDFs, COL1A1 expression was decreased by ~0.4 and ~0.1 fold in premiR 5nM and 50 nM HDFs respectively (figure 7.16A), and FN1-EDA expression was decreased by ~0.3 and ~0.2 in 5 nM and 50 nM premiR-145 transfection respectively (figure 7.16B). COL1A1 levels in induced myofibroblasts increased by ~3 fold compared to untreated HDFs, the higher overexpression (50nM dose) of miR-145 caused a significant reduction in COL1A1 (~1.5 fold) (figure 7.16A). However, the lower dose (5 nM) caused a small reduction in COL1A1 transcript (~2 fold), however this was not a significant change. FN1-EDA levels in TGF-β1 induced myofibroblasts increased by ~4 fold compared to untreated HDFs (figure 7.16B). The doses of

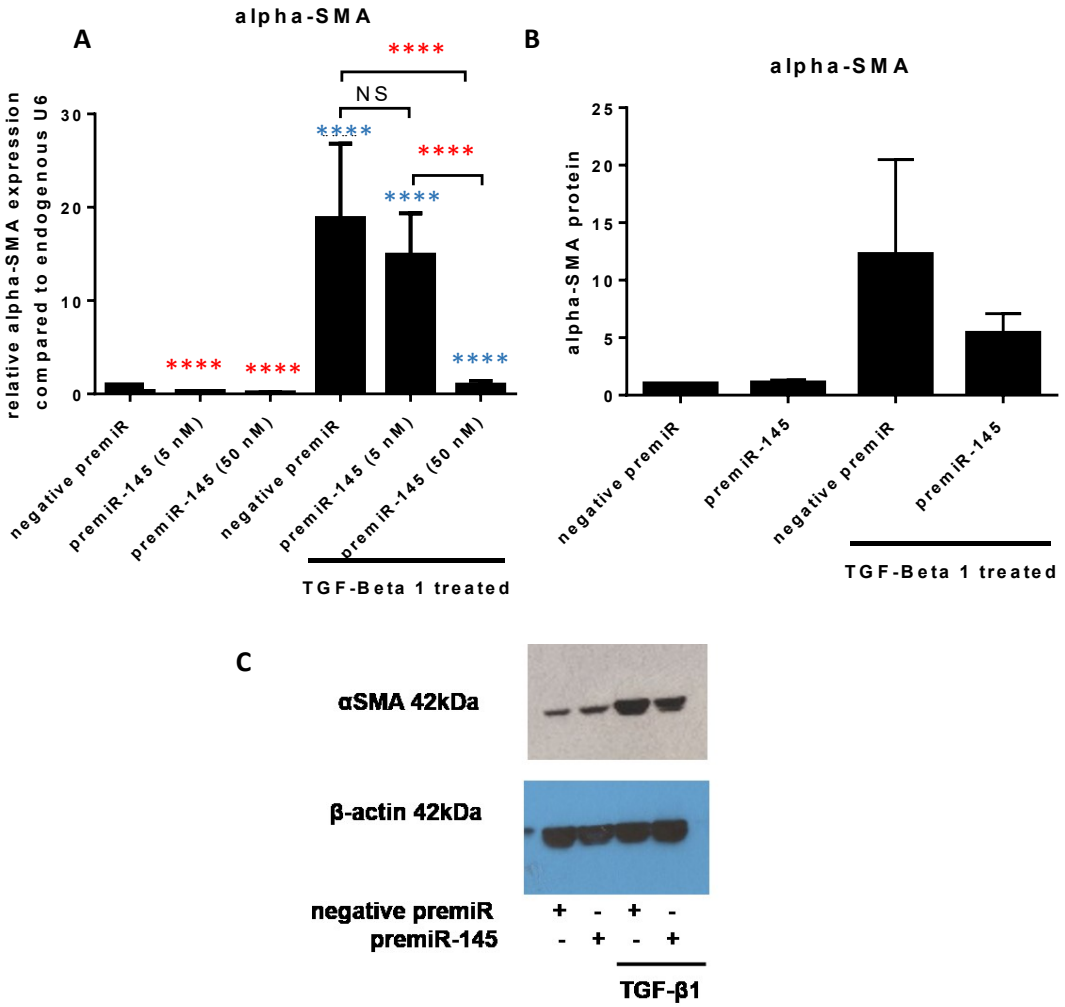

Figure 7.14: Overexpression of miR-145 in dermal induced myofibroblasts reduced αSMA transcript levels, but not protein levels. HDF286 were treated with 5 ng/ml TGF-β1 or serum free media, then transiently transfected with 5 nM premiR-145, 50 nM premiR-145 or a negative non-targeting premiR. The transfection was left for 48 h before being harvested. RNA was isolated and used to generate total cDNA for qRT-PCR analysis using primers for αSMA and U6, as an endogenous control. Total protein lysates were also extracted, and 20 µg was resolved on a 3-8% (w/v) tris acetate gradient gel and transferred to a nitrocellulose membrane and used for immunoblotting using antibodies raised to human αSMA and β-actin as a loading control. Each bar on the figure **A** represents the mean relative quantification of αSMA transcript levels compared to endogenous U6, for each transfection plus/minus treatment relative to untreated negative premiR. Protein changes were quantified by densitometry using Image J and are shown in figure **B**, relative to GAPDH. Figure **C** shows a representative blot. Statistical analysis was performed by a paired two tailed student's t-test, and statistical significance is shown on the figure by *p<0.05, **p<0.01, ***p<0.001, ****p<0.0001. If not indicated by a bar, the black significance asterix are compared to the untreated, negative premiR transfected, negative control. Blue significance asterix indicate significance compared to the untreated counterpart, e.g. premiR-145 transfected, TGF-β1 treated compared with premiR-145 transfected untreated. Bars also indicate statistical comparisons. Important significant data is shown in red. Error bars represent the SEM. N=3, independent experiments for each NOF.

A

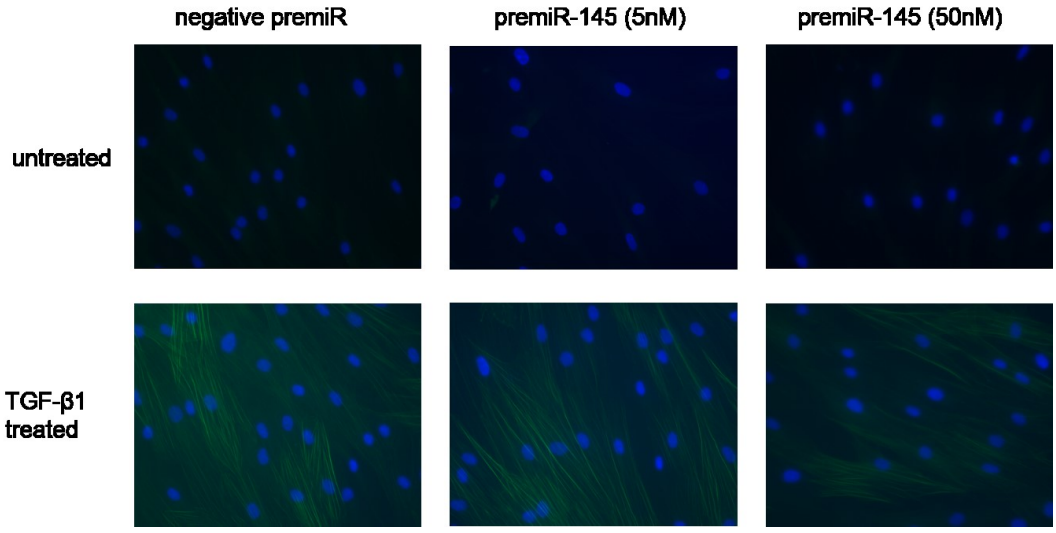

B

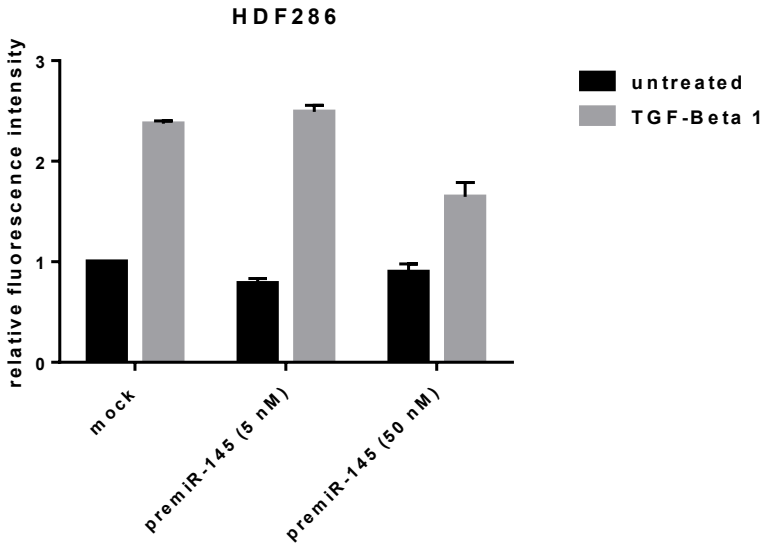

Figure 7.15: miR-145 overexpression reduced αSMA stress fibre formation in dermal fibroblasts. HDF286s were seeded onto coverslips overnight, treated with 5 ng/ml TGF-β1 for 48 h, or serum free media, then were transiently transfected with negative premiR, or premiR-145 (at two doses 5 nM or 50 nM). The coverslips were washed in PBS, before being fixed in 100% methanol for 10 min, they were then permeablised using 4 mM sodium deoxycholate for 10 min, and blocked using 2.5% (w/v) BSA in PBS for 30 min before incubation with a primary FITC-conjugated αSMA antibody at 4 ^{o}C overnight. The coverslips were then washed in PBS before mounting on microscope slides using DAPI containing mounting medium. Fluorescent images were taken using a fluorescent light microscope, using Pro-plus 7 imaging software at 40x magnification. Representative pictures are shown in **A.** The amount of fluorescence intensity per cell was quantified using Image J, and displayed in **B** as the mean relative fluorescent intensity for DENF319. Statistical analysis was performed by a paired two tailed student's t-test, and statistical significance is shown on the figure by *p<0.05, premiR-145 (5nM) treated compared to treated. N=3, independent experiments. Error bars show the SEM.

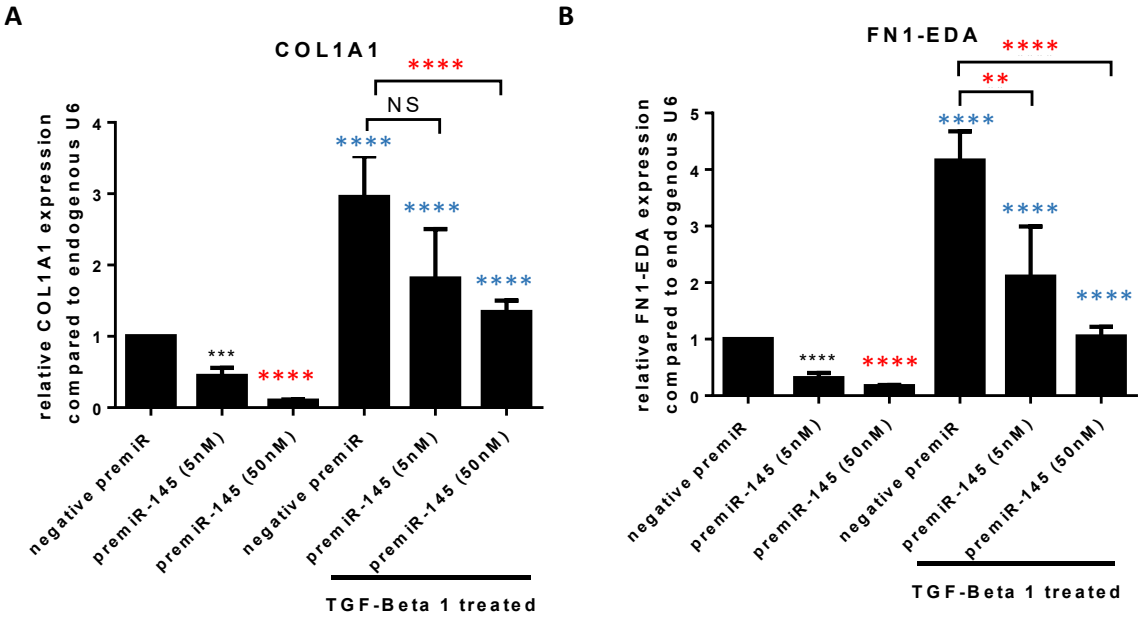

Figure 7.16: Overexpression of microRNA-145 in induced dermal myofibroblasts reduced the transcript levels of myofibroblast markers COL1A1 and FN1-EDA. HDF286s were treated with 5 ng/ml TGF-β1 or serum free media, then transiently transfected with 5 nM premiR-145, 50 nM premiR-145 or a negative non-targeting premiR. The transfection was left for 48 h before being harvested. RNA was isolated and used to generate total cDNA for qRT-PCR analysis using primers for COL1A1, FN1-EDA and U6, as an endogenous control. Each bar on the figure represents the mean relative quantification of COL1A1 (**A**) and FN1-EDA (**B**) transcript levels compared to endogenous U6, for each transfection plus/minus treatment relative to untreated negative premiR. Statistical analysis was performed by a paired two tailed student's t-test, and statistical significance is shown on the figure by **p<0.01, ***p<0.001 and ****p<0.0001. If not indicated by a bar, the black significance asterix are compared to the untreated, negative premiR transfected, negative control. Blue significance asterix indicate significance compared to the untreated counterpart, e.g. premiR-145 transfected, TGF-β1 treated compared with premiR-145 transfected untreated. Bars also indicate statistical comparisons. Important significant data is shown in red. Error bars represent the SEM. N=3, independent experiments.

premiR-145 transfected into these myofibroblasts caused a stepwise reduction in FN1-EDA levels, the low dose (5 nM) decreased expression to ~2 fold, and the high dose completely restored FN1-EDA levels back to untreated levels, around 1 fold.

The expression of proteoglycan versican was assessed by qRT-PCR and immunoblotting in treated then transfected dermal fibroblasts. TGF-β1 induced myofibroblasts had elevated expression of both versican isoforms ~3 fold for V0 and ~2 fold for V1 (figure 7.17), a lower fold change to that seen in the dermal fibroblasts that were transfected prior to the TGF-β1 treatment (figure 7.8). miR-145 overexpression was able to cause a significant dose response decrease in versican expression of both the isoforms in untreated HDFs (for V0:~0.2 and ~0.02 fold, for V1:~0.5 and ~0.2 fold; in 5 nM and 50 nM overexpression respectively) and HDFs induced to be myofibroblasts. Induced myofibroblasts versican V0 expression was decreased to ~2 and ~0.5 fold in treated HDFs transfected transfected with premiR-145 5 nM and 50 nM respectively. Overexpression of miR-145, reversed the myofibroblast associated increase in versican V1 expression at both of the doses of premiR used (~1 fold and 0.8 fold). Interestingly, premiR-145 was able reduce the expression of V1 versican in HDFs, but was unable to inhibit its increase in expression (figure above 7.8B). miR-145 overexpression in induced myofibroblasts was able to reverse the TGF-β1 myofibroblasts associated increase in versican protein levels (figure 7.18).

The efficacy of the overexpression of miR-145 using premiR-145 to transfect TGF-β1 induced dermal myofibroblasts was validated by qRT-PCR. Transfection using premiR-145 (5 nM) caused an average of ~10 fold increase in mature miR-145 levels in normal HDFs, and this was similar in to the level of overexpression in induced dermal myofibroblast which had a ~14 fold overexpression (figure 7.19). The transfection of the higher dose of premiR-145 (50nM) caused an average of ~200 fold increase in mature miR-145 levels in normal HDF, and in TGF-β1 induced myofibroblasts, the transfection only caused a ~33 fold increase.

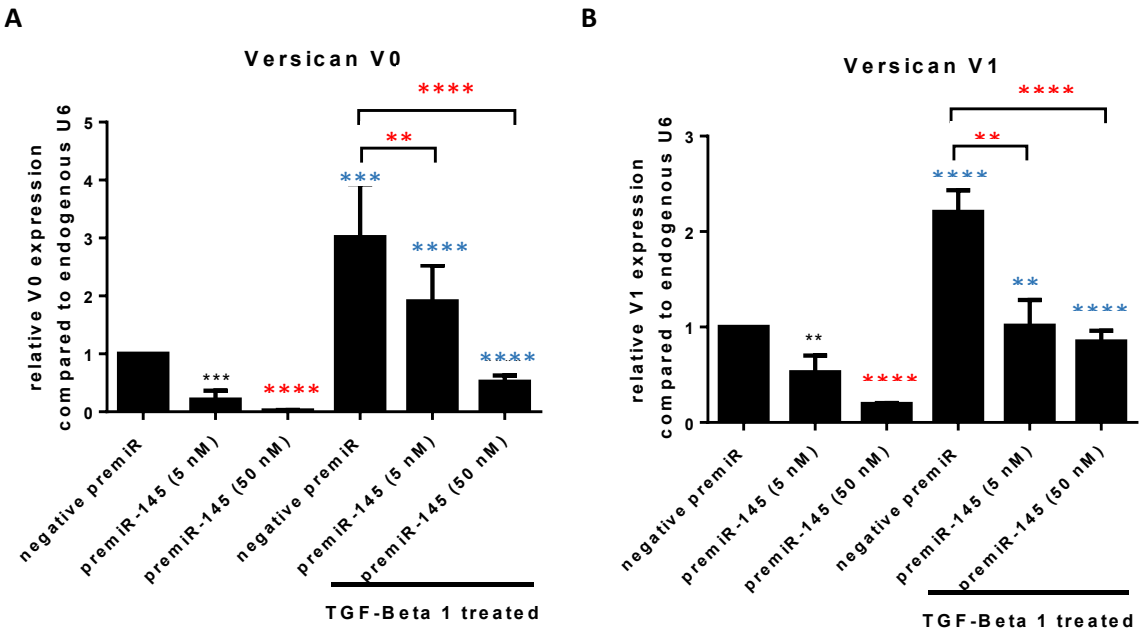

Figure 7.17: Overexpression of microRNA-145 in induced dermal myofibroblasts reduced V0 and V1 versican isoform transcript levels. HDF286s were treated with 5 ng/ml TGF-β1 or serum free media, then transiently transfected with 5 nM premiR-145, 50 nM premiR-145 or a negative non-targeting premiR. The transfection was left for 48 h before being harvested. RNA was isolated and used to generate total cDNA for qRT-PCR analysis using primers for V0 and V1 versican isoforms and U6, as an endogenous control. Each bar on the figure represents the mean relative quantification of versican V0 (**A**) and versican V1 (**B**) transcript levels compared to endogenous U6, for each transfection plus/minus treatment relative to untreated negative premiR. Statistical analysis was performed by a paired two tailed student's t-test, and statistical significance is shown on the figure by *p<0.05. If not indicated by a bar, the black significance asterix are compared to the untreated, negative premiR transfected, negative control. Blue significance asterix indicate significance compared to the untreated counterpart, e.g. premiR-145 transfected, TGF-β1 treated compared with premiR-145 transfected untreated. Bars also indicate statistical comparisons. Important significant data is shown in red. Error bars represent the SEM. N=3, independent experiments.

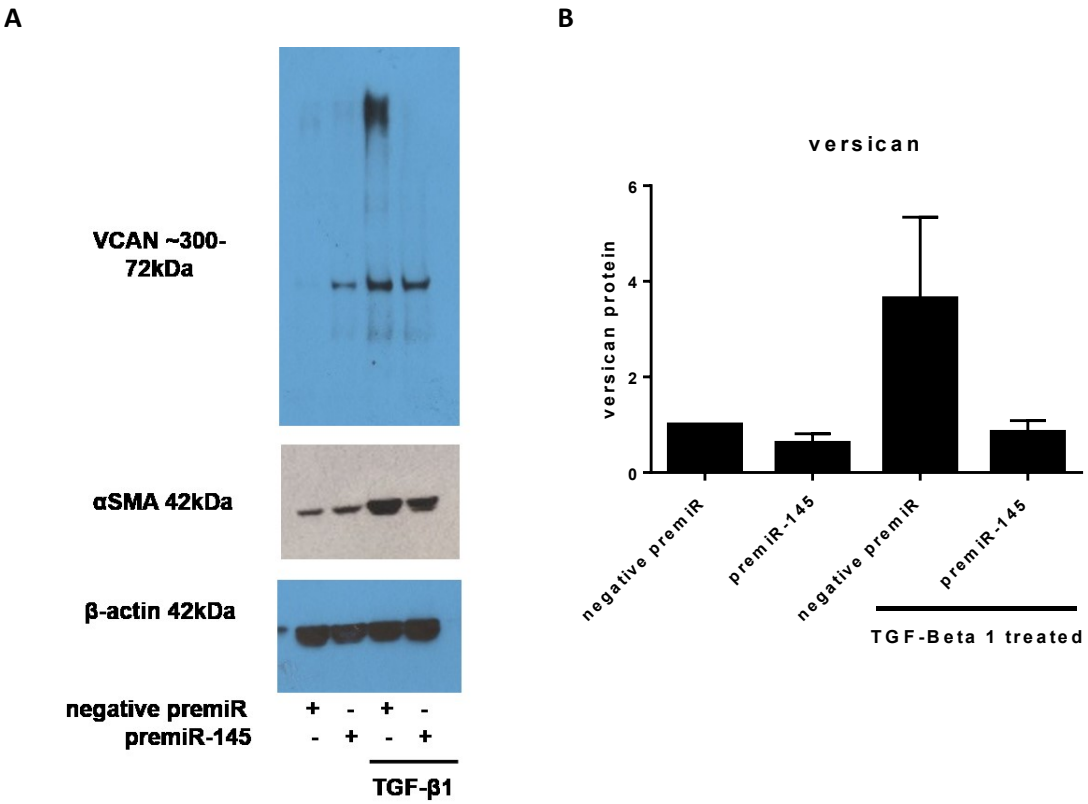

Figure 7.18: miR-145 overexpression caused a non-significant attenuation of TGF-β1 induced versican protein expression in human dermal fibroblasts. HDF286 (data shown) and Promocell (data not shown), were treated with 5 ng/ml TGF-β1 for 48 h, then transiently transfected with a negative non-targeting premiR or premiR-145 (50 nM) for 48 h. After transfection, fibroblasts were harvested and total protein lysates were prepared. Protein lysate (20 µg) was run on a 3–8% (w/v) tris acetate gradient gel and transferred to a nitrocellulose membrane and immunoblotted for versican, αSMA and β-actin as the loading control. Figure **A** shows a representative blot. Protein changes were quantified by densitometry using Image J and are shown in figure **B**, relative to β-actin. The figure shows a representative blot. N=3, independent experiments for each NOF.

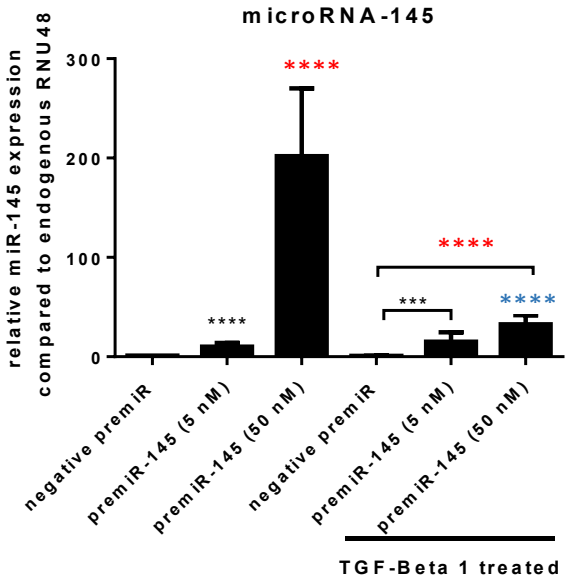

Figure 7.19: PremiR-145 caused overexpression of mature microRNA-145 in dermal fibroblasts. HDF286s were treated with 5 ng/ml TGF-β1 or serum free media, then transiently transfected with 5 nM premiR-145, 50 nM premiR-145 or a negative non-targeting premiR. Fibroblasts were harvested 48 h after initial transfection and the RNA was isolated and used to generate specific miR-145 and RNU 48 cDNA for qRT-PCR analysis using primers for miR-145 and RNU 48, as an endogenous control. Each bar on the figure represents the mean relative quantification of miR-145 transcript levels compared to endogenous U6, for each transfection plus/minus treatment relative to untreated negative premiR. Statistical analysis was performed by a paired two tailed student's t-test, and statistical significance is shown on the figure by ***p<0.001 and ****p<0.0001. If not indicated by a bar, the black significance asterix are compared to the untreated, negative premiR transfected, negative control. Blue significance asterix indicate significance compared to the untreated counterpart, e.g. premiR-145 transfected, TGF-β1 treated compared with premiR-145 transfected untreated. Bars also indicate statistical comparisons. Important significant data is shown in red. Error bars represent the SEM. N=3, independent experiments.

7.6 ***Summary***

miR-145 was able to inhibit and reverse TGF-β1 induced dermal myofibroblasts. TGF-β1 treatment in dermal fibroblasts caused an upregulation of miR-145, versican V0 and V1 expression. Loss of function of versican had no effect on TGF-β1's ability to induce dermal myofibroblasts.

Chapter 8: Discussion

8.1 *Introduction*

Gradual modifications between the tumour and its surrounding stromal microenvironment result in tumour progression. It is thought that transformed epithelial cells have altered paracrine signalling which can promote pro-tumourigenic stromal remodelling, which in turn helps to create a more permissive environment to encourage tumour growth, invasion and metastasis (Pietras & Ostman, 2010). Cancer associated fibroblasts (CAFs), in particular, have been shown to modulate many important aspects of tumour progression: ECM remodelling, cancer cell migration/invasion, angiogenesis, immune cell infiltrate. Myofibroblasts, like CAFs, promote invasive tumours and are predictors of poor prognosis (Kellermann *et al*., 2007; Tsujino *et al*., 2007; Surowiak *et al*., 2007). In OSCC, the presence of myofibroblasts is the strongest predictor of mortality compared to any of tumour characteristics including stage, grade or lymph node status (Marsh *et al*., 2011). Therefore, it is crucial to discover how myofibroblasts arise and identify their contribution towards tumour development. A significant proportion of myofibroblast-like CAFs found in the tumour microenvironment are thought to have arisen from resident normal fibroblasts. Understanding the molecular mechanism of myofibroblast transdifferentiation is therefore key in developing future therapeutics to halt the pro-tumourigenic contributions of these CAFs.

Previously our lab found that the downregulation of miR-145 was important for orchestrating stromal epithelial interactions between fibroblasts and an OSCC cell line, induced by cigarette smoke extract (Pal *et al*., 2013). The current study investigated the role of miR-145 in the fibroblasts within the tumour microenvironment, and found convincing evidence revealing that this small non-coding RNA inhibits and partially reverses oral and dermal myofibroblast transdifferentiation. It was shown to be involved in stromal remodelling, regulating an oncogenic matricellular proteoglycan versican, and regulating paracrine cell migration; identifying the tantalising therapeutic potential of microRNA-145 for the treatment of desmoplastic stroma and fibrotic disorders.

8.2 *Stromal fibroblasts in oral squamous cell carcinomas*

Cancer associated fibroblasts (CAFs) have been found to arise by a number of different mechanisms in the tumour microenvironment, including from tumour/normal epithelial cells undergoing EMT, adipocytes, fibrocytes, endocytes, pericytes, bone marrow derived and resident mesenchymal stem cells (MSCs) (Otranto *et al*., 2012). This study used normal oral fibroblast (NOFs) extracted from normal human gingiva, and treated them with factors that

trans-activate them into phenotypes like that of CAFs found within the tumour microenvironment. Primary CAFs, fibroblasts isolated from various OSCCs, were also used and compared to the NOFs phenotypes. The main CAF under investigation was the myofibroblast-like CAF, therefore myofibroblast molecular markers αSMA, COL1A1 and FN1-EDA were used to assess the fibroblast phenotype.

Studies have shown OSCC cell lines be able to provoke transdifferentiation of oral fibroblasts into myofibroblasts, by co-culture or conditioned media treatment. In most of these cases, the growth factor found to be necessary for transdifferentiation is TGF-β1 (Lewis *et al*., 2004; Marsh *et al*., 2011). Exogenous treatment of fibroblasts with recombinant TGF-β1 is often used to induce oral myofibroblast *in vitro* (Sobral *et al*., 2011). In this study the optimal treatment of TGF-β1 was found to be 5 ng/ml for 48 h to induce NOFs to express markers of myofibroblast transdifferentiation. When NOFs were treated with OSCC cell line conditioned media from Cal27, H357 and VB6, there was little effect on myofibroblast transdifferentiation, in contrast to previous studies. It is likely that the differences seen between the studies are the result of differences in precise methodology of the experiments, for example the collection of cancer cell line conditioned media.

In this study when NOFs were treated with conditioned media from VB6 (a H357 cell line stably overexpressing integrin αvβ6), there was a slight decrease in αSMA transcript levels and a small increase in αSMA protein expression. Marsh *et al*., (2011) found convincing evidence that co-culturing VB6 and NOFs resulted in myofibroblast transdifferentiation through promoting TGF-β1 activation. Marsh *et al*., (2011) used equal numbers of each VB6 cell line and primary oral fibroblasts seeded on coverslips overnight, then after media changed left for 48 h. Whereas our study used NOFs treated with conditioned media which was collected for 24 h, and used as a treatment for 48 h. Conditioned media growth factors can be exhausted, whereas co-cultures provide continual stimulation of both cells. NOFs may require longer exposure to VB6 conditioned media, or may require cross-talk between the VB6 and fibroblasts or contact dependent signalling to induce myofibroblasts.

Four different NOFs were used in this study, OF26, DENF008, DENF316 and DENF319, although most of the experiments used just DENF316 and DENF319. There was a certain amount of biological variability observed from the NOFs throughout the results, especially in response to TGF-β1 treatment. The best read out for TGF-β1 response was the induced expression of αSMA, consistently there was a larger increase in αSMA in DENF316 than DENF319, however even within the same primary fibroblasts there was a range of different responses varying from ~ 4

fold increase- ~100 fold increase, and sometimes the αSMA increase was not significant due to variability. An explanation these differences in the levels of stimulation may be due to the recombinant protein itself, when it was prepared, the batch number, storage, number of freeze thaw cycles etc. In addition, the response could also be altered by the condition of the NOFs, the passage number, stress in culture or confluency of the cells.

There was some variability of the NOFs in their expression of other myofibroblast markers, suggesting that different NOFs express slightly different markers of activation. DENF319, for example, consistently had no TGF-β1 mediated increase in COL1A1 expression whereas DENF316 mostly showed an increase in COL1A with TGF-β1 treatment.

8.3 ***Molecular comparison of NOFs and CAFs***

There was no difference in expression of myofibroblast markers between fibroblasts isolated from OSCC (CAFs) and NOFs. However, analysis of the myofibroblast markers within NOFs showed that NOFs isolated in Sheffield and Beatson Institute had different molecular expression, for example BICR NOFs had a higher expression of FN1-EDA.

The CAFs used, were previously characterised (Hassona *et al*., 2014; Hassona *et al*., 2013; Lim *et al*., 2011), and were classified into separate subtypes depending on the classification of the OSCC that they are extracted from. The tumours were classified as genetically stable or unstable depending on the number of copy number alterations, amount of loss of heterozygosity, and the presence/absence of mutations in p53 and p16 INK4A. Previously CAFs from genetically stable OSCC were shown to be molecularly distinct from CAFs from genetically unstable OSCCs, which were easily induced into a senescent phenotype by TGF-β1 released from OSCC cell lines and could promote invasion through MMP2 secretion. On comparing gene expression of the CAF subtypes αSMA was significantly upregulated in GU-OSCC CAFs compared to GS-OSCC CAFs and NOFs (Lim *et al*., 2011).

Contrary to the findings outlined in Lim *et al*., (2011), using the same cells, this study found that there was no difference in the expression of myofibroblast markers between the GU-OSCC CAFs and GS-OSCC CAFs, or NOFs. This surprising result suggests that some of the CAF phenotype may have been lost in culture. Some CAFs were very slow growing, therefore extended time in culture may have resulted in their gradual change in phenotype. However, in line with the previous reports, senescence associated β-galactosidase assays were used in our lab (data not reported here) and confirmed that the GU-OSCC CAFs used were senescent. The majority of the CAFs

looked microscopically very similar to phenotypically normal fibroblasts, however a number of them had a stretched flattened looking appearance, consistent with a senescent cell. In addition, immunocytochemistry showed no difference in αSMA staining and observed cell shapes between CAFs and NOFs. When NOFs and CAFs were stimulated with TGF-β1 there appeared to be no difference between the cell types' responses; they both displayed bright, vivid αSMA stress fibres in response to TGF-β1 treatment.

CAFs treated with TGF-β1 transdifferentiated readily into myofibroblasts, and generally expressed higher levels of myofibroblast markers relative to untreated controls when compared to TGF-β1 stimulated NOFs. However, MCA, a CAF from Brazil, showed little response to stimulation from TGF-β1, or conditioned media from Cal27 or VB6 OSCC-derived cells. BICR CAFs had a greater induction of expression of αSMA and a greater amount of quantified αSMA stress fibres, in response to TGF-β1. TGF-β1 also caused a greater increase in FN1-EDA expression in CAFs compared to NOFs, however the increase in FN1-EDA in TGF-β1 treated BICR-3 CAFs was not significant. Overall, this data suggests that fibroblasts extracted from the tumour more readily respond to TGF-β1 than normal fibroblasts.

The ability of NOFs and CAFs to stimulate paracrine migration was also compared, and no difference was found. The result was contrary to previous studies, which found that oral myofibroblasts and CAFs promoted the paracrine migration and invasion of cancer cells (Sobral *et al*., 2011; Marsh *et al*., 2011; Hassona *et al*., 2014). CAFs and myofibroblasts are known to have a migratory and invasive secretome, releasing factors such as EGF, HGF, SF, MMPs, TGF-β, etc. which are known to promote EMT and invasion (Ostman & Augsten, 2009), therefore the data that suggests CAFs did not promote migration and invasion was surprising. The reasons for this unexpected result are unclear, but again point to the possibility of phenotypic characteristics of CAFs being lost in culture.

8.4 *miR-143 and miR-145 cluster in CAFs and TGF-β1 induced myofibroblasts*

Molecularly the only difference observed between NOFs and CAFs was the expression of the miR-143/5 cluster. CAFs had a ~20 fold and ~4 fold greater expression of mature miR-143 and miR-145 respectively. For both miR-143 and miR-145, the expression was highest in CAFs from GS-OSCC and this was the only subtype of fibroblast where there was a significant difference compared to NOFs. This result was the opposite of what was expected, as miR-145 was downregulated in CAFs from invasive bladder cancers (Enkelmann *et al*., 2011), however this was only in the microRNA microarray data and was not validated by qRT-PCR. Published data

from our lab also suggested that miR-145 is downregulated in in the tumour microenvironment as the treatment of NOFs with cigarette smoke extract promoted the downregulation of miR-145, which stimulated paracrine cancer cell migration. Our lab and others (Coppe *et al*., 2008) have shown that oral fibroblasts can promote paracrine cancer cell migration in response to cigarette smoke extract, suggesting this may be a stromal event in oral tumourigenesis.

Consistent with higher miR-145 expression in CAFs, TGF-β1 treatment caused an increase in mature miR-145 levels in NOFs. For DENF319 and OF26 NOFs this was a significant increase, but for DENF008 and DENF316 NOFs the trend indicates that TGF-β1 upregulates mature miR145 expression, however due to variability in the responses it was not found to be statistically significant. In addition, CAFs showed a similar response of the cluster to TGF-β1. TGF-β1 caused an upregulation of miR-145 levels in BICR-59, BICR-3 and BIR-63. Taken together, this data is consistent with other studies which have previously shown TGF-β1 to increase the expression of miR-145 transcription in human coronary smooth muscle cells (Long & Miano, 2011), dermal (Gras et al.) and pulmonary fibroblasts (Yang *et al*., 2013). The study in smooth muscle cells revealed the presence of a CArG box and SBE (smad binding element) upstream in miR-143/5 enhancer elements, therefore revealing how TGF-β1 signalling and myocardin/SRF activates the expression of miR-145 (Long & Miano, 2011).

In light of CAFs and TGF-β1 treated NOFs having elevated miR-145 expression, it was surprising that treatment of NOFs with conditioned media from VB6, a cell line overexpressing αvβ6, a known activator of TGF-β1 signalling (Thomas *et al*., 2002), caused a significant downregulation of mature miR-145 levels in DENF316 NOFs and CAFs. The only NOFs used in this experiment was DENF316, which did not shown an increase in miR-145 expression in response to TGF-β1, it would be interesting to perform the experiment again using DENF319 NOFs, which have TGF-β1 mediated miR-145 upregulation, to confirm this result. VB6 conditioned media failed to transdifferentiate NOFs into myofibroblasts perhaps reflecting the lack of activation of TGF-β1 signalling.

However, the VB6 mediated downregulation of miR-145 is interesting, and implies that miR-145 may play a key role in both TGF-β1 signalling and myofibroblasts transdifferentiation, if indeed VB6 is capable of inducing myofibroblasts transdifferentiation. This result supports the data in this thesis which suggests miR-145 may play an anti-myofibroblastic role. The downregulation of miR-145 may be an early response of fibroblasts in the transdifferentiation process, it may allow TGF-β1 that has been activated by αvβ6 to have its effect. Further work to test this hypothesis needs to be done, miR-145 expression should be analysed in NOFs at timepoints in

the TGF-β1 and potentially VB6-mediated transdifferentiation process. To investigate whether VB6 conditioned media is able to induce myofibroblasts, NOFs could be treated with conditioned media for longer time periods. If this is achieved then the effect of overexpression of miR-145 could be tested to evaluate whether it is able to prevent VB6 induced transdifferentiation.

8.5 *Effect of microRNA-145 in oral fibroblasts and CAFs.*

A number of microRNAs have been implicated in orchestrating myofibroblast transdifferentiation, for example miR-21 and miR-146a (Sachdeva *et al*., 2012; Yao *et al*., 2011). One study in ovarian CAFs found that miR-31, miR-214 and antimiR-155 transfection into CAFs was able to reverse the CAF phenotype (Mitra *et al*., 2012). In this study, gain of function assays revealed that miR-145 was able to block the and partially reverse TGF-β1 induced oral myofibroblasts transdifferentiation in all NOFs tested. miR-145 inhibited the TGF-β1 induction of the transcripts of all myofibroblasts markers, with the most dramatic effect on αSMA. The inhibition of αSMA expression was also shown by miR-145 preventing protein expression and myofibroblasts αSMA stress fibre formations. miR-145 also was able to inhibit the functional effect of TGF-β1 induced contractility and paracrine migration (only performed in DENF316).

There was a certain amount of variability in the response to miR-145 overexpression, which in part can be accounted for by the efficiency of individual transfections, due to NOFs being or different passages or confluency. Also the biological variability of the NOFs was apparent, miR-145 is capable of decreasing the endogenous expression of αSMA, COL1A1 and FN1-EDA in DENF319, but is only capable of decreasing COL1A1 expression in DENF316. These differences in the responses to TGF-β1 and miR-145 can help to reveal information about the genetic pathways allowing myofibroblast transdifferentiation. For example, TGF-β1 only caused significant upregulation of miR-145 in DENF319 NOFs and not DENF316, and in both NOFs the overexpression of miR-145 results in the downregulation of COL1A1. Only in DENF316 and not DENF319 TGF-β1 is able to stimulate COL1A1 expression. Therefore, it can be hypothesised that DENF319 fail to have an increase in COL1A1 expression as TGF-β1 upregulates miR-145 in these cells which in turn decreases the COL1A1. A possible reason why DENF319 NOFs do not show as much as a response to TGF-β1 as DENF316, could be that TGF-β1 induces miR-145 expression to decrease the activation of the myofibroblast markers. However, the data from the CAFs shows that they generally have a higher miR-145 expression, TGF-β1 generally increases miR-145 expression and they have big responses to TGF-β1 which does not fit with the above reasoning.

miR-143, which is co-transcribed and often processed with miR-145, but is known to have a distinct set of targets, also had some effect on oral myofibroblast transdifferentiation, but it was less marked than the effects of miR-145. Overexpression of miR-143 significantly reduced the DENF316 TGF-β1-induced αSMA expression only at the mRNA level, miR-143 had no effect on the other myofibroblast markers or on any markers in DENF319s. It was able to prevent the some functional effects, preventing some myofibroblasts associated contractility of the fibroblasts and ability to promote paracrine migration.

miR-145 was also able to inhibit TGF-β1 myofibroblast transdifferentiation in CAFs, and reduce endogenous levels of myofibroblast markers in these cells, suggesting that exogenous delivery of miR-145 could be used to reduce myofibroblast activation in CAFs within the tumour microenvironment. miR-145 was also able to partially reverse the TGF-β1 induced myofibroblast phenotypes, furthering the therapeutic potential of this miRNA. After 48 h of premiR-145 transfection, miR-145 was able to reduce the activation of αSMA transcript levels, but no other myofibroblast markers. miR-145 was also able to reduce the amount of total fluorescence of the αSMA stress fibres, however TGF-β1 treated NOFs, transfected with miR-145 still had visible stress fibres. As the effect on αSMA protein level was minimal in comparison to the effect on transcript levels, it was thought that αSMA protein may have a long half-life therefore it would take longer for miR-145 mediated knock-down of αSMA protein. A cycloheximide chase assay was used to assess the half-life of αSMA protein; this approach was unsuccessful. Studies from mammary fibroblasts highlighted that activated TGF-β1 and SDF autocrine signalling was capable of maintaining myofibroblast activation (Kojima *et al*., 2010), perhaps once transdifferentiated, oral fibroblasts may maintain their differentiation through the secretion of key cytokines.

8.6 ***miR-145 effect on protumourigenic effects on myofibroblasts***

TGF-β1 is known to induce EMT in cancer cells (Siegel & Massagué, 2003). Treatment of NOFs with TGF-β1 has been shown to secrete factors which promote proliferation and invasion of oral cancer cells (Kellermann *et al*., 2008; Lewis *et al*., 2004). In this study, the treatment of NOFs with TGF-β1 was able to promote paracrine migration in DENF316 NOFs in line with previous studies, DENF319 NOFs were not investigated. The TGF-β1 mediated increase in migration was inhibited by miR-145 overexpression, but miR-145 had no effect on NOFs endogenous paracrine effect on migration. miR-145 therefore may inhibit the myofibroblast associated release the chemokines to promote migration of cancer cells. This could be investigated by collecting the

conditioned media from NOFs transfected with premiR-145 or negative control premiR then treating with TGF-β1 or serum free control and incubating the conditioned media with a cytokine array to assess the secretome of the fibroblasts.

Our group previously showed ET-1 was able to stimulate paracrine migration through ET-1 activating ADAM-17 mediated cleavage of EGF ligands (Hinsley, *et al*., 2012). ADAM-17 is a known target of miR-145 (Doberstein *et al*., 2013), therefore miR-145 overexpression in NOFs could be preventing ET-1 and perhaps TGF-β1 induced increased in paracrine migration through reducing EGF signalling through lack of ADAM-17 mediated release of EGF receptor ligands. Myofibroblasts are known to release a myriad factors which could promote paracrine invasion, therefore the extent at which the hypothesised ADAM-17 release of ligands contributes to TGF-β1 induced myofibroblasts paracrine stimulation of migration/ invasion could be assessed through using inhibitors of ADAM or knocking down ADAM-17 and measuring ADAM-17 expression on ET-1 and TGF-β1 treatment.

Another role for ADAM-17 could be in the regulation of TGF-β1 signalling. In VSMCs, ADAM-17 has been shown to cleave a transmembrane protein vasorin into the extracellular environment where it can bind to a sequester TGF-β1 and inhibit its action (Ikeda *et al*., 2004; Malapeira, Esselens, Bech-Serra, Canals, & Arribas, 2011). Vasorin may also be a target of miR-145 as there is a putative binding site in its 3'UTR (Target Scan 6), therefore vasorin may be another mechanism how miR-145 can fine-tune the response of a cell to TGF-β1. It is not known whether vasorin is expressed in fibroblasts or whether it is exclusive to VMSCs.

The presence of myofibroblast are often implicated to lead to invasive tumours (De Wever *et al*., 2008). Inhibitors of TGF-β1 have been shown to inhibit CAF and normal fibroblasts ability to stimulate paracrine migration/invasion in several studies (Hassona *et al*., 2013; Yeung *et al*., 2013). Conditioned media from GU-OSCC CAFs, which were shown to senescent, promoted invasion which was inhibited by inhibitors to both TGF-β1 and MMP2 (Hassona *et al*., 2014). In this study, TGF-β1 had different effects in stimulating paracrine invasion on the two different NOFs used. TGF-β1 stimulated paracrine invasion in DENF316s and inhibited invasion in DENF319s. miR-145 overexpression was able to inhibit the TGF-β1 increase in paracrine invasion, in a dose wise response. This change in invasion closely correlated with the expression of MMP2 from these cells, suggesting that miR-145 may regulate TGF-β1 induced invasion through the regulation of MMP2 expression. In DENF319, again the pro-invasiveness of the NOFs was similar to the pattern of MMP2 expression. miR-145 overexpression was able to downregulate MMP2 expression, therefore TGF-β1 may have caused a decrease in invasion

through miR-145 mediated downregulation of MMP2 in DENF319. TGF-β1 regulation of miR-145 appears to be key in the fibroblasts response. Unfortunately, the loss of function experiments did not work in this study; it would have been useful to assess whether transient knock-down of miR-145 could ameliorate the TGF-β1 decrease in paracrine invasion. It would also be useful to determine by zygmography the activity of the expressed MMP2 and other MMPs, for example MMP9, together with MMP2 they are both able to promote latent TGF-β1 activation (Yu & Stamenkovic, 2000).

miR-145 was able to reverse the ability of TGF-β1 induced myofibroblasts to promote paracrine migration in DENF316 but not DENF319. Overexpression of miR-145 also had less effect on invasion when introduced after TGF-β1 treatment in DENF316. However, the levels of MMP2 were not assessed in these fibroblasts to determine if they also correlated with the level of invasion as before.

CAFs treated with TGF-β1 had a reduced ability to stimulate paracrine migration. This was unexpected as previous studies have shown that TGF-β1 treatment of CAFs encourages paracrine migration (Yeung *et al*., 2013) and invasion (Casey *et al*., 2008; Gaggioli *et al*., 2007), although the effect of CAFs on paracrine invasion was not investigated in this study. miR-145 had no significant effect on paracrine migration, and in some CAFs the trend of migration looked as though it increased on miR-145 overexpression, highlighting doubt for whether miR-145 mimics would be a suitable drug.

8.7 ***miR-145 in fibrosis***

Fibrosis is generally described as a failure for normal wound healing to appropriately finish (Eckes *et al*., 2000). Fibrosis and fibrotic disorders are mainly characterised by the appearance of an extensive scar produced by extensive deposition of ECM (Leask & Abraham, 2004). Myofibroblasts are one of the main cell types orchestrating fibrosis, producing ECM and secreting cytokines which promote further fibroblast and immune cell recruitment: TGF-β, PDGF, MMPs, IL-1 CTGF (reviewed in Wynn & Ramalingam, 2012). There are many similarities between fibrosis and the tumour microenvironment. Therefore, data regarding myofibroblasts found in fibrotic disorders is important for understanding the role of miR-145 in myofibroblasts in the tumour microenvironment. miR-145 is reported to be downregulated in scleroderma (Zhu *et al*., 2012) an autoimmune fibrotic disorder and in keloids (hypertrophic scars; Li *et al*., 2013). This suggests, in agreement with our data, that miR-145 is anti-fibrotic. However, miR-145 is increased in hypertrophic scars (Gras et al.) and idiopathic lung fibrosis (Yang *et al*., 2013), and

has recently been shown to be involved in inducing dermal, cardiac and pulmonary myofibroblasts transdifferentiation (Gras *et al*., 2015; Wang *et al*., 2014; Yang *et al*., 2013), suggesting that miR-145 is important in producing myofibroblasts and promoting fibrotic disease.

These studies in pulmonary and cardiac fibroblasts, outlined that miR-145 overexpression was able to induce functional myofibroblasts via increasing the expression of myofibroblast marker αSMA. Anti-miR-145 was able to prevent TGF-β1 induced dermal and pulmonary myofibroblasts transdifferentiation in vitro (Gras *et al*., 2015; Yang *et al*., 2013). Knockout mice lacking miR-143/145 showed reduced bleomycin induced pulmonary fibrosis, and in vitro miR-143/145 $^{-/-}$ fibroblasts showed a reduced TGF-β1 induced pulmonary myofibroblast transdifferentiation. In addition in the cardiac study, a tail injection of antimiR-145 before coronary artery occlusion to induce myocardium infarction, significantly reduced the number of myofibroblasts present, hence resulted in a bigger infarct size as there was impaired wound healing and a reduced scar thickness (Wang *et al*., 2014).

The studies suggested that miR-145 has a similar mechanism of action. They provided evidence that miR-145 controls the myofibroblast phenotype, via targeting the KLF4/KLF5 myocardin regulators (dermal and pulmonary/cardiac fibroblasts respectively). In lung fibroblasts miR-145 overexpression resulted in the decrease of KLF4 protein levels, which lead to the authors identifying KLF4 as a target of miR-145 (Yang *et al*., 2013). In the dermal study the authors showed that overexpression of KLF4 can inhibit myofibroblast transdifferentiation (Gras et al.). Similarily in the cardiac study, KLF5 re-expression was able to 'rescue' and prevent the acquisition of the myofibroblast phenotype when mouse cardiac fibroblasts were treated with a miR-145 mimic. miR-145 was validated to directly target KLF5 in human HEK293 cells and an increase myocardin expression in cardiac fibroblasts (Wang *et al*., 2014).

In oral fibroblasts, some evidence of miR-145 regulating KLF4 and KLF5 was found. Overexpression of miR-145 showed no significant effect on KLF4/5 expression, however in NOFs transfected then treated with TGF-β1 KLF4 expression was significantly decreased, and miR-145 was able to significantly attenuate the TGF-β1 dependent KLF5 increase. Suggesting that unlike these two studies, miR-145 does not control the myofibroblast phenotype solely through the regulation KLF4/5. One similarity in our results and these studies results is miR-145s effect on myocardin (Wang *et al*., 2014) where miR-145 overexpression caused an increase on myocardin expression, they conclude this was through negative regulator KLF5.

The majority of the key experiments were performed in murine fibroblasts or *in vivo* mouse models, differences between human and murine fibroblasts may help explain why these studies opposite to the results in this thesis. miR-145 is conserved (miRbase), but it may well have a distinct mechanism of action in the different species, as they may have different targets in mouse/human and binding sites on targets may not be conserved. However, the areas of KLF4/5 where miR-145 is reported to bind to is conserved between mouse and human.

The pulmonary study used some human fibroblasts, they used some primary cells, but MRC-5, a pulmonary fibroblast cell line derived from a human foetus, were used for the majority of the key experiments. There is a strong possibility that miR-145 has distinct roles in foetal fibroblasts compared to adult, especially due to its key roles in smooth muscle differentiation. Several studies have highlighted some of the differences between adult and foetal fibroblast (reviewed in Larson, Longaker, & Lorenz, 2010). There seems to be key differences with the fibroblast produced ECM, foetal fibroblasts have a greater amount of hyaluronic acid and glycosaminoglycans and less TGF-β signalling (Ellis & Schor, 1996). In humans, scars are known to begin to form around 24 weeks gestation (Lorenz *et al.,* 1995), before then the foetal wound healing is scarless and there are no documented myofibroblasts (Clark & Henson, 1988). The MRC-5 fibroblasts cell line was derived from 14 week foetus, therefore at a stage where there is no myofibroblast activation, so it seems illogical to use it as the main fibroblast cell line to investigate myofibroblast transdifferentiation.

8.8 ***miR-145 effect in dermal myofibroblasts***

Wound healing in the oral cavity is notably different to skin. Oral mucosal wound healing is associated with a fast, scarless wound closure, with a short inflammatory response, compared to dermal wound healing which often results in scar formation due to excessive collagen rich ECM accumulation (reviewed in Larson *et al.,* 2010). To determine whether oral myofibroblasts have separate molecular mechanisms than dermal myofibroblasts, the miR-145 gain of function were repeated in TGF-β1 induced dermal fibroblasts. Experiments performed in 3 different human primary dermal fibroblasts consistently revealed very similar results to that observed in oral fibroblasts. Contrary to the study by Gras *et al*., (2015) miR-145 significantly inhibited and reversed dermal myofibroblasts transdifferentiation. TGF-β1 significantly induced each molecular marker, and, similar to the previous dermal study, most TGF-β1 dermal fibroblasts had increased miR-145 expression. There was a marked difference between the efficiency of miR-145 in reversing dermal TGF-β1 induced myofibroblast than in oral induced myofibroblasts.

Overexpression of miR-145 caused a dose responsive reduction of myofibroblast markers αSMA, COL1A1 and FN1-EDA in both HDF and TGF-β1 treated HDFs, elegantly showing miR-145 inhibiting the myofibroblast phenotype.

Studies have highlighted the differential gene expressions between dermal and gingival fibroblasts grown in 3D cultures (Mah *et al.*, 2014; Stephens *et al.,* 2001). Mah *et al.,* (2014) showed that fibroblasts from breast skin were more profibrotic than gingival fibroblasts, and showed that they had elevated TGF-β signalling, ECM remodelling and myofibroblastic markers (αSMA, tenascin c, COL1A, and SDF-1) compared to skin fibroblasts. The reason why mir-145 appeared to have a more dramatic effect in dermal myofibroblasts than oral myofibroblasts, in this study, may be due to their comparatively more inherent profibrotic nature, again reflected by their ability to form a scar. miR-145 was able to reduce each marker of myofibroblast in dermal myofibroblasts, whereas miR-145 only reduced TGF-β1 mediated αSMA expression in oral fibroblasts, and not COL1A or FN1-EDA. However, no functional assays were performed, therefore it is unknown whether TGF-β1 induces functional myofibroblasts and whether miR-145 reverses their functional effects. Contractility or 'scratch' wound healing assay could have been performed to further validate the dermal myofibroblast phenotype.

Overall the data from dermal and gingival fibroblasts suggest that miR-145 is indeed anti-fibrotic and discrepancies between the previous studies saying the opposite are likely to be due to the fibroblasts which they used, mouse and foetal (Wang *et al*., 2014; Yang *et al*., 2013). To confirm this human primary fibroblasts from heart and lung, amongst other locations should be tested in the future. It would also be interesting to assess the role of miR-145 in oral fibroblasts from different sites of the oral cavity as phenotypic differences have been described for periodontal and buccal fibroblasts (Lepekhin *et al*., 2002).

8.9 ***Versican***

Versican has been shown to be necessary for dermal myofibroblast transdifferentiation (Hattori *et al*., 2011) and is associated with invasion (Cattaruzza *et al*., 2004; Yee *et al*., 2007) and with poor outcomes in many cancers including OSCC (Pukkila *et al*., 2004; Pukkila *et al*., 2007; Ricciardelli *et al*., 2002; Said *et al*., 2012). Versican is an extracellular chondroitin proteoglycan, of around 74 - 450kDa apparent molecular weight (Ricciardelli *et al*., 2009). The antibody used in this study binds to versican at the Gly1344-Asp1554 epitope in the GAG-β domain which is only in V0 and V1 isoforms, therefore the antibody should detect 2 isoforms of differing sizes 450 kDa and 274 kDa, with different numbers of chondroitin sulphate chains. Therefore, the

antibody used produced an immunoblot of many clear bands of different sizes. Versican is an integral structural component of the ECM which is involved in cell signalling and maintaining ECM, therefore is involved in many cellular processes including adhesion, proliferation, apoptosis and motility.

Loss of function experiments in dermal and oral normal fibroblasts, and oral CAFs, showed that versican had little effect on TGF-β1 induced myofibroblast transdifferentiation. Versican siRNA had some effect on reducing the TGF-β1 mediated activation of myofibroblasts markers in DENF316 and the one tested CAF (BICR-59) but not DENF319, but in dermal fibroblasts versican knock-down had no effect on TGF-β1 induced myofibroblast markers. In all fibroblasts assessed, versican had no effect on αSMA protein expression or stress fibre formation, suggesting that versican may have a small effect on inducing myofibroblasts but is not necessary for transdifferentiation, in contrast to previous reports (Hattori *et al*., 2011). However, this study was mainly in mice, which as suggested previously may have distinct molecular mechanisms of myofibroblast transdifferentiation; the only human experiments performed were gain of function studies showing that a versican overexpression vector had increased TGF-β signalling and caused human dermal fibroblasts to transdifferentiate (Hattori *et al*., 2011).

Versican expression has been shown to cause a reduction in cancer cell adhesion and increased migration (Ang *et al*., 1999; Onken *et al*., 2014; Ricciardelli *et al*., 2007). The TGF-β1 mediated release of versican from ovarian CAFs stimulated migration and invasion of ovarian cancer cell lines (Yeung *et al*., 2013). In line with previous studies (Haase *et al*., 1998; Kähäri, Larjava, & Uitto, 1991) here it was found that TGF-β1 stimulated an up regulation of versican expression in in oral and dermal fibroblasts, which in NOFs transfected with negative premiR caused an increase in paracrine migration, however in negative siRNA transfected NOFs and CAFs there was no increase in paracrine migration. This suggests that this particular 'non-targeting' siRNA control has some off target effects. Versican knock-down was able to decrease paracrine migration in NOFs but not in CAFs. Suggesting that versican does promote paracrine migration, and TGF-β1 may cause some of its pro-migratory effects via versican upregulation. It also suggests that CAFs tested are a distinct phenotype from TGF-β1 treated oral fibroblasts.

This thesis convincingly outlines that miR-145 negatively regulates versican, more so than previously published miR-143 (Wang *et al*., 2010). microRNAs are thought to generally bind to complementary regions in 3'UTR of gene transcripts, however recent studies have shown evidence for functional binding sites for miRNA in coding regions (Duursma *et al*., 2008), promoters (Place *et al*., 2008) and in 5' UTRs (Moretti, Thermann, & Hentze, 2010). miR-145s

regulation of versican is unlikely to be a direct regulation as there are no putative binding sites in the versican 3'UTR (TargetScan).

To further investigate the regulation of versican by mir-145, the versican promoter was cloned. The versican promoter contains AP1 and TCF/LEF transcription factor binding sites. AP1 is a transcription factor which is pleiotropically utilised by several cytokines and growth factors (Hess, Angel, & Schorpp-Kistner, 2004), providing further evidence that versican is transcriptionally regulated by a range of cytokines. β-Catenin, the active transcription factor of Wnt signalling, binds to the TCF/LEF sites and actives the transcription of the gene. P53 has also been shown to transcriptionally regulate versican through binding to a p53 response element in intron 1 of versican (Yoon *et al.,* 2002). However, Pukkila *et al.*, (2004) found no correlation between p53 status and versican expression in immunohistological examination of pharyngeal squamous cell carcinomas.

miR-145 overexpression did not have any effect on the activity of the versican promoter in a reporter assay. Using microPIR, a bioinformatics database predicting which microRNAs can bind with gene promoters, confirmed that there was not a predicted miR-145 interaction with the VCAN promoter (Piriyapongsa *et al.,* 2014). Importantly, this assay suggested that miR-145 does not control the regulation of versican through regulating a transcription factor acting on versican promoter.

An alignment was performed using multalin online alignment software (Corpet, 1988) and found miR-145 seed sequence can bind the versican transcript with 7 out of 8 nucleotide complementary, in a coding region exon region. This near perfect seed sequence complementary in coding region has been shown to promote negative regulation in several previous plant studies (reviewed in Brennecke *et al.,* 2005) Therefore, it is possible that this interaction may produce the profound downregulation of versican seen in this study. However, studies have indicated that binding sites with 3' UTRs are much more effective at leading to the mRNA transcript degradation than binding sites in coding regions (Baek *et al.*, 2008; Fang & Rajewsky, 2011). To further investigate the functionality of this potential binding site, mutagenesis of the putative binding site in coding region of versican should be performed.

TGF-β1 may also regulate versican processing in the oral tumour microenvironment by the positive regulation of ADAMTS-1 and -4. Higher expression of ADAMTS-1 and -4 have been reported in prostate tumours (Ricciardelli *et al*., 2009). These ADAMTSs are capable of proteolytically cleaving versican V1 at the Glu441-Ala442 bond in the GAG-α domain producing a DPEAAE neo-epitope (Ricciardelli *et al.*, 2009). This form of versican has been shown to

promote invasion in prostate cancer studies (Arslan *et al*., 2007). Unexpectedly, here it was expressed in NOFs but not TGF-β1 treated NOFs, however the immunoblotting was only effective once therefore other means of detecting versican cleavage should be carried out. It may be that the antibody is not optimised for immunoblotting but is effective in immunohistochemistry. miR-145 overexpression was able to decrease endogenous ADAMTS-1 and -4 expression and completely block TGF-β1 stimulated expression, but this is unlikely to be a direct effect as there is no putative miR-145 binding site in their 3' UTRs. ADAMTS-1 is upregulated in wound healing (Krampert *et al*., 2005) and lung fibrosis, and has been implicated in TGF-β activation (Bourd-Boittin *et al*., 2011).

Chondroitinase treatment of versican was performed in this study, however it was unsuccessful. Other groups successfully achieved complete digestion of the chondroitin sulphate chains at similar doses of 0.02 units/ml for 1 h at 37 ^{o}C (Russell *et al.,* 2003). This left 2 immunoreactive bands reflecting V0 and V1 isoforms, when a full length versican antibody was used. Optimisation of the technique is required to see further see differences in TGF-β1 and the effect of miR-145, but also to ensure the immunoreactivity of the neoepitope antibody. Most studies, but not all (Didangelos *et al.,* 2012), that have used an antibody to the cleaved DPEAAE neo-epitope versican have used the chondroitinase treatment before (Hattori *et al*., 2011; Russell, Doyle, *et al*., 2003), suggesting that the epitope may be hidden by chondroitin sulphate chains. This view is supported by data suggesting TGF-β1 induces more GAGs and upregulates the posttranscriptional GAG modifying enzymes responsible for the synthesis and adding chondroitin sulphate chains to versican in lung fibrosis (Venkatesan *et al*., 2014), perhaps explaining why TGF-β1 caused a decrease in the immunoreactivity of truncated VCAN.

8.10 *miR-145 effect on smooth muscle transcription factors*

Many of the same growth factors involved that are involved in fibrosis are also known to play roles in regulating smooth muscle and myofibroblast differentiation – PDGF, TGF-β and Ang II (Bai *et al*., 2013; Swigris & Brown, 2010). TGF-β1 and PDGF are the two main growth factors known to control smooth muscle cell phenotypes, the synthetic and contractile. The synthetic phenotype is where cells are more migratory and proliferative and contractile/differentiated is where there is a high expression of contractile genes. Both growth factors regulate the miR-143/5 cluster (Long & Miano, 2011; Quintavalle, Elia, Condorelli, & Courtneidge, 2010) which is known to mediate these phenotypes by regulating key smooth muscle effector genes (Xin *et al*., 2009). Myocardin, Myocardin related transcription factors (MRTFs) and serum response factor

are all also able to promote the expression of the miR-143/5 cluster in a feedback loop, through the presence of a CArG box in the clusters enhancer.

Myocardin is an activator of the SMC phenotype with SRF turns on CArG box smooth muscle genes including αSMA. Myocardin is responsible for repression of versican (Wang *et al*., 2010) in smooth muscle cells. In several cell lines overexpression of myocardin resulted in a marked downregulation of versican mRNA, however this also was accompanied by an increase in αSMA in a mouse embryonic fibroblast cell line 10T1/2. The authors showed that myocardin regulated miR-143 which directly targeted versican via its 3'UTR, and miR-143 was shown to be necessary for the myocardin regulation of versican. In our study, although myocardin expression was elevated on miR-145 overexpression, miR-143 overexpression in oral fibroblasts did not result in down-regulation of versican, whereas miR-145 did. In addition αSMA expression is attenuated when myocardin expression is activated; this is the opposite of that observed in smooth muscle differentiation.

In this study, NOFs did not express a detectable background level of myocardin transcript, miR-145 overexpression caused the detection of myocardin suggesting that it may regulate a negative regulator of myocardin. KLF4/5 both negatively regulate myocardin in smooth muscle cells, and are putative targets of miR-145. miR-145 has been shown to directly target KLF4 and KLF5 in smooth muscle studies (Cheng *et al*., 2009; Xin *et al*., 2009) and in pulmonary and cardiac fibroblasts respectively (Wang *et al*., 2014; Yang *et al*., 2013). However, our qRT-PCR data shows that miR-145 does not significantly regulate KLF4/5 at the transcriptional level, this of course does not rule out that miR-145 could interfere with KLF4/5 translation in oral fibroblasts. For KLF4, both miR-145 overexpression and TGF-β1 led to a small decrease in KLF4, however miR-145 overexpressing NOFs treated with TGF-β1 had a significant downregulation of KLF4 suggesting that both high miR-145 expression and TGF-β1 signalling may be needed to regulate KLF4. A decreased KLF4 expression in these NOFs correlated with increased myocardin expression consistent with miR-145 upregulating myocardin expression via the regulation of KLF4.

Myocardin Related Transcription Factor A and B (MRTF-A/B) are transcription factors that, like myocardin, work with SRF to activate smooth muscle contractile genes. MRTF-A/B have also been reported to be important for promoting myofibroblast transdifferentiation in rat embryonic fibroblasts (Crider et al., 2011). According to TargetScan, miR-145 has 4 putative binding sites in MRTF-B 3'UTR (Lewis, Burge, & Bartel, 2005) and has been shown to directly bind to the UTR (Xin *et al*., 2009). Consistent with this miR-145 and TGF-β caused a decrease in

MRTF-B expression in NOFs (in OF26 and DENF319), allowing it to become a potential candidate gene to be regulating the oral myofibroblast transdifferentiation. However, in DENF316 miR-145 caused a significant increase in MRTF-B, nonetheless a MRTF-B targeting siRNA was used to investigate whether it plays a significant role in oral myofibroblasts transdifferentiation.

MRTF-B knock-down had little effect on myofibroblast transdifferentiation. MRTF-B knock-down was only able to reduce myofibroblasts activation in DENF316, not in DENF319. Interestingly in DENF319 NOFs TGF-β1 caused a downregulation of MRTF-B transcripts, consistent with this NOF having TGF-β1 mediated increase in miR-145 expression. As TGF-β1 treatment increased MRTF-A levels in NOFs tested, a possible amount of redundancy between MRTF-A and B may explain why MRTF-B knock-down did not prevent oral myofibroblast transdifferentiation as expected. miR-145 was able to prevent the TGF-β1 activation of MRTF-A signalling, this is likely to be due to miR-145 dampening TGF-β1 signalling.

There are many other genes are involved in the regulation of αSMA, some of which are mediated by or mediate the expression of miR-145. A positive regulator of αSMA is CCAAT/ enhancer binding protein β (C/EBP-β), this is able to decrease miR-145 expression through binding to and preventing the p53-mediated regulation of miR-145 (Sachdeva *et al*., 2012). Homeobox transcription factor NK 2 homeobox, (NK2 transcription factor related, locus 5) a coactivator of CArG boxes (C. Y. Chen & Schwartz, 1996), transcriptionally activates αSMA and miR-145 (Cordes *et al*., 2009). PPAR-γ activates miR-145 to downregulate smad3 (Zhu *et al*., 2015). On the other hand, a negative regulation of αSMA in myofibroblasts (Jeon *et al*., 2014), peroxisome proliferator-activated receptor (PPAR-γ) also leads to the upregulation of miR-145 (Cordes *et al*., 2009). Therefore, αSMA and miR-145 seem to be involved in a complex regulatory loop which seems to differ between myo/fibroblasts and smooth muscle cells.

The miR-145 regulation of Sox-9 was also investigated, as miR-145 has been previously shown to target sox-9 and regulate chondrocyte differentiation from mesenchymal stem cells (Yang *et al*., 2011). Sox-9 has been shown to promote oncogenic proliferation and inhibit senescence (Matheu *et al*., 2012). miR-145 has been shown to target sox-9 aiding in preventing tumourigenesis in gliomas (Rani *et al*., 2013). In a HNSCC study, miR-145 was shown to regulate ADAM-17 though its direct interaction with its 3'UTR but also through sox-9 regulation (Yu *et al*., 2013). The loss of miR-145 in tumour initiating cells resulted in higher sox-9 and ADAM-17 expression and mediated release of IL-6 and soluble IL-6 receptor promoting paracrine migration and invasion. Sox-9 has even been shown to regulate versican expression (Lee *et al.,* 2008) perhaps providing a mechanism by which miR-145 can regulate versican expression in oral

fibroblasts. Our study found that both TGF-β1 and miR-145 was able to downregulate sox-9 expression, however this was a small change in expression suggesting if it does play a role in the regulation of versican, it would not be sufficient to to fully explain the effect miR-145 on versican expression.

8.11 *miR-145 regulation of the ECM and actin cytoskeleton*

The importance of ECM modulation by MMPs was shown by a study using 'TIMPless' a quadruple TIMP knockout mouse in which fibroblasts had a myofibroblast like CAF phenotype. The main MMP responsible for this phenotypic change was ADAM-10 as an ADAM-10 knockout rescued the fibroblasts (Shimaoda *et al.,* 2014). Futhermore, Hinz has outlined 3 things that must occur to induce myofibroblast transdifferentiation (Hinz *et al.,* 2007). The presence of activated of TGF-β1, specialised ECM, for example FN1-EDA, and extracellular mechanical stress. Mechanical stress generated by stiff ECM and cell-matrix junctions such as cadherins. This mechanical tension is produced by the increase production of ECM: collagens, fibronectins and proteoglycans for example versican. The mechanical stiffness has additional roles in promoting myofibroblasts, TGF-β1 can be activated from its latent form through contraction (Wipff *et al*., 2007) and mechanical stimulation can cause CTGF expression has been found to increase in gingival fibroblasts (Guo, Carter, & Leask, 2011).

In this study, in both oral (only DENF319) and dermal fibroblasts miR-145 was able to prevent the TGF-β1 induction of myofibroblasts ECM markers and regulated endogenous levels of COL1A1 and FN1-EDA. This is consistent with data from Zhao *et al.,* (2015) study in vascular smooth muscle cells, which revealed miR-145 as being able to orchestrate the TGF-β1 cellular response by inhibiting TGF-βRII and resulting in the inhibition of TGF-β1 upregulated ECM rather than regulating αSMA.

Connective tissue growth factor (CTGF/ CCN2) is an important in stromal remodelling in both fibrosis and tumours including HNSCC (Mullis, Tang, & Chong, 2008). It modulates EMT within the tumour microenvironment (Chang *et al.,* 2013) and has been reported to be involved in ECM remodelling in fibrosis and to be necessary for dermal myofibroblast TGF-β1 stimulated transdifferentiation (Garrett *et al*., 2004). miR-145 has been shown to directly target CTGF in glioma cells (Lee *et al*., 2013), therefore CTGF expression was assessed in the oral fibroblasts characterised here. Like the previous study miR-145 overexpression was able to downregulate CTGF transcript levels in DENF319 and OF26 NOFS, but not DENF316 where there was an increase. TGF-β1 caused a marked increase in CTGF, suggesting CTGF is as previous studies have

suggested a key mediator of TGF-β1 induced transdifferentiation. miR-145 was able to reduce the TGF-β1 mediated CTGF increase, but there was still a large fold increase in CTGF expression compared to other genes investigated. As CTGF plays a significant role in HNSCCs and fibrosis, it would be interesting to further investigate its effects in oral myofibroblasts transdifferentiation.

Cadherin 11 is important in myofibroblasts phenotype, it can act as a marker as it becomes neo-expressed in myofibroblasts, but is also important for their contractility (Hinz *et al.,* 2004) and mechanoperception. miR-145 negatively regulates cadherin 11 through mucin in breast cancer cell lines (Sachdeva & Mo, 2010), miR-145 may in part disrupt TGF-β1 induced myofibroblasts contractility through the regulation of cadherin 11. Another role for cadherin 11 is to bind to β catenin The activation of the Wnt pathway has been shown to induce MSCs to become myofibroblasts (Sun *et al*., 2014).

miR-145 regulates several genes involved in actin cytoskeletal organization and remodelling (reviewed Xin *et al*., 2009) e.g. cofilin, actin-related protein 2/3 complex, Rho kinase ROCK and various actin binding proteins. Collectively these are involved in the maintenance of the actin cytoskeleton. miR-145 may act to prevent myofibroblast transdifferentiation and prevent stress fibre formation in part by collectively targeting the actin machinery.

8.12 *miR-145 regulation of the TGF-β signalling pathway*

One explanation of how miR-145 is able to inhibit and reverse TGF-β1 induced oral and dermal myofibroblasts is that it can regulate the TGF-β1 pathway itself. Diana pathway software identified a number of potential targets of miR-145 within the TGF-β1 pathway including TGF-β receptor II, smad3, smad4 and smad5. From the literature, most of these look like promising targets (Vlachos *et al.,* 2012). Smad3 negatively correlates with miR-145 expression (Megiorni *et al.,* 2013) and recently the smad3 3'UTR was shown to be a direct target of miR-145 in a nasopharyngeal cancer study and contributed to miR-145s tumour suppressive effects (Huang *et al*., 2015). Smad4 and Smad5 were both upregulated in miR-145 knockout mice (Caruso *et al.,* 2012). It has also been previously shown that miR-145 targets TGF-βRII (Zhao *et al.,* 2015) and our results confirmed this regulation.

To further understand how miR-145 regulates TGF-β signalling. A method of assessing TGF-β1 signalling needs to establish in these cells. Primers for smad3, 4 and 5 and antibodies for the smads phosphorylated and unphosphorylated form could be used to assess the relative activity of TGF-β1 signalling, however, a smad reporter assay may be the most sensitive measure of

overall TGF-β1 signalling. These are dual luciferase assays using a reporter luciferase gene downstream of multiple smad transcriptional response elements under the control of a strong promoter.

In addition miR-145 has been shown to target Ca^{2+} /calmodulin kinase (CAMKII δ) (Cordes *et al.,* 2009) which has been previously indicated to be involved with TGF-β1 signal transduction (Midgley *et al.,* 2013).

8.13 *miR-145 as a protective mechanism.*

A previous study in VSMCs, led authors to hypothesise that miR-145 serves as a checkpoint in TGF-β1 based diseases (Zhao *et al.,* 2015). This study validated TGF-βRII as a target of miR-145 and showed that miR-145 is capable of having differential effects within smooth muscle cells. Interestingly, the authors showed that miR-145 can function to prevent TGF-β1 induced matrix gene expression, but allow the TGF-β1 mediated increase in αSMA. They suggested that in the presence of miR-145, TGF-β1 promotes a 'contractile' phenotype, where matrix genes are downregulated, but in the absence of miR-145 it promotes a 'synthetic', matrix rich phenotype, like that of fibrosis. The study also found evidence for miR-145 having an anti-fibrotic role, as the loss of miR-145 increases cardiovascular fibrosis.

This study supports the data outlined in this thesis outlining an anti-fibrotic role for miR-145, the expression of miR may be lost in the acquisition of a myofibroblast phenotype. Data from this thesis and published work from this lab has shown miR-145 expression is downregulated in response to VB6 conditioned media and cigarette smoke extract in fibroblasts (Pal *et al.,* 2013), perhaps the loss of miR-145 is the first checkpoint leading to myofibroblast transdifferentiation.

8.14 *Limitations of the study*

The study assessed the myofibroblast phenotype by looking at 3 molecular markers of myofibroblasts; αSMA, FN1-EDA and COL1A1, as well as the ability of the fibroblasts to contract, although is this enough evidence to confirm that the cells are myofibroblasts. After all, some TGF-β1 induced myofibroblasts did not express higher levels of some markers. Some fibroblasts display some characteristics of myofibroblasts without expressing αSMA, these cells are thought to be *en route* to complete myofibroblasts transdifferentiation, termed protomyofibroblast (Tomasek *et al.,* 2002). It would be valuable to assess extra markers of CAFs and myofibroblasts, to confirm that the phenotype assessed in this study were really myofibroblast – like CAFs.

In particular tenascin-c, could be an important marker to investigate as it has been documented to be important for oral myofibroblast transdifferentiation. Tenascin-c and its receptor αvβ6, which were both found to be only expressed in OSCC specimens not normal controls (Ramos *et al*., 1997). Although in vitro tenascin-c was found to be secreted by both the OSCC cell lines and fibroblasts, when human SCC cell lines were injected in a murine model tenascin-c was only expressed in reactive stroma, where it was identified to be secreted only by the murine CAFs. Suggesting tenascin-c could be a suitable marker for CAFs in OSCCs.

Another marker of myofibroblasts is an increased number of focal adhesions, this could be assessed by Scanning Electron Microscopy. In addition the orientation of the smooth muscle filaments in indicative of myofibroblasts, a method of assessing the percentage of the same orientated fibroblasts could further validate the myofibroblast transdifferentiation. However, in line with other studies it is reasonable to assume that the αSMA positive fibroblasts observed in this study were myofibroblasts, despite some not consistently expressing other myofibroblast markers COL1A (DENF319) or in some cases, FN1-EDA.

Within the fibroblasts isolated from a tumour there will be a heterogenous population of fibroblasts. By using CAFs from OSCC in theory you would be studying an array of different CAF subtypes, however due to some being senescent and others growing at different rates and, there is a danger the in culture fibroblasts will lose their heterogeneity. FACs sorting CAFs from OSCCs immediately and sub culturing individual clones to assess the contribution of different CAFs would be one way to address this heterogeneity. In addition by studying just myofibroblast markers, and not markers for the senescent phenotype or any other CAF marker, the effect of TGF-β1, miR-145 or versican on other CAF populations is unknown.

The functional assays used in this study often produced varied results, these *in vitro* assays oversimplify a very complex multistep paracrine migration and invasion processes that result from a contribution of many different cells of the tumour microenvironment. Using 3D organotypic models may be a more physiologically relevant way of assessing invasion. In addition another way of quantifying fluorescence in immunocytochemistry, rather than total fluorescence, would be useful as the ImageJ software used was not very sensitive to the intensity of the stress fibres.

8.15 *Future work*

The data described in this study has raised many questions regarding the molecular mechanisms of myofibroblast transdifferentiation and has pointed to further experiments that could be carried out to aspire to complete the study.

Loss of function experiments were performed in this study, but the antimiR-145 was not effective at knocking down miR-145 transcripts; to fully investigate its role within CAFs another method of loss of function should be implemented. MiRNA sponges, plasmid constructs containing multiple miR-145 binding sites can sequester endogenous miR-145 levels and result in stable or transient knock-down. This especially would be important for assessing if miR-145 acts as a checkpoint, and needs to be downregulated to allow fibrosis. Stable knock-down of miR-145 would also help to explain the mechanism behind miR-145s regulation of myofibroblasts markers. In addition, it would help to assess whether DENF319 mediates TGF-β1 effects through miR-145, as the data suggests that both TGF-β1 and miR-145 downregulate MMP2 and COL1A, and TGF-β1 leads to the upregulation of miR-145.

As mentioned previously, the ECM surrounding fibroblasts seems key in the regulation of cellular signalling and promoting a stiff mechanical environment to promote myofibroblast transdifferentiation. The data presented here has pointed to some of the ways in which fibroblasts may remodel the ECM, e.g. TGF-β1 induction of metalloproteases. The TGF-β1 mediated deposition and remodelling of the ECM, and the potential miR-145 prevention/reversal of this ECM should be investigated further. Optimisation of the versican neo-epitope and chondroitin free immunoblotting should be carried out. MMP2 and MMP9 are important for ECM remodelling but also for activating TGF-β1 signalling, therefore zymography should be performed to investigate whether they are active in the induced myofibroblasts.

As experiments performed produced different data than previous myofibroblast studies, a greater number of fibroblasts from different sites should be used in future study to reinforce our data from oral and dermal fibroblasts. Human adult pulmonary and cardiac fibroblasts would be included to see if miR-145 is anti-myofibroblastic in these cells. It would also be useful to obtain MRC-5, the foetal pulmonary fibroblasts to confirm what other authors found (Yang *et al*., 2013). Also, increasing the size of the CAF cohort would be important for future study. Unfortunately a small cohort of CAFs was used in this study, with only one fibroblast from an oral dysplasia, therefore nothing can be deduced from the dysplastic CAF data. The study could also look at normal oral fibroblasts from different sites within the oral cavity, e.g. periodontal or

buccal fibroblasts, to assess whether the data described could translate to treat myofibroblasts in other oral lesions (Pinisetti *et al.,* 2014).

To assess the true therapeutic value of miR-145 further analysis of miR-145s functional effects of myofibroblasts need to be evaluated. More invasion studies could be performed, especially as TGF-β1 produced opposite effects in the two NOFs used. In addition the use of *in vivo* animal models would be invaluable to assess whether miR-145 could treat myofibroblasts in models of fibrosis or in desmoplastic stroma of cancers. As mentioned previously it may be possible that the miR-145 regulation of the myofibroblasts phenotype is different in humans and in mice, therefore it may be more appropriate to use 3D organotypic models of carcinomas (Moharamzadeh *et al*., 2012) built using fibroblasts or CAFs that are stably transfected with miR-145 mimics or antimiR-145, to see the effect on cancer cell invasion. These 3D models are also excellent tools for assessing drug delivery efficacy, myofibroblast could be used in the 3D model of oral carcinoma and used to test the effect of exogenous miR-145 delivery.

Tissue specimens from OSCCs should be used to assess myofibroblasts in patients. Immunohistochemistry using antibodies to αSMA, versican and cleaved versican could be performed to assess its expression in normal oral mucosa, dysplasias, moderate OSCCs and metatastic OSCCs. The location of the myofibroblasts within tumour may reveal more information about tumourigenesis, Lewis *et al*., (2004) found myofibroblasts in close proximity to the tumour and suggested that the fibroblasts must be transdifferentiated by the tumour itself.

The study has highlighted some similarities and some differences in myofibroblasts and smooth muscle cells regulation of αSMA, further experiments investigating the effect of miR-145 in the regulation of smooth muscle related transcription factors should be performed in human smooth muscle cells to compare the distinct molecular mechanisms controlling the expression of contractile genes in the different cell types. In addition, to further delineate miR-145s actions in the tumour microenvironment it is important to identify and validate novel transcriptional targets and confirm previously published targets.

8.16 *Conclusions and clinical relevance*

Data described in this thesis outlines miR-145 as being a key regulator of myofibroblasts transdifferentiation, a pro-tumourigenic and pro-fibrotic phenotype. miR-145 overexpression was able to prevent and partially reverse TGF-β1 induced oral and dermal myofibroblastic

phenotype and associated pro-tumourigenic paracrine effects. Another important finding is that miR-145 negatively regulates oncogenic extracellular proteoglycan versican, more so than miR-143, which had been previously published to target versican, although the mechanism of this regulation remains to be delineated.

Although the exact mechanisms need further investigation, the data suggests that miR-145 is able to negatively regulate TGF-β1 signalling and is able to prevent TGF-β1 from stimulating pro-tumourigenic paracrine effects. The results presented here have pointed to miR-145 being a master regulator of myofibroblast phenotype. It suggests that miR-145, regulates smooth muscle transcription factors (MRTF-B and KLF4), which can control the expression of contractile genes and also several genes that modulate the ECM and cell signalling (versican, ADAMTS-1, ADAMTS-4, Sox-9, TGF-RII) that combined have a large effect on the whole myofibroblast phenotype. miR-145 has several predicted targets in the TGF-β1 signalling pathway itself, but also dramatically prevents TGF-β1 signalling from inducing genes which aid in facilitating myofibroblast transdifferentiation and stromal remodelling, e.g. CTGF, MMP2, KLF5, versican, ADAMTS-1, ADAMTS-4, FN1-EDA and COL1A1.

The study has highlighted the exciting potential of exogenously delivering miR-145 to reverse the detrimental effects of myofibroblast in chronic fibrotic disorders and in the tumour microenvironment. Specialised delivery techniques to target miRs to the tumour microenvironment are currently in development, a miR conjugation to a low pH induced transmembrane structure which inserts into the cell membrane of cells within a low pH environment, for example a tumour, is a recent promising breakthrough (Cheng *et al*., 2014). miR-145 gene therapy could be an excellent therapy in HNSCC as miR-145, also a potent tumour suppressor, is often downregulated, therefore miR-145 could treat collectively the tumour cells and the tumour microenvironment. So far miR-145 delivery via lentiviral transfection to xenografts has been successful in halting tumour progression (Yu *et al*., 2013). The same study also showed a non-gene therapy of curcumin had the same effect of preventing tumour progression by the upregulation of miR-145 by direct promoter activation. However, despite the exciting potential miR-145 has shown for a potential therapy for treating both the tumour microenvironment and tumour itself, future work to investigate miR-145 exact targets and molecular mechanisms in the regulation of myofibroblast transdifferentiation *in vitro* and *in vivo* are required to progress towards the clinic.

References

Akao, Y., Nakagawa, Y., Hirata, I., Iio, A., Itoh, T., Kojima, K.,Nakashima, R., Kitade, Y., & Naoe, T. (2010). Role of anti-oncomirs miR-143 and -145 in human colorectal tumors. *Cancer Gene Therapy, 17*(6), 398–408.

Akimoto, T., Mitsuhashi, N., Saito, Y., Ebara, T., & Niibe, H. (1998). Effect of radiation on the expression of E-cadherin and alpha-catenin and invasive capacity in human lung cancer cell line in vitro. *International Journal of Radiation Oncology, Biology, Physics, 41*(5), 1171–6.

Alexa, A., Baderca, F., Lighezan, R., & Izvernariu, D. (2009). Myofibroblasts reaction in urothelial carcinomas. *Romanian Journal of Morphology and Embryology = Revue Roumaine de Morphologie et Embryologie, 50*(4), 639–43.

Allen, M., & Louise Jones, J. (2011). Jekyll and Hyde: the role of the microenvironment on the progression of cancer. *The Journal of Pathology, 223*(2), 162–76.

Ambros, V., Bartel, B., Bartel, D. P., Burge, C. B., Carrington, J. C., Chen, X., Dreyfuss, G., Eddy, S. R., Griffiths-Jones, S., Marshall, M., Matzke, M., Ruvkuo, M., & Tuschl, T. (2003). A uniform system for microRNA annotation. *RNA, 9*(3), 277–9.

Ang, K. K., Harris, J., Wheeler, R., Weber, R., Rosenthal, D. I., Nguyen-Tân, P. F., Westra, W. H., Chung, C. H., Jordan, R. C., Lu, C., Kin, H., Axelrod, R., Silverman, C., Redmond, K. P., & Gillison, M. L. (2010). Human papillomavirus and survival of patients with oropharyngeal cancer. *The New England Journal of Medicine, 363*(1), 24–35.

Ang, L. C., Zhang, Y., Cao, L., Yang, B. L., Young, B., Kiani, C., Lee, V., Allan, K., & Yang, B. B. (1999). Versican enhances locomotion of astrocytoma cells and reduces cell adhesion through its G1 domain. *Journal of Neuropathology and Experimental Neurology, 58*(6), 597–605.

Annes, J. P., Chen, Y., Munger, J. S., & Rifkin, D. B. (2004). Integrin alphaVbeta6-mediated activation of latent TGF-beta requires the latent TGF-beta binding protein-1. *The Journal of Cell Biology, 165*(5), 723–34.

Annes, J. P., Munger, J. S., & Rifkin, D. B. (2003). Making sense of latent TGFbeta activation. *Journal of Cell Science, 116*(Pt 2), 217–24.

Aprelikova, O., Yu, X., Palla, J., Wei, B.-R., John, S., Yi, M., Stephens, R., Simpson, R. M., Risinger, J. I., Jazaeri, A., & Niederhuber, J. (2010). The role of miR-31 and its target gene SATB2 in cancer-associated fibroblasts. *Cell Cycle, 9*(21), 4387–98.

Arora, P. D., Narani, N., & McCulloch, C. A. (1999). The compliance of collagen gels regulates transforming growth factor-beta induction of alpha-smooth muscle actin in fibroblasts. *The American Journal of Pathology, 154*(3), 871–82.

Arslan, F., Bosserhoff, A.-K., Nickl-Jockschat, T., Doerfelt, A., Bogdahn, U., & Hau, P. (2007). The role of versican isoforms V0/V1 in glioma migration mediated by transforming growth factor-beta2. *British Journal of Cancer, 96*(10), 1560–8.

Augsten, M. (2014). Cancer-associated fibroblasts as another polarized cell type of the tumor microenvironment. *Frontiers in Oncology, 4,* 62.

Baek, D., Villén, J., Shin, C., Camargo, F. D., Gygi, S. P., & Bartel, D. P. (2008). The impact of microRNAs on protein output. *Nature, 455*(7209), 64–71.

Bai, J., Zhang, N., Hua, Y., Wang, B., Ling, L., Ferro, A., & Xu, B. (2013). Metformin inhibits angiotensin II-induced differentiation of cardiac fibroblasts into myofibroblasts. *PloS One, 8*(9), e72120.

Balza, E., Borsi, L., Allemanni, G., & Zardi, L. (1988). Transforming growth factor beta regulates the levels of different fibronectin isoforms in normal human cultured fibroblasts. *FEBS Letters, 228*(1), 42–4.

Bar, J., Feniger-Barish, R., Lukashchuk, N., Shaham, H., Moskovits, N., Goldfinger, N., Simansky, D., Perlman, M., Papa, M., Yosepovich, A., Rechavi, G., Rotter, V., & Oren, M. (2009). Cancer cells suppress p53 in adjacent fibroblasts. *Oncogene, 28*(6), 933–6.

Bar, J., Moskovits, N., & Oren, M. (2010). Involvement of stromal p53 in tumor-stroma interactions. *Seminars in Cell & Developmental Biology, 21*(1), 47–54.

Barcellos-Hoff, M. H. (1993). Radiation-induced transforming growth factor beta and subsequent extracellular matrix reorganization in murine mammary gland. *Cancer Research, 53*(17), 3880–6.

Barcellos-Hoff, M. H., & Ravani, S. A. (2000). Irradiated mammary gland stroma promotes the expression of tumorigenic potential by unirradiated epithelial cells. *Cancer Research, 60*(5), 1254–60.

Baroukh, N., Ravier, M. A., Loder, M. K., Hill, E. V, Bounacer, A., Scharfmann, R., Rutter, G. A., & Van Obberghen, E. (2007). MicroRNA-124a regulates Foxa2 expression and intracellular signaling in pancreatic beta-cell lines. *The Journal of Biological Chemistry, 282*(27), 19575–88.

Barth, P. J., Schenck zu Schweinsberg, T., Ramaswamy, A., & Moll, R. (2004). CD34+ fibrocytes, alpha-smooth muscle antigen-positive myofibroblasts, and CD117 expression in the stroma of invasive squamous cell carcinomas of the oral cavity, pharynx, and larynx. *Virchows Archiv : An International Journal of Pathology, 444*(3), 231–4.

Bates, R. C., Bellovin, D. I., Brown, C., Maynard, E., Wu, B., Kawakatsu, H., Sheppard, D., Oettgen, P., & Mercurio, A. M. (2005). Transcriptional activation of integrin beta6 during the epithelial-mesenchymal transition defines a novel prognostic indicator of aggressive colon carcinoma. *The Journal of Clinical Investigation, 115*(2), 339–47.

Bebek, G., Orloff, M., & Eng, C. (2011). Microenvironmental genomic alterations reveal signaling networks for head and neck squamous cell carcinoma. *Journal of Clinical Bioinformatics, 1*(1), 21.

Bello, I. O., Vered, M., Dayan, D., Dobriyan, A., Yahalom, R., Alanen, K., Nieminen, P., Kantola, S., Läärä, E., & Salo, T. (2011). Cancer-associated fibroblasts, a parameter of the tumor microenvironment, overcomes carcinoma-associated parameters in the prognosis of patients with mobile tongue cancer. *Oral Oncology, 47*(1), 33–8.

Bennett, J. H., Morgan, M. J., Whawell, S. A., Atkin, P., Roblin, P., Furness, J., & Speight, P. M. (2000). Metalloproteinase expression in normal and malignant oral keratinocytes: stimulation of MMP-2 and -9 by scatter factor. *European Journal of Oral Sciences, 108*(4), 281–91.

Bhattacharyya, S., Tamaki, Z., Wang, W., Hinchcliff, M., Hoover, P., Getsios, S., White, E. S., & Varga, J. (2014). FibronectinEDA promotes chronic cutaneous fibrosis through Toll-like receptor signaling. *Science Translational Medicine, 6*(232), 232ra50.

Bhowmick, N. A., Chytil, A., Plieth, D., Gorska, A. E., Dumont, N., Shappell, S., Washington, M. K., Neilson, E. G., & Moses, H. L. (2004). TGF-beta signaling in fibroblasts modulates the oncogenic potential of adjacent epithelia. *Science, 303*(5659), 848–51.

Bhowmick, N. A., Neilson, E. G., & Moses, H. L. (2004). Stromal fibroblasts in cancer initiation and progression. *Nature, 432*(7015), 332–7.

Bierie, B., & Moses, H. L. TGF-beta and cancer. *Cytokine & Growth Factor Reviews, 17*(1-2), 29–40.

Bierie, B., & Moses, H. L. (2006). Tumour microenvironment: TGFbeta: the molecular Jekyll and Hyde of cancer. *Nature Reviews. Cancer, 6*(7), 506–20.

Bingle, L., Brown, N. J., & Lewis, C. E. (2002). The role of tumour-associated macrophages in tumour progression: implications for new anticancer therapies. *The Journal of Pathology, 196*(3), 254–65.

Blobel, C. P. (2005). ADAMs: key components in EGFR signalling and development. *Nature Reviews. Molecular Cell Biology, 6*(1), 32–43.

Bode-Lesniewska, B., Dours-Zimmermann, M. T., Odermatt, B. F., Briner, J., Heitz, P. U., & Zimmermann, D. R. (1996). Distribution of the large aggregating proteoglycan versican in adult human tissues. *The Journal of Histochemistry and Cytochemistry : Official Journal of the Histochemistry Society, 44*(4), 303–12.

Borsi, L., Castellani, P., Risso, A. M., Leprini, A., & Zardi, L. (1990). Transforming growth factor-beta regulates the splicing pattern of fibronectin messenger RNA precursor. *FEBS Letters, 261*(1), 175–8.

Bourd-Boittin, K., Bonnier, D., Leyme, A., Mari, B., Tuffery, P., Samson, M., Ezan, F., Baffet, G., & Theret, N. (2011). Protease profiling of liver fibrosis reveals the ADAM metallopeptidase with thrombospondin type 1 motif, 1 as a central activator of transforming growth factor beta. *Hepatology, 54*(6), 2173–84.

Bourguignon, L. Y. W., Singleton, P. A., Zhu, H., & Zhou, B. (2002). Hyaluronan promotes signaling interaction between CD44 and the transforming growth factor beta receptor I in metastatic breast tumor cells. *The Journal of Biological Chemistry, 277*(42), 39703–12.

Boussif, O., Lezoualc'h, F., Zanta, M. A., Mergny, M. D., Scherman, D., Demeneix, B., & Behr, J. P. (1995). A versatile vector for gene and oligonucleotide transfer into cells in culture and in vivo: polyethylenimine. *Proceedings of the National Academy of Sciences of the United States of America, 92*(16), 7297–301.

Boy, J. (2002). The Extracellular Matrix of Animals. In Alberts, B., Johnson, A., Lewis, J., Martin, R., &Roberts, K., *The Molecular Biology of the Cell* (4th Ed). New York, NY: Garland Science.

Brennecke, J., Stark, A., Russell, R. B., & Cohen, S. M. (2005). Principles of microRNA-target recognition. *PLoS Biology, 3*(3), e85.

Breuss, J. M., Gallo, J., DeLisser, H. M., Klimanskaya, I. V, Folkesson, H. G., Pittet, J. F., Nishimura, S. L., Aldape, D. V., Landers, W., Carpenter, W., Gillet, N., Sheppard, D., Matthay, M. A., Albelda, S. M., Kramer, R. H., & Pytela, R. (1995). Expression of the beta 6 integrin subunit in development, neoplasia and tissue repair suggests a role in epithelial remodeling. *Journal of Cell Science, 108*(6), 2241–51.

Bullock, M. D., Pickard, K. M., Nielsen, B. S., Sayan, A. E., Jenei, V., Mellone, M., Mitter, R., Primrose, J. N., Thomas, G. J., Packham, G. K., & Mirnezami, A. H. (2013). Pleiotropic actions of miR-21 highlight the critical role of deregulated stromal microRNAs during colorectal cancer progression. *Cell Death & Disease,* 4, e684.

Burtness, B., Goldwasser, M. A., Flood, W., Mattar, B., & Forastiere, A. A. (2005). Phase III randomized trial of cisplatin plus placebo compared with cisplatin plus cetuximab in metastatic/recurrent head and neck cancer: an Eastern Cooperative Oncology Group study. *Journal of Clinical Oncology : Official Journal of the American Society of Clinical Oncology, 23*(34), 8646–54.

Calin, G. A., Dumitru, C. D., Shimizu, M., Bichi, R., Zupo, S., Noch, E., Alder, H., Rattan, S., Keating, M., Rai, K., Rassenti, L., Kipps, T., Negripi, M., Bullrich, F., & Croce, C. M. (2002). Frequent deletions and down-regulation of micro- RNA genes miR15 and miR16 at 13q14 in chronic lymphocytic leukemia. *Proceedings of the National Academy of Sciences of the United States of America, 99*(24), 15524–9.

Calin, G. A., Ferracin, M., Cimmino, A., Di Leva, G., Shimizu, M., Wojcik, S. E., Iorio, M. V., Visone, R., Sever, N. I., Fabbri, M., Iuliano, R., Palumbo, T., Pichiorri, F., Roldo, C., Garzon, R., Sevignani, C., Rassenti, L., Alder, H., Volinia, S., Liu, C. G., Kipps, T. J., Negrini, M., & Croce, C. M. (2005). A MicroRNA signature associated with prognosis and progression in chronic lymphocytic leukemia. *The New England Journal of Medicine, 353*(17), 1793–801.

Calin, G. A., Sevignani, C., Dumitru, C. D., Hyslop, T., Noch, E., Yendamuri, S., Shimizu, M., Rattan, S., Bullrich, F., Negrini, M., & Croce, C. M. (2004). Human microRNA genes are frequently located at fragile sites and genomic regions involved in cancers. *Proceedings of the National Academy of Sciences of the United States of America, 101*(9), 2999–3004.

Campisi, J., & d'Adda di Fagagna, F. (2007). Cellular senescence: when bad things happen to good cells. Nature Reviews. *Molecular Cell Biology, 8*(9), 729–40.

Cardone, A., Tolino, A., Zarcone, R., Borruto Caracciolo, G., & Tartaglia, E. (1997). Prognostic value of desmoplastic reaction and lymphocytic infiltration in the management of breast cancer. *Panminerva Medica, 39*(3), 174–7.

Carmeliet, P., Ferreira, V., Breier, G., Pollefeyt, S., Kieckens, L., Gertsenstein, M., Fahrig, M., Vandenhoeck, A., Harpal, K., Eberhardt, C., Declercg, C., Pawling, J., Moons, L., Collen, D., Risau, W., & Nagy, A. (1996). Abnormal blood vessel development and lethality in embryos lacking a single VEGF allele. *Nature, 380*(6573), 435–9.

Carmeliet, P., & Jain, R. K. (2000). Angiogenesis in cancer and other diseases. *Nature, 407*(6801), 249–57.

Caruso, P., Dempsie, Y., Stevens, H. C., McDonald, R. A., Long, L., Lu, R., White, K., Mair, K. M., McClure, J. D., Southwood, M., Upton, P., Xin, M., van Rooii, E., Olson, E. N., Morrell, N. W.,

MacLean, M. R., & Baker, A. H. (2012). A role for miR-145 in pulmonary arterial hypertension: evidence from mouse models and patient samples. *Circulation Research, 111*(3), 290–300.

Casey, T. M., Eneman, J., Crocker, A., White, J., Tessitore, J., Stanley, M., Tessitore, J., Stanley, M., Harlow, S., Bunn, J. Y., Weaver, D., Muss, H., & Plaut, K. (2008). Cancer associated fibroblasts stimulated by transforming growth factor beta1 (TGF-beta 1) increase invasion rate of tumor cells: a population study. *Breast Cancer Research and Treatment, 110*(1), 39–49.

Cattaruzza, S., Schiappacassi, M., Kimata, K., Colombatti, A., & Perris, R. (2004). The globular domains of PG-M/versican modulate the proliferation-apoptosis equilibrium and invasive capabilities of tumor cells. *FASEB Journal : Official Publication of the Federation of American Societies for Experimental Biology, 18*(6), 779–81.

Chang, C.-C., Hsu, W.-H., Wang, C.-C., Chou, C.-H., Kuo, M. Y.-P., Lin, B.-R., Chen, S. T., Tai, S. K., Kuo, M. L., & Yang, M.-H. (2013). Connective tissue growth factor activates pluripotency genes and mesenchymal-epithelial transition in head and neck cancer cells. *Cancer Research, 73*(13), 4147–57.

Chen, C., Bhalala, H. V, Qiao, H., & Dong, J.-T. (2002). A possible tumor suppressor role of the KLF5 transcription factor in human breast cancer. *Oncogene, 21*(43), 6567–72.

Chen, C. Y., & Schwartz, R. J. (1996). Recruitment of the tinman homolog Nkx-2.5 by serum response factor activates cardiac alpha-actin gene transcription. *Molecular and Cellular Biology, 16*(11), 6372–84.

Chen, H.-C., Chen, G.-H., Chen, Y.-H., Liao, W.-L., Liu, C.-Y., Chang, K.-P., Chang, Y.S., & Chen, S.-J. (2009). MicroRNA deregulation and pathway alterations in nasopharyngeal carcinoma. *British Journal of Cancer, 100*(6), 1002–11.

Chen, J.-H., Chen, W. L. K., Sider, K. L., Yip, C. Y. Y., & Simmons, C. A. (2011). β-catenin mediates mechanically regulated, transforming growth factor-β1-induced myofibroblast differentiation of aortic valve interstitial cells. *Arteriosclerosis, Thrombosis, and Vascular Biology, 31*(3), 590–7.

Chen, X., Guo, X., Zhang, H., Xiang, Y., Chen, J., Yin, Y., Cai, X., Wang, K., Wang, G., Ba, Y., Zhu, L., Wang, J., Yang, R., Zhang, Y., Ren, Z., Zen, K., Zhang, J., & Zhang, C.-Y. (2009). Role of miR-143 targeting KRAS in colorectal tumorigenesis. *Oncogene, 28*(10), 1385–92.

Cheng, C. J., Bahal, R., Babar, I. A., Pincus, Z., Barrera, F., Liu, C., Syoronos, A., Braddock, D. T., Glazer, P. M., Engelman, D. M., Saltzman, W. M., & Slack, F. J. (2014). MicroRNA silencing for cancer therapy targeted to the tumour microenvironment. *Nature, 518*(7537), 107–10.

Cheng, Y., Liu, X., Yang, J., Lin, Y., Xu, D.-Z., Lu, Q., Deitch, E. A., Huo, Y., Delphin, E. S., & Zhang, C. (2009). MicroRNA-145, a novel smooth muscle cell phenotypic marker and modulator, controls vascular neointimal lesion formation. *Circulation Research, 105*(2), 158–66.

Chien, W., O'Kelly, J., Lu, D., Leiter, A., Sohn, J., Yin, D., Karlan, B., Vadgama, J., Lyon, K. M., & Koeffler, H. P. (2011). Expression of connective tissue growth factor (CTGF/CCN2) in breast cancer cells is associated with increased migration and angiogenesis. *International Journal of Oncology, 38*(6), 1741–7.

Chivukula, R. R., Shi, G., Acharya, A., Mills, E. W., Zeitels, L. R., Anandam, J. L., Abdelnaby, A. A., Balch, G. C., Mansour, J. C., Yopp, A. C., Maitra, A., & Mendell, J. T. (2014). An essential

mesenchymal function for miR-143/145 in intestinal epithelial regeneration. *Cell, 157*(5), 1104–16.

Chong, M. M. W., Zhang, G., Cheloufi, S., Neubert, T. a, Hannon, G. J., & Littman, D. R. (2010). Canonical and alternate functions of the microRNA biogenesis machinery. *Genes & Development, 24*(17), 1951–60.

Chuang, J.-Y., Yang, W.-Y., Lai, C.-H., Lin, C.-D., Tsai, M.-H., & Tang, C.-H. (2011). CTGF inhibits cell motility and COX-2 expression in oral cancer cells. *International Immunopharmacology, 11*(8), 948–54.

Cimmino, A., Calin, G. A., Fabbri, M., Iorio, M. V, Ferracin, M., Shimizu, M., Woicik, S. E., Ageilan, R. I., Zuno, S., Dono, M. I., Rassenti, L., Alder, H., Volinia, S., Liu, C. G., Kipps, T. J., Negrini, M., & Croce, C. M. (2005). miR-15 and miR-16 induce apoptosis by targeting BCL2. *Proceedings of the National Academy of Sciences of the United States of America, 102*(39), 13944–9.

Clark, R. A. F., & Henson, P. M. (Eds.). (1988). The Molecular and Cellular Biology of Wound Repair. Boston, MA: Springer US.

Climent-Salarich, M., Quintavalle, M., Miragoli, M., Chen, J., Condorelli, G., & Elia, L. (2015). TGFβ Triggers miR-143/145 Transfer from Smooth Muscle Cells to Endothelial Cells, Thereby Modulating Vessel Stabilization. *Circulation Research, CIRCRESAHA*, *116*(11):1753-64.

Colotta, F., Allavena, P., Sica, A., Garlanda, C., & Mantovani, A. (2009). Cancer-related inflammation, the seventh hallmark of cancer: links to genetic instability. *Carcinogenesis, 30*(7), 1073–81.

Coppe, J.-P., Boysen, M., Sun, C. H., Wong, B. J. F., Kang, M. K., Park, N.-H., Desprez, P. Y., Campisi, J., & Krtolica, A. (2008). A role for fibroblasts in mediating the effects of tobacco-induced epithelial cell growth and invasion. *Molecular Cancer Research : MCR, 6*(7), 1085–98.

Cordes, K. R., Sheehy, N. T., White, M. P., Berry, E. C., Morton, S. U., Muth, A. N., Lee, T. H., Miano, J. M., Ivey, K. N., & Srivastava, D. (2009). miR-145 and miR-143 regulate smooth muscle cell fate and plasticity. *Nature, 460*(7256), 705–10.

Corpet, F. (1988). Multiple sequence alignment with hierarchical clustering. *Nucleic Acids Research, 16*(22), 10881–90.

Crider, B. J., Risinger, G. M., Haaksma, C. J., Howard, E. W., & Tomasek, J. J. (2011). Myocardin-related transcription factors A and B are key regulators of TGF-β1-induced fibroblast to myofibroblast differentiation. *The Journal of Investigative Dermatology, 131*(12), 2378–85.

Dameron, K. M., Volpert, O. V, Tainsky, M. A., & Bouck, N. (1994). Control of angiogenesis in fibroblasts by p53 regulation of thrombospondin-1. *Science, 265*(5178), 1582–4.

Darby, I. A., Laverdet, B., Bonté, F., & Desmoulière, A. (2014). Fibroblasts and myofibroblasts in wound healing. *Clinical, Cosmetic and Investigational Dermatology, 7*, 301–11.

Davis-Dusenbery, B. N., Chan, M. C., Reno, K. E., Weisman, A. S., Layne, M. D., Lagna, G., & Hata, A. (2011). down-regulation of Kruppel-like factor-4 (KLF4) by microRNA-143/145 is critical for modulation of vascular smooth muscle cell phenotype by transforming growth factor-beta and bone morphogenetic protein 4. *The Journal of Biological Chemistry, 286*(32), 28097–110.

De Wever, O., Demetter, P., Mareel, M., & Bracke, M. (2008). Stromal myofibroblasts are drivers of invasive cancer growth. *International Journal of Cancer. Journal International Du Cancer, 123*(10), 2229–38.

De Wit, M., Belt, E. J. T., Delis-van Diemen, P. M., Carvalho, B., Coupé, V. M. H., Stockmann, H. B., Beljen, J. A., Fiineman, R. J., & Meijer, G. A. (2012). Lumican and Versican Are Associated with Good Outcome in Stage II and III Colon Cancer. *Annals of Surgical Oncology, 20*(3),:S348-59.

Desmoulière, A., Geinoz, A., Gabbiani, F., & Gabbiani, G. (1993). Transforming growth factor-beta 1 induces alpha-smooth muscle actin expression in granulation tissue myofibroblasts and in quiescent and growing cultured fibroblasts. *The Journal of Cell Biology, 122*(1), 103–11

Desmoulière, A., Redard, M., Darby, I., & Gabbiani, G. (1995). Apoptosis mediates the decrease in cellularity during the transition between granulation tissue and scar. *The American Journal of Pathology, 146*(1), 56–66.

Didangelos, A., Mayr, U., Monaco, C., & Mayr, M. (2012). Novel role of ADAMTS-5 protein in proteoglycan turnover and lipoprotein retention in atherosclerosis. *The Journal of Biological Chemistry, 287*(23), 19341–5.

Doberstein, K., Steinmeyer, N., Hartmetz, A.-K., Eberhardt, W., Mittelbronn, M., Harter, P. N., Juengel, E., Blaheta, R., Pfeilschifter, J., & Gutwein, P. (2013). MicroRNA-145 targets the metalloprotease ADAM17 and is suppressed in renal cell carcinoma patients. *Neoplasia, 15*(2), 218–30

Dours-Zimmermann, M. T., & Zimmermann, D. R. (1994). A novel glycosaminoglycan attachment domain identified in two alternative splice variants of human versican. *The Journal of Biological Chemistry, 269*(52), 32992–8.

Duursma, A. M., Kedde, M., Schrier, M., le Sage, C., & Agami, R. (2008). miR-148 targets human DNMT3b protein coding region. *RNA, 14*(5), 872–877.

Dvorak, H. F. (1986). Tumors: wounds that do not heal. Similarities between tumor stroma generation and wound healing. *The New England Journal of Medicine, 315*(26), 1650–9.

Eckes, B., Zigrino, P., Kessler, D., Holtkötter, O., Shephard, P., Mauch, C., & Krieg, T. (2000). Fibroblast-matrix interactions in wound healing and fibrosis. *Matrix Biology, 19*(4), 325–332.

Elayadi, A. N., Samli, K. N., Prudkin, L., Liu, Y.-H., Bian, A., Xie, X.-J., Wistuba, I. I., Roth, J. A., McGuire, M. J., & Brown, K. C. (2007). A peptide selected by biopanning identifies the integrin alphavbeta6 as a prognostic biomarker for nonsmall cell lung cancer. *Cancer Research, 67*(12), 5889–95.

Elenbaas, B., Spirio, L., Koerner, F., Fleming, M. D., Zimonjic, D. B., Donaher, J. L., Popescu, N. C., Hahn, W. C., & Weinberg, R. A. (2001). Human breast cancer cells generated by oncogenic transformation of primary mammary epithelial cells. *Genes & Development, 15*(1), 50–65.

Ellis, I. R., & Schor, S. L. (1996). Differential effects of TGF-beta1 on hyaluronan synthesis by fetal and adult skin fibroblasts: implications for cell migration and wound healing. *Experimental Cell Research, 228*(2), 326–33.

Enkelmann, A., Heinzelmann, J., von Eggeling, F., Walter, M., Berndt, A., Wunderlich, H., & Junker, K. (2011). Specific protein and miRNA patterns characterise tumour-associated fibroblasts in bladder cancer. *Journal of Cancer Research and Clinical Oncology, 137*(5), 751–9.

Evanko, S. P., Johnson, P. Y., Braun, K. R., Underhill, C. B., Dudhia, J., & Wight, T. N. (2001). Platelet-derived growth factor stimulates the formation of versican-hyaluronan aggregates and pericellular matrix expansion in arterial smooth muscle cells. *Archives of Biochemistry and Biophysics, 394*(1), 29–38.

Fabbri, M., Paone, A., Calore, F., Galli, R., Gaudio, E., Santhanam, R., Lovat, F., Fadda, P., Mao, C., Nuovo, G. J., Zanesi, N., Crawford, M., Ozer, G. H., Wernicke, D., Alder, H., Caligiuri, M. A., Nana-Sinkam P., Perrotti, D., & Croce, C. M. (2012). MicroRNAs bind to Toll-like receptors to induce prometastatic inflammatory response. *Proceedings of the National Academy of Sciences of the United States of America, 109*(31), E2110–6.

Fang, R., Xiao, T., Fang, Z., Sun, Y., Li, F., Gao, Y., Feng, Y., Li, L., Wang, Y., Liu, X., Chen, H., Liu, X. Y., & Ji, H. (2012). MicroRNA-143 (miR-143) Regulates Cancer Glycolysis via Targeting Hexokinase 2 Gene. *The Journal of Biological Chemistry, 287*(27), 23227–35.

Fang, Z., & Rajewsky, N. (2011). The impact of miRNA target sites in coding sequences and in 3'UTRs. *PloS One, 6*(3), e18067.

Forrester, E., Chytil, A., Bierie, B., Aakre, M., Gorska, A. E., Sharif-Afshar, A.-R., Muller, W. J., & Moses, H. L. (2005). Effect of conditional knockout of the type II TGF-beta receptor gene in mammary epithelia on mammary gland development and polyomavirus middle T antigen induced tumor formation and metastasis. *Cancer Research, 65*(6), 2296–302.

Gabriely, G., Wurdinger, T., Kesari, S., Esau, C. C., Burchard, J., Linsley, P. S., & Krichevsky, A. M. (2008). MicroRNA 21 promotes glioma invasion by targeting matrix metalloproteinase regulators. *Molecular and Cellular Biology, 28*(17), 5369–80.

Gaggioli, C., Hooper, S., Hidalgo-Carcedo, C., Grosse, R., Marshall, J. F., Harrington, K., & Sahai, E. (2007). Fibroblast-led collective invasion of carcinoma cells with differing roles for RhoGTPases in leading and following cells. *Nature Cell Biology, 9*(12), 1392–400.

Galie, P. A., Westfall, M. V, & Stegemann, J. P. Reduced serum content and increased matrix stiffness promote the cardiac myofibroblast transition in 3D collagen matrices. *Cardiovascular Pathology : The Official Journal of the Society for Cardiovascular Pathology, 20*(6), 325–33.

Garrett, Q., Khaw, P. T., Blalock, T. D., Schultz, G. S., Grotendorst, G. R., & Daniels, J. T. (2004). Involvement of CTGF in TGF-beta1-stimulation of myofibroblast differentiation and collagen matrix contraction in the presence of mechanical stress. *Investigative Ophthalmology & Visual Science, 45*(4), 1109–16.

Gebert, L. F. R., Rebhan, M. A. E., Crivelli, S. E. M., Denzler, R., Stoffel, M., & Hall, J. (2014). Miravirsen (SPC3649) can inhibit the biogenesis of miR-122. *Nucleic Acids Research, 42*(1), 609–21.

Giraldez, A. J., Mishima, Y., Rihel, J., Grocock, R. J., Van Dongen, S., Inoue, K., Enright, A. J., & Schier, A. F. (2006). Zebrafish MiR-430 promotes deadenylation and clearance of maternal mRNAs. *Science, 312*(5770), 75–9.

Goffin, J. M., Pittet, P., Csucs, G., Lussi, J. W., Meister, J.-J., & Hinz, B. (2006). Focal adhesion size controls tension-dependent recruitment of alpha-smooth muscle actin to stress fibers. *The Journal of Cell Biology, 172*(2), 259–68.

Gras, C., Ratuszny, D., Hadamitzky, C., Zhang, H., Blasczyk, R., & Figueiredo, C. (2015). miR-145 contributes to hypertrophic scarring of the skin by inducing myofibroblast activity. *Molecular Medicine*. Epub ahead of print.

Greer, R. O. (2006). Pathology of malignant and premalignant oral epithelial lesions. *Otolaryngologic Clinics of North America, 39*(2), 249–75, v.

Grum-Schwensen, B., Klingelhofer, J., Berg, C. H., El-Naaman, C., Grigorian, M., Lukanidin, E., & Ambartsumian, N. (2005). Suppression of tumor development and metastasis formation in mice lacking the S100A4(mts1) gene. *Cancer Research, 65*(9), 3772–80.

Gulyás, M., & Hjerpe, A. (2003). Proteoglycans and WT1 as markers for distinguishing adenocarcinoma, epithelioid mesothelioma, and benign mesothelium. *The Journal of Pathology, 199*(4), 479–87.

Guo, F., Carter, D. E., & Leask, A. (2011). Mechanical Tension Increases CCN2/CTGF Expression and Proliferation in Gingival Fibroblasts via a TGFβ-Dependent Mechanism. *PLoS ONE, 6*(5), e19756.

Haase, H. R., Clarkson, R. W., Waters, M. J., & Bartold, P. M. (1998). Growth factor modulation of mitogenic responses and proteoglycan synthesis by human periodontal fibroblasts. *Journal of Cellular Physiology, 174*(3), 353–61.

Hanahan, D., & Weinberg, R. A. (2000). The hallmarks of cancer. *Cell, 100*(1), 57–70.

Hanna, E., Quick, J., & Libutti, S. K. (2009). The tumour microenvironment: a novel target for cancer therapy. *Oral Diseases, 15*(1), 8–17.

Hassona, Y., Cirillo, N., Heesom, K., Parkinson, E. K., & Prime, S. S. (2014). Senescent cancer-associated fibroblasts secrete active MMP-2 that promotes keratinocyte dis-cohesion and invasion. *British Journal of Cancer, 111*(6), 1230–7.

Hassona, Y., Cirillo, N., Lim, K. P., Herman, A., Mellone, M., Thomas, G. J., Pitiyage, G. N., Parkinson, E. K., & Prime, S. S. (2013). Progression of genotype-specific oral cancer leads to senescence of cancer-associated fibroblasts and is mediated by oxidative stress and TGF-β. *Carcinogenesis, 34*(6), 1286–95.

Hattori, N., Carrino, D. a, Lauer, M. E., Vasanji, A., Wylie, J. D., Nelson, C. M., & Apte, S. S. (2011). Pericellular versican regulates the fibroblast-myofibroblast transition: a role for ADAMTS5 protease-mediated proteolysis. *The Journal of Biological Chemistry, 286*(39), 34298–310.

Hayashi, N., & Cunha, G. R. (1991). Mesenchyme-induced changes in the neoplastic characteristics of the Dunning prostatic adenocarcinoma. *Cancer Research, 51*(18), 4924–30.

Hazelbag, S., Kenter, G. G., Gorter, A., Dreef, E. J., Koopman, L. A., Violette, S. M., Weinreb, P. H., & Fleuren, G. J. (2007). Overexpression of the alpha v beta 6 integrin in cervical squamous cell carcinoma is a prognostic factor for decreased survival. *The Journal of Pathology, 212*(3), 316–24.

Hedbäck, N., Jensen, D. H., Specht, L., Fiehn, A.-M. K., Therkildsen, M. H., Friis-Hansen, L., Dabelsteen, E., & von Buchwald, C. (2014). MiR-21 expression in the tumor stroma of oral squamous cell carcinoma: an independent biomarker of disease free survival. *PloS One, 9*(4), e95193.

Hess, J., Angel, P., & Schorpp-Kistner, M. (2004). AP-1 subunits: quarrel and harmony among siblings. *Journal of Cell Science, 117*(25), 5965–73.

Hezel, A. F., Deshpande, V., Zimmerman, S. M., Contino, G., Alagesan, B., O'Dell, M. R., Rivera, L. B., Harper, J., Lonning, S., Brekken, R. A., & Bardeesy, N. (2012). TGF-β and αvβ6 integrin act in a common pathway to suppress pancreatic cancer progression. *Cancer Research, 72*(18), 4840–5.

Hill, R., Song, Y., Cardiff, R. D., & Van Dyke, T. (2005). Selective evolution of stromal mesenchyme with p53 loss in response to epithelial tumorigenesis. *Cell, 123*(6), 1001–11.

Hinsley, E. E., Hunt, S., Hunter, K. D., Whawell, S. A., & Lambert, D. W. (2012). Endothelin-1 stimulates motility of head and neck squamous carcinoma cells by promoting stromal-epithelial interactions. *International Journal of Cancer, 130*(1), 40–47.

Hinsley, E. E., Kumar, S., Hunter, K. D., Whawell, S. A., & Lambert, D. W. (2012). Endothelin-1 stimulates oral fibroblasts to promote oral cancer invasion. *Life Sciences. 91*(13-14):557-61

Hinz, B. (2007). Formation and function of the myofibroblast during tissue repair. *The Journal of Investigative Dermatology, 127*(3), 526–37.

Hinz, B., Celetta, G., Tomasek, J. J., Gabbiani, G., & Chaponnier, C. (2001). Alpha-smooth muscle actin expression upregulates fibroblast contractile activity. *Molecular Biology of the Cell, 12*(9), 2730–41.

Hinz, B., Phan, S. H., Thannickal, V. J., Galli, A., Bochaton-Piallat, M.-L., & Gabbiani, G. (2007). The myofibroblast: one function, multiple origins. *The American Journal of Pathology, 170*(6), 1807–16.

Hinz, B., Pittet, P., Smith-Clerc, J., Chaponnier, C., & Meister, J.-J. (2004). Myofibroblast development is characterized by specific cell-cell adherens junctions. *Molecular Biology of the Cell, 15*(9), 4310–20.

Huang, H., Sun, P., Lei, Z., Li, M., Wang, Y., Zhang, H.-T., & Liu, J. (2015). miR-145 inhibits invasion and metastasis by directly targeting Smad3 in nasopharyngeal cancer. *Tumour Biology : The Journal of the International Society for Oncodevelopmental Biology and Medicine.* Epub ahead of print.

Huang, X., Yang, N., Fiore, V. F., Barker, T. H., Sun, Y., Morris, S. W., Ding, Q., Thannickal, V. J., & Zhou, Y. (2012). Matrix stiffness-induced myofibroblast differentiation is mediated by intrinsic mechanotransduction. *American Journal of Respiratory Cell and Molecular Biology, 47*(3), 340–8.

Huntzinger, E., & Izaurralde, E. (2011). Gene silencing by microRNAs: contributions of translational repression and mRNA decay. *Nature Reviews. Genetics, 12*(2), 99–110.

Hurst, D. R., Edmonds, M. D., & Welch, D. R. (2009). Metastamir: the field of metastasis-regulatory microRNA is spreading. *Cancer Research, 69*(19), 7495–8.

Ikeda, Y., Imai, Y., Kumagai, H., Nosaka, T., Morikawa, Y., Hisaoka, T., Manabe, I., Maemura, K., Nakaora, T., Imamura, T., Miyazono, K., Komuro, I., Naqai, R., & Kitamura, T. (2004). Vasorin, a transforming growth factor -binding protein expressed in vascular smooth muscle cells, modulates the arterial response to injury in vivo. *Proceedings of the National Academy of Sciences, 101*(29), 10732–10737.

Iozzo, R. V. (2000). Proteoglycans: Structure, Biology And Molecular Interactions. New York, NY Marcel Dekker. CRC Press.

Ito, T., Williams, J. D., Fraser, D., & Phillips, A. O. (2004). Hyaluronan attenuates transforming growth factor-beta1-mediated signaling in renal proximal tubular epithelial cells. *The American Journal of Pathology, 164*(6), 1979–88.

Jacobson, A., & Cunningham, J. L. (2012). Connective tissue growth factor in tumor pathogenesis. *Fibrogenesis & Tissue Repair, 5*(1), S8.

Jeon, K.-I., Kulkarni, A., Woeller, C. F., Phipps, R. P., Sime, P. J., Hindman, H. B., & Huxlin, K. R. (2014). Inhibitory effects of PPARγ ligands on TGF-β1-induced corneal myofibroblast transformation. *The American Journal of Pathology, 184*(5), 1429–45.

Johansson, A.-C., Ansell, A., Jerhammar, F., Lindh, M. B., Grénman, R., Munck-Wikland, E., Ostman, A., & Roberg, K. (2012). Cancer-associated fibroblasts induce matrix metalloproteinase-mediated cetuximab resistance in head and neck squamous cell carcinoma cells. *Molecular Cancer Research : MCR, 10*(9), 1158–68.

Joyce, J. a, & Pollard, J. W. (2009). Microenvironmental regulation of metastasis. *Nature Reviews. Cancer, 9*(4), 239–52.

Jun, J.-I., & Lau, L. F. (2010). Cellular senescence controls fibrosis in wound healing. *Aging, 2*(9), 627–31.

Kadera, B. E., Li, L., Toste, P. A., Wu, N., Adams, C., Dawson, D. W., & Donahue, T. R. (2013). MicroRNA-21 in pancreatic ductal adenocarcinoma tumor-associated fibroblasts promotes metastasis. *PloS One, 8*(8), e71978.

Kähäri, V. M., Larjava, H., & Uitto, J. (1991). Differential regulation of extracellular matrix proteoglycan (PG) gene expression. Transforming growth factor-beta 1 up-regulates biglycan (PGI), and versican (large fibroblast PG) but down-regulates decorin (PGII) mRNA levels in human fibroblasts in cult. *The Journal of Biological Chemistry, 266*(16), 10608–15.

Kalluri, R., & Neilson, E. G. (2003). Epithelial-mesenchymal transition and its implications for fibrosis. *The Journal of Clinical Investigation, 112*(12), 1776–84.

Kalluri, R., & Weinberg, R. A. (2009). The basics of epithelial-mesenchymal transition. *The Journal of Clinical Investigation, 119*(6), 1420–8.

Kalluri, R., & Zeisberg, M. (2006). Fibroblasts in cancer. *Nature Reviews. Cancer, 6*(5), 392–401.

Kalyankrishna, S., & Grandis, J. R. (2006). Epidermal growth factor receptor biology in head and neck cancer. *Journal of Clinical Oncology : Official Journal of the American Society of Clinical Oncology, 24*(17), 2666–72.

Kawashima, H., Atarashi, K., Hirose, M., Hirose, J., Yamada, S., Sugahara, K., & Miyasaka, M. (2002). Oversulfated chondroitin/dermatan sulfates containing GlcAbeta1/IdoAalpha1-3GalNAc(4,6-O-disulfate) interact with L- and P-selectin and chemokines. *The Journal of Biological Chemistry, 277*(15), 12921–30.

Kawashiri, S., Tanaka, A., Noguchi, N., Hase, T., Nakaya, H., Ohara, T., Kato, K., & Yamamoto, E. (2009). Significance of stromal desmoplasia and myofibroblast appearance at the invasive front in squamous cell carcinoma of the oral cavity. *Head & Neck, 31*(10), 1346–53.

Kellermann, M. G., Sobral, L. M., da Silva, S. D., Zecchin, K. G., Graner, E., Lopes, M. A., Nishimoto, I., Kowalski, L. P., & Coletta, R. D. (2007). Myofibroblasts in the stroma of oral squamous cell carcinoma are associated with poor prognosis. *Histopathology, 51*(6), 849–53.

Kellermann, M. G., Sobral, L. M., da Silva, S. D., Zecchin, K. G., Graner, E., Lopes, M. A., Kowalski., L. P., & Coletta, R. D. (2008). Mutual paracrine effects of oral squamous cell carcinoma cells and normal oral fibroblasts: Induction of fibroblast to myofibroblast transdifferentiation and modulation of tumor cell proliferation. *Oral Oncology, 44*(5), 509–517.

Kent, O. A., Chivukula, R. R., Mullendore, M., Wentzel, E. A., Feldmann, G., Lee, K. H., Liu, S., Leach S. D., Maitra, A., & Mendell, J. T. (2010). Repression of the miR-143/145 cluster by oncogenic Ras initiates a tumor-promoting feed-forward pathway. *Genes & Development, 24*(24), 2754–9.

Kessenbrock, K., Plaks, V., & Werb, Z. (2010). Matrix metalloproteinases: regulators of the tumor microenvironment. *Cell, 141*(1), 52–67.

Kiaris, H., Chatzistamou, I., Trimis, G., Frangou-Plemmenou, M., Pafiti-Kondi, A., & Kalofoutis, A. (2005). Evidence for nonautonomous effect of p53 tumor suppressor in carcinogenesis. *Cancer Research, 65*(5), 1627–30.

Kim, S., Takahashi, H., Lin, W.-W., Descargues, P., Grivennikov, S., Kim, Y., Luo, J.-L., & Karin, M. (2009). Carcinoma-produced factors activate myeloid cells through TLR2 to stimulate metastasis. *Nature, 457(*7225), 102–6.

Kim, S.-H., Turnbull, J., & Guimond, S. (2011). Extracellular matrix and cell signalling: the dynamic cooperation of integrin, proteoglycan and growth factor receptor. *The Journal of Endocrinology, 209*(2), 139–51.

Kinugasa, Y., Matsui, T., & Takakura, N. (2014). CD44 expressed on cancer-associated fibroblasts is a functional molecule supporting the stemness and drug resistance of malignant cancer cells in the tumor microenvironment. *Stem Cells, 32*(1), 145–56.

Kitade, Y., & Akao, Y. (2010). MicroRNAs and their therapeutic potential for human diseases: microRNAs, miR-143 and -145, function as anti-oncomirs and the application of chemically modified miR-143 as an anti-cancer drug. *Journal of Pharmacological Sciences, 114*(3), 276–80.

Kitamura, T., Kometani, K., Hashida, H., Matsunaga, A., Miyoshi, H., Hosogi, H., Aoki, M., Oshima, M., Hattori, M., Takabavashi, A., Minato, N., & Taketo, M. M. (2007). SMAD4-deficient intestinal tumors recruit CCR1+ myeloid cells that promote invasion. *Nature Genetics, 39*(4), 467–75.

Kohan, M., Muro, A. F., White, E. S., & Berkman, N. (2010). EDA-containing cellular fibronectin induces fibroblast differentiation through binding to alpha4beta7 integrin receptor and MAPK/Erk 1/2-dependent signaling. *FASEB Journal : Official Publication of the Federation of American Societies for Experimental Biology, 24*(11), 4503–12.

Kojima, Y., Acar, A., Eaton, E. N., Mellody, K. T., Scheel, C., Ben-Porath, I., Onder, T. T., Wang, Z. C., Richardson, A. L., Weinberg, R. A., & Orimo, A. (2010). Autocrine TGF-β and stromal cell-derived factor-1 (SDF-1) signaling drives the evolution of tumor-promoting mammary stromal myofibroblasts. *Proceedings of the National Academy of Sciences of the United States of America, 107*(46), 20009–20014.

Korpal, M., & Kang, Y. The emerging role of miR-200 family of microRNAs in epithelial-mesenchymal transition and cancer metastasis. *RNA Biology, 5*(3), 115–9.

Koshkin, A. A., Singh, S. K., Nielsen, P., Rajwanshi, V. K., Kumar, R., Meldgaard, M., Olsen, C. E., & Wengel, J. (1998). LNA (Locked Nucleic Acids): Synthesis of the adenine, cytosine, guanine, 5-methylcytosine, thymine and uracil bicyclonucleoside monomers, oligomerisation, and unprecedented nucleic acid recognition. *Tetrahedron, 54(*14), 3607–3630.

Krampert, M., Kuenzle, S., Thai, S. N.-M., Lee, N., Iruela-Arispe, M. L., & Werner, S. (2005). ADAMTS1 proteinase is up-regulated in wounded skin and regulates migration of fibroblasts and endothelial cells. *The Journal of Biological Chemistry, 280*(25), 23844–52.

Kuhn, C., & McDonald, J. A. (1991). The roles of the myofibroblast in idiopathic pulmonary fibrosis. Ultrastructural and immunohistochemical features of sites of active extracellular matrix synthesis. *The American Journal of Pathology, 138*(5), 1257–65.

Kuperwasser, C., Chavarria, T., Wu, M., Magrane, G., Gray, J. W., Carey, L., Richardson, A., & Weinberg, R. A. (2004). Reconstruction of functionally normal and malignant human breast tissues in mice. *Proceedings of the National Academy of Sciences of the United States of America, 101*(14), 4966–71.

Kurose, K., Gilley, K., Matsumoto, S., Watson, P. H., Zhou, X.-P., & Eng, C. (2002). Frequent somatic mutations in PTEN and TP53 are mutually exclusive in the stroma of breast carcinomas. *Nature Genetics, 32*(3), 355–7.

La Rocca, G., Badin, M., Shi, B., Xu, S.-Q., Deangelis, T., Sepp-Lorenzinoi, L., & Baserga, R. (2009). Mechanism of growth inhibition by MicroRNA 145: the role of the IGF-I receptor signaling pathway. *Journal of Cellular Physiology, 220*(2), 485–91.

Lajer, C. B., Garnæs, E., Friis-Hansen, L., Norrild, B., Therkildsen, M. H., Glud, M., Rossing, M., Laier, H., Svane, D., Skotte, L., Specht, L., Buchwald, C., & Nielsen, F. C. (2012). The role of miRNAs in human papilloma virus (HPV)-associated cancers: bridging between HPV-related head and neck cancer and cervical cancer. *British Journal of Cancer, 106*(9), 1526–34.

Laoui, D., Movahedi, K., Van Overmeire, E., Van den Bossche, J., Schouppe, E., Mommer, C., Nikolaou, A., Morias, Y., De Baetselier, P., & Van Ginderachter, J. A. (2011). Tumor-associated macrophages in breast cancer: distinct subsets, distinct functions. *The International Journal of Developmental Biology, 55*(7-9), 861–7.

Larson, B. J., Longaker, M. T., & Lorenz, H. P. (2010). Scarless fetal wound healing: a basic science review. *Plastic and Reconstructive Surgery, 126*(4), 1172–80.

Leask, A., & Abraham, D. J. (2004). TGF-beta signaling and the fibrotic response. *FASEB Journal : Official Publication of the Federation of American Societies for Experimental Biology, 18*(7), 816–27.

Lebaron, R. G. (1996). Versican. *Perspectives on Developmental Neurobiology, 3*(4), 261–71.

LeBaron, R. G., Zimmermann, D. R., & Ruoslahti, E. (1992). Hyaluronate binding properties of versican. *The Journal of Biological Chemistry, 267(*14), 10003–10.

Lee, H. K., Bier, A., Cazacu, S., Finniss, S., Xiang, C., Twito, H., Poisson, L. M., Mikkelsen, T., Slavin, S., Jacoby, E., Yalon, M., Toren, M., Rempel, S.A., & Brodie, C. (2013). MicroRNA-145 is

downregulated in glial tumors and regulates glioma cell migration by targeting connective tissue growth factor. *PloS One, 8*(2), e54652.

Lee, Y.-J., Kong, M.-H., Song, K.-Y., Lee, K.-H., & Heo, S.-H. (2008). The Relation Between Sox9, TGF-beta1, and Proteoglycan in Human Intervertebral Disc Cells. *Journal of Korean Neurosurgical Society, 43*(3), 149–54.

Leemans, C. R., Braakhuis, B. J. M., & Brakenhoff, R. H. (2011). The molecular biology of head and neck cancer. *Nature Reviews. Cancer, 11*(1), 9–22.

Lepekhin, E., Grøn, B., Berezin, V., Bock, E., & Dabelsteen, E. (2002). Differences in motility pattern between human buccal fibroblasts and periodontal and skin fibroblasts. *European Journal of Oral Sciences, 110*(1), 13–20.

Levy, L., & Hill, C. S. Alterations in components of the TGF-beta superfamily signaling pathways in human cancer. *Cytokine & Growth Factor Reviews, 17*(1-2), 41–58.

Lewis, B. P., Burge, C. B., & Bartel, D. P. (2005). Conserved seed pairing, often flanked by adenosines, indicates that thousands of human genes are microRNA targets. *Cell, 120*(1), 15–20.

Lewis, M. P., Lygoe, K. A., Nystrom, M. L., Anderson, W. P., Speight, P. M., Marshall, J. F., & Thomas, G. J. (2004a). Tumour-derived TGF-beta1 modulates myofibroblast differentiation and promotes HGF/SF-dependent invasion of squamous carcinoma cells. *British Journal of Cancer, 90*(4), 822–32.

Lewis, M. P., Lygoe, K. A., Nystrom, M. L., Anderson, W. P., Speight, P. M., Marshall, J. F., & Thomas, G. J. (2004b). Tumour-derived TGF-beta1 modulates myofibroblast differentiation and promotes HGF/SF-dependent invasion of squamous carcinoma cells. *British Journal of Cancer, 90*(4), 822–32. Li, C., Bai, Y., Liu, H., Zuo, X., Yao, H., Xu, Y., & Cao, M. (2013). Comparative study of microRNA profiling in keloid fibroblast and annotation of differential expressed microRNAs. *Acta Biochimica et Biophysica Sinica, 45*(8), 692–9.

Lim, K. P., Cirillo, N., Hassona, Y., Wei, W., Thurlow, J. K., Cheong, S. C., Pitiyage, G., Parkinson, E. K., & Prime, S. S. (2011). Fibroblast gene expression profile reflects the stage of tumour progression in oral squamous cell carcinoma. *The Journal of Pathology, 223*(4), 459–469.

Lim, L. P., Lau, N. C., Garrett-Engele, P., Grimson, A., Schelter, J. M., Castle, J., Bartel, D. P., Linsley, P. S., & Johnson, J. M. (2005). Microarray analysis shows that some microRNAs downregulate large numbers of target mRNAs. *Nature, 433*(7027), 769–73.

Lin, C. J., Grandis, J. R., Carey, T. E., Gollin, S. M., Whiteside, T. L., Koch, W. M., Ferris, R. L., & Lai, S. Y. (2007). Head and neck squamous cell carcinoma cell lines: established models and rationale for selection. *Head & Neck, 29*(2), 163–88.

Liu, R., Liao, J., Yang, M., Sheng, J., Yang, H., Wang, Y., Pan, E., Guo, W., Pu, Y., Kim, S. J., & Yin, L. (2012). The cluster of miR-143 and miR-145 affects the risk for esophageal squamous cell carcinoma through co-regulating fascin homolog 1. *PloS One, 7*(3), e33987.

Liu, Y., Sinha, S., McDonald, O. G., Shang, Y., Hoofnagle, M. H., & Owens, G. K. (2004). Kruppel-like Factor 4 Abrogates Myocardin-induced Activation of Smooth Muscle Gene Expression. *Journal of Biological Chemistry, 280*(10), 9719–9727.

Liu, Z., Lu, C.-L., Cui, L.-P., Hu, Y.-L., Yu, Q., Jiang, Y., Ma, T., Jiao, D. K., Wang, D., & Jia, C.-Y. (2012). MicroRNA-146a modulates TGF-β1-induced phenotypic differentiation in human dermal fibroblasts by targeting SMAD4. *Archives of Dermatological Research, 304*(3), 195–202.

Livak, K. J., & Schmittgen, T. D. (2001). Analysis of relative gene expression data using real-time quantitative PCR and the 2(-Delta Delta C(T)) Method. *Methods, 25*(4), 402–8.

Long, X., & Miano, J. M. (2011). Transforming growth factor-beta1 (TGF-beta1) utilizes distinct pathways for the transcriptional activation of microRNA 143/145 in human coronary artery smooth muscle cells. *The Journal of Biological Chemistry, 286*(34), 30119–29.

Lorenz, H. P., Lin, R. Y., Longaker, M. T., Whitby, D. J., & Adzick, N. S. (1995). The fetal fibroblast: the effector cell of scarless fetal skin repair. *Plastic and Reconstructive Surgery, 96*(6), 1251–9; 1260–1.

Lotfi, A., Mohammadi, G., Tavassoli, A., Mousaviagdas, M., Chavoshi, H., & Saniee, L. (2015). Serum Levels of MMP9 and MMP2 in Patients with Oral Squamous Cell Carcinoma. *Asian Pacific Journal of Cancer Prevention : APJCP, 16*(4), 1327–30.

Lu, S.-L., Reh, D., Li, A. G., Woods, J., Corless, C. L., Kulesz-Martin, M., & Wang, X.-J. (2004). Overexpression of transforming growth factor beta1 in head and neck epithelia results in inflammation, angiogenesis, and epithelial hyperproliferation. *Cancer Research, 64*(13), 4405–10.

Lu, Y., Chopp, M., Zheng, X., Katakowski, M., Buller, B., & Jiang, F. (2013). MiR-145 reduces ADAM17 expression and inhibits in vitro migration and invasion of glioma cells. *Oncology Reports, 29*(1), 67–72.

Lv, H., Zhang, S., Wang, B., Cui, S., & Yan, J. (2006). Toxicity of cationic lipids and cationic polymers in gene delivery. *Journal of Controlled Release: Official Journal of the Controlled Release Society, 114*(1), 100–9.

Lyons, R. M., Keski-Oja, J., & Moses, H. L. (1988). Proteolytic activation of latent transforming growth factor-beta from fibroblast-conditioned medium. *The Journal of Cell Biology, 106*(5), 1659–65.

Mah, W., Jiang, G., Olver, D., Cheung, G., Kim, B., Larjava, H., & Häkkinen, L. (2014). Human gingival fibroblasts display a non-fibrotic phenotype distinct from skin fibroblasts in three-dimensional cultures. *PloS One, 9*(3), e90715.

Malapeira, J., Esselens, C., Bech-Serra, J. J., Canals, F., & Arribas, J. (2011). ADAM17 (TACE) regulates TGFβ signaling through the cleavage of vasorin. *Oncogene, 30*(16), 1912–22.

Marsh, D., Suchak, K., Moutasim, K. A., Vallath, S., Hopper, C., Jerjes, W., Upile, T., Kalavrezos, N., Weinreb, P. H., Chester, K A., Chana, J. S., Marshall, J. F., Hart, I. R., Hackshaw, A. K., Piper, K., & Thomas, G. J. (2011). Stromal features are predictive of disease mortality in oral cancer patients. *The Journal of Pathology, 223*(4), 470–81.

Martinelli-Kläy, C. P., Mendis, B. R. R. N., & Lombardi, T. (2009). Eosinophils and oral squamous cell carcinoma: a short review. *Journal of Oncology, 2009*, 310132.

Massagué, J. (2008). TGFbeta in Cancer. *Cell, 134*(2), 215–30.

Masszi, A., Speight, P., Charbonney, E., Lodyga, M., Nakano, H., Szászi, K., & Kapus, A. (2010). Fate-determining mechanisms in epithelial-myofibroblast transition: major inhibitory role for Smad3. *The Journal of Cell Biology, 188*(3), 383–99.

Matheu, A., Collado, M., Wise, C., Manterola, L., Cekaite, L., Tye, A. J., Canamero, M., Buianda, L., Schedl, A., Cheah, K. S., Skotheim, R. I., Lothe, R. A., Lopez de Munain, A., Briscoe, J., Serrano, M., & Lovell-Badge, R. (2012). Oncogenicity of the developmental transcription factor Sox9. *Cancer Research, 72*(5), 1301–15.

Matrisian, L. M., & Hogan, B. L. (1990). Growth factor-regulated proteases and extracellular matrix remodeling during mammalian development. *Current Topics in Developmental Biology, 24*, 219–59.

Mayr, C., Hemann, M. T., & Bartel, D. P. (2007). Disrupting the pairing between let-7 and Hmga2 enhances oncogenic transformation. *Science, 315*(5818), 1576–9.

McLendon, J., Joshi, S., Fewell, J., Oka, M., McMurtry, I., & Gerthoffer, W. (2014). AntimiR-145 therapy improves right ventricular structure in experimental pulmonary arterial hypertension (1090.1). *FASEB J, 28*, 1090.1–.

Megiorni, F., Cialfi, S., Cimino, G., De Biase, R. V., Dominici, C., Quattrucci, S., & Pizzuti, A. (2013). Elevated levels of miR-145 correlate with SMAD3 down-regulation in cystic fibrosis patients. *Journal of Cystic Fibrosis : Official Journal of the European Cystic Fibrosis Society, 12*(6), 797–802.

Meran, S., Thomas, D., Stephens, P., Martin, J., Bowen, T., Phillips, A., & Steadman, R. (2007). Involvement of hyaluronan in regulation of fibroblast phenotype. *The Journal of Biological Chemistry, 282*(35), 25687–97.

Merlos-Suárez, A., Ruiz-Paz, S., Baselga, J., & Arribas, J. (2001). Metalloprotease-dependent protransforming growth factor-alpha ectodomain shedding in the absence of tumor necrosis factor-alpha-converting enzyme. *The Journal of Biological Chemistry, 276*(51), 48510–7.

Michael, M. Z., O' Connor, S. M., van Holst Pellekaan, N. G., Young, G. P., & James, R. J. (2003). Reduced Accumulation of Specific MicroRNAs in Colorectal Neoplasia. Mol. *Cancer Res., 1*(12), 882–891.

Midgley, A. C., Rogers, M., Hallett, M. B., Clayton, A., Bowen, T., Phillips, A. O., & Steadman, R. (2013). Transforming growth factor-β1 (TGF-β1)-stimulated fibroblast to myofibroblast differentiation is mediated by hyaluronan (HA)-facilitated epidermal growth factor receptor (EGFR) and CD44 co-localization in lipid rafts. *The Journal of Biological Chemistry, 288*(21), 14824–38.

miRagen Therapeutics | microRNA Based Therapeutics. Retrieved May 9, 2015, from http://miragentherapeutics.com/

Mitra, A. K., Zillhardt, M., Hua, Y., Tiwari, P., Murmann, A. E., Peter, M. E., & Lengyel, E. (2012). MicroRNAs reprogram normal fibroblasts into cancer-associated fibroblasts in ovarian cancer. *Cancer Discovery, 2*(12), 1100–8.

Moharamzadeh, K., Colley, H., Murdoch, C., Hearnden, V., Chai, W. L., Brook, I. M., Thornhill, M. H., & Macneil, S. (2012). Tissue-engineered oral mucosa. *Journal of Dental Research, 91*(7), 642–50.

Moore, K. M., Thomas, G. J., Duffy, S. W., Warwick, J., Gabe, R., Chou, P., Ellis, I. O., Green A. R., Haider, S., Brouilette, K., Saha, A., Vallath, S., Bowen, R., Chelala, C., Eccles, D., Tapper, W. J., Thompson, A. M., Quinlan, P., Jordan, L., Gillett, C., Brentnall, A., Violette, S., Weinreb, P. H., Kendrew, J., Barry, S. T., Hart, I. R., Jones, J. L., & Marshall, J. F. (2014). Therapeutic targeting of integrin αvβ6 in breast cancer. *Journal of the National Cancer Institute, 106*(8), dju169–.

Moretti, F., Thermann, R., & Hentze, M. W. (2010). Mechanism of translational regulation by miR-2 from sites in the 5' untranslated region or the open reading frame. *RNA, 16*(12), 2493–502.

Moritani, N. H., Kubota, S., Nishida, T., Kawaki, H., Kondo, S., Sugahara, T., & Takigawa, M. (2003). Suppressive effect of overexpressed connective tissue growth factor on tumor cell growth in a human oral squamous cell carcinoma-derived cell line. *Cancer Letters, 192*(2), 205–14.

Moskovits, N., Kalinkovich, A., Bar, J., Lapidot, T., & Oren, M. (2006). p53 Attenuates cancer cell migration and invasion through repression of SDF-1/CXCL12 expression in stromal fibroblasts. *Cancer Research, 66(*22), 10671–6.

Mullis, T. C., Tang, X., & Chong, K. T. (2008). Expression of connective tissue growth factor (CTGF/CCN2) in head and neck squamous cell carcinoma*. Journal of Clinical Pathology, 61*(5), 606–10.

Munger, J. S., Huang, X., Kawakatsu, H., Griffiths, M. J., Dalton, S. L., Wu, J., Pittet, J. F., Kaminski, N., Garat, C., Matthay, M. A., Rifkin D. B., & Sheppard, D. (1999). The integrin alpha v beta 6 binds and activates latent TGF beta 1: a mechanism for regulating pulmonary inflammation and fibrosis. *Cell, 96*(3), 319–28.

Murdoch, C., Muthana, M., Coffelt, S. B., & Lewis, C. E. (2008). The role of myeloid cells in the promotion of tumour angiogenesis. *Nature Reviews. Cancer, 8*(8), 618–31.

Muro, A. F., Moretti, F. A., Moore, B. B., Yan, M., Atrasz, R. G., Wilke, C. A., Flaherty, K. R., Martinez, F. J., Tsui, J. L., Sheppard, D., Baralle, F. E., Toews, G. B., & White, E. S. (2008). An essential role for fibronectin extra type III domain A in pulmonary fibrosis*. American Journal of Respiratory and Critical Care Medicine, 177*(6), 638–45.

Najm, P., & El-Sibai, M. (2014). Palladin regulation of the actin structures needed for cancer invasion. *Cell Adhesion & Migration, 8*(1), 29–35.

Nasos, M. F., Zimmermanng, D. R., & Iozzon, R. V. (1994). Characterization of the Complete Genomic Structure of the Human Versican Gene and Functional Analysis of Its Promote*. The Journal of Biological Chemistry, 269*(52), 32999–33008.

Noël, A., De Pauw-Gillet, M. C., Purnell, G., Nusgens, B., Lapiere, C. M., & Foidart, J. M. (1993). Enhancement of tumorigenicity of human breast adenocarcinoma cells in nude mice by matrigel and fibroblasts. *British Journal of Cancer, 68*(5), 909–15.

Olumi, A. F., Grossfeld, G. D., Hayward, S. W., Epithelium, P., Carroll, P. R., Tlsty, T. D., & Cunha, G. R. (1999). Carcinoma-associated Fibroblasts Direct Tumor Progression of Initiated Human Prostatic Epithelium Carcinoma-associated Fibroblasts Direct Tumor Progression of Initiated Human. *Cancer Research, 59*(19):5002-11.

Onken, J., Moeckel, S., Leukel, P., Leidgens, V., Baumann, F., Bogdahn, U., Vollmann-Zwerenz, A., & Hau, P. (2014). Versican isoform V1 regulates proliferation and migration in high-grade gliomas. *Journal of Neuro-Oncology, 120*(1), 73–83.

Orimo, A., Gupta, P. B., Sgroi, D. C., Arenzana-Seisdedos, F., Delaunay, T., Naeem, R., Carey V. J., Richardson, A. L., & Weinberg, R. a. (2005). Stromal fibroblasts present in invasive human breast carcinomas promote tumor growth and angiogenesis through elevated SDF-1/CXCL12 secretion. *Cell, 121*(3), 335–48.

Ostman, A., & Augsten, M. (2009). Cancer-associated fibroblasts and tumor growth--bystanders turning into key players. *Current Opinion in Genetics & Development, 19*(1), 67–73.

Otranto, M., Sarrazy, V., Bonté, F., Hinz, B., Gabbiani, G., & Desmouliere, A. (2012). The role of the myofibroblast in tumor stroma remodeling. *Cell Adhesion & Migration, 6*(3), 203–19.

Ou, J., Peng, Y., Deng, J., Miao, H., Zhou, J., Zha, L., Zhou, R., Yu, L., Shi, H., & Liang, H. (2014). Endothelial cell-derived fibronectin extra domain A promotes colorectal cancer metastasis via inducing epithelial-mesenchymal transition. *Carcinogenesis, 35*(7), 1661–70.

Pai, S. I., & Westra, W. H. (2009). Molecular pathology of head and neck cancer: implications for diagnosis, prognosis, and treatment. *Annual Review of Pathology, 4,* 49–70.

Pal, A., Melling, G., Hinsley, E. E., Kabir, T. D., Colley, H. E., Murdoch, C., & Lambert, D. W. (2013). Cigarette smoke condensate promotes pro-tumourigenic stromal-epithelial interactions by suppressing miR-145. *Journal of Oral Pathology & Medicine : Official Publication of the International Association of Oral Pathologists and the American Academy of Oral Pathology, 42*(4), 309–14.

Pankov, R., & Yamada, K. M. (2002). Fibronectin at a glance. *Journal of Cell Science, 115*(Pt 20), 3861–3.

Patocs, A., Zhang, L., Xu, Y., Weber, F., Caldes, T., Mutter, G. L., Platzer, P., & Eng, C. (2007). Breast-cancer stromal cells with TP53 mutations and nodal metastases. *The New England Journal of Medicine, 357*(25), 2543–51.

Peng, X., Guo, W., Liu, T., Wang, X., Tu, X., Xiong, D., Chen, S., Lai, Y., Du, H., Chen, G., Liu, G., Tang, Y., Huang, S., & Zou, X. (2011). Identification of miRs-143 and -145 that is associated with bone metastasis of prostate cancer and involved in the regulation of EMT. *PloS One, 6*(5), e20341.

Peschiaroli, A., Giacobbe, A., Formosa, A., Markert, E. K., Bongiorno-Borbone, L., Levine, A. J., Candi, E., D'Alessandro, A., Zolla, L., Finazzi Agro, A., & Melino, G. (2012). miR-143 regulates hexokinase 2 expression in cancer cells. *Oncogene. 32*(6):797-802.

Pickard, A., Cichon, A.-C., Barry, A., Kieran, D., Patel, D., Hamilton, P., Salto- Tellez, M., James, J., & McCance, D. J. (2012). Inactivation of Rb in stromal fibroblasts promotes epithelial cell invasion. *The EMBO Journal, 31*(14), 3092–103.

Pietras, K., & Ostman, A. (2010). Hallmarks of cancer: interactions with the tumor stroma. *Experimental Cell Research, 316*(8), 1324–31.

Pinisetti, S., Manyam, R., Suresh, B., & Aparna, V. (2014). Myofibroblasts in oral lesions: A review. *Journal of Oral and Maxillofacial Pathology : JOMFP, 18*(1), 52–7.

Piriyapongsa, J., Bootchai, C., Ngamphiw, C., & Tongsima, S. (2014). microPIR2: a comprehensive database for human-mouse comparative study of microRNA-promoter interactions. *Database : The Journal of Biological Databases and Curation,* 2014, bau115.

Place, R. F., Li, L.-C., Pookot, D., Noonan, E. J., & Dahiya, R. (2008). MicroRNA-373 induces expression of genes with complementary promoter sequences. *Proceedings of the National Academy of Sciences of the United States of America, 105*(5), 1608–13.

Pukkila, M. J., Kosunen, A. S. T., Virtaniemi, J. A., Kumpulainen, E. J., Johansson, R. T., Kellokoski, J. K., Nuutinen, J., & Kosma, V.-M. (2004). Versican expression in pharyngeal squamous cell carcinoma: an immunohistochemical study. *Journal of Clinical Pathology, 57*(7), 735–9.

Pukkila, M., Kosunen, A., Ropponen, K., Virtaniemi, J., Kellokoski, J., Kumpulainen, E., Pirinen, R., Nuutinen, J., Johansson, R., & Kosma, V.-M. (2007). High stromal versican expression predicts unfavourable outcome in oral squamous cell carcinoma. *Journal of Clinical Pathology, 60*(3), 267–72.

Quintavalle, M., Elia, L., Condorelli, G., & Courtneidge, S. A. (2010). MicroRNA control of podosome formation in vascular smooth muscle cells in vivo and in vitro. *The Journal of Cell Biology, 189*(1), 13–22.

Qwarnström, E. E., Järveläinen, H. T., Kinsella, M. G., Ostberg, C. O., Sandell, L. J., Page, R. C., & Wight, T. N. (1993). Interleukin-1 beta regulation of fibroblast proteoglycan synthesis involves a decrease in versican steady-state mRNA levels. *The Biochemical Journal, 294*(20), 613–20.

Rahmani, M., Read, J. T., Carthy, J. M., McDonald, P. C., Wong, B. W., Esfandiarei, M., Si, X., Luo, Z., Luo, H., Rennie, P. S., & McManus, B. M. (2005). Regulation of the versican promoter by the beta-catenin-T-cell factor complex in vascular smooth muscle cells. *The Journal of Biological Chemistry, 280*(13), 13019–28.

Ramos, D. M., Chen, B. L., Boylen, K., Stern, M., Kramer, R. H., Sheppard, D., Nishimura, S. L., Greenspan, D., Zardi, L., & Pytela, R. (1997). Stromal fibroblasts influence oral squamous-cell carcinoma cell interactions with tenascin-C. *International Journal of Cancer. Journal International Du Cancer, 72*(2), 369–76.

Rangrez, A. Y., Massy, Z. A., Metzinger-Le Meuth, V., & Metzinger, L. (2011). miR-143 and miR-145: molecular keys to switch the phenotype of vascular smooth muscle cells. *Circulation. Cardiovascular Genetics, 4*(2), 197–205.

Rani, S. B., Rathod, S. S., Karthik, S., Kaur, N., Muzumdar, D., & Shiras, A. S. (2013). MiR-145 functions as a tumor-suppressive RNA by targeting Sox9 and adducin 3 in human glioma cells. *Neuro-Oncology, 15*(10), 1302–16.

Read, J. T., Rahmani, M., Boroomand, S., Allahverdian, S., McManus, B. M., & Rennie, P. S. (2007). Androgen receptor regulation of the versican gene through an androgen response element in the proximal promoter. *The Journal of Biological Chemistry, 282*(44), 31954–63.

Reed, M. J., Vernon, R. B., Abrass, I. B., & Sage, E. H. (1994). TGF-beta 1 induces the expression of type I collagen and SPARC, and enhances contraction of collagen gels, by fibroblasts from young and aged donors. *Journal of Cellular Physiology, 158*(1), 169–79.

Rettig, W. J., Garin-Chesa, P., Healey, J. H., Su, S. L., Ozer, H. L., Schwab, M., Albino, A.P., & Old, L. J. (1993). Regulation and heteromeric structure of the fibroblast activation protein in normal

and transformed cells of mesenchymal and neuroectodermal origin. *Cancer Research, 53*(14), 3327–35.

Ricciardelli, C., Brooks, J. H., Suwiwat, S., Sakko, A. J., Mayne, K., Raymond, W. A., Seshadri, R., LeBaron, R. G., & Horsfall, D. J. (2002). Regulation of stromal versican expression by breast cancer cells and importance to relapse-free survival in patients with node-negative primary breast cancer. *Clinical Cancer Research : An Official Journal of the American Association for Cancer Research, 8*(4), 1054–60.

Ricciardelli, C., Russell, D. L., Ween, M. P., Mayne, K., Suwiwat, S., Byers, S., Marshall, V. R., Tilley, W. D., & Horsfall, D. J. (2007). Formation of Hyaluronan- and Versican-rich Pericellular Matrix by Prostate Cancer Cells Promotes Cell Motility. *Journal of Biological Chemistry, 282*(14), 10814–10825.

Ricciardelli, C., Sakko, A. J., Ween, M. P., Russell, D. L., & Horsfall, D. J. (2009). The biological role and regulation of versican levels in cancer. *Cancer Metastasis Reviews, 28*(1-2), 233–45.

Rodemann, H. P., & Müller, G. A. (1991). Characterization of human renal fibroblasts in health and disease: II. In vitro growth, differentiation, and collagen synthesis of fibroblasts from kidneys with interstitial fibrosis. *American Journal of Kidney Diseases : The Official Journal of the National Kidney Foundation, 17*(6), 684–6.

Rodier, F., & Campisi, J. (2011). Four faces of cellular senescence. *The Journal of Cell Biology, 192*(4), 547–56.

Rolfe, K. J., & Grobbelaar, A. O. (2012). A review of fetal scarless healing. *ISRN Dermatol.* 2012;698034.

Rønnov-Jessen, L., & Petersen, O. W. (1993). Induction of alpha-smooth muscle actin by transforming growth factor-beta 1 in quiescent human breast gland fibroblasts. Implications for myofibroblast generation in breast neoplasia. *Laboratory Investigation; a Journal of Technical Methods and Pathology, 68*(6), 696–707.

Russell, D. L., Doyle, K. M. H., Ochsner, S. A., Sandy, J. D., & Richards, J. S. (2003). Processing and localization of ADAMTS-1 and proteolytic cleavage of versican during cumulus matrix expansion and ovulation. *The Journal of Biological Chemistry, 278*(43), 42330–9.

Russell, D. L., Ochsner, S. A., Hsieh, M., Mulders, S., & Richards, J. S. (2003). Hormone-regulated expression and localization of versican in the rodent ovary. *Endocrinology, 144*(3), 1020–31.

Sachdeva, M., Liu, Q., Cao, J., Lu, Z., & Mo, Y.-Y. (2012). Negative regulation of miR-145 by C/EBP-β through the Akt pathway in cancer cells. *Nucleic Acids Research, 40*(14), 6683–92.

Sachdeva, M., & Mo, Y.-Y. (2010a). MicroRNA-145 suppresses cell invasion and metastasis by directly targeting mucin 1. *Cancer Research, 70*(1), 378–87.

Sachdeva, M., & Mo, Y.-Y. (2010b). miR-145-mediated suppression of cell growth, invasion and metastasis. *American Journal of Translational Research, 2*(2), 170–80.

Sachdeva, M., Zhu, S., Wu, F., Wu, H., Walia, V., Kumar, S., Elble, R., Watabe, K., & Mo, Y.-Y. (2009). p53 represses c-Myc through induction of the tumor suppressor miR-145. *Proceedings of the National Academy of Sciences of the United States of America, 106*(9), 3207–12.

Sadlonova, A., Novak, Z., Johnson, M. R., Bowe, D. B., Gault, S. R., Page, G. P., Thottassery, J. V., Welch, D. R., & Frost, A. R. (2005). Breast fibroblasts modulate epithelial cell proliferation in three-dimensional in vitro co-culture. *Breast Cancer Research : BCR, 7*(1), R46–59.

Said, N., Sanchez-Carbayo, M., Smith, S. C., & Theodorescu, D. (2012). RhoGDI2 suppresses lung metastasis in mice by reducing tumor versican expression and macrophage infiltration. *The Journal of Clinical Investigation, 122*(4), 1503–18.

Sakko, A. J., Ricciardelli, C., Mayne, K., Tilley, W. D., Lebaron, R. G., & Horsfall, D. J. (2001). Versican accumulation in human prostatic fibroblast cultures is enhanced by prostate cancer cell-derived transforming growth factor beta1. *Cancer Research, 61*(3), 926–30.

Sanderson, R. J., & Ironside, J. A. D. (2002). Squamous cell carcinomas of the head and neck. *BMJ (Clinical Research Ed.), 325*(7368), 822–7.

Santos, A. M., Jung, J., Aziz, N., Kissil, J. L., & Puré, E. (2009). Targeting fibroblast activation protein inhibits tumor stromagenesis and growth in mice. *The Journal of Clinical Investigation, 119*(12), 3613–25.

Schmidt-Ullrich, R. K., Valerie, K., Fogleman, P. B., & Walters, J. (1996). Radiation-induced autophosphorylation of epidermal growth factor receptor in human malignant mammary and squamous epithelial cells. *Radiation Research, 145*(1), 81–5.

Schultz-Cherry, S., & Murphy-Ullrich, J. E. (1993). Thrombospondin causes activation of latent transforming growth factor-beta secreted by endothelial cells by a novel mechanism. *The Journal of Cell Biology, 122*(4), 923–32.

Serini, G., Bochaton-Piallat, M. L., Ropraz, P., Geinoz, A., Borsi, L., Zardi, L., & Gabbiani, G. (1998). The fibronectin domain ED-A is crucial for myofibroblastic phenotype induction by transforming growth factor-beta1. *The Journal of Cell Biology, 142*(3), 873–81.

Sharafinski, M. E., Ferris, R. L., Ferrone, S., & Grandis, J. R. (2010). Epidermal growth factor receptor targeted therapy of squamous cell carcinoma of the head and neck. *Head & Neck, 32*(10), 1412–21.

Shekhar, M. P., Werdell, J., Santner, S. J., Pauley, R. J., & Tait, L. (2001). Breast stroma plays a dominant regulatory role in breast epithelial growth and differentiation: implications for tumor development and progression. *Cancer Research, 61*(4), 1320–6.

Sheng, W., Wang, G., Wang, Y., Liang, J., Wen, J., Zheng, P.-S., Wu, Y., Lee, V., Slingerland, J., Dumont, D., & Yang, B. B. (2005). The roles of versican V1 and V2 isoforms in cell proliferation and apoptosis. *Molecular Biology of the Cell, 16*(3), 1330–40.

Sheu, J. J.-C., Hua, C.-H., Wan, L., Lin, Y.-J., Lai, M.-T., Tseng, H.-C., Jinawath, N., Tsai, M. H., Chang, N. W., Lin, C. F., Lin, C. C., Hsieh, L. H., Wang, T. L., Shihle, M., & Tsai, F.-J. (2009). Functional genomic analysis identified epidermal growth factor receptor activation as the most common genetic event in oral squamous cell carcinoma. *Cancer Research, 69*(6), 2568–76.

Shimasaki, N., Kuroda, N., Miyazaki, E., Hayashi, Y., Toi, M., Hiroi, M., Enzan, H., & Shuin, T. (2006). The distribution pattern of myofibroblasts in the stroma of human bladder carcinoma depends on their invasiveness. *Histology and Histopathology, 21*(4), 349–53.

Shimoda, M., Principe, S., Jackson, H. W., Luga, V., Fang, H., Molyneux, S. D., Shao, Y. W., Aiken, A., Waterhouse, P. D., Karamboulas, C., Hess, F. M., Ohtsuka, T., Okada, Y., Ailles, L., Ludwig, A.,

Wrana, J. L., Kislinger, T., & Khokha, R. (2014). Loss of the Timp gene family is sufficient for the acquisition of the CAF-like cell state. *Nature Cell Biology, 16*(9), 889–901.

Shinde, A. V, Kelsh, R., Peters, J. H., Sekiguchi, K., Van De Water, L., & McKeown-Longo, P. J. (2015). The α4β1 integrin and the EDA domain of fibronectin regulate a profibrotic phenotype in dermal fibroblasts. *Matrix Biology : Journal of the International Society for Matrix Biology, 41,* 26–35.

Siegel, P. M., & Massagué, J. (2003). Cytostatic and apoptotic actions of TGF-beta in homeostasis and cancer. *Nature Reviews. Cancer, 3*(11), 807–21.

Simpson, R. M. L., Wells, A., Thomas, D., Stephens, P., Steadman, R., & Phillips, A. (2010). Aging fibroblasts resist phenotypic maturation because of impaired hyaluronan-dependent CD44/epidermal growth factor receptor signaling. *The American Journal of Pathology, 176*(3), 1215–28.

Siomi, H., & Siomi, M. C. (2010). Posttranscriptional regulation of microRNA biogenesis in animals. *Molecular Cell, 38*(3), 323–32.

Skobe, M., & Fusenig, N. E. (1998). Tumorigenic conversion of immortal human keratinocytes through stromal cell activation. *Proceedings of the National Academy of Sciences of the United States of America, 95*(3), 1050–5.

Sobral, L. M., Bufalino, A., Lopes, M. A., Graner, E., Salo, T., & Coletta, R. D. (2011). Myofibroblasts in the stroma of oral cancer promote tumorigenesis via secretion of activin A. *Oral Oncology, 47*(9), 840–6. doi:10.1016/j.oraloncology.2011.06.011

Sok, J. C., Coppelli, F. M., Thomas, S. M., Lango, M. N., Xi, S., Hunt, J. L., … Grandis, J. R. (2006). Mutant epidermal growth factor receptor (EGFRvIII) contributes to head and neck cancer growth and resistance to EGFR targeting. *Clinical Cancer Research : An Official Journal of the American Association for Cancer Research, 12*(17), 5064–73.

Sotiriou, C., Lothaire, P., Dequanter, D., Cardoso, F., & Awada, A. (2004). Molecular profiling of head and neck tumors. *Current Opinion in Oncology, 16*(3), 211–4.

Stephens, P., Davies, K. J., Occleston, N., Pleass, R. D., Kon, C., Daniels, J., Khaw, P. T., & Thomas, D. W. (2001). Skin and oral fibroblasts exhibit phenotypic differences in extracellular matrix reorganization and matrix metalloproteinase activity. *The British Journal of Dermatology, 144*(2), 229–37.

Strutz, F., Okada, H., Lo, C. W., Danoff, T., Carone, R. L., Tomaszewski, J. E., & Neilson, E. G. (1995). Identification and characterization of a fibroblast marker: FSP1. *The Journal of Cell Biology, 130*(2), 393–405.

Studebaker, A. W., Storci, G., Werbeck, J. L., Sansone, P., Sasser, A. K., Tavolari, S., Huang, T., Chan, M.W., Marini, F. C., Rosol, T. J., Bonafe, M., & Hall, B. M. (2008). Fibroblasts isolated from common sites of breast cancer metastasis enhance cancer cell growth rates and invasiveness in an interleukin-6-dependent manner. *Cancer Research, 68*(21), 9087–95.

Stuelten, C. H., DaCosta Byfield, S., Arany, P. R., Karpova, T. S., Stetler-Stevenson, W. G., & Roberts, A. B. (2005). Breast cancer cells induce stromal fibroblasts to express MMP-9 via secretion of TNF-alpha and TGF-beta. *Journal of Cell Science, 118*(Pt 10), 2143–53.

Sugimoto, H., Mundel, T. M., Kieran, M. W., & Kalluri, R. (2006). Identification of fibroblast heterogeneity in the tumor microenvironment. *Cancer Biology & Therapy, 5*(12), 1640–6.

Suh, S. O., Chen, Y., Zaman, M. S., Hirata, H., Yamamura, S., Shahryari, V., Liu, J., Tabatabai, Z. L., Kakar, S., Deng, G., Tanaka, Y., & Dahiya, R. (2011). MicroRNA-145 is regulated by DNA methylation and p53 gene mutation in prostate cancer. *Carcinogenesis, 32*(5), 772–8.

Sun, X., Fa, P., Cui, Z., Xia, Y., Sun, L., Li, Z., Tang, A., Gui, Y., & Cai, Z. (2014). The EDA-containing cellular fibronectin induces epithelial-mesenchymal transition in lung cancer cells through integrin α9β1-mediated activation of PI3-K/AKT and Erk1/2. *Carcinogenesis, 35*(1), 184–91.

Sun, Z., Wang, C., Shi, C., Sun, F., Xu, X., Qian, W., Nie, S., & Han, X. (2014). Activated Wnt signaling induces myofibroblast differentiation of mesenchymal stem cells, contributing to pulmonary fibrosis. *International Journal of Molecular Medicine, 33*(5), 1097–109.

Surowiak, P., Murawa, D., Materna, V., Maciejczyk, A., Pudelko, M., Ciesla, S., Breborowicz, J., Murawa, P., Zabel, M., Dietel, M., & Lage, H. Occurence of stromal myofibroblasts in the invasive ductal breast cancer tissue is an unfavourable prognostic factor. *Anticancer Research, 27*(4C), 2917–24.

Suwan, K., Choocheep, K., Hatano, S., Kongtawelert, P., Kimata, K., & Watanabe, H. (2009). Versican/PG-M Assembles Hyaluronan into Extracellular Matrix and Inhibits CD44-mediated Signaling toward Premature Senescence in Embryonic Fibroblasts. *The Journal of Biological Chemistry, 284*(13), 8596–604.

Suwiwat, S., Ricciardelli, C., Tammi, R., Tammi, M., Auvinen, P., Kosma, V.-M., LeBaron, R. G., Raymond, W. A., Tilley, W. D., & Horsfall, D. J. (2004). Expression of extracellular matrix components versican, chondroitin sulfate, tenascin, and hyaluronan, and their association with disease outcome in node-negative breast cancer. *Clinical Cancer Research : An Official Journal of the American Association for Cancer Research, 10*(7), 2491–8.

Suzuki, H. I., Yamagata, K., Sugimoto, K., Iwamoto, T., Kato, S., & Miyazono, K. (2009). Modulation of microRNA processing by p53. *Nature, 460*(7254), 529–33.

Swigris, J. J., & Brown, K. K. (2010). The role of endothelin-1 in the pathogenesis of idiopathic pulmonary fibrosis. *BioDrugs : Clinical Immunotherapeutics, Biopharmaceuticals and Gene Therapy, 24*(1), 49–54.

Syrokou, A., Tzanakakis, G. N., Hjerpe, A., & Karamanos, N. K. (1999). Proteoglycans in human malignant mesothelioma. Stimulation of their synthesis induced by epidermal, insulin and platelet-derived growth factors involves receptors with tyrosine kinase activity. *Biochimie, 81*(7), 733–44.

Tarin, D., & Croft, C. B. (1969). Ultrastructural features of wound healing in mouse skin. *Journal of Anatomy, 105*(Pt 1), 189–90.

Teofoli, P., Barduagni, S., Ribuffo, M., Campanella, A., De Pita', O., & Puddu, P. (1999). Expression of Bcl-2, p53, c-jun and c-fos protooncogenes in keloids and hypertrophic scars. *Journal of Dermatological Science, 22*(1), 31–7.

Thiery, J. P. (2002). Epithelial-mesenchymal transitions in tumour progression. *Nature Reviews. Cancer, 2*(6), 442–54.

Thomas, G. J., Hart, I. R., Speight, P. M., & Marshall, J. F. (2002). Binding of TGF-beta1 latency-associated peptide (LAP) to alpha(v)beta6 integrin modulates behaviour of squamous carcinoma cells. *British Journal of Cancer, 87*(8), 859–67.

Thomas, G. J., Lewis, M. P., Whawell, S. A., Russell, A., Sheppard, D., Hart, I. R., Speight, P. M., & Marshall, J. F. (2001). Expression of the alphavbeta6 integrin promotes migration and invasion in squamous carcinoma cells. *The Journal of Investigative Dermatology, 117*(1), 67–73..

Thomas, G. J., Nyström, M. L., & Marshall, J. F. (2006). Alphavbeta6 integrin in wound healing and cancer of the oral cavity. *Journal of Oral Pathology & Medicine : Official Publication of the International Association of Oral Pathologists and the American Academy of Oral Pathology, 35*(1), 1–10.

Tomasek, J. J., Gabbiani, G., Hinz, B., Chaponnier, C., & Brown, R. A. (2002). Myofibroblasts and mechano-regulation of connective tissue remodelling. *Nature Reviews. Molecular Cell Biology*, 3(5), 349–63.

Touab, M., Villena, J., Barranco, C., Arumí-Uría, M., & Bassols, A. (2002). Versican is differentially expressed in human melanoma and may play a role in tumor development. *The American Journal of Pathology, 160*(2), 549–57.

Trimboli, A. J., Cantemir-Stone, C. Z., Li, F., Wallace, J. A., Merchant, A., Creasap, N., Thompson, J. C., Caserta, E., Wang, H., Chong, J. L., Naidu, S., Wei, G., Sharma, M. S., Stephens, J. A., Fernandez, S. A., Gurcan, M. N., Weinstein, M. B., Barsky, S. H., Yee, L., Rosol, T. J., Stromberg, P. C., Robinson, M. L., Pepin, F., Hallett, M., Park, M., Ostrowski, M. C., & Leone, G. (2009). Pten in stromal fibroblasts suppresses mammary epithelial tumours. *Nature, 461*(7267), 1084–91.

Tsujino, T., Seshimo, I., Yamamoto, H., Ngan, C. Y., Ezumi, K., Takemasa, I., Ikeda, M., Sekimoto, M., Matsuura, N., & Monden, M. (2007). Stromal Myofibroblasts Predict Disease Recurrence for Colorectal Cancer. *Clinical Cancer Research, 13*(7), 2082–2090.

Uozaki, H., Morita, S., Kumagai, A., Aso, T., Soejima, Y., Takahashi, Y., & Fukusato, T. (2014). Stromal miR-21 is more important than miR-21 of tumour cells for the progression of gastric cancer. *Histopathology, 65*(6), 775–83.

Van Baal, J. W. P. M., Verbeek, R. E., Bus, P., Fassan, M., Souza, R. F., Rugge, M., ten Kate, F. J., Vleggaar, F. P., & Siersema, P. D. (2012). microRNA-145 in Barrett's oesophagus: regulating BMP4 signalling via GATA6. *Gut. 62*(5):664-75.

Van Rooij, E., Purcell, A. L., & Levin, A. A. (2012). Developing microRNA therapeutics. *Circulation Research, 110*(3), 496–507.

Velasquez, L. S., Sutherland, L. B., Liu, Z., Grinnell, F., Kamm, K. E., Schneider, J. W., Olsen, E. N., & Small, E. M. (2013). Activation of MRTF-A-dependent gene expression with a small molecule promotes myofibroblast differentiation and wound healing. *Proceedings of the National Academy of Sciences of the United States of America, 110*(42), 16850–5.

Venkatesan, N., Tsuchiya, K., Kolb, M., Farkas, L., Bourhim, M., Ouzzine, M., & Ludwig, M. S. (2014). Glycosyltransferases and glycosaminoglycans in bleomycin and transforming growth factor-β1-induced pulmonary fibrosis. *American Journal of Respiratory Cell and Molecular Biology, 50*(3), 583–94.

Vered, M., Dayan, D., Yahalom, R., Dobriyan, A., Barshack, I., Bello, I. O., Kantola, S., & Salo, T. (2010). Cancer-associated fibroblasts and epithelial-mesenchymal transition in metastatic oral tongue squamous cell carcinoma. *International Journal of Cancer. Journal International Du Cancer, 127*(6), 1356–62.

Vered, M., Dobriyan, A., Dayan, D., Yahalom, R., Talmi, Y. P., Bedrin, L., Barshack, I., & Taicher, S. (2010). Tumor-host histopathologic variables, stromal myofibroblasts and risk score, are significantly associated with recurrent disease in tongue cancer. *Cancer Science, 101*(1), 274–80.

Vikram, B., Strong, E. W., Shah, J. P., & Spiro, R. Failure at distant sites following multimodality treatment for advanced head and neck cancer. *Head & Neck Surgery, 6*(3), 730–3.

Villadsen, S. B., Bramsen, J. B., Ostenfeld, M. S., Wiklund, E. D., Fristrup, N., Gao, S., Hansen, T. B., Jensen, T. I., Borre, M., Orntoft, T. F., Dyrskiot, L., & Kjems, J. (2012). The miR-143/-145 cluster regulates plasminogen activator inhibitor-1 in bladder cancer. *British Journal of Cancer, 106*(2), 366–74.

Vlachos, I. S., Kostoulas, N., Vergoulis, T., Georgakilas, G., Reczko, M., Maragkakis, M., Paraskeyopoulou, M. D., Prionidis, K., Dalamagas, T., & Hatzigeorgiou, A. G. (2012). DIANA miRPath v.2.0: investigating the combinatorial effect of microRNAs in pathways Nucleic Acids Research.

Walraven, M., Gouverneur, M., Middelkoop, E., Beelen, R. H. J., & Ulrich, M. M. W. Altered TGF-β signaling in fetal fibroblasts: what is known about the underlying mechanisms? *Wound Repair and Regeneration : Official Publication of the Wound Healing Society [and] the European Tissue Repair Society, 22*(1), 3–13.

Wang, G., Chan, E. S.-Y., Kwan, B. C.-H., Li, P. K.-T., Yip, S. K.-H., Szeto, C.-C., & Ng, C.-F. (2012). Expression of microRNAs in the urine of patients with bladder cancer. *Clinical Genitourinary Cancer, 10*(2), 106–13.

Wang, S. J., & Bourguignon, L. Y. W. (2011). Role of hyaluronan-mediated CD44 signaling in head and neck squamous cell carcinoma progression and chemoresistance. *The American Journal of Pathology, 178*(3), 956–63.

Wang, S. J., Wong, G., de Heer, A.-M., Xia, W., & Bourguignon, L. Y. W. (2009). CD44 variant isoforms in head and neck squamous cell carcinoma progression. *The Laryngoscope, 119*(8), 1518–30.

Wang, W., Li, Q., Yamada, T., Matsumoto, K., Matsumoto, I., Oda, M., Watanabe, G., Kayang, Y., Nishioka, Y., Sone, S., & Yano, S. (2009). Crosstalk to stromal fibroblasts induces resistance of lung cancer to epidermal growth factor receptor tyrosine kinase inhibitors. *Clinical Cancer Research : An Official Journal of the American Association for Cancer Research, 15*(21), 6630–8.

Wang, X., Hu, G., & Zhou, J. (2010). Repression of versican expression by microRNA-143. *The Journal of Biological Chemistry, 285(*30), 23241–50.

Wang, Y.-S., Li, S.-H., Guo, J., Mihic, A., Wu, J., Sun, L., Davis, K., Weisel, R. D., & Li, R.-K. (2014). Role of miR-145 in cardiac myofibroblast differentiation. *Journal of Molecular and Cellular Cardiology*, 66, 94–105.

Webber, J., Steadman, R., Mason, M. D., Tabi, Z., & Clayton, A. (2010). Cancer exosomes trigger fibroblast to myofibroblast differentiation. *Cancer Research, 70*(23), 9621–30.

Weinberg, R. A. (2006). Biology of Cancer. (R. A. Weinberg, Ed.). New York: Garland Science.

Weiss, A., & Attisano, L. (2013). The TGFbeta superfamily signaling pathway. *Wiley Interdisciplinary Reviews. Developmental Biology, 2*(1), 47–63.

Wentz-Hunter, K. K., & Potashkin, J. A. (2011). The Role of miRNAs as Key Regulators in the Neoplastic Microenvironment. *Molecular Biology International*, 2011, 1–8.

Wicki, A., & Christofori, G. (2006). The potential role of podoplanin in tumour invasion. *British Journal of Cancer, 96*(1), 1–5.

Wiklund, E. D., Gao, S., Hulf, T., Sibbritt, T., Nair, S., Costea, D. E., Villadsen, S. B., Bakholdt, V., Bramsen, J. B., Sorensen, J A., Krogdahl, A., Clark, S. J., & Kjems, J. (2011). MicroRNA alterations and associated aberrant DNA methylation patterns across multiple sample types in oral squamous cell carcinoma. *PloS One, 6*(11), e27840.

Wipff, P.-J., Rifkin, D. B., Meister, J.-J., & Hinz, B. (2007). Myofibroblast contraction activates latent TGF-beta1 from the extracellular matrix. *The Journal of Cell Biology, 179*(6), 1311–23.

Wszolek, M. F., Rieger-Christ, K. M., Kenney, P. A., Gould, J. J., Silva Neto, B., Lavoie, A. K., Logyinenko, T., Libertino, J. A., & Summerhayes, I. C. (2009). A MicroRNA expression profile defining the invasive bladder tumor phenotype. *Urologic Oncology, 29*(6), 794–801.e1.

Wu, B.-L., Xu, L.-Y., Du, Z.-P., Liao, L.-D., Zhang, H.-F., Huang, Q., Fang, G. Q., & Li, E.-M. (2011). MiRNA profile in esophageal squamous cell carcinoma: downregulation of miR-143 and miR-145. *World Journal of Gastroenterology : WJG, 17*(1), 79–88.

Wu, D., Li, M., Wang, L., Zhou, Y., Zhou, J., Pan, H., & Qu, P. (2014). microRNA 145 inhibits cell proliferation, migration and invasion by targeting matrix metallopeptidase-11 in renal cell carcinoma. *Molecular Medicine Reports, 10*(1), 393–8.

Wu, Y. J., La Pierre, D. P., Wu, J., Yee, A. J., & Yang, B. B. (2005). The interaction of versican with its binding partners. *Cell Research, 15*(7), 483–94.

Wynn, T. A., & Ramalingam, T. R. (2012). Mechanisms of fibrosis: therapeutic translation for fibrotic disease. *Nature Medicine, 18*(7), 1028–40.

Xiang, L., Xie, G., Ou, J., Wei, X., Pan, F., & Liang, H. (2012). The extra domain A of fibronectin increases VEGF-C expression in colorectal carcinoma involving the PI3K/AKT signaling pathway. *PloS One, 7*(4), e35378.

Xin, M., Small, E. M., Sutherland, L. B., Qi, X., McAnally, J., Plato, C. F., Richardson, J. A., Bassel-Duby, R., & Olson, E. N. (2009). MicroRNAs miR-143 and miR-145 modulate cytoskeletal dynamics and responsiveness of smooth muscle cells to injury. *Genes & Development, 23*(18), 2166–78.

Xu, N., Papagiannakopoulos, T., Pan, G., Thomson, J. A., & Kosik, K. S. (2009). MicroRNA-145 regulates OCT4, SOX2, and KLF4 and represses pluripotency in human embryonic stem cells. *Cell, 137*(4), 647–58.

Xu, Q., Liu, L.-Z., Qian, X., Chen, Q., Jiang, Y., Li, D., Lai, L., & Jiang, B.-H. (2012). MiR-145 directly targets p70S6K1 in cancer cells to inhibit tumor growth and angiogenesis. *Nucleic Acids Research, 40*(2), 761–74.

Yamada, T., Matsumoto, K., Wang, W., Li, Q., Nishioka, Y., Sekido, Y., Sone, E., & Yano, S. (2010). Hepatocyte growth factor reduces susceptibility to an irreversible epidermal growth factor receptor inhibitor in EGFR-T790M mutant lung cancer. *Clinical Cancer Research : An Official Journal of the American Association for Cancer Research, 16*(1), 174–83.

Yang, B., Guo, H., Zhang, Y., Chen, L., Ying, D., & Dong, S. (2011). MicroRNA-145 regulates chondrogenic differentiation of mesenchymal stem cells by targeting Sox9. *PloS One, 6*(7), e21679.

Yang, L., Huang, J., Ren, X., Gorska, A. E., Chytil, A., Aakre, M., Carbone, D. P., Matrisan, L. M., Richmond, A., Lin, P. C., & Moses, H. L. (2008). Abrogation of TGF beta signaling in mammary carcinomas recruits Gr-1+CD11b+ myeloid cells that promote metastasis. *Cancer Cell, 13*(1), 23–35.

Yang, L., & Moses, H. L. (2008). Transforming growth factor beta: tumor suppressor or promoter? Are host immune cells the answer? *Cancer Research, 68*(22), 9107–11.

Yang, M.-H., Lin, B.-R., Chang, C.-H., Chen, S.-T., Lin, S.-K., Kuo, M. Y.-P., Jeng, Y. M., Kuo, M. L., & Chang, C.-C. (2012). Connective tissue growth factor modulates oral squamous cell carcinoma invasion by activating a miR-504/FOXP1 signalling. *Oncogene, 31*(19), 2401–11.

Yang, S., Cui, H., Xie, N., Icyuz, M., Banerjee, S., Antony, V. B., Abraham, E., Thannickal, V. J., & Liu, G. (2013). miR-145 regulates myofibroblast differentiation and lung fibrosis. *FASEB Journal : Official Publication of the Federation of American Societies for Experimental Biology, 27*(6), 2382–91.

Yao, L. Y., Moody, C., Schönherr, E., Wight, T. N., & Sandell, L. J. (1994). Identification of the proteoglycan versican in aorta and smooth muscle cells by DNA sequence analysis, in situ hybridization and immunohistochemistry. *Matrix Biology : Journal of the International Society for Matrix Biology, 14*(3), 213–25.

Yao, Q., Cao, S., Li, C., Mengesha, A., Kong, B., & Wei, M. (2011). Micro-RNA-21 regulates TGF-β-induced myofibroblast differentiation by targeting PDCD4 in tumor-stroma interaction. *International Journal of Cancer. Journal International Du Cancer, 128*(8), 1783–92.

Yee, A. J. M., Akens, M., Yang, B. L., Finkelstein, J., Zheng, P.-S., Deng, Z., & Yang, B. (2007). The effect of versican G3 domain on local breast cancer invasiveness and bony metastasis. *Breast Cancer Research : BCR, 9*(4), R47.

Yeung, T.-L., Leung, C. S., Wong, K.-K., Samimi, G., Thompson, M. S., Liu, J., Zaid, T. M., Ghosh, S., Birrer, M. J., & Mok, S. C. (2013). TGF-β modulates ovarian cancer invasion by upregulating CAF-derived versican in the tumor microenvironment. *Cancer Research, 73*(16), 5016–28.

Yoon, H., Liyanarachchi, S., Wright, F. A., Davuluri, R., Lockman, J. C., de la Chapelle, A., & Pellegata, N. S. (2002). Gene expression profiling of isogenic cells with different TP53 gene dosage reveals numerous genes that are affected by TP53 dosage and identifies CSPG2 as a direct target of p53. *Proceedings of the National Academy of Sciences of the United States of America, 99*(24), 15632–7.

Yu, C.-C., Tsai, L.-L., Wang, M.-L., Yu, C.-H., Lo, W.-L., Chang, Y.-C., Chiou, G. Y., Chou, M. Y., & Chiou, S.-H. (2013). miR145 targets the SOX9/ADAM17 axis to inhibit tumor-initiating cells and IL-6-mediated paracrine effects in head and neck cancer. *Cancer Research, 73*(11), 3425–40.

Yu, Q., & Stamenkovic, I. (1999). Localization of matrix metalloproteinase 9 to the cell surface provides a mechanism for CD44-mediated tumor invasion. *Genes & Development, 13*(1), 35–48.

Yu, Q., & Stamenkovic, I. (2000). Cell surface-localized matrix metalloproteinase-9 proteolytically activates TGF-beta and promotes tumor invasion and angiogenesis. *Genes & Development, 14*(2), 163–76.

Yue, J., & Mulder, K. M. (2001). Transforming growth factor-beta signal transduction in epithelial cells. *Pharmacology & Therapeutics, 91*(1), 1–34.

Yue, X., Li, X., Nguyen, H. T., Chin, D. R., Sullivan, D. E., & Lasky, J. A. (2008). Transforming growth factor-beta1 induces heparan sulfate 6-O-endosulfatase 1 expression in vitro and in vivo. *The Journal of Biological Chemistry, 283*(29), 20397–407.

Zahran, F., Ghalwash, D., Shaker, O., Al-Johani, K., & Scully, C. (2015). Salivary Micro-RNAs in Oral Cancer. *Oral Diseases.* Epub ahead of print.

Zeng, L., Carter, A. D., & Childs, S. J. (2009). miR-145 directs intestinal maturation in zebrafish. *Proceedings of the National Academy of Sciences of the United States of America, 106*(42), 17793–8.

Zhang, J., Chen, L., Xiao, M., Wang, C., & Qin, Z. (2011). FSP1+ fibroblasts promote skin carcinogenesis by maintaining MCP-1-mediated macrophage infiltration and chronic inflammation. *The American Journal of Pathology, 178*(1), 382–90.

Zhang, Y., Wang, Z., & Gemeinhart, R. A. (2013). Progress in microRNA delivery. *Journal of Controlled Release : Official Journal of the Controlled Release Society, 17*2(3), 962–74.

Zhao, N., Koenig, S. N., Trask, A. J., Lin, C.-H., Hans, C. P., Garg, V., & Lilly, B. (2015). MicroRNA miR145 regulates TGFBR2 expression and matrix synthesis in vascular smooth muscle cells. *Circulation Research, 116*(1), 23–34.

Zhu, H., Li, Y., Qu, S., Luo, H., Zhou, Y., Wang, Y., Zhao, H., You, Y., Xiao, X., & Zuo, X. (2012). MicroRNA expression abnormalities in limited cutaneous scleroderma and diffuse cutaneous scleroderma. *Journal of Clinical Immunology, 32*(3), 514–22.

Zhu, H.-Y., Li, C., Zheng, Z., Zhou, Q., Guan, H., Su, L.-L., Zhu, X. X., Wang, S. Y., Li, J., & Hu, D.-H. (2015). Peroxisome proliferator-activated receptor-γ (PPAR-γ) agonist inhibits collagen synthesis in human hypertrophic scar fibroblasts by targeting Smad3 via miR-145. *Biochemical and Biophysical Research Communication, 459*(1):49-53.

Zhu, S., Wu, H., Wu, F., Nie, D., Sheng, S., & Mo, Y.-Y. (2008). MicroRNA-21 targets tumor suppressor genes in invasion and metastasis. *Cell Research, 18*(3), 350–9.

Zimmermann, D. R., & Ruoslahti, E. (1989). Multiple domains of the large fibroblast proteoglycan, versican. *The EMBO Journal, 8(*10), 2975–81.

Zur Hausen, H. (2002). Papillomaviruses and cancer: from basic studies to clinical application. Nature Reviews. *Cancer, 2*(5), 342–50.

Appendix

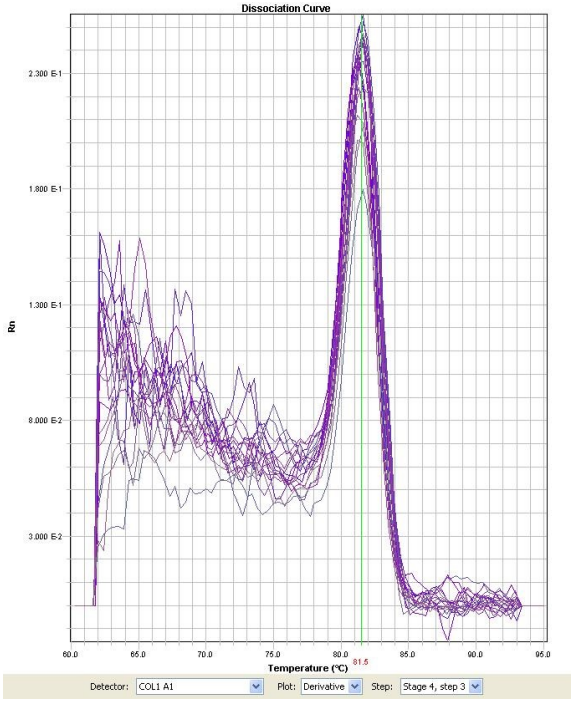

Appendix figure 1: An example of a dissociation curve. A melt curve was performed using a 7900HT fast Real Time-PCR system and shown in appendix figure 1 where change Rn (fluorescence/ change in temperature) is plotted against temperature. A clear single peak indicating the amplication of one PCR product.

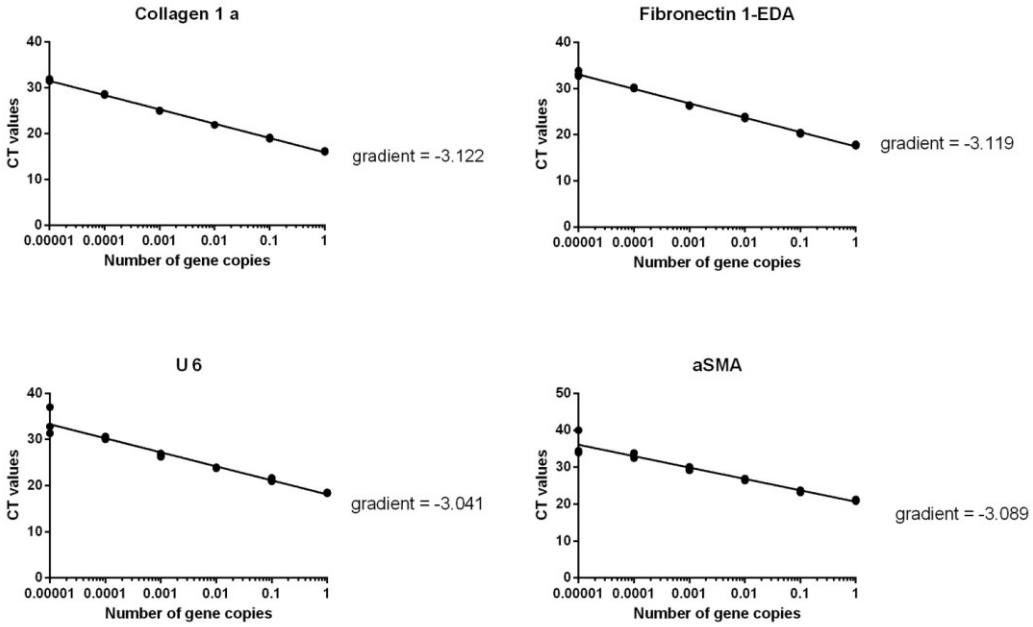

Appendix figure 2: Primer efficiencies CT values vs log of gene number. 2 μg RNA was reverse transcribed and the cDNA was serially diluted to create 6 standard dilutions, which were used in a qRT-PCR reaction for a particular SYBR green primer. CT values were plotted against the number of gene copies on a semi-log scale the line of best fit was calculated and used to calculate the amplification efficiencies. This figure shows the graphs for the primer efficiencies CT vs log number of gene copies, with the calculated gradients adjacent.

Primers	Gradient	Amplification Factor	Amplification efficiency (%)
αSMA	-3.089	2.11	110.73%
COL1A	-3.122	2.09	109.08%
FN1-EDA	-3.119	2.09	109.23%
U 6	-3.041	2.13	113.23%
KLF4	-3.728	1.85	85.46%
KLF5	-3.171	2.07	106.71%
SOX9	-2.837	2.25	125.16%
TGFBRII	-3.070	2.12	111.71%
CTGF	-3.076	2.11	111.40%
MRTF-A	-3.897	1.81	80.55%
MRTF-B	-3.170	2.07	106.76%
SMAD3	-3.058	2.12	112.33%
VCAN	-3.834	1.82	82.32%
MMP2	-3.717	1.86	85.80%

Appendix table 1: Primer amplification efficiencies. The gradient from CT vs semi log gene number graphs were used in an equation to calculate the amplication factor $E = 10^{-1/slope}$. This could then be used to calculate the % amplification efficiency using this equation: $\%\, E = (E - 1) \times 100\%$. According to Bio-Rad, primers with amplification efficiencies between 90-110 % are acceptable for use in qPCR.